Role of Passivity and Surface Modification on the Corrosion Behaviour of AISI 304L Stainless Steel in Nitric Acid Medium

By

Nilamadhab Padhy

Indira Gandhi Centre for Atomic Research
Kalpakkam, India

A thesis submitted to the
Board of Studies in Chemical Sciences
In partial fulfillment of requirement
For the Degree of

DOCTOR OF PHILOSOPHY

of

Homi Bhabha National Institute (HBNI)
Deemed University
Mumbai, India

December, 2010

Role of Passivity and Surface Modification on the Corrosion Behaviour of AISI 304L Stainless Steel in Nitric Acid Medium

A thesis submitted to the
Board of Studies in Chemical Sciences
Homi Bhabha National Institute
in partial fulfillment of requirement
for the degree of

DOCTOR OF PHILOSOPHY

in

Chemical Science

By

Nilamadhab Padhy
Enrolment No: CHEM 022007040003
Indira Gandhi Centre for Atomic Research

Research Supervisor

Prof. Dr. U. Kamachi Mudali

Head, Corrosion Science and Technology Division

Head, Reprocessing Research and Development Division

Indira Gandhi Centre for Atomic Research

Kalpakkam, 603 102, India

Homi Bhabha National Institute

Recommendations of the Viva Voce Board

As members of the Viva Voce Board, we certify that we have read the dissertation prepared by **Mr. Nilamadhab Padhy** entitled ***"Role of Passivity and Surface Modification on the Corrosion Behaviour of AISI Type 304L Stainless Steel in Nitric Acid Medium"*** and recommend that it may be accepted as fulfilling the dissertation requirement for the Degree of Doctor of Philosophy.

C Mallika **Date:** 12-4-2011

Chairperson - **Prof. C. Mallika**

UKamachi Mudali **Date:** 12-4-2011

Supervisor -Convener – **Prof. U. Kamachi Mudali**

Date: 12-4-2011

Member 1 – External Examiner – **Prof. N. Palaniswamy, CECRI**

Date: 12-4-2011

Member 2 – **Prof. S. Rangarajan**

Date: 12-4-2011

Member N – **Prof. B. K.Panigrahi**

Final approval and acceptance of this dissertation is contingent upon the candidate's submission of the final copies of the dissertation to HBNI.

I hereby certify that I have read this dissertation prepared under my direction and recommend that it may be accepted as fulfilling the dissertation requirement.

Date: April 12, 2011

Place: Indira Gandhi Centre for Atomic Research, Kalpakkam

STATEMENT BY AUTHOR

This dissertation has been submitted in partial fulfillment of requirements for an advanced degree at Homi Bhabha National Institute (HBNI) and is deposited in the library to be made to borrowers under rules of the HBNI.

Brief quotations from this dissertation are allowable without special permission, provided that accurate acknowledgement of source is made. Requests for permission for extended quotation from or reproduction of this manuscript in whole or in part may be granted by the Competent Authority of HBNI when in his or her judgment the proposed use of the material is in the interest of scholarship. In all other instances, permission must be obtained from the author.

Nilamadhab Padhy

Nilamadhab Padhy

DECLARATION

I, hereby declare that the thesis entitled "***Role of passivity and surface modification on the corrosion behaviour of AISI 304L stainless steel in nitric acid medium***" submitted to **Homi Bhabha National Institute (HBNI)**, Mumbai, India, for the award of **Doctor of Philosophy** in **Chemical Science** is the record of work carried out by me under the guidance of **Prof. Dr. U. Kamachi Mudali**, Head, Corrosion Science and Technology Group (CSTD), and Reprocessing Research and Development Division (RRDD), Indira Gandhi Centre for Atomic Research (IGCAR). The work is original and has not been submitted earlier as a whole or in part for a degree, diploma, associateship, fellowship at this or any other Institution/University of higher learning.

Nilamadhab Padhy

Nilamadhab Padhy

ACKNOWLEDGMENT

The author wish to express sincere respect and gratitude to **Prof. Dr. U. Kamachi Mudali**, Head, Corrosion Science and Technology Division (CSTD), and Reprocessing Research and Development Division (RRDD), Indira Gandhi Centre for Atomic Research (IGCAR), for his wholehearted support, encouragement and guidance during the whole research work. Thanks are due to his constant inspiration, legacy towards learning, and keen interest in the subject. I am deeply obliged to his constructive suggestions, meticulous planning, and effective analytic approach.

I would like to extend my heartfelt thanks to **Padmashree Dr. Baldev Raj,** his excellency, Director, IGCAR, for moral support, permission to use various facilities in the centre, and most importantly providing direction in this investigation.

I sincerely thank my Doctoral Committee chairman **Dr. C. Mallika**, and members **Dr. S. Rangarajan**, **Dr. B. K. Panigrahi** for time to time evaluation of the research work, and useful suggestion which definitely improved the dissertation. I would also like to express my heartfelt thank to **Dr. S. Ningshen** for technical support.

I take this opportunity to thank with great pleasure for strong support from the officers and research scholars working in Corrosion Science and Technology Division, IGCAR, Dr. A. R. Hasan Shaikh, Shri. R. V. Subba Rao, Dr. Rani. P. George, Dr. S. Ramya, Smt. Girija Suresh, Shri. K. Thyagarajan, Shri. R. K. Sole, Shri. A. Ravi Shankar, Smt. Ranita Paul, Shri. M. Arumugam, Shri. K. Kamalnathan, Shri. A. Ramakrishnan, Shri. R. Thiruvaluvan, Shri. T. Nanda Kumar, Smt. Lipika Rani Bairi, Mr. Praddep Kumar Samantroy, Mr. Jagdeesh Sure, Ms. S. D. Ruth Nithila, Mr. Pinaki Paul, Mr. Arun Chandran, Ms. P. V. Mahalaxmi, and Ms. Indira. K.

Nevertheless, nor the least, I am thankful, and indebted to all the research scholars working in the centre for their help and kind cooperation in every possible way. In fact, they are the source of inspiration during the doctoral study.

I am thankful to my parents, brother and sisters for their kind cooperation and support.

Finally, I thank almighty for providing me the opportunity to step into the exciting world of science, merciful blessing, and enabling me to write the thesis.

Nilamadhab Padhy

Nilamadhab Padhy

CONTENTS

Spent Nuclear Fuel Reprocessing
&
Material Challenges

Corrosion Issues of Austenitic Stainless Steel in Nitric Acid

Material, Medium & Mechanism

3 CHAPTER 3 42

Experimental Details

Morphological and Compositional Analysis of Passive Film on AISI 304L Stainless Steel in Nitric Acid Medium

Corrosion Behaviour of Nitrogen Ion Implanted AISI 304L Stainless Steel in Nitric Acid Medium

6 **C H A P T E R 6** 116

Corrosion Performance of Ti, TiO_2 and Duplex Ti-TiO_2 Coated 304L Stainless Steel in Nitric Acid Medium

7 **CHAPTER 7** 155

Conclusions, Summary & Scope for Future Work

I SYNOPSIS

American Iron and Steel Institute (AISI) type 304L stainless steel (SS) is the largest material of construction used in spent nuclear fuel reprocessing plants due to its good corrosion resistance, adequate mechanical properties, and affordable cost [1,2]. Moreover, these materials are readily available, and are easy to weld and fabricate. The versatile application of 304L SS in the fuel reprocessing plant have been critically evaluated over the years for predicting the corrosion rate, reliability in aggressive situations, and their economic competence. Special emphasis was given towards their structure, properties, and maintenance free aspects in order to perform satisfactorily for decades leading to uninterrupted operation of the plant. Major applications of 304L SS in the nuclear fuel reprocessing plant includes as vessels and tanks for dissolver and solvent extraction equipments, evaporators, lining of floors and walls of the contaminate area, off-gas treatment systems, piping for the flow of process fluid, and in many other critical components. In addition, type 304L SS is used for storage and transportation of waste generated from spent nuclear fuel reprocessing plant. The choice of 304L SS is also due to low absorption of radioactivity, and easiness in decontaminating by specific reagents without substantial corrosion to the material. Thus, the large scale use of 304L SS for process vessels, and as hundreds of kilometers of piping involves possible use of several hundred tons of material in the overall construction of a reprocessing plant.

Nitric acid at various concentrations and at different temperatures is the main process medium for spent nuclear fuel dissolution as well as for various stages of extraction and separation process in aqueous nuclear fuel reprocessing [3-7]. The selection of nitric acid for spent fuel dissolution is due to fastest reaction kinetics with spent fuel in the finely divided state. Moreover, the advantage of using nitric acid is because, it is a good salting agent, posses low viscosity, surface tension, and easy to separate from the raffinate. Nitric acid after reprocessing can be recovered, and concentrated for reuse in the reprocessing plant. Due to this acid recovery, the regent cost for the neutralization of aqueous waste is also lowered giving considerable economic advantage. However, the undesirable feature is that its relative inextractability to organic phase compelling to change in salting agent concentration during the separation process. The off gases generated such as NO_x, non-volatile iodates, and undissolved metals also create problem in the overall recovery process, and lets down the neediness of reprocessing. Moreover, the concentration of nitric acid in high level waste after spent fuel dissolution should be adjusted, otherwise sever corrosion problem will occur in the container material [8].

As 304L SS is the major constructional material, and nitric acid is the main process medium, the compatibility between these two determines the overall performance of the material in the reprocessing plant. Stainless steels are well known for their good passivity and corrosion resistance to uniform corrosion in nitric acid, nevertheless the susceptibility to localized corrosion in the oxidizing environment is also largely known [1-4, 6,7]. Various forms of corrosion that have been noticed for 304L SS are, (a) intergranular corrosion, (b) transpassive corrosion, (c) end-grain attack etc. Apart from this, galvanic corrosion, pitting corrosion, crevice corrosion and stress corrosion cracking have also been observed. Specific example includes, (a) intergranular corrosion of austenitic stainless steel in nitric acid containing oxidizing species, (b) end-grain attack in presence of dissolver fluid, (c) corrosion in distillation columns in contact with concentrated acid, (d) corrosion in equipments due to acid fumes, and mist generated from dissolver off-gas, and (e) corrosion of container materials due to presence of nitric acid in high level waste generated etc [1-4, 9,10].

The corrosion behaviour of austenitic stainless steel is largely determined by the properties of adherent, tenacious, and self-healing passive film present over the surface [11-14]. The passive film in general has a thickness of 10 Å to 100 Å. However, the thickness of the passive film as well as composition is largely dependent on the electrochemical environment, composition of stainless steel on which it is formed, concentration of the solution, *p*H of the solution, etc. Similarly, the degradation of passive film is dependent on many factors such as aggressivity of the electrochemical environment as well as defects generated on the passivated surface such as, (a) local heterogeneities, (b) variation of stoichiometric composition on atomic scale, and (c) difference in space charge neutrality etc. Apart from this, the hydrodynamics of the process fluid also has a significant effect on the formation of the passive film. Over the years extensive study has been carried out to understand their electrical properties (capacitance, resistance, space charge), thermodynamical properties for growth and range of stability, morphological study to understand the topographical features, chemical analysis to locally resolve the chemical composition, spectroscopic measurements to elucidate the structural features, mechanical test to study the stresses generated within the film, and other various combined measurements to get a reliable picture regarding structure-property of the passive film. Many theories have been proposed which gave a comprehensive understanding regarding passive film, but there is no general consensus exists to any particular theory [15-19]. Even though, progress has been made in this direction, debate still continues for in-depth study for making a unified approach.

Thus, the major work of the present thesis includes investigation of the passive film property of AISI type 304 SS in both ex-situ, and in-situ condition in nitric acid medium [20]. *Apart from this for improving the corrosion resistance of AISI type 304L SS surface modification techniques were used as corrosion is mostly a surface phenomenon. In the present investigation nitrogen ion implantation* [21] *and anti-corrosive Ti,* TiO_2 *and duplex Ti-*TiO_2 *coatings were used to study the degree of improvement in corrosion resistance* [22]. *To the best of knowledge, the studies and the results reported in the thesis are original and contribute to the understanding of the "role of passivity and surface modification on the corrosion behaviour of AISI 304L stainless steel in nitric acid medium".*

The ex-situ study of passive film was carried out using atomic force microscope (AFM) after exposing AISI 304L SS in various concentrations of nitric acid for different duration to understand the time-dependent surface morphological changes in passive film. The in-situ study was carried out using Electrochemical AFM (EC-AFM) at a particular location of the specimen (without changing specimen position) for increasing concentration of nitric acid to examine the sequential change in passive film morphology to elucidate the process of formation and dissolution. Apart from this the change in chemical composition of the passive film in nitric acid medium has been analyzed using X-ray photoelectron spectroscopy.

The effect of surface modification of AISI 304L SS by nitrogen ion implantation, and sputter deposited Ti, TiO_2 *and Ti-*TiO_2 *coating on the corrosion behaviour in nitric acid medium have been investigated as corrosion is mostly a surface phenomenon. The sub-surface modification of AISI 304L SS has been carried out by nitrogen ion implantation. The surface modifications occurring and the extent of improvement in corrosion resistance in nitric acid medium by nitrogen ion implantation have been analyzed as compared to unimplanted specimen. Similarly, the top-surface modification of AISI 304L SS has been carried out by anti-corrosive Ti,* TiO_2 *and duplex Ti-*TiO_2 *coating using magnetron sputtering. The coating properties and its corrosion resistance have been examined from dilute to concentrated nitric acid medium as compared to uncoated specimens.*

II LIST OF FIGURES

III LIST OF TABLES

IV LIST OF ABBREVIATIONS

AISI: American Institute of Steel Industries

SS: Stainless Steel

GHG: Green House Gas

GoI: Government of India

DAE: Department of Atomic Energy

FBR: Fast Breeder Reactor

AHWR: Advanced Heavy Water Reactor

PUREX: Plutonium Uranium Reduction Extraction

NAG: Nitric Acid Grade

SCC: Stress Corrosion Cracking

TRIM: Transport of Ions in Maters

PVD: Physical Vapour Deposition

AFM: Atomic Force Microscopy

GIXRD: Glancing Incidence X-ray Diffraction

JCPDS: Joint Committee on Powder Diffraction Standards

SIMS: Secondary Ion Mass Spectroscopy

XPS: X-ray Photoelectron Spectroscopy

OCP: Open Circuit Potential

EIS: Electrochemical Impedance Spectroscopy

EC-AFM: Electrochemical Atomic Force Microscopy

EC-SPM: Electrochemical Scanning Probe Microscope

CHAPTER 1

Spent Nuclear Fuel Reprocessing
&
Material Challenges

CHAPTER 1

Spent Nuclear Fuel Reprocessing & Material Challenges

The chapter introduces the Indian nuclear power programme towards meeting the increasing energy requirement. The requirement for spent nuclear fuel reprocessing, and various problems and challenges in spent nuclear fuel reprocessing is briefly explained. Out of several problems the chapter focuses on the material selection, and their implementation for successful reprocessing plant application.

1.1 Introduction to Indian nuclear power programme

To date nuclear energy [23] is considered as an important part of energy source by several countries with rising energy demand. The growing interest of nuclear energy is due to large part to its negligible Green House Gas (GHG) emission, and its long term economic competitiveness [24]. The projected energy demand for future (2032) published by Government of India (GoI) is 60 GWe. To meet the demand India needs 25 % of total power production from nuclear sector, a 22% hike from the current level and towards this, Department of Atomic Energy (DAE) has chalked out a three stage power programme [25]. With the utilization of the available resources, it is expected that nuclear power production capacity will increase up to 20, 000 MWe by the year 2020. This involves setting up of pressurized heavy water reactors, and imported light water reactors. The second stage envisages building a chain of Fast Breeder Reactors (FBR) multiplying fissile material inventory along with power production. Subsequently, FBRs will be the stronghold of India’s nuclear power programme. Third stage consists of exploiting the vast resources of thorium through the route of fast, thermal or accelerator driven sub-critical reactors. Thorium is present in a larger quantity in the total estimated reserves of monazite in India to about 8 million tonnes in association with other heavy minerals. An Advanced Heavy Water Reactor (AHWR) designed to draw about two-third power from thorium fuel is under development, and will provide experience in all aspects of technology related to thorium fuel cycle. Overall, with these long-term strategies, the nuclear industry is expected to undergo a paradigm shift from a mere electricity producer to being an indispensable part of India's energy policy.

1.2 Necessity of spent nuclear fuel reprocessing

Reprocessing of spent nuclear fuel [25,26] refers to a chemical separation process with the fractionation of useful radionuclide, and safe waste management. Over the last five decades the prime objective of the spent nuclear fuel reprocessing is to recover the plutonium, and unused uranium for contribution towards energy security as well as avoiding wastage of valuable energy resources. The recovered materials can effectively close the fuel cycle, thereby lowering the large extent dependence on fossil fuel, and improving the energy security. In once-through cycle advantage is that it avoids the difficulties of reprocessing, however it can only extract about half a percent of energy content of mined uranium. Moreover, the recovered material can directly be enriched reducing the demand of mining and milling of new uranium.

The initiatives for nuclear fuel reprocessing in India started in 1964 as the known sources of uranium is inadequate to meet the long-term nuclear power programme [27]. At present India is having three nuclear fuel reprocessing plants, one at Trombay of reprocessing capacity 60 tonne per year, the second and third plants located at Tarapur and Kalpakkam, respectively with capacity of 100 tonne of power reactor fuel per year. As India moved into reprocessing of spent nuclear fuel, PUREX (Plutonium Uranium Reduction EXtraction) was the main separation process. Thus reprocessing programme initiated with design, construction and commissioning of demonstration plant at Trombay using PUREX as aqueous reprocessing process. The schematic of a typical PUREX process is shown in Fig.1.1 [28].

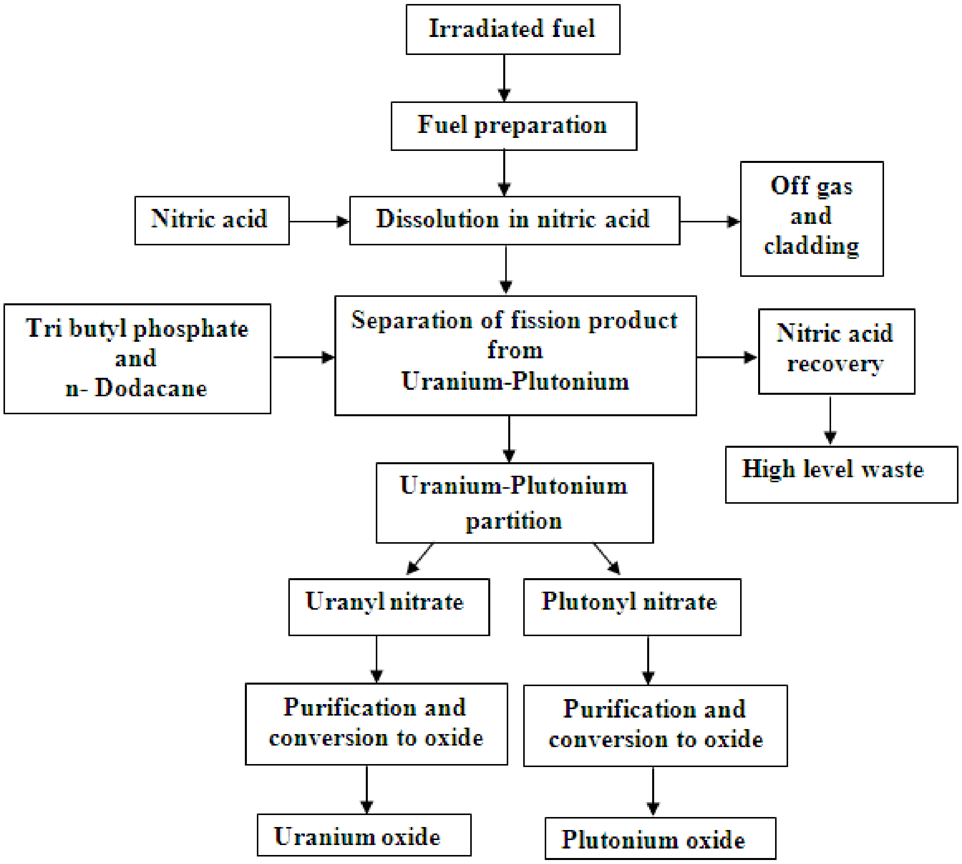

Fig. 1.1: Schematic of a typical PUREX process [28]

1.3 Challenges in spent nuclear fuel reprocessing

Nuclear fuel reprocessing plant faces the same problems as associated with any other process industry. Moreover, the problems encountered in fuel reprocessing plant are more stringent due to radiological impacts such as presence of radioactivity, build-up of heavy isotopes, and contaminated equipments. The major problems associated with reprocessing are safety concerns, problems in selection of materials of construction, cost of fuel reprocessing, and radioactive disposal. Out of several critical issues, material challenges [1] are of utmost important for safe operation of fuel reprocessing plant as well as determining the overall plant life. The selection criteria of materials of construction for nuclear fuel reprocessing plant is a complicated procedure involving various parameters such as their availability, cost, mechanical properties and corrosion resistance etc. The demanding criteria are the presence of radiation, corrosive chemicals, and materials operating in these areas are difficult to access for maintenance. In these acute conditions materials have to perform for a prolonged period. Thus, development of high corrosion resistant materials with prolonged integrity is considered one of the challenging area for ensuring the safety, and economical operation of commercial reprocessing plants**.**

1.4 Overview of material selection and application

Nuclear fuel reprocessing plant uses a verity of materials in different environments depending upon the circumstances prevailing, such as presence of radioactivity, corrosive chemicals, high temperature and areas where maintenance is restricted etc. Thus material selection is dictated by requirement of avoidance to radiation damage, their corrosion resistance, ability to decontaminate, availability and cost effectiveness. Hence, selection of the proper material as well as effective shielding design is most important in order to ensure adequate attenuation of the penetrating radiation. Corrosion is one of the most challenging issues, and a wide spread problem in spent nuclear fuel reprocessing plant. Corrosion problems arise at various stages of fuel reprocessing such as in dissolution of spent fuel, due to dissolver off gases, during solvent extraction, and during storage of waste generated from reprocessed spent fuel. Out of several materials used for application in spent nuclear fuel reprocessing plant, austenitic stainless steel (300 series), titanium and its variants, and zirconium are used for construction of structural components as summarized below.

1.4.1 Austenitic stainless steel

The nuclear fuel reprocessing plant uses vast quantity of austenitic stainless steel in the form of plates, tubes, forgings and other critical components. Over last three decades these materials are finding applications in plant as well as waste-storage vessels involving concentrated nitric acid. The choice is with respect to nature of process stream, hazard to radiation and corrosion resistance. The corrosion resistance of austenitic stainless steel depends on the concentration of nitric acid, for lower concentration (< 50 %) corrosion susceptibility is determined by chromium content in the alloy, and for higher concentration containing Cr^{6+} ions it is determined by impurity elements in the alloy. Mainly, AISI type 304L SS (18 % Cr-8 % Ni-0.03% C) finds large scale application because of good passivity, corrosion resistance, and appropriate practical aspects such as working, welding, cost competitiveness etc. Despite many beneficial effects, type 304L SS fails in the oxidizing environment of nitric acid leading to intergranular corrosion, end-grain attack, transpassivity etc [2]. To overcome these problems different grades of austenitic stainless steels have been evolved over time. Fe-18Cr-15Ni-4Si-0.01C austenitic stainless steel was developed to keep the intergranular and uniform corrosion low in the process environment of hot nitric acid. The addition of titanium and niobium to these alloys gives still improved property, however due to high silicon, and low carbon content these materials tend to form crack in the welded region. Similarly, special nitric acid grade (NAG) austenitic stainless steel such as URANS-16 (18 Cr-12 Ni) and URANS-65 (25 Cr-20 Ni) are designed with sharp control of carbon, silicon, sulphur and phosphorus. Because of high chromium content and tighter control of impurities, nitric acid grade stainless steel performs satisfactorily up to 65 % concentration in boiling condition. Nevertheless, these materials fail in nitric acid solution containing hexavalent chromium (Cr^{6+}) at elevated temperature due to transpassivity [3]. Thus, use of these materials in these extreme conditions is restricted. Moreover, large scale use is also not possible due to extra cost in the manufacturing process because of controlling the impurity level.

1.4.2 Titanium

Titanium is a unique material, as strong as stainless steel with less than 60 % of its density, and possessing excellent corrosion resistance. Titanium is used in critical components such as spent nuclear fuel dissolvers handling hot concentrated nitric acid where austenitic stainless steel experiences intergranular corrosion. Higher resistance of titanium to corrosion is due to the formation of titanium dioxide (TiO_2) film on the surface due to formation of Ti^{4+} ions [1]. However, the composition of oxide film depends upon the film formation conditions such as electrolyte composition, hydro-dynamic flow, and temperature etc. The oxide film formed on titanium is more protective than that of austenitic stainless steel, and often performs better in oxidizing environment of nitric acid. In boiling condition titanium corrosion resistance is very sensitive to nitric acid purity, and higher the metallic ion content in the acid, the better titanium performs. This is in contrast to austenitic stainless steel which is often adversely affected by the acid contaminants. This is because, titanium corrosion product (Ti^{4+}) is highly inhibitive, and titanium exhibits superb performance in recycled nitric acid streams such as reboiler loops. Despite many advantages, the use of titanium in spent nuclear fuel reprocessing plant is limited. One of the factors to this is the high cost relative to austenitic stainless steel. Moreover, even if titanium is having excellent corrosion resistance, it is not cure-for all corrosion problems. Failures in acid condensers and evaporators have been observed in spent nuclear fuel reprocessing plant [1]. Under these vapour and condensate conditions semi-protective oxide films forms on the surface which do not fully retard the oxidizing action of nitric acid. The presence of iron greater than 0.05 % in titanium enhances the corrosion rate due to formation, and segregation of iron rich ilmenite ($FeTiO_3$) intermetallic particles. In such situations advanced alloys such as Ti-5% Ta-1.8% Nb were recommended which is titanium alloyed with more noble metals like tantalum and niobium which have similar size to that of titanium. The oxide film formed on such alloys shows low solubility and high stability in nitric acid medium.

1.4.3 Zirconium

Zirconium is an important constructional material for spent fuel dissolver, and for many other critical applications in nuclear fuel reprocessing plant in highly oxidizing condition. The choice of zirconium is due to its high corrosion resistance as compared to titanium and austenitic stainless steel with or without the presence of oxidizing species. As compared to austenitic stainless steel, zirconium does not undergo intergranular corrosion, and compared to titanium it does not suffer from vapour and condensate phase corrosion problems in boiling nitric acid. Comparative analysis on the corrosion resistance of 20 Cr-20 Ni austenitic stainless steel, Ti, and Zr in 17-70 % nitric acid concentration in boiling condition in presence of hexavalent chromium (Cr^{6+}) showed high corrosion resistance for zirconium as compared to others [29]. The high corrosion resistance is attributed to natural formation of dense, stable and self healing zirconium oxide (ZrO_2) film on the surface which protects the material from corrosive environments [1]. Moreover, it does not form non-adherent oxide with poor corrosion resistance under condensing condition as seen in case of titanium. Recent corrosion study [30] on zirconium, and its welds showed superior corrosion resistance as compared to other candidate material like Ti, Ti-5% Ta, and Ti- 5% Ta-1.8 % Nb. No corrosion attack was observed in liquid, vapor and condensate zones of boiling 11.5 M nitric acid. Due to high corrosion resistance, inspection, and maintenance is also a less concern for zirconium.

Even though, zirconium shows outstanding corrosion resistance in nitric acid medium, certain factors require thorough investigation, such as fluoride content in the process medium and stress corrosion cracking. The presence of fluoride ions as complexing agent is detrimental to passive film stability, and increases the dissolution rate of the material even at low concentration of fluoride ion [31]. However, the effect of fluoride ion can be reduced by adding corrosion inhibitor such as zirconium sponge and zirconium nitrate to convert to non-corrosive compound. Stress corrosion cracking (SCC), can occur in Zr exposed to hot boiling nitric acid (> 70 %) [29]. Particularly, heat effected zones of zirconium welds are considered to be sensitive to SCC. However, recent study shows that zirconium has excellent corrosion resistance, and do not show susceptibility to SCC in simulated dissolver solution carried out in small-scale mock-up test even after 7 yrs [32]. However, unlike austenitic stainless steel, large scale application of zirconium is restricted to demanding conditions only, because it is seven times expensive and fabrication cost is five times more compared to conventional 304L austenitic stainless steel.

CHAPTER 2

Corrosion Issues of Austenitic Stainless steel in Nitric acid

Material, Medium & Mechanism

CHAPTER 2

Corrosion Issues of Austenitic Stainless Steel in Nitric Acid

Material, Medium & Mechanism

The chapter gives brief introduction to the austenitic stainless steel with respect to their formation using Fe-C, Fe-Cr, Fe-Cr-Ni phase diagram, microstructure, physical, mechanical, and chemical properties. Apart from this, the chapter introduces to the process environment of nuclear fuel reprocessing, and the various corrosion problems of austenitic steel in the oxidizing environment of nitric acid.

2. 1 Introduction

Economy in the production and construction of industrial plant, and equipment depends upon the existence of good processing properties as well as the cost of the materials to be used. The satisfactorily performance of the materials depends upon many features, such as selection of proper material, appropriate design, fabricability, sustainable mechanical and physical properties of the designed structure/equipment, chemical conditions of the process environment, and their maintenance aspect. However, the interplay between these chemical, mechanical and physical properties produces a wide range of requirements which must be considered in choosing the correct material for the application in question. The most important material properties required are mechanical strength and ductility, machinability, sufficient cold and hot formability, excellent weldability, and good corrosion resistance. Austenitic stainless steels [33] are widely used as constructional materials in various industries such as nuclear and other chemical processing industries, food processing industry, hydro-power generation, and for many other engineering applications. The advantages with this class of materials are (a) exceptional formability, (b) resistance to brittle cleavage at low temperature, and good mechanical strength at higher temperature, (c) higher intrinsic creep strength for lower stresses at elevated temperature (d) good resistance to uniform corrosion and oxidation behaviour, and (e) economical from overall life cycle cost [33,34]. However, austenitic steels possess low yield strength, and thus several process are used to improve the yield strength, such as thermomechanical treatments, hardening with nitrogen and precipitation hardening etc [35]. Apart from this, austenitic stainless steels are susceptible to stress corrosion cracking in the presence of aggressive ions [15]. This type of failure occurs under applied stress or as a result of residual stress in fabricated materials. Similarly, localized corrosion along the grain boundaries can be a serious problem due to chromium depletion, and formation of chromium carbide precipitates. Pitting and crevice corrosion are the other localized corrosion type which occur in the environment containing halide ions [15].

2. 2 Fe-C equilibrium diagram and austenitic stainless steel

A study of the constitution and structure of all steels starts from Fe-C equilibrium diagram. A portion of the Fe-C phase diagram is presented in Fig. 2.1 [15].

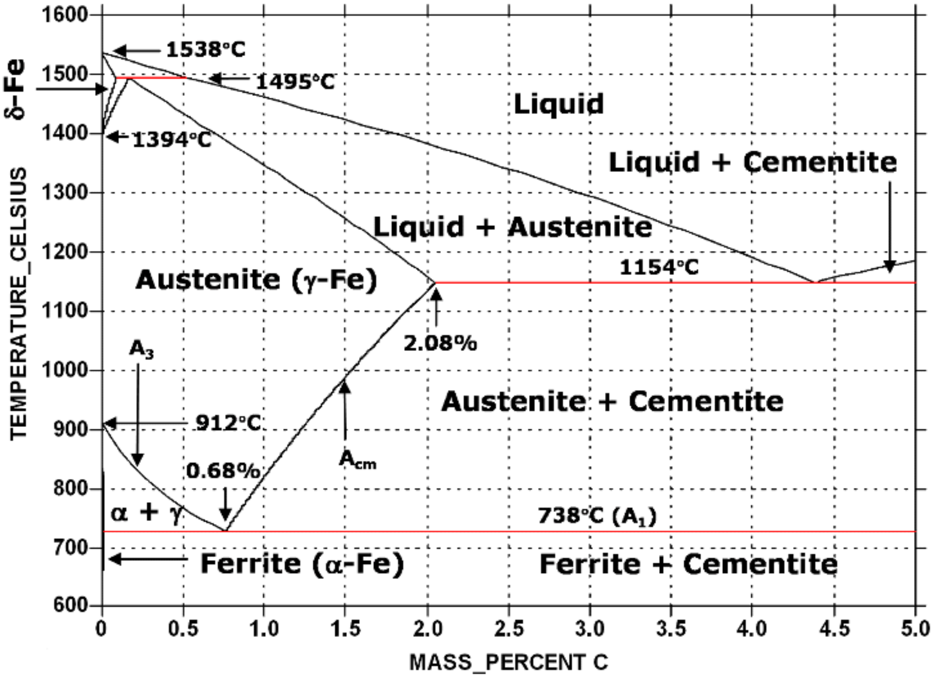

Fig. 2.1: Fe-C equilibrium phase diagram [15]

Pure iron upon heating experiences two changes in crystal structure before it melts. At room temperature the stable form is called as ferrite (α-iron) has body centred cubic (bcc) crystal structure. Ferrite experiences a polymorphic phase transformation to austenite (γ-iron) at 912 °C which has a face centred cubic (fcc) crystal structure. The austenite phase persists up to 1394 °C, and at this temperature the austenite reverts back to the bcc phase known as δ-ferrite. Carbon as an interstitial element forms solid solution with both α and δ ferrite, and also with γ-austenite as indicated by α, δ and γ phase field in Fig. 2.1. Moreover, the much larger phase field of γ-iron compared to that of α-iron reflects the greater solubility of carbon in γ-iron, with a maximum value of 2.08 wt% at 1147 °C. Austenite is characterized as non-magnetic, high ductility, rapid work hardening rates, and excellent toughness.

However, the iron-carbon equilibrium diagram as shown in Fig. 2.1 is modified by the addition of alloying elements such as chromium (Cr), Nickel (Ni), and other minor alloying elements, resulting in poly-component systems. Fig. 2.2 shows the Fe-Cr equilibrium phase diagram [15].

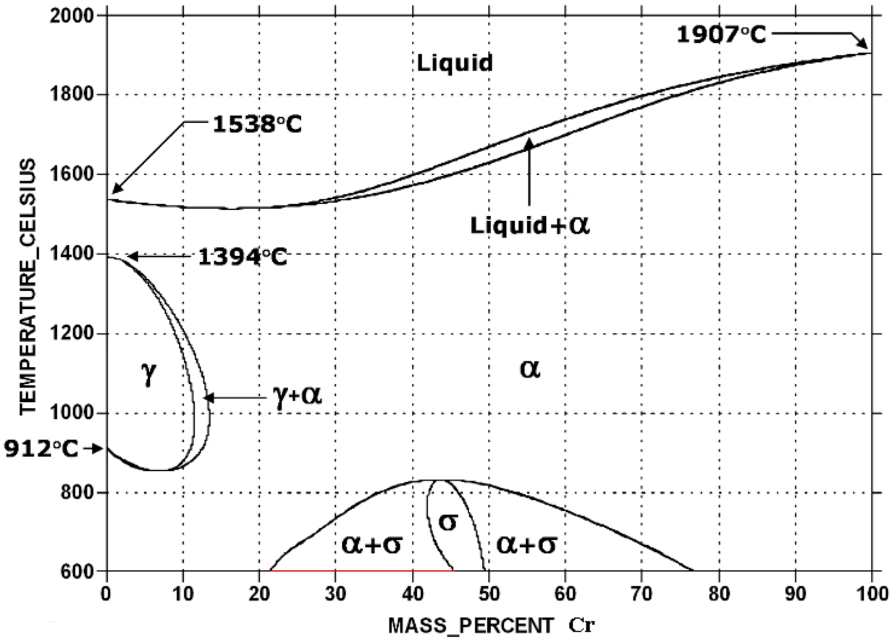

Fig. 2.2: Fe-Cr equilibrium phase diagram [15]

Chromium in excess of 12 wt % by weight is required to impart "stainless" characteristics of iron alloys. Thus, all stainless steels contain large amount of chromium from 12% to a maximum of 25 %. Chromium as major alloying element stabilizes the body-centred cubic (bcc) phase of iron, therefore with increasing chromium content the low temperature and high temperature α and δ ferrite field expands. As the ferrite field expands the austenite field contracts, and produces what is often called as the gamma (γ) loop. However, the addition of carbon to the Fe-Cr binary alloy extends the gamma loop to higher chromium content, and also widens the (alpha plus gamma) phase field, and above 0.40 wt % C, the steel can be made fully austenitic if cooled directly from the gamma loop region. Moreover, nickel with a face-centred-cubic structure favours the formation of fcc austenite solid solution, and the stability range of austenite phase expands at the expanse of bcc α-ferrite phase. The Fe-Cr-Ni ternary phase diagram is shown in Fig. 2.3 [33].

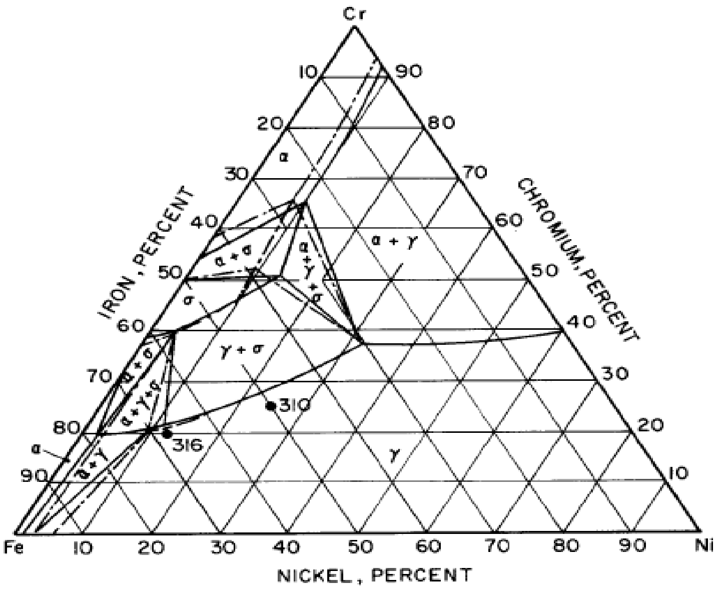

Fig. 2.3: Fe-Cr-Ni ternary phase diagram [33]

Thus, if nickel is added to a low carbon-Fe-18 wt % Cr alloy, the gamma phase field expands, and at about 8 wt % Ni, the gamma phase persist at room temperature leading to familiar group of austenitic stainless steel based upon 18 Cr-8 Ni (wt %). This particular composition arises because minimum nickel content (8 wt %) is required to retain gamma at room temperature. With both lower and higher chromium content more nickel is required for room temperature stability of austenite phase. For example with more corrosion resistance 25 wt% Cr-steels, about 15 wt % nickel is required to retain the austenite at room temperature. The family of austenitic and other stainless steel formed with addition of alloying elements starting from 18 % Cr-8 % Ni is shown in Fig. 2.4 [15].

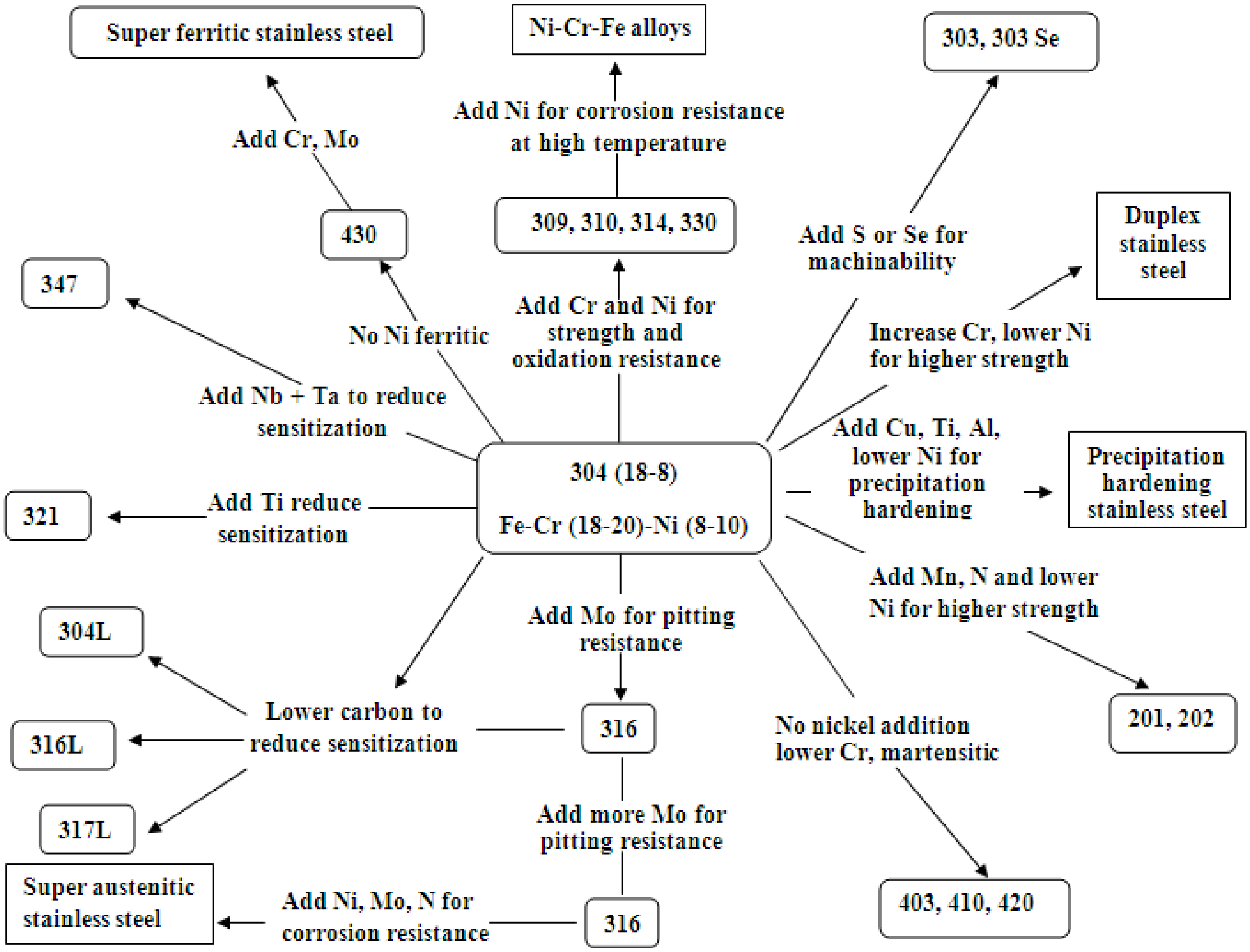

Fig. 2.4: Different type of stainless steel with addition of alloying element starting from 18-8 stainless Steel [15].

2. 3 Effect of alloying elements on the properties of austenitic stainless steel

Apart from major alloying elements such as chromium and nickel, certain minor alloying elements such as nitrogen, molybdenum, manganese etc also influences the physical, mechanical and chemical properties of austenitic stainless steel. The combined effect of the alloying elements and heat treatment procedures gives enormous varieties, microstructure and properties of different types of austenitic stainless steel (Fig. 2.4). Residual elements which are inherently present in raw materials, and entering during steel making practices also profoundly affect the properties of steel. General effects of the alloying elements commonly found in austenitic stainless steel are as summarized below [15,34,35].

2.3.1 Carbon

Carbon is one of the extremely powerful austenite stabilizers, and the solubility of carbon decreases as the temperature decreases giving chromium rich precipitates. Austenitic stainless steels in general contain carbon from 0.02 wt % to 0.15 wt %. Carbon is the key alloying element which controls maximum attainable hardness, and increasing the carbon content is the least expansive way for increasing hardness. High carbon content increases the tensile strength but decreases the ductility. Moreover, with high carbon content chromium carbide precipitates at the grain boundaries leading to depletion of chromium which increase the susceptibility to intergranular corrosion.

2.3.2 Nitrogen

Nitrogen is one of the important elements for stabilizing γ-field similar to carbon. It can expand and stabilize the austenite phase. It is used as an alloying element in austenitic stainless steel for precipitation or solid solution strengthening for increasing the yield strength. Nitrogen in solid solution makes austenitic stainless steel more wear and fatigue resistance. Apart from this, nitrogen provides beneficial effects to avoid localized corrosion.

2.3.3 Manganese

Manganese is an austenite former, a deoxidizer, and a desulfurizer. In general, it is added to austenitic stainless steel to assist in de-oxidation during melting, and to prevent iron sulphide inclusions in order to avoid hot cracking. The manganese sulphides formed increases machinability. However, it is a weak carbide former, and favorably effects forgeability and weldability. The manganese sulphide inclusion acts as precursor site of pitting.

2.3.4 Molybdenum

Molybdenum increases the hardenability of austenitic stainless steel, particularly effective in maintaining the hardenability between specified limits. It minimizes the susceptibility to temper embrittlement, and is unique in the extent to which it increases the high temperature tensile, and creep resistance of austenitic stainless steel. Apart from this, molybdenum is very effective in stabilizing the passive film in presence of aggressive ions, and increases the pitting, intergranular and crevice corrosion resistance of austenitic stainless steels.

2.3.5 Titanium

The main use of titanium as an alloying element in austenitic stainless steel is for stabilization of carbides. It combines with carbon to form titanium carbide which is quite stable, and hard to dissolve in austenite matrix. This tends to minimize the occurrence of intergranular corrosion. Moreover, carbon preferentially combines with titanium than chromium preventing depletion of chromium at the grain boundaries. Titanium also increases the hardness of austenitic stainless steel.

2. 4 Microstructural properties of austenitic stainless steel

If properly processed austenitic stainless steels are truly single phase without carbides, ferrite, and all alloying elements in solid solution. In single phase austenite the grains are equiaxed, many of which contain annealing twins.

The twins are identified as bands with parallel sides, and are formed when changes in the stalking of atoms on close-packed (1 1 1) planes occur during crystallization and grain growth. However, single phase austenite structure is an ideal structure, and steels heated into austenite phase in general contain other phases such as inclusions, carbides, and precipitates of alloying elements. Austenitic stainless steels are annealed at high temperatures to accomplish recrystallization. The microstructure of austenitic stainless steel is shown in Fig. 2.5 [36].

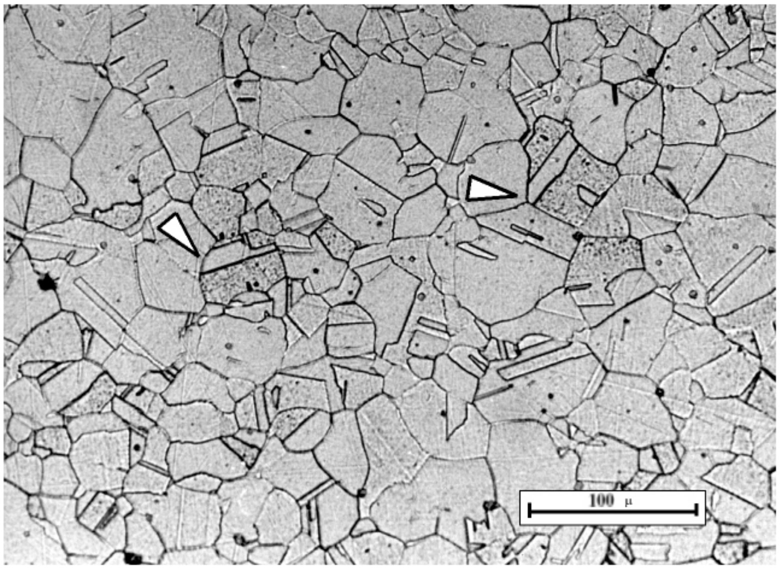

Fig. 2.5: Microstructure of austenitic stainless steel [36]

In as cast state, the microstructure is characterised by an austenite matrix with some precipitated carbide. The carbides lie along the grain boundaries, and in interdendritic areas within grains. Occasionally, interdendritic carbides can be fairly massive especially at triple points and are sometimes surrounded by lamellar carbide zones.

2. 5 Physical properties of austenitic stainless steel

The major physical properties of austenitic stainless steel considered important in regard to the functional application and successful implementation includes; (a) density, (b) modulus of elasticity, (c) melting range, (d) coefficient of thermal expansion, (e) thermal conductivity, (f) heat transfer coefficient, (g) specific heat, (h) magnetic and electrical resistivity [33,34]. The change in density for austenitic grade stainless steel is small, and generally remains in between 7.5 to 8 g/cm^3. The coefficient of thermal expansion for austenitic grades is considerably higher (17 µm/m °C), and dimensional changes in structural parts occur during heating and cooling. The thermal conductivity of austenitic grade stainless is low around one-fifth of that of iron. The ability of this class of material to remain cleanness enhances the heat transfer process. The electrical resistivity increases with increase in temperature. The magnetic permeability of austenitic stainless steel is low, and their non-magnetic nature is useful for certain application in measuring and controlling equipments.

2. 6 Mechanical properties of austenitic stainless steel

Mechanical properties of austenitic stainless steel are of major concern in order to safe guard the structural integrity of numerous components in various process industries. The mechanical properties which are of prime importance are hardness, strength, ductility, and stiffness etc. Austenitic stainless steels are in general hardened by cold work, and in highly cold work conditions, they show extra ordinary strength [33,34]. They have high ductility but the ductility decreases with increase in cold work. Austenitic stainless steels show good impact strength at low temperature, and are useful in cryogenic applications. However, at elevated temperature the impact strength decreases with temperature [33]. Austenitic stainless steel has low yield strength. Nevertheless, different methods are used to improve the yield strength such as hardening with addition of nitrogen, precipitation hardening, and appropriate thermo-mechanical treatment [35]. The addition of nitrogen is the most convenient way for improving the hardness in low carbon austenitic stainless steel. The fatigue limit of austenitic stainless steel is 40 % of the yield strength, and it increases with work hardening in proportion with tensile strength [34]. Austenitic stainless steel can best resist high temperature creep, and can be used at lower stresses, and at temperature around 1150 °C [33]. These materials can be readily welded and exhibit good toughness, however in weld metal and heat affected zones, cracking can be observed [34].

2. 7 Chemical properties of austenitic stainless steel

The major chemical properties that affect austenitic stainless steel are high temperature oxidation, and corrosion resistance. In general austenitic stainless steel has high oxidation resistance up to high temperature and other forms of high temperature corrosion [34]. Oxidation resistance of austenitic steel depends upon oxygen partial pressure, temperature, time and type of service, surrounding atmosphere, and the selection of material for specific application etc. Austenitic stainless steels are largely known for their corrosion resistance in aqueous media [17,18]. Always the material selection process for service in corrosive environment begins with type 304L SS or its variants (Fig. 2.4). The useful corrosion resistance of austenitic stainless steel is to the fact that it exhibits passivity in wide range of environments. The passive film is thin, adherent, self-healing, and tenacious having thickness around 10-100 Å. The structure-composition of this ultrathin passive film is a vast and complex subject, and depends upon the alloy composition, and also on the nature of environment they are exposed. Based on the research over the years, passivity is believed to occur due to the formation of oxide layer or a process that can be considered as adsorption of oxygen as summarized below.

2.7.1 Oxide film theory

Oxide layer formation is one of the important hypothesis to account for the cause of passivity of metals, and alloys including different types of stainless steel. The theory is usually ascribed to Micheal Farady on the study of passivation of iron in nitric acid [17]. Later on, the protective oxide film theory gained support from the studies carried out by many researchers on different material and in different environment. In the year 1934, Tronstad and Borgmann showed that some kind of film exists on 18-8 stainless steel, and assumed that it must be an oxide layer

[17]. They concluded from their study that the air formed film on 18-8 stainless steel gets strengthened when passivated in nitric acid media. According to this theory, the surface of the metal/alloy is oxidized or the atoms on the surface are in such a relation with the oxygen of the electrolyte, that it is equivalent to an oxidation process. The properties characterizing a typical oxide film are of low ionic conductivity, and low solubility. Moreover, it is assumed that such oxide layers are formed as a diffusion barrier separating metal/alloy from electrochemical environment thereby decreasing the reaction rate. Due to these properties, the oxide layer prevents a large extent transport of metal ions from sites in crystal lattice to the electrochemical environment i.e., it prevents the anodic dissolution. Nevertheless, there is slow dissolution corresponding to passive state of the materials since oxide layers directly formed in close connection with crystal structure often contains defects which allow electron conduction, and electrochemical reaction can occur at the top surface of the oxide layer.

2.7.2 Adsorption theory

The oxide film theory suffered set beck, when it was observed that, the lack of coincidence of the potential marking the active to passive state transition with the potential for the reverse transition [17]. It was thought that the lack of coincidence in passivation potential could not be explained by oxide layer theory rather by a variable layer of adsorbed oxygen on the surface either by physical or chemical adsorbtion. Later on, Uhlig [19] proposed that adsorbed oxygen film is commonly the source of passivity, and such film forms on transition metals (Fe, Cr) as well as 18-8 stainless steel in accord with their uncoupled d-electrons interacting with oxygen atoms to form stable bond. The high sublimation energy of these metal-oxygen bond favours retention of the metal atoms in their lattice in preference to their removal to form the oxide lattice as per oxide layer theory. Even less than a monolayer of adsorbed film has passivating effect, increases the anodic overvoltage and decreases the exchange current density. The characteristics of high energy of adsorption of oxygen on transition metals (Fe, Cr) mostly favours the formation chemisorbed films as compared to low-energy films formed on non-transition elements due to physical adsorption [19]. Thus, the chemisorbed film formed on the surface is thermodynamically more stable then the oxide layer formed on the surface due to oxidation according to oxide layer theory.

However, the large recognition of adsorbtion theory does not preclude the existence of oxide layer theory. It is argued that both the theories are supplementary to each other because the adsorbed film in the process of nucleation and growth gradually changes into an oxide layer. The inclusion of adsorbtion is necessary to explain the observed property of passive film, and by and large is an overlap between the oxide layer and adsorbtion theory. The evidence for the change over from adsorbed layer to oxide layer was first pointed out by Flade on the observation that passive film on iron becomes more resistance to disruption when kept for longer duration in the passive state [17]. The observation was subsequently confirmed by others and can be explained on the basis of oxide film theory by formation of a thicker oxide film with time.

2. 8 Passivity of austenitic stainless steel

The passivation property of austenitic stainless steels primarily dependent upon chromium (Cr) although iron (Fe) is the major alloying element. In addition, the contribution of austenite stabilizers such as Ni, N and Mn also strengthen the passive film property. Apart from this, molybdenum also significantly contributes to the passivity in the corrosive environments containing aggressive ions. However, it is found that passive film formed on austenitic stainless steel does not contain all the alloying elements those are added to stabilize the austenite phase [18].

The thickness, composition, and structure of passive film in austenitic stainless steel are highly dependent on the chromium content of the alloy as well as their formation potential. In austenitic stainless steels passivation occurs by the rapid adsorbtion of hydrated complex largely associated with chromium in the form of bound water which deprotonates and changes to oxide layer over time and applied potential. Surface analysis of the passivated surface showed the existence of M-H_2O (aquo), M-OH (olation), and M-O (oxo) type of bonding between chromium and oxygen in the passive film [16-19, 37]. All the above type of bonding between chromium and oxygen depends on the chromium content of the alloy and increase in chromium increases the bonding tendency [16-19, 37]. However, with increase in passivation potential, the olation (M-OH) type bonding decreases, and the oxo (M-O) type of bonding increases in proportion. The passivation potential, and the electrical field strength play an important role in deprotonation and influence the oxidation state of chromium which in turn governs the solubility of oxide layer. Iron, even though is the largest alloying element in austenitic stainless steel, is found to present in less quantity in the passive film as the Cr/Fe ratio is always higher with increasing potential irrespective of specimen preparation conditions [16-19, 37]. In general, iron is present in two oxidation states of Fe^{3+} and Fe^{2+}, the higher proportion of latter being observed on higher chromium alloys [16-19, 37].

The beneficial effect of nitrogen on the passivity of austenitic stainless steel is due to its segregation to the oxide-metal interface thereby forms the interstitial nitrides which largely hinder the anodic dissolution [38]. Apart from this, in acidic solutions nitrogen forms ammonium ions which buffers the local *p*H, and increases the repassivation tendency by forming the nitrate compounds and providing local inhibition effects. Nevertheless, nitrogen is having solubility from 0.2 to 0.7 %, and higher content affects the hot ductility of austenitic stainless steel.

Molybdenum is one of the most effective elements added to austenitic stainless steel to improve the pitting resistance. Extensive study was carried out to elucidate the role of molybdenum on the passivity of austenitic stainless steel, and several mechanisms have been proposed. It is proposed that, molybdenum forms complex with CrOOH, thereby inhibiting the transpassive dissolution [39]. According to another mechanism [40], the active sites in the passive film are rapidly blocked by molybdenum oxyhydroxide or molybdate salts, thereby inhibiting the localized corrosion.

2. 9 Corrosion mechanism of austenitic stainless steel in nitric acid

Nitric acid is a clear colorless liquid having boiling point 107 °C, melting point -42 °C and specific gravity 1.4, respectively. It is completely soluble in water, and is stable in ambient condition**.** It is highly ionized acid, and has all the properties of strong acid. Apart from being a strong acid it is a powerful oxidizing agent even in very dilute solution. The reduction mechanism of nitric acid is widely investigated due to large industrial applications, and in relation to the corrosion of stainless steel as well as disposal of radiolytic waste containing nitric acid from spent nuclear fuel reprocessing plant. Reduction mechanism of nitric acid is dependent on the concentration of nitric acid, and the auto-catalytic activity of nitrous acid produced as a result of reduction [3-7, 20-22, 41,42]. Being a strong acid, nitric acid completely ionizes to hydrogen ions (H^+), and nitrate ions (NO_3^-) as shown below.

$$HNO_3 \longleftrightarrow H^+ + NO_3^- \qquad (1)$$

In the ionized state NO_3^- ions are more oxidizing as compared to that of H^+ ions. Thus, in most acidic media nitrate ions get reduced to the nitrous acid as given below.

$$NO_3^- + 3\,H^+ + 2e^- \longleftrightarrow (HNO_2)_{aq} + H_2O \qquad (2)$$

Nitrous acid produced maintains the auto-catalytic activity by a heterogeneous electron transfer reaction followed by a chemical reaction leading to its regeneration as presented below.

$$(HNO_2)_{aq} + H^+ + e^- \longleftrightarrow (NO)_g + H_2O \qquad (3)$$

$$HNO_3 + (NO)_g \longleftrightarrow (HNO_2)_{aq} + (NO_2)_g \qquad (4)$$

In the overall reduction process the nature of the product formed depends upon the concentration of nitric acid. Thermodynamic study for the equilibrium between gaseous and liquid phase has shown the predominant existence of aqueous nitrous acid (HNO_2) species and gaseous species such as nitric oxide (NO) and nitrous oxide (N_2O), respectively. The final reduction product is nitric oxide (NO) for the concentration low to moderate i.e. 8 M/litre and nitrous oxide (N_2O) for the concentration above 8 M/litre. The schematic of reduction of nitric acid is shown in Fig. 2.6 [42].

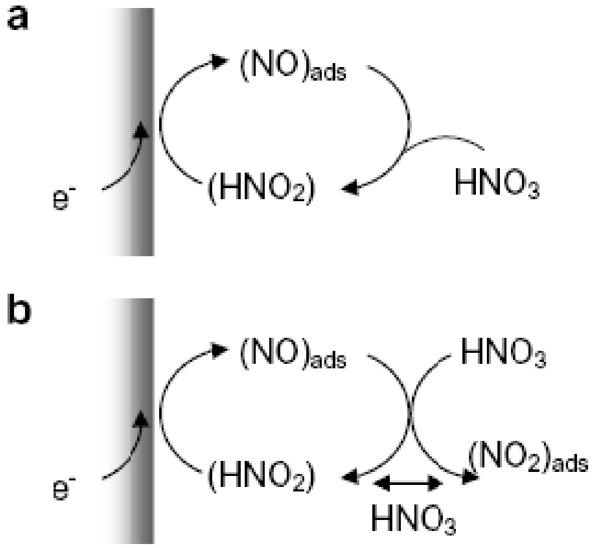

Fig. 2.6: Schematic of reduction mechanism of nitric acid; (a) low to moderate concentration (< 8 M/Litre) (b) high concentration (>8 M/Litre) [42].

2. 10 Corrosion issues of austenitic stainless steel in nitric acid

The choice of materials for nitric acid service is quite complicated and limited due to unexpected corrosion problems limiting their life. For industrial applications, the choice is between austenitic stainless steel and high silicon-iron alloys. Again the choice is limited for high silicon-iron alloys, as it is available only in cast form, and have poor mechanical property. Thus, austenitic stainless steels are by and large the material of choice, and are compatible with nitric acid in boiling condition up to 50 % concentration. The good corrosion resistance of austenitic stainless steel in nitric acid is due to their inherent tendency to form thin, adherent, and self-healing chromium oxide film on the surface [34]. Even though, austenitic stainless steels are having good passivation property and corrosion resistance in nitric acid environment, they are not without problems and failures. In fact, these alloys are not immune to corrosion attack, and different types of corrosion may occur in the reprocessing environment of nitric acid [1-7, 42-46]. In general, the corrosion resistance decreases with increase in concentration and temperature, and high corrosion rate at elevated temperature has been realized in actual plant condition. It has also been observed that in more sever condition such as 65 % concentration in boiling condition, these material fail severely leading to grain loss [1,42]. The type of corrosion attack in austenitic stainless steels in nitric acid medium depends upon the chromium content of the alloy, presence of other minor alloying elements, metallurgical condition, fabrication process, and the electrochemical environment. Major problems associated with these materials in nitric acid are (a) intergranular corrosion, (b) end-grain attack, (c) transpassive corrosion, (d) pitting corrosion, and (e) crevice corrosion as summarized below. The occurrence of these problems act as life-limiting factor of the structural components, and have direct effect on the performance of the plant.

2.10.1 Intergranular corrosion

Austenitic stainless steel, although protected by a passive layer rich in chromium oxide can suffer from intergranular corrosion due to selective attack at the grain boundaries. The localized attack on the grain boundaries in corrosive media results in loss of strength and ductility. The usual form of intergranular corrosion occurs due to sensitization i.e. depletion of chromium and formation of chromium carbide precipitate adjacent to grain boundary. This happens when austenitic stainless steel is heated in the temperature range from 450 °C to 800 °C. The alloy becomes sensitized and susceptible to intergranular corrosion. Apart from this, intergranular corrosion can occur in non-sensitized austenitic stainless steel as a result of segregation of certain impurity elements to grain boundaries. However, this is known to occur in highly oxidizing solutions containing metallic ions (Cr^{6+}, V^{5+}, Ce^{4+}, Fe^{3+}) and is an unusual form of intergranular corrosion.

According to accepted mechanism, in sensitized alloys intergranular corrosion occurs due to the depletion of chromium at the grain boundaries, and formation chromium rich carbide precipitates ($Cr_{23}C_6$), if the carbon concentration is 0.03 % or higher. The degree of sensitization depends on the chromium and carbon content of the alloy and in generally increases with increase in carbon content and decrease in chromium content. Chromium from the solid solution is utilized for Cr-rich $Cr_{23}C_6$ formation resulting in lower chromium content adjacent to such carbides along the grain boundaries. Such chromium depleted regions are venerable to corrosive attack, because it does not contain sufficient chromium to form passive film. The intergranular corrosion of austenitic stainless steel due to depletion of chromium is shown in Fig. 2.7 [2].

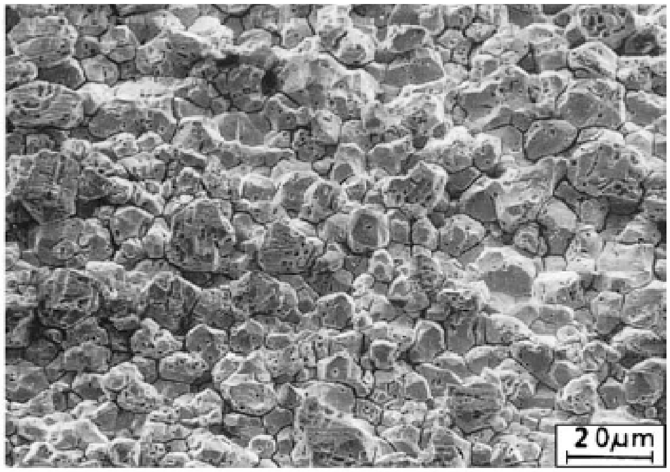

Fig. 2.7: Intergranular corrosion of austenitic stainless steel in nitric acid [2].

Nonsensitized austenitic stainless steels also undergo intergranular corrosion in highly corrosive solutions containing metallic ions in their higher valance state. This happens when austenitic stainless steels are used in the transpassive region. The effect of minor alloying elements such as sulphur, silicon, and phosphorus have deleterious effect on such type of corrosion due to their segregation to the grain boundaries. The mechanism of attack is not understood fully, however it is suggested that dissolution of weak passive film formed at the grain boundaries causes the intergranular corrosion [15]. Increase in phosphorus content results in progressive increase in intergranular corrosion. The effect of silicon is more complex, and no intergranular corrosion attack is observed in low (< 0.1 %) and high (> 2 %) silicon levels. Maximum rate of attack occurs at approximately 0.7 % silicon.

2.10.2 End-grain attack

This is an unusual form of localized corrosion in austenitic stainless steel that occurs in nuclear fuel reprocessing plant as well as other chemical processing plant handling concentrated nitric acid. End-grain attack otherwise known as tunnel corrosion occurs along the cross section normal to the rolling direction, and is considered to have significant effect on the corrosion resistance of austenitic stainless steel in highly oxidizing nitric acid solution. The schematic of end-grain attack is shown in Fig. 2.8a and a typical example of end-grain attack in 18 Cr-10 Ni austenitic stainless steel in simulated dissolver solution containing highly oxidizing nitric acid is shown in Fig. 2.8b [43].

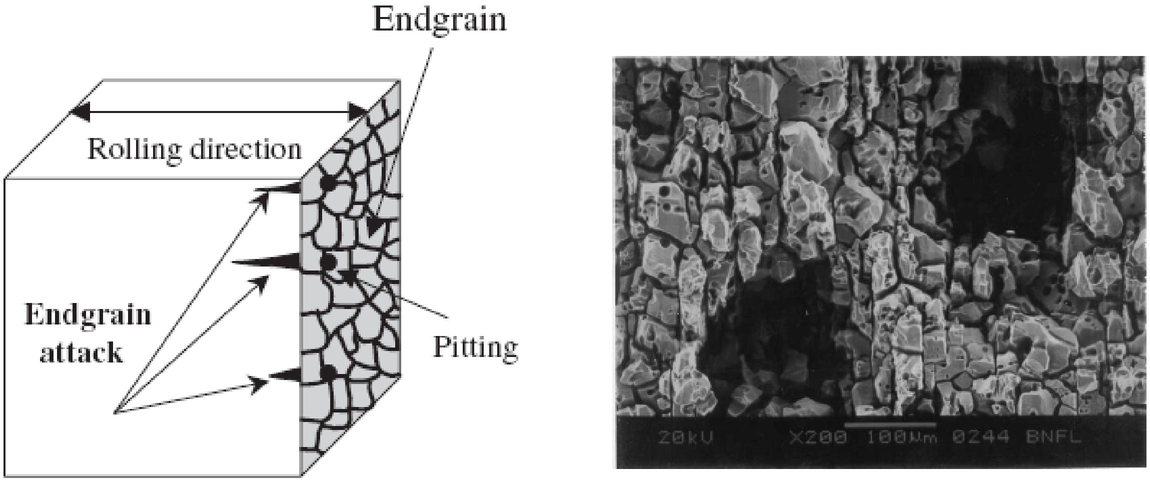

Fig. 2.8 (a)

Fig. 2.8 (b)

Fig. 2.8: (a) Schematic of end-grain (b) a typical end-grain attack in austenitic stainless steel [43].

The end-grains (Fig. 2.8a) i.e. exposed grains normal to the rolling direction in austenitic stainless steel shows inferior corrosion resistance in nitric acid solution as compared to other grains. The general corrosion rate of austenitic stainless steel in nitric acid depends up on the exposed part of the surface follows the order top surface < side << end. The end-grain corrosion often ends in preferential localized corrosion similar to pitting corrosion in aggressive medium. Moreover, end-grain corrosion is considered to be enhanced by the presence of non-metallic inclusions. Austenitic stainless steel plates which are usually manufactured by continuous casting, non-metallic constituents such as silicon and phosphorous tend to gather towards the core of the ingot, and are then drawn out along the hot working direction forming segregated bands. These segregated bands of non-metallic constituents accelerate the dissolution rate forming deep tunnel like structures. For stabilized grades of austenitic stainless steel, the dissolution of NbC precipitates and MnS inclusions oriented in the rolling direction contribute significantly to enhanced end grain corrosion. Hence, segregation of the non-metallic elements is the most causative factor for end-grain corrosion. End-grain corrosion also occurs in forgings, where the effect can be particularly sever and observed penetration of the end-grain pits are 5-10 times higher than the intergranular corrosion.

2.10.3 Transpassivity

Transpassivity in restricted sense is defined as the dissolution of metal/alloy by oxidation of an insoluble passive film to a soluble substance. Phenomenon wise it is defined as metal dissolution resulting from anodic polarization to potentials nobler to that of passive region where continuous increase in current with increasing potential is observed. However, transpassive metal dissolution, and oxygen evolution can occur simultaneously leading to increase the current density. Thus, in general transpassivity is said to be attained with increase in current density prior to or before the onset of oxygen evolution. The nature and mechanism of transpassive dissolution is intimately related to the stability of the protective passive film on the material, electrochemical environment, presence of other oxidizing and reducing species, and rate of cathodic and anodic process. Austenitic stainless steels, even though are protected by passive film on the surface, undergo transpassive corrosion when their corrosion potential shifted to the transpassive domain in some particular nitric acid media especially in presence of hexavalent chromium ion (Cr^{6+}). The characteristic feature of transpassive dissolution is mainly intergranular corrosion with opening up of grain boundaries and observed intergranular ditches [1-7]. The schematic of transpasive corrosion of austenitic stainless steel in nitric acid medium containing hexavalent chromium ion is shown in Fig. 2.9 [45].

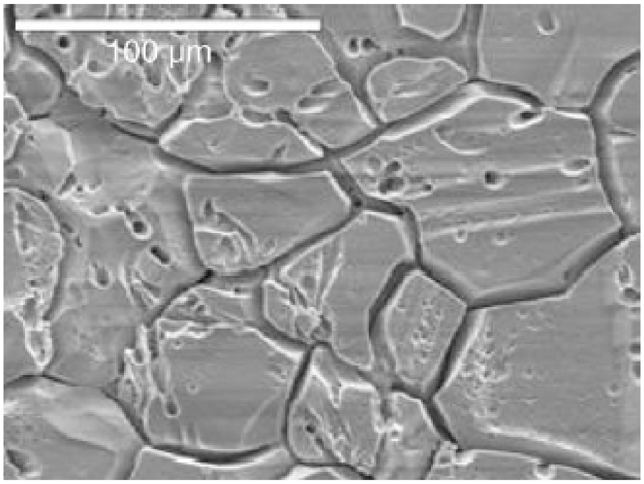

Fig. 2.9: Transpassive dissolution of austenitic stainless steel in nitric acid [45].

If the conditions are sufficiently reducing austenitic stainless steel under goes uniform dissolution in the active state. If the medium is moderately oxidizing, austenitic stainless steel are in the passive state. In passive state also austenitic stainless steels are characterized by uniform passive film but with low surface dissolution. If the medium becomes excessively oxidizing, the dissolution of passive film initiates specially with oxidation of insoluble Cr_2O_3 to soluble $Cr_2O_7^-$. The dissolution of passive film results in accelerated transpassive dissolution of oxide covered material. In the more sever oxidizing medium, grain losses occur, and successive rows of material gets lost. Metallic ions such as Cr^{6+}, $V_2O_5^{2-}$ present in nitric acid solution in general greatly increases the transpassive corrosion of austenite stainless steel.

2.10.4 Pitting corrosion

Pitting corrosion is one of the localized corrosion where small area on the surface corrodes preferentially leading to formation of cavities or holes leaving the bulk surface unattacked. In general austenitic stainless steel undergoes pitting corrosion, and passivation property decreases when nitric acid is contaminated with halide ions [47,48].

Pitting corrosion is one of the major concerns for austenitic grade stainless steels used in spent nuclear fuel reprocessing plant as these plants are mostly located in the saline atmosphere of coastal region. The combined action of both powerful oxidizing (HNO_3) and de-passivating (Cl^-) agents on the corrosion properties of austenitic stainless steel depends upon the alloy composition, solution composition and *p*H of the solution.

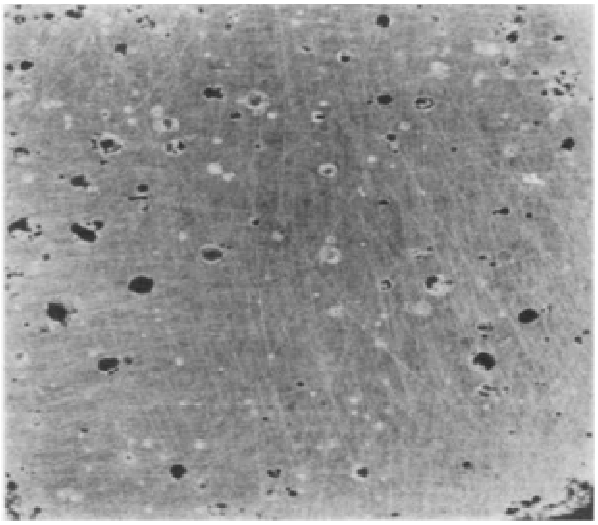

Fig. 2.10: Pitting corrosion austenitic stainless steel in nitric acid medium containing chloride ions [48].

The general effect of the chloride ions is that they inhibit the cathodic reaction by adsorption on the passivated surface resulting in the easy breakdown of passive film. Apart from this the surface dissolution in the combined action of nitric acid and chloride ions is auto-catalytic in nature because the dissolved ions also act as oxidizing agent, and increase the dissolution rate. Alloying composition and solution composition play greater role on the susceptibility of austenitic stainless steel to pitting corrosion. Alloying elements such as Cr, Mo, N, etc increase the passive film breakdown potential, and C, S, P reduce the breakdown potential [15,34]. Solution composition also has effect on the pitting susceptibility of austenitic stainless steel, and the inhibiting action to pitting corrosion decreases in the order, $OH^- > NO_3^- >$ acetate $> SO_4^{2-} > ClO_4^-$. In acidic range of *p*H, the pitting potential remains unaffected, in alkaline region the pitting potential shifts in noble direction. The induction time for pitting depends upon the chloride concentration, and in general decreases with increase in chloride concentration.

2.10.5 Stress corrosion cracking

Austenitic stainless steel in general possess inferior stress corrosion cracking resistance. The contributing factors for the stress corrosion cracking of austenitic stainless steel are presence of aggressive media, temperature, hydrogen ion concentration, and residual, applied or thermal stress. Nitric acid is a strong oxidizing agent, and generates hydrogen as a result of ionisation. The generated hydrogens at the alloy/solution interface in combination with residual or thermal stress in the material can cause hydrogen-embrittlement initiating stress corrosion cracking [15,48]. Moreover, the liberated atomic hydrogens are readily absorbed by non-metallic inclusions or at grain boundaries producing high pressure area within the matrix. The adsorbtion of hydrogen in the intermetallic inclusions leads to formation of metal hydrides which are known to be brittle. In the transition states such as active to passive, and passive to transpassive the susceptibility to stress corrosion cracking is generally higher [34]. These transition regions provide active surface which is necessary for passive film rupture to initiate the stress corrosion cracking. Apart from this, solute (phosphorus, silicon) segregation brings compositional changes in the grain boundary region as compared to the matrix which provides active anodic areas for stress corrosion cracking.

2.10.6 Crevice corrosion

This type of corrosion occurs in crevices, gasket, and in lap joints of the fabricated material and equipments. In general, systems that show pitting behaviour are susceptible to crevice corrosion [36]. However, the reverse is not true always. Austenitic stainless steel does suffer from crevice corrosion in nitric acid medium containing aggressive ions. Crevice corrosion indeed has been observed in nuclear fuel reprocessing plant behind weld backing strip at the closing seam of 304L SS vessels handling hot concentrated nitric acid [15]. Corrosion by stagnant acid in the crevices creates hexavalent chromium ions (Cr^{6+}) which causes accelerated attack while other exposed surfaces remains unaffected.

2. 11 Need for present study

Based upon the literature survey it is found that even though the mechanism of different forms of corrosion of austenitic stainless steel in nitric acid medium has been investigated, the passive film initiation, formation and dissolution has not been addressed to date either in ex-situ or in-situ condition combining electrochemical mechanism and surface morphology. Thus, in the present thesis major emphasis has been given to understand the important aspects of passive film such as nucleation, agglomeration, formation, dissolution, morphology and composition of the passive film of AISI 304L SS in nitric acid medium in both ex-situ and in-situ condition using electrochemical polarization and atomic force microscope. Similarly, the effect of surface modification either by sub-surface or top-surface for understanding the corrosion resistance and protection efficiency in nitric acid environment is not significantly investigated. Hence, an attempt has been made to investigate the effects of sub-surface modification by nitrogen ion implantation and top surface modification using protective coating (Ti, TiO_2 and duplex Ti-TiO_2) on the corrosion resistance of AISI 304L SS in nitric acid medium.

CHAPTER 3

Experimental Details

CHAPTER 3

Experimental Details

The chapter introduces to the various experimental techniques used for the investigation. This comprises material of investigation, electrochemical medium and experimental techniques such as surface modification techniques, surface morphological techniques, surface analytical techniques and electrochemical techniques that have been used in the present study.

3.1 Experimental details

3.1.1 Material and electrochemical environment

3.1.1.1 Introduction to material of investigation

The material chosen for the present investigation was AISI (American Institute of Steel Institute) type 304L stainless steel. The chemical composition (wt %) of AISI 304L SS is as given in Table. 3.1. The alloy investigated was used for the construction of a demonstration spent nuclear fuel reprocessing plant. To get a uniform metallurgical microstructure the as received alloy was given solution annealing heat treatment at 1050 °C for 30 minutes.

Element	Cr	Ni	Mn	Si	S	P	C	N	Fe
Content (wt%)	19.00	9.37	1.63	0.52	0.027	0.025	0.017	0.02	Balance

Table.3.1: Chemical composition of AISI 304L stainless steel (wt %).

3.1.1.2 Specimen preparation

The size of the specimen prepared for the whole investigation varies depending upon the suitability and requirement of the particular experimental technique. Mostly, the specimens are either of square type of size 1 cm × 1cm × 1.5 cm or of circular of size of 12 mm diameter. Specimens of the aforementioned size were cut from the sheet or rod, mechanically grinded using emery paper (SiC) up to 1200 grade, and then finely polished in 0.25 μ diamond paste. All the specimens are cleaned with acetone, and then ultrasonically in double distilled water prior to any surface modification or electrochemical investigations.

3.1.1.3 Solution preparation

The test solution for corrosion study was nitric acid. The solution used for different type of electrochemical corrosion investigation varies from dilute to concentrated medium depending upon the requirement of the test, and the equipment used for the investigation. The nitric acid solutions were prepared from Ranbaxy make analytical grade chemical reagent of specific gravity 1.41, and maximum permissible impurity was around 0.00005 %.

3.1.2 Surface modification techniques

3.1.2.1 Ion implantation

Ion implantation using accelerator is one of the important surface modification techniques in the field of corrosion science for different type of engineering materials. It has been found that by doping metallic surfaces with suitable elements by ion implantation technique the rate of anodic reaction is lowered significantly [49,50]. Due to this, the technique is fast developing as a research tool in the corrosion study of conventional and non-conventional alloys. Ions of almost any atom species can be implanted, but nitrogen is generally implanted to improve corrosion resistance, and tribological properties of austenitic stainless steel, and is already commercialized in an expanding scale. The large scale use of nitrogen is because, (1) it stabilizes the austenite phase, (2) enhances passivation property in aggressive solutions, (3) provides beneficial effects from intergranular and pitting corrosion, (4) increases hardness, friction coefficient, load bearing capacity and wear behaviour, and (5) improves fatigue resistance and cavitation corrosion behaviour [38, 51-54].

Ion implantation is generally carried out by accelerators consisting of an *ion source* where ions of the desired element are produced, an *accelerator* where the ions are accelerated to high energy, and a *target* chamber where the ions impinge on the target which is the material to be implanted. A schematic of ion implantation process is shown in Fig. 3.1 [55].

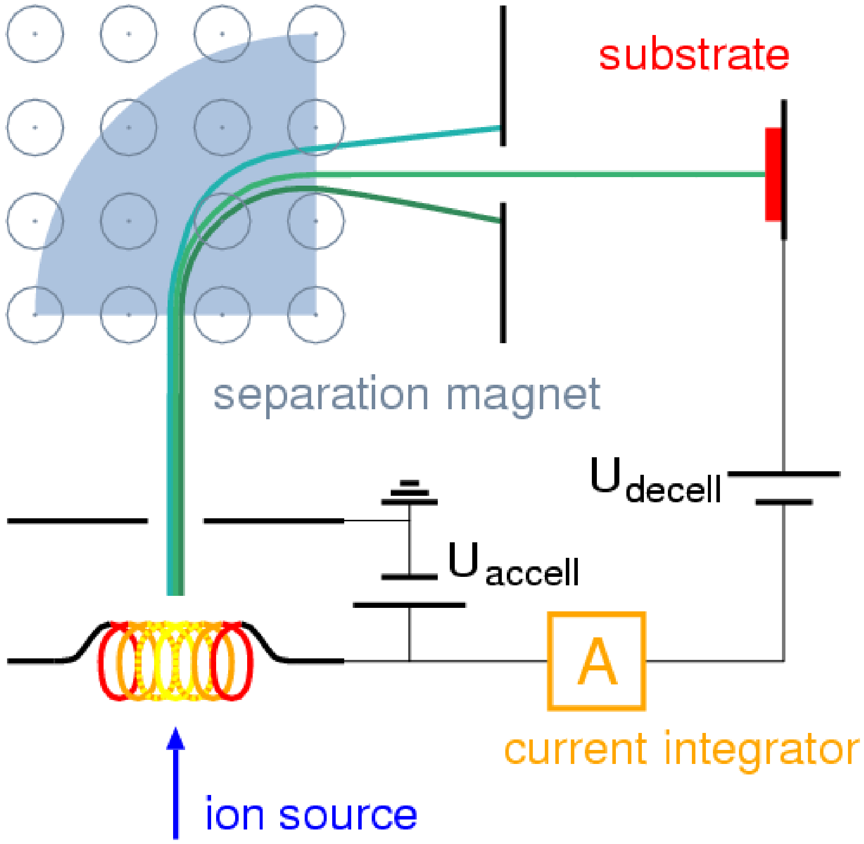

Fig. 3.1: Schematic of ion implantation using accelerator [55].

Ion sources are the most important component of ion implantation equipment, and almost all the sources (hallow cathode ion source, penning discharge ion source etc) [56] produce ions by means of confined electrical discharge which is sustained by gas or vapour of the material to be ionized. However, differences arise in the method of ionization, and in the formation of gas phase of the required species. The plasma from the ion source has a positive charge, and is extracted by accelerating them from the source by applying a negative potential. The ion generation and extraction system affects significantly the final beam qualities, thus careful selection of the process parameters are required. The generated ions are mass analyzed according to their e/m ratio, for allowing the single species in a defined charge state for the implantation purpose. The mass analyzer magnet is positioned along the beam path between the source and the process chamber. As the ions travel through the analyzer, magnetic field moves the ions in a circular path and the ions of mass to charge ratio that have equal centrifugal and centripetal force pass through the chamber. The magnetostatic field does not change the kinetic energy of the ions, but only changes the direction. The dose control system for an ion implantation system mounts the specimen, and also moves in a radial direction relative to an ion beam. The control system senses the beam current by a Faraday cup. This current is integrated using Eq. (1) over time of implantation to obtain the flux of charge (ions/cm^2) required for the desired ion dosage [57].

$$\Phi = \frac{1}{qA}\int_0^t I\, dt \qquad (1)$$

Where, Φ is the flux of charge for the required ion dose, q is charge on the ion, A is the area of the ion beam, I is the beam current, and t is the time required for implantation.

As the ions travel inside the target it undergoes series of collisions with host atoms until it finally stops at some depth known as projected range (R_p). The energy loss is due to elastic collision of the positive ions with the nuclei of the target material, and inelastic collision with the electron cloud of the target atoms. Thus, the total stopping power (S) of the target material is defined as the energy loss per unit path length travelled by the ion as represented in Eq. (2) [57].

$$S = \left(\frac{dE}{dx}\right)_{nuclear} + \left(\frac{dE}{dx}\right)_{electronic} \tag{2}$$

$$= \quad S_n + S_e \tag{3}$$

Where S_n and S_e are the energy loss due to nuclear and electronic stopping power. From the stopping power (S) the projected range (R_p) of the ions with initial energy E_0 inside the target can be estimated using Eq. (4) [57].

$$R_p = \int_{E_0}^{0} \frac{dE}{S_n + S_e} \tag{4}$$

In the present investigation, to study the effect of sub-surface modification on the corrosion resistance of 304L SS, nitrogen ion implantation was carried out at 70 keV energy by 150 keV accelerator at room temperature using 99.999 % high purity nitrogen on 12 mm diameter specimens of 304L SS. The doses given were in the range of 1×10^{15}, 1×10^{16}, 1×10^{17} and 2.5×10^{17} N^+/cm^2, respectively (Eq. 1). The vacuum in the target side during implantation was maintained at 1×10^{-5} Pa. The projected range of the ions in 304L SS was calculated using Monte-Carlo simulation code Transport of Ions in Matters (TRIM) [57]. TRIM is based upon binary ion-atom collision approximation assuming moving atom as ion and the target atom as atoms for calculating the range distribution of ions inside the target. The Monte-Carlo simulation as applied in TRIM has number of advantages over analytic formulation. It allows rigorous treatment of elastic scattering, explicit consideration of surface and interfaces leading to easy determination of projected range and distribution of particles.

3.1.2.2 Magnetron sputtering

Magnetron sputtering is a high vacuum coating process for depositing metals, alloys and ceramic coatings. Developed in 1970's, magnetron sputtering is finding increasing application in various industrial applications because of, (a) its simplicity and reliability, (b) capability for operating in different physical conditions, (3) sputtering sources can be designed up to industrial scale, and (4) as an alternative to meet the functional and economical industrial requirements compared to the traditional process. Moreover, the process limitations in conventional sputtering process, such as low deposition rate, low ionisation efficiency in plasma, and substrate heating effect is not encountered in magnetron sputtering. Today, magnetron sputtering technology is largely used in different applications such as (a) decorative coating on items in everyday life such as jewellery and glasses (b) in semi-conductor industries for application in Si integrated circuits, and (c) to improve the surface properties of base material particularly wear, load bearing and corrosion resistance etc [58-60]. The driving force for the fast development of magnetron sputtering technology is due to the requirement of advanced thin films with prescribed physical and functional properties in many diverse technological applications.

The basic sputtering process has been known for many years. In the basic sputtering process, a target (cathode) is bombarded by energetic ions generated in a glow discharge plasma situated in front of the plasma. The bombardment process causes the removal i.e. sputtering of the target atoms, which may then condense as a thin film on the substrate. However, secondary electrons are also generated from the target surface as a result of ion bombardment and these electrons do not significantly contribute in maintaining the plasma and cause unnecessary heating of the substrate.

Magnetrons make use of the fact that a magnetic field configured parallel to the target surface can constrain secondary electron motion to the vicinity of the target [61,62]. The schematic of magnetron sputtering is shown in Fig. 3.2 [62]. The magnets are arranged in such a way that one pole is placed at the central axis of the target and the second pole is formed by a ring of magnets arranged around the outer edge of the target.

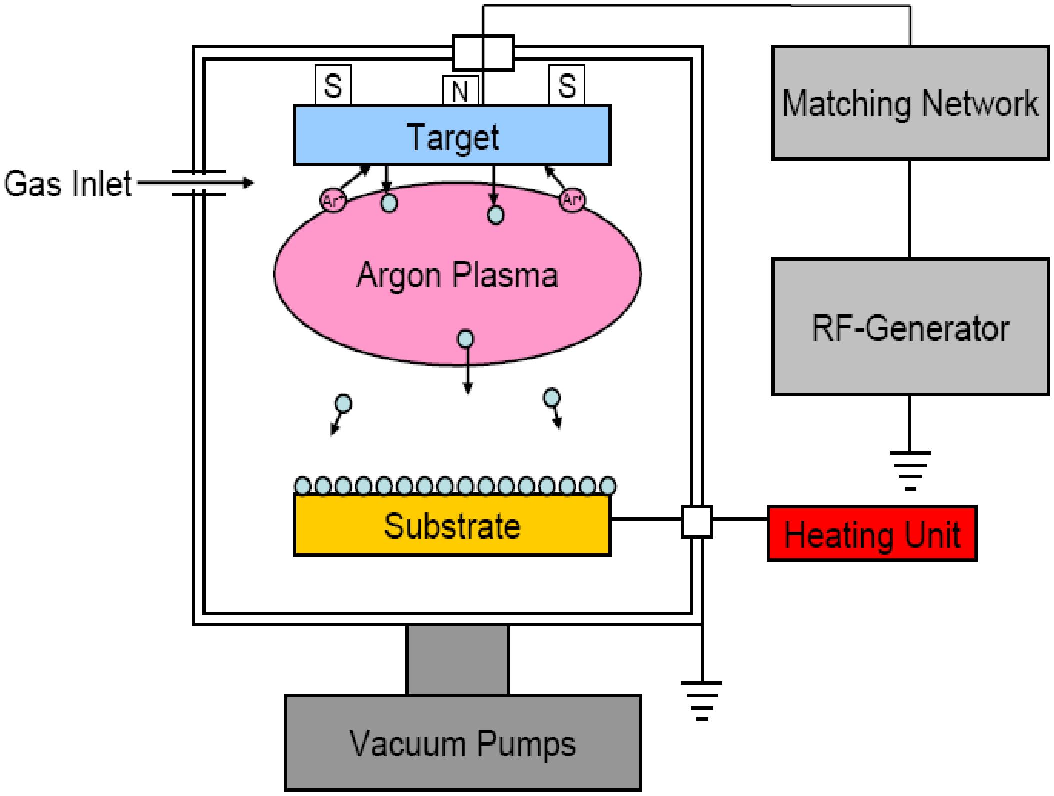

Fig. 3.2: Schematic of magnetron sputtering [62].

Trapping the electron in this way substantially increases the probability of an ionising electron-target atom collision. This in turn, leads to increased ion bombardment of the target giving higher sputtering rates and therefore higher deposition rate at the substrate. The increased deposition rate results in denser films at the substrate. Nevertheless, magnetron sputtering faces many challenges such as poisoning effect of the sputtering target due to formation of compounds on the surface. One more disadvantage of magnetron sputtering configuration is that plasma is confined near the target and is not available to activate the reactive gas near the substrate. This disadvantage can be overcome by an unbalanced magnetron configuration, where some electron can escape from the target region towards substrate [63]. However, despite these drawbacks, it is one of the widely used physical vapour deposition (PVD) techniques for thin film deposition, and researchers are striving to overcome the shortcomings to bring the technology for wider industrial application.

In the present investigation magnetron sputtering was used to deposit thin films of titanium (Ti), titanium dioxide (TiO_2) and duplex Ti-TiO_2 coating on 304L SS to investigate the effect of top-surface coating on the passive film stability and corrosion resistance in 1 M and 8 M nitric acid medium compared to uncoated specimens. The coatings were deposited by RF magnetron sputtering (Excel Instruments, India) in a custom designed 12 inch diameter chamber. Titanium (Ti) coating was deposited over 304L SS (1 cm×1 cm×1.5 cm) by sputtering titanium with 99.99 % purity at temperature of 400 °C and pressure 1×10^{-1} Pa after pre-sputtering for 10 min. Titanium dioxide (TiO_2) coating was deposited on the polished specimens of 304L SS by reactive magnetron sputtering of titanium of 99.99 % purity using Ar^+ and adding oxygen in the ratio of 80 sccm and 20 sccm, respectively. Prior to introduction of sputtering gas, the base pressure was 5×10^{-4} Pa, and then pre-sputtering was performed for 10 min at pressure of 1×10^{-1} Pa to remove the carbon contamination and hydrated layers present on the surface of target. The magnetron power used was 100 W and bias voltage applied to the target was 200 V. The distance between substrate and target was 10 cm and the substrate temperature was maintained around 200 °C during deposition. Thickness of Ti and TiO_2 coating was maintained at 1 μ, respectively. Similarly, duplex Ti-TiO_2 coated specimens were prepared by first depositing Ti followed by TiO_2 as explained above. The thickness of the Ti interlayer was maintained at 100 nm and the total thickness of the duplex Ti-TiO_2 coating was 1.2 μ.

3.1.3 Morphological study

3.1.3.1 Optical microscopy

Optical microscope is the oldest and most common instrument for characterization of materials. Over the past decade enormous growth in the application of optical microscope has been witnessed in wide variety of material characterization from micron to sub-micron level. Moreover, with continued development of specialized techniques such as new light source, electronic detection system, video enhancement, advancement in chemical markers for visualizing biological structures has led to many advanced optical microscopes. Nevertheless, despite recent developments conventional optical microscopy still maintains its position as the easiest, fastest, and most widely used method of micro-characterization. The schematic of an optical microscope consisting of (a) illuminating source, (b) condenser lens, (c) stage to support specimen, and (d) objective lens are shown in Fig. 3.3 [64].

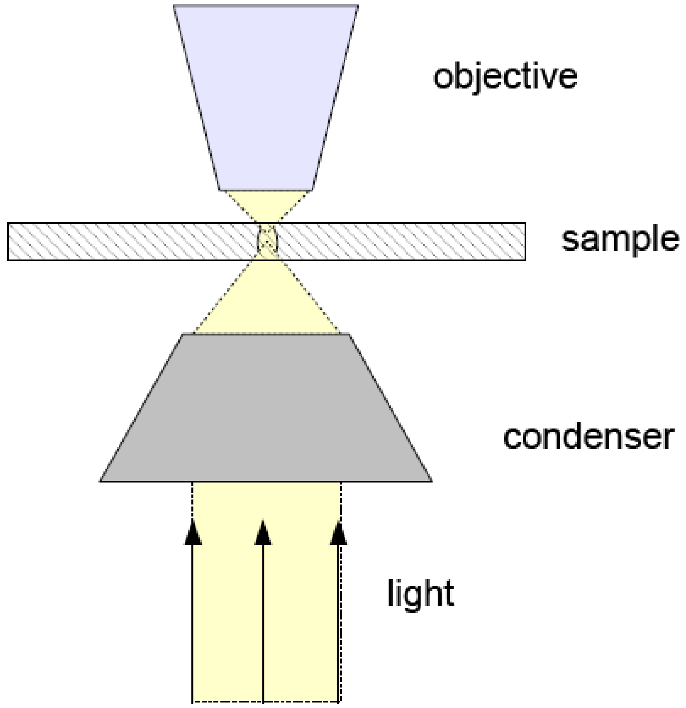

Fig. 3.3: Schematic of an optical microscope [64].

In the present investigation, optical microscope was used to investigate the microstructure of unimplanted, and nitrogen ion implanted 304L SS. The as polished samples and the nitrogen implanted samples were examined by optical microscope (Leica BFC280) after etching with three different etchants i.e. by (a) Oxalic acid, (b) Murakami's reagent (10 g KOH + 10 g of $K_4[Fe(CN)_6]$ + 100 ml H_2O), and (c) Vilella's reagent (2 g of $C_6H_3N_3O_7$ (picric acid) + 5 ml of HCl + 95 ml of CH_3OH).

3.1.3.2 Atomic force microscopy

Atomic Force Microscope (AFM) is one of the important equipment in the field of material science for surface investigation from micron to nano-meter range in ultrahigh vacuum, ambient condition and liquid environment. The advantage of this microscope is that it is capable for studying all types of surfaces such as conducting, semi-conducting and insulating of materials. Major applications of atomic force microscope includes, (a) polymer crystallization studies, (b) physical property measurement of thin films (c) failure analysis of integrated circuits, (d) presence of phases in metals and alloys, (e) study of morphology of oxide films present on the surface, (f) topographical variation due to process of corrosion, and (g) microscopic imaging of biological specimens [65-69].

Atomic force microscope scans the surface in rastering pattern with the help of a probe to obtain the information about the surface [70]. The schematic of an atomic force microscope is shown in Fig. 2.4 [71]. It consists of (a) probe, (b) scanner (c) detection system, and (d) feedback loop. The probe consists of a sharp tip made up of Si or Si_3N_4 at the end of a cantilever which scans the surface. The scanner which is made up piezo-ceramic elements and moves the tip in X, Y and Z directions. The three dimensional movement of the tip is detected by the deflection of the laser from the cantilever by photodiode. The feedback loop helps in detecting the force of interaction between the tip and sample, and alters the tip-sample distance.

The basic modes of operation of AFM are; (a) contact mode, (b) semi-contact mode, and (c) non-contact mode, respectively. In contact mode, tip scans the sample in close contact with the surface, and is the most common mode of operation. In semi-contact mode, the tip oscillates near the surface, and the reduction in amplitude of oscillation of cantilever is used to identify the surface topography. In non-contact mode, tip measures the surface topography by sensing the van der Walls force between tip and sample.

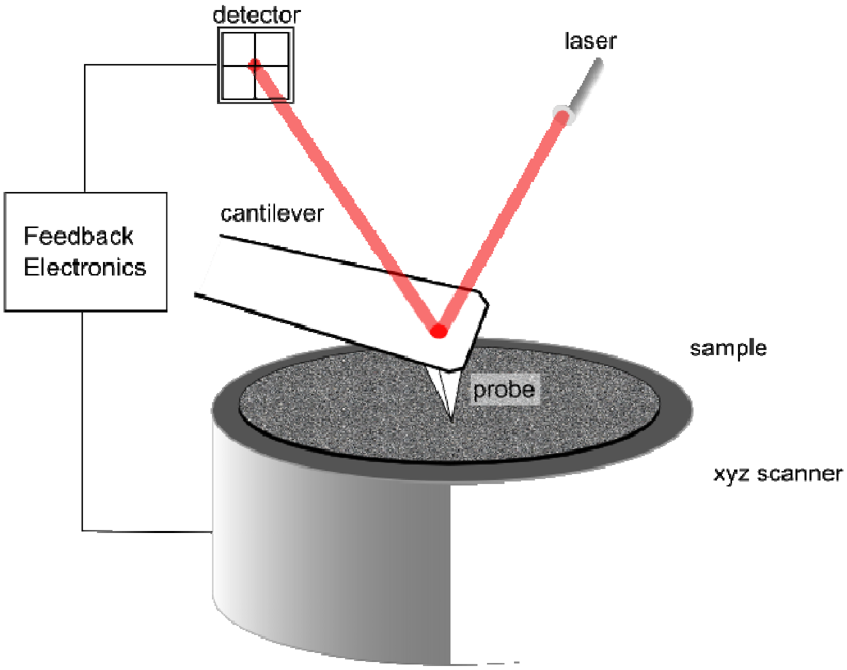

Fig. 3.4: Schematic of atomic force microscope [71].

In the present investigation, a NT-MDT make scanning probe microscope (Solver ProEC) consisting of scanning tunnelling microscope (STM) and atomic force microscope was used particularly with AFM to measure the surface topographical features of as polished, nitrogen ion implanted, and after electrochemical potentiodynamic polarization study to examine the surface condition before and after nitrogen ion implantation, and the extent of surface dissolution taking place after polarization study. Similarly, it was used to study the surface topography, particle and pore size determination of the Ti, TiO_2 and duplex Ti-TiO_2 coated 304L SS and to study the change in surface morphology after electrochemical polarization in 1 M and 8 M nitric acid. All the measurements were carried out in semi-contact mode using standard conical silicon tip with cone angle less than 20°, attached to cantilever having force constant 5 nN/m with frequency range from 50 to 150 Hz in ambient condition. Average (R_a), and root mean square (R_q) roughness values were calculated using Eq. 5 and Eq. 6 to get quantitative idea regarding the roughness present on the surface for nitrogen ion implanted, and coated (Ti, TiO_2 and duplex Ti-TiO_2) 304L SS.

$$R_a = \sum_{i=1}^{n} Z_i - \overline{Z} \tag{5}$$

$$R_q = \sqrt{\frac{\sum_{i=1}^{n} \left(Z_i - \overline{Z}\right)^2}{n}} \tag{6}$$

Where, Z_i is the height value of each single point, $\overline{Z}$ is the mean of all the height values and, n is the number of data points within the image.

3.1.4 Surface analytical studies

3.1.4.1 Glancing Incidence X-ray Diffraction

Glancing Incidence X-ray Diffraction (GIXRD) is a versatile non-destructive technique and is widely used for obtaining the information from thin top most layer of the materials. Conventional X-ray diffraction technique reveals information about the top layer of a thickness in the order 5-10 μm. In contrast, by employing glancing angle ($\leq 1.5°$) this thickness becomes an order of magnitude smaller. Important informations that can be obtained from the GIXRD analysis are; (a) structural changes occurring on materials by the process of ion implantation, (b) particle size and phase analysis of thin films, (c) micro-strain present in the specimen, (d) analysis of passive film, and (e) the characterization of corrosive deposits on the surface [72-75]. Of course, the technique has some limitation. The first one is that it works only on very smooth surfaces, and all the surfaces cannot be sufficiently smooth. Second is that at glancing angle most of the incoming X-rays are wasted passing over the surface.

Glancing incidence is a scattering geometry i.e. a combination of Bragg's condition with the conditions for X-ray total external reflection from crystal surfaces [76,77]. The advantage of small penetration depth and enhanced X-ray intensities at the surface makes glancing angle X-rays suitable for non-destructive characterization of various material properties. The geometry for Glancing Incidence X-ray Diffraction is shown in Fig. 2.5 [76].

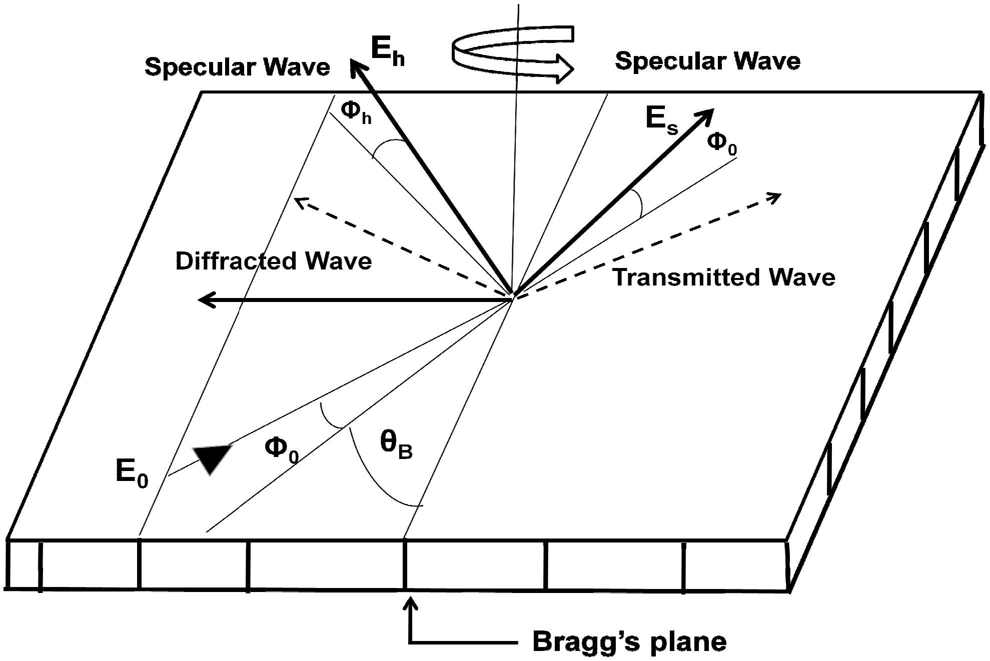

Fig. 3.5: Schematic of Glancing Incidence X-ray Diffraction [76].

The wave E_0 incidents on the surface at small angle Φ_0 produces specularly reflected wave E_S. However, in order to diffraction to occur from the surface, the incident wave E_0 has to meet some atomic planes perpendicular to the surface at a Bragg angle of θ_B. This is usually carried out by rotating the specimen about a normal to the surface, preserving the small angle Φ_0 as shown in Fig. 3.5. Though, the diffracted wave will be directed inwards to the plane, the reciprocal lattice vector being parallel to the surface, its specularly reflected counterpart E_h appears, taking off the crystal at small angle Φ_h. The wave E_h can also be treated as Bragg's diffraction of specularly reflected wave E_s, and E_h contains the structural information of very thin layer surface. The necessary condition is that the Φ_0 and Φ_h should be less then critical angle Φ_c for total external reflection.

In the present investigation GIXRD analysis was carried out by STOE make diffractometer to study the structural modification occurring on 304L SS with increasing dose of nitrogen ion implantation, and for the phase analysis, and particle size determination of the sputter deposited titanium (Ti) and titanium dioxide (TiO_2) and duplex Ti-TiO_2 coating on 304L SS. To study the structural modification as well as formation of certain phases with increase in nitrogen ion implantation dose, specimens from unimplanted and nitrogen ion implanted 304L SS with dose of 1×10^{16}, 1×10^{17} and 2.5×10^{17} N^+/cm^2 were analyzed. All the measurements were carried out at glancing angle of 1° for Cu Kα ($\lambda = 1.5487$ Å) with rotation of the sample at a measuring rate of 1° per sec in the 2θ range from 30°-90°. The angle of incidence was kept 1° because the depth of nitrogen ion implanted layer as calculated by TRIM simulation code [57] was 76 nm with straggling of 33 nm, and at this angle of incidence information about the phase components can be obtained up to a depth of 110 nm. Similarly, GIXRD analysis of titanium (Ti), titanium dioxide (TiO_2) and duplex Ti-TiO_2 coated specimen were carried out in the 2θ range from 20°-80° to analyze the phase composition as well as to determine the particle size using Scherrer’s formula. The data obtained were analyzed using JCPDS data base as well as compared with available literature.

3.1.4.2 Secondary Ion Mass Spectroscopy

Secondary Ion Mass Spectroscopy (SIMS) is one of the versatile analytical techniques to obtain chemical composition information at the surface, sub-surface, and in the bulk of the specimen. In general SIMS can characterize specimens with high spatial, and in-depth resolution, due to inherent sensitivity of mass spectroscopy coupled with high detection sensitivity down to ppb levels. Some of the interesting applications of SIMS include, (a) concentration profiles of diffused and ion implanted materials, (b) in-depth composition of profiles of oxide layers, (c) analysis of corrosion films, (d) depth profile of embrittled materials, (e) vapour deposited thin films, and (f) oxidation of different species [78-82]. However, the interpretation of SIMS spectra is quite difficult, and thus is not used for the unknown specimens without certain degree of prior information about the elemental composition. Similarly, quantification of SIMS data is also quite difficult due to matrix effect problem arising as function of ionization potential of the sputtered species, and due to the presence of electronegative atoms such as oxygen on the surface. Apart from this, the bombardment of primary ions modifies the surface due to mixing of atoms, and fragmentation of surface molecules etc [83].

In SIMS an energetic ion beam (1-20 keV) of focused primary ions is directed at the sample surface in a high or ultra high vacuum environment. The sputtered ions are termed as secondary ions. The secondary ions are then mass analyzed using double focusing mass spectrometer or an energy filtered quadruple mass spectrometer [84]. The principle of SIMS is schematically represented in Fig. 3.6 [84]. The primary ion beam can be of noble gases (Ar^+, Xe^+), oxygen (O^-, O^{2-}) and cesium (Cs^+). The choice of the ion species depends up on the required current, required beam size, and the specimen to be analyzed. The transfer of momentum from the impinging primary ions to the specimen surface causes collision cascade resulting sputtering of surface atoms and ions since most of the momentum transfer is redirected towards the surface. The secondary ion current is represented in Eq. 7,

$$I_m = I_p Y_m \alpha \theta_m \eta \qquad (7)$$

where

I_m is the secondary ion current of the species m.

I_p is the primary ion flux.

Y_m is the sputter yield.

α is the ionization probability.

θ_m is the fractional concentration of m in the surface layer.

η is the transmission of the analysis system.

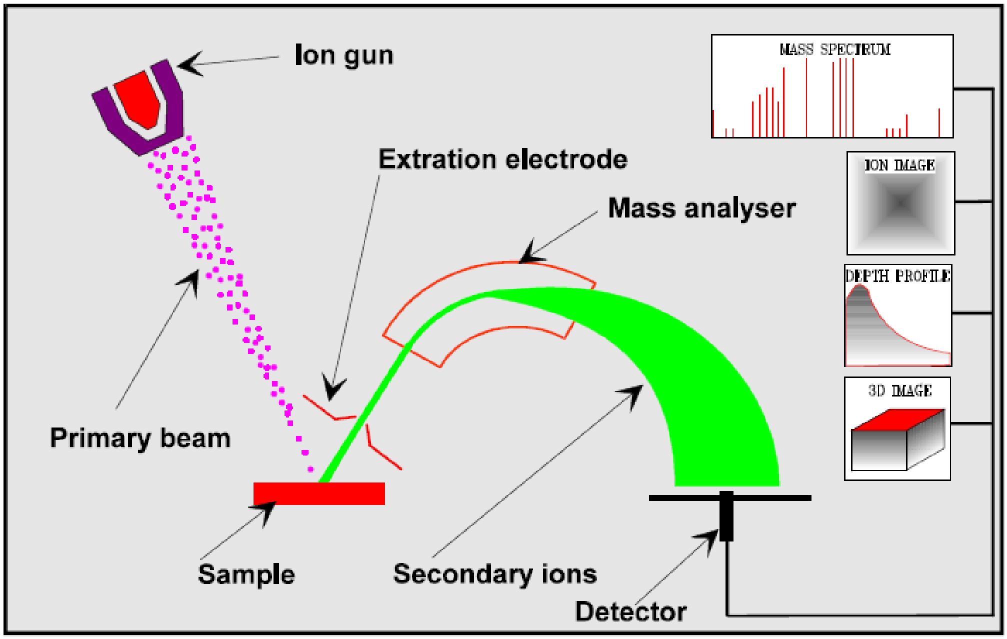

Fig. 3.6: Schematic of Secondary Ion Mass Spectroscopy [84].

In the present investigation, elemental depth profile analysis of unimplanted, and nitrogen ion implanted 304L SS with dose of 2.5×10^{17} N^+/cm^2 was carried out using dynamic SIMS (Cameca IMS 4f). All the measurements were carried out in positive SIMS mode using Cs^+ as primary ion source. The relative elemental sensitivity for all kinds of element is within the factor of two in case of Cs-complex except for the elements having higher electronegativity where the order of sensitivity is around five. The primary ion source (Cs^+) of 1.75 keV energy, and 10 nA beam current was rastered over an area of 100 µm × 100 µm in order to get an uniform bombardment on the surface, and the secondary ion species CCs^+, OCs^+, $CrCs^+$, $FeCs^+$, $NiCs^+$, and NCs^+ were collected with respect to time over an area of 30 μm^2 circular area. The process was repeated over three different places on the surface, and the data presented is a representative of the whole surface. The pressure inside the chamber during measurement was around 10^{-7} Pa.

3.1.4.3 X-ray Photoelectron Spectroscopy

X-ray Photoelectron Spectroscopy (XPS) or Electron Spectroscopy for Chemical Analysis (ESCA) is a surface analysis technique that is unique in providing the information regarding the bonding in different chemical states of elements. Its application is wide spread involving oxidation state determination of elements, identification of the chemical state of the metal oxide films, surface analysis of semi-conducting and insulating materials, and elemental depth profiling etc [85-87]. XPS in combination with traditional electrochemical techniques has long been used for understanding and solution of different types of corrosion problems. It is invaluable in the field of corrosion science, and the areas of corrosion research which are finding major applications are (a) for understanding the phenomenon of passivity, (b) compositional analysis at interface, (c) selective oxidation phenomenon, (d) assessment of mass transport process, and (e) the interaction of materials in different electrochemical environment [88-90]. However, the inability to detect hydrogen is one of the limitations in understanding greater details of overlapping mechanism of various corrosion phenomena [91].

XPS involves irradiating a sample with X-rays of a characteristic energy and measuring the energy of flux of electrons leaving the surface [92]. The energy spectrum for the ejected electrons is a combination of an overall trend due to energy loss processes within the sample, transmission characteristics of the spectrometer, and resonance structures that derive from electronic states of the material under analysis. In principle it consists of (a) X-ray source, (b) electronic focusing system, (c) electron energy analyzer, and (d) detector. The schematic of X-ray photoelectron spectroscopy is shown in Fig. 3.7 [92].

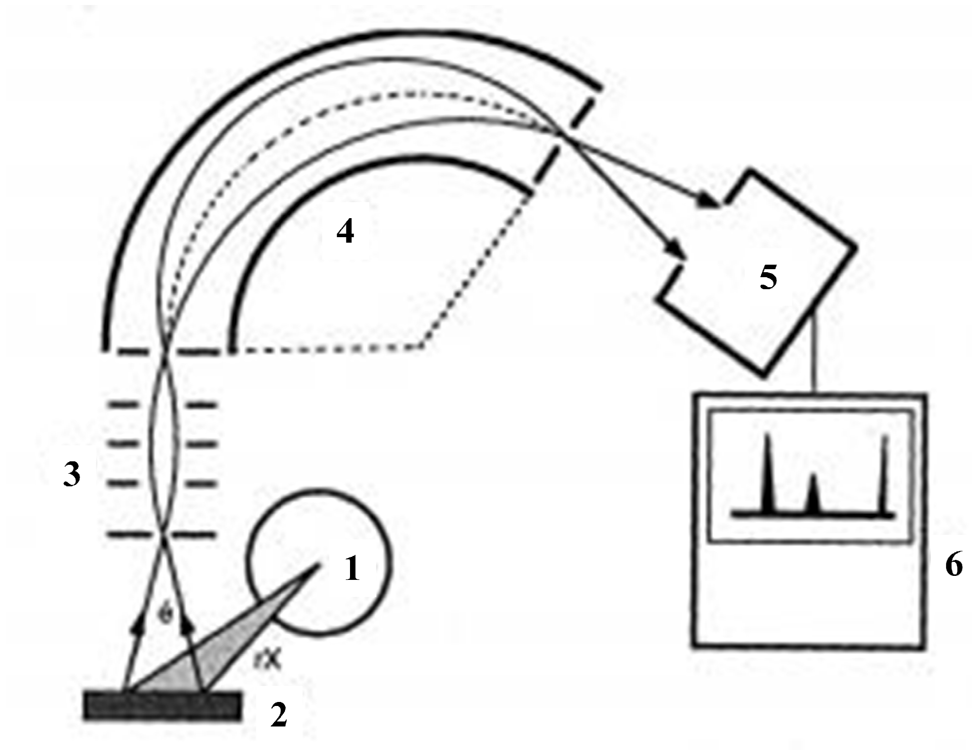

Fig. 3.7: Schematic of X-ray photoelectron spectroscopy showing (1) X-ray source, (2) sample, (3) electronic focusing system, (4) spectrometer (5) electron detector or channeltron and (6) data acquisition system [92].

The selection of X-ray source depends on many factors such as (a) energy resolution of X-ray, (b) energy of the photons that are produced, and (c) the ease of application as an anode material. Based upon these criteria, Al Kα (1486.6 eV) and Mg Kα (1253.6 eV) are universally used in laboratory XPS studies. The monochromatization of the X-ray source is carried out according to the Bragg's relation by diffraction of a crystal for reduced back ground, narrow peak width, and filtering of satellite peaks. The monochromatized X-ray source is then refocused to a point where the specimen is located. The irradiation of the specimen with X-ray source causes emission of electrons (photoelectrons) of discrete energy by means of photoelectric effect. The analysis of energies of these photoelectrons escaped from the surface of the specimen is the most important part of XPS measurement. Thus, an electron energy analyzer (spectrometer) is often used to measure the kinetic energy of the ejected electrons. The basic function of the spectrometer is to separate out electrons in a desired band of energies from all other electrons entering the spectrometer with wide range of energies. The most common type of spectrometers used is concentric hemispherical analyzer (CHA). The current reaching the exist slit of the energy analyzer from the energy analyzed electrons is very low, and usually requires electron multiplier for detecting the photoelectrons of different energy. There are two types of electron multiplier currently in use, those are (a) discrete dynode and (b) channel electron multiplier. The current gains from such electron multipliers are within 10^4-10^8. In the detector, photoelectron spectra give directly the detected electron density versus their binding energy. The identification of elements on the surface is realised with their characteristics peaks appearing on wide range energy spectrum.

In the present investigation, XPS was used to investigate the passive film composition of 304L SS in nitric acid medium developed in in-situ condition using electrochemical atomic force microscope (EC-AFM), and the bonding state of nitrogen in nitrogen ion implanted 304L SS. Measurements were carried out using XPS system (SPECS) that employed monochromatized Al Kα radiation as probe and a hemispherical analyzer for energy analysis with pass energy of 20 eV having an optimum energy resolution of 0.6 eV. The passive film as formed on 304L SS in 0.1 M, 0.6 M and 1 M nitric acid in in-situ EC-AFM study were analyzed to understand the overall change in chemical composition of the passive film as a function of increasing nitric acid concentration. Survey scans and high resolution spectra of major alloying elements in as polished condition as well as nitric acid passivated condition were acquired to analyze the chemical state of the alloying elements in aforementioned condition. Similarly, XPS analysis of nitrogen ion implanted 304L SS was carried out to study the bonding of implanted nitrogen with certain alloying elements in 304L SS leading to the formation of certain phases. XPS spectra for nitrogen ion implanted specimens were carried out after different sputtering time interval at a sputtering rate of 10Å/min using 5 keV Ar^+ ion beam with current of 50 μA/cm^2 at an incidence angle of 45°, and at a pressure of 1×10^{-5} Pa. The pressure in the analyzer chamber was of the order 1×10^{-7} Pa throughout the measurement.

3.1.5 Electrochemical corrosion studies

3.1.5.1 Open circuit potential vs. time measurement

Out of several electrochemical techniques used for the investigation of corrosion, open circuit potential (OCP) measurement over time of immersion is successfully employed over the years for understanding the corrosion process by analyzing the natural fluctuation of the corrosion potential. When a specimen is immersed in corrosive solution both oxidation and reduction reaction takes place, and in general specimen oxidizes and the solution reduces. Thus, open circuit potential or free corrosion potential is defined as the potential of a working electrode in steady state measured with respect to a reference electrode in absence of any perturbation to the working electrode surface [93]. The magnitude of open circuit potential is dependent on the metal/alloy itself, composition of the solution, temperature, and hydrodynamics of the electrolyte. OCP-time measurement provides insight into the instantaneous electrochemical process occurring in the electrode surface, and is important for determining tendency of materials to free corrosion [94]. Moreover, variation in OCP is an indication of the protective power of the passive film building on the surface, and its stability from surface electro-chemical phenomenon occurring in a corrosive environment as a function of time. The change in potential in the anodic direction is termed as noble potential, and indicates the presence of stable passive film whereas the shift of potential in the cathodic direction i.e. active direction indicates the onset of corrosion process. Apart from this, it provides the idea regarding the transient steps in the passive film formation from the signals spontaneously generated from the corroding surface. However, the OCP measurement gives only qualitative information of the corrosion behaviour, and is limited regarding kinetics and mechanism of the electrochemical reaction occurring on the surface of an electrode in contact with corrosive reagent.

In the present investigations open circuit potential vs. time measurements were carried out using a standard electrochemical cell as shown in Fig. 2.8 [93] in different concentration of nitric acid for unimplanted, nitrogen ion implanted, uncoated, titanium (Ti), titanium dioxide (TiO_2), and duplex Ti-TiO_2 coated 304L SS.

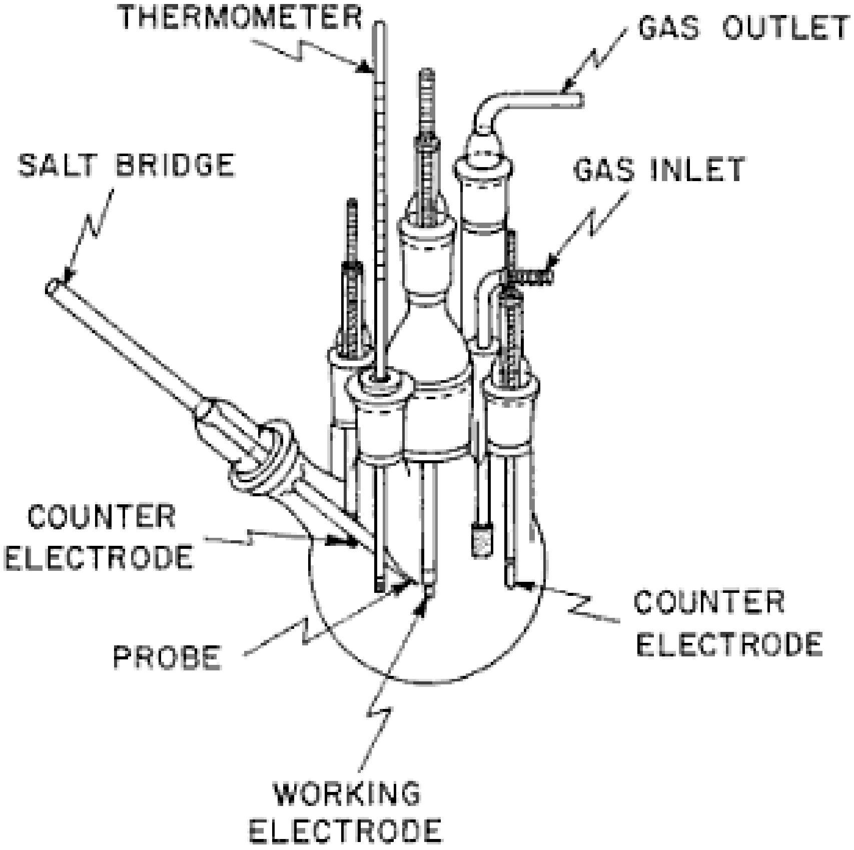

Fig. 3.8: Schematic of an electrochemical cell for corrosion study [93].

The electrochemical cell comprises of specimen as working electrode, platinised platinum counter electrode and Ag/AgCl reference electrode. The OCP was measured by potentiometric circuit with negligible current generation until the potential remained stable over a reasonable time period. The specimens analyzed are unimplanted, and nitrogen ion implanted 304L SS with different doses of nitrogen (1×10^{15}, 1×10^{16}, 1×10^{17}, 2.5×10^{17} N^+/cm^2) in 1 M nitric acid. Similarly, OCP-time measurements for uncoated, titanium (Ti) titanium dioxide (TiO_2), and duplex Ti-TiO_2 coated 304L SS were carried out in 1 M and 8 M nitric acid, respectively. The solutions used in the investigations were not de-aerated, and the specimens were immersed at least for 30 minutes for attaining stability at the electrode-electrolyte interface. At least three tests were carried out to check the reproducibility for various types of specimens examined in the present investigation at different concentration of nitric acid.

3.1.5.2 Electrochemical impedance analysis

Electrochemical impedance spectroscopy (EIS) is one of the versatile electrochemical techniques for characterizing electrochemical properties of the materials, and their interfaces in different electrochemical environments. It is defined as the impedance of an electrode-electrolyte interface as a function of frequency of the applied alternating current [95]. Today, it is widely used to analyze the complex material properties such as dielectric properties, mass transport, defect density, passive film stability, coating degradation, microstructural and compositional effects on the conductance of solids, and impedance study of biological membranes [96-101]. The wide spread use of impedance technique is due to the possibility of using very small amplitude signal without disturbing the desired properties of materials to be measured. Moreover, the tests are non destructive and provide a rapid and convenient way of characterizing physico-chemical properties. However, the primary problem associated with EIS technique is the ambiguity associated with data interpretation i.e. what equivalent circuit model [102] should be used out of several possibilities. Even when, the equivalent circuit model is known, component values may not able to be resolved properly. Nevertheless, the added dimension of frequency can provide essential mechanistic information which would be otherwise unavailable from complimentary electrochemical techniques [103]. Out of several applications, EIS is largely used in the field of corrosion science in recent years due to development of sophisticated electronics which employs latest digital electronics and computer control overcoming the earlier limitations.

EIS study is carried out in properly designed standard electrochemical cell consisting of specimen as working electrode, counter electrode, and a reference electrode as shown in Fig. 3.8 [93]. The basic design feature of the electrochemical cell is to measure the impedance at the working electrode-electrolyte interface only, and to eliminate the impedance contribution from the counter electrode. This is done by making the resistance of the counter electrode negligible compared to that of working electrode, and capacitance of the counter electrode very large compared to that of working electrode [98]. Since, resistance in series add and capacitance in series add reciprocally, the influence of the counter electrode can be eliminated by making its area large compared to that of working electrode. Often platinised platinum with large area is used as counter electrode.

In EIS measurements a perturbing sinusoidal voltage $E = E_0 \text{ Sin } (\omega t)$ with frequency ω is applied to the electrode system under test [95,102,103]. The response is analysed in terms of the resultant current $I = I_0 \text{ Sin } (\omega t + \alpha)$, where α represents a characteristics phase angle shift. The frequency response is analyzed by instruments known as Frequency Response Analyzers (FRA) interfaced with potentiostat. Frequency response analyzer provides scope for studying wide range of frequencies, faster analysis, and removal of harmonic distortions. The corresponding complex impedance spectrum $Z(\omega)$ obtained by varying the signal frequency ω is expressed in terms of displacement vector $Z(\omega)$. In the plane of cartesian coordinates impedance is expressed by its real and imaginary parts as presented in Eq. 8.

$$\mathbf{Z}(\omega) = Z_{Re} + jZ_{Im.} \qquad (8)$$

The modulus of electrochemical impedance |Z|, and phase angle (α) are obtained by the following Eq. 9 & 10.

$$|\mathbf{Z}| = \sqrt{(Z_{Re})^2 + (Z_{Im})^2} \tag{9}$$

$$\alpha = \arctan\,(Z_{Re}/Z_{Im}) \tag{10}$$

The relationship between the modulus of impedance, frequency, and phase angle is expressed in two ways i.e. (a) Nyquist plot, and (b) Bode plot. In the format known as Nyquist plot, the frequency response of the complex plane is obtained by plotting the imaginary component of the impedance (jZ_{im}) against the real component Z_{Re}. In Bode plot the magnitude of total impedance is plotted against the frequency on a log-log scale and phase angle α against log frequency. Nyquist plot allows an easy prediction of the properties of the electrode-electrolyte interface, however it does not provide the information regarding the frequency dependence of impedance [95,102,103]. Bode plot contains all the necessary information for clear interpretation of the results. The interpretation of the impedance data from Nyquist or Bode plot is carried out by means of electrical equivalent circuit consisting of circuit elements, and the whole arrangement should represent the physical phenomenon occurring in the electrochemical cell. In general the circuit contains following basic elements,

(a) Charge transfer resistance (R_P) whose impedance is |Z| = R

(b) Capacitance of double layer (C_{dl}) at electrode-electrolyte interface whose impedance is given by |Z| = 1/jωC. In order to consider non-ideal capacitance behaviour, real capacitance is replaced by constant phase element whose impedance is given by Eq. 11,

$$\mathbf{Z}_{CPE} = \frac{1}{T(j\omega)^n} \tag{11}$$

where T and n are frequency independent parameters, ω is the angular frequency, and j is the imaginary number equal to $\sqrt{-1}$.

(c) Solution resistance (R_S).

The schematic of an electrical equivalent circuit consisting of above circuit elements is shown in Fig. 3.9 [21]. However, the circuit diagram varies depending upon the nature of working electrode, and the physico-chemical process occurring at the electrode-electrolyte interface. The total impedance of the system can be calculated as a combination of the aforementioned circuit elements.

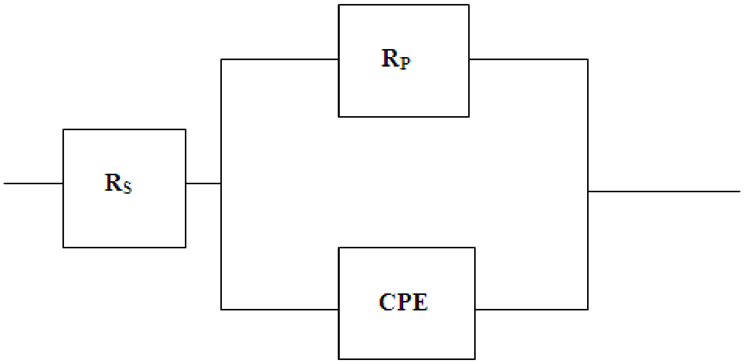

Fig. 3.9: Schematic of electrode-electrolyte interface in electrochemical impedance spectroscopy [21].

In the present investigation, electrochemical impedance spectroscopy was used for investigating the passive film stability of unimplanted and nitrogen ion implanted 304L SS in 1 M nitric acid. Similarly, EIS study was carried out for uncoated, titanium (Ti), titanium dioxide (TiO_2), and duplex Ti-TiO_2 coated 304L SS for comparing the passive film stability of uncoated, and coated 304L SS specimens in 1 M and 8 M nitric acid. For unimplanted and nitrogen ion implanted specimens electrical equivalent circuit as shown in Fig. 3.9 was used to evaluate the effect of nitrogen on polarization resistance, double layer capacitance, and on the passive film stability with increase in dose of nitrogen implantation. Similarly, two different electrical equivalent circuit as shown in Fig.3.10a-b was used for uncoated, Ti, TiO_2 and duplex Ti-TiO_2 coated specimens to study the effect top-surface coating on the polarization resistance, double layer capacitance, coating capacitance and pore resistance in 1 M and 8 M nitric acid as compared to uncoated specimen. Fig. 3.10a consisting of circuit elements such as R_s as solution resistance, CPE_2 as constant phase element characterized by double layer capacitance (Cdl_2) and Rct_2 as charge transfer resistance respectively was used for uncoated specimens. Electrical equivalent circuit as shown in Fig. 3.10b consisting of R_s as solution resistance, CPE_1 as constant phase element representing coating capacitance (Cdl_1), CPE_2 as constant phase element representing double layer capacitance (Cdl_2), Rct_1 as coating resistance (pore resistance) and Rct_2 as interfacial charge transfer resistance respectively was used for Ti, TiO_2 and duplex Ti-TiO_2 coated specimen.

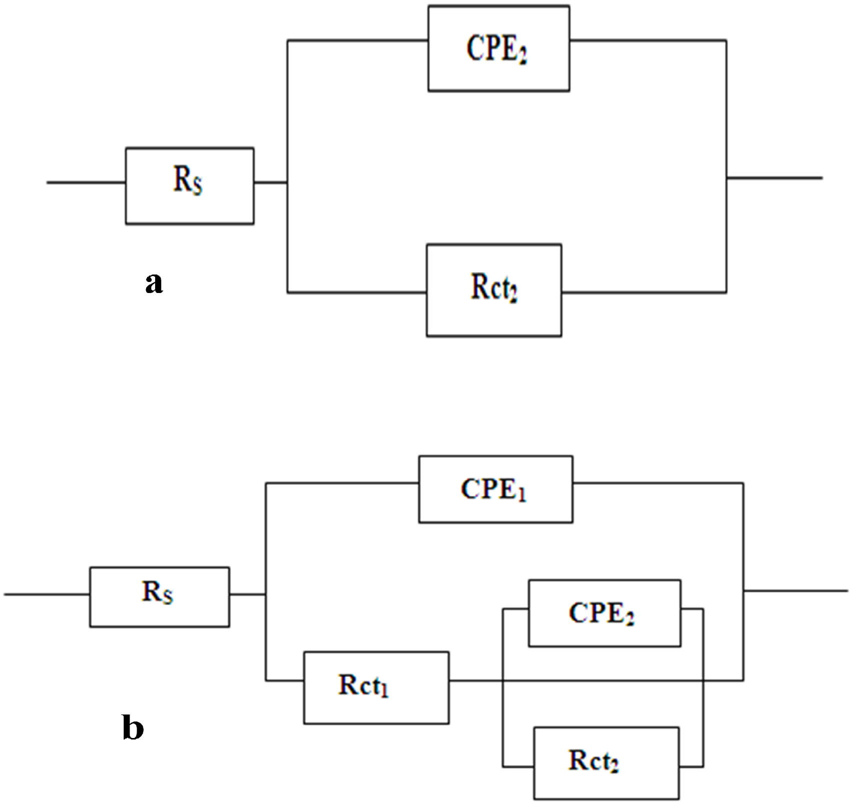

Fig. 3.10a-b: Schematic of electrical equivalent circuit for (a) uncoated, and (b) Ti, TiO_2 and duplex Ti-TiO_2 coated 304L SS [22].

All the measurements were carried out in open circuit potential condition in standard electrochemical cell as mentioned earlier consisting of specimen as working electrode, Ag/AgCl as reference electrode, and platinised platinum as counter electrode using Solatron 1255 Frequency Response Analyzer associated with 1287 electrochemical interface. The experiments were carried out in the frequency range from 10^{-1} Hz to 10^{5} Hz by superimposing an AC voltage of 10 mV amplitude with data density of 5 points per decade.

3.1.5.3 Potentiodynamic polarization study

Potentiodynamic polarization is probably the most commonly used polarization technique often used for testing corrosion susceptibility. This technique can provide significant information regarding corrosion mechanism, corrosion rate, and corrosion of specific materials in designated environments. A polarization curve can provide evidences whether or not a material is active, passive or active-passive. Apart from this, passivity and corrosivity can be determined in presence of oxidizing-reducing species also. One of the major advantages of potentiodynamic polarization study is quick determination of corrosion rate as compared to traditional weight loss methods. In this technique the corrosion rate is determined by extrapolating linear segments of cathodic and anodic regions (Tafel lines) [104]. The intersection of the Tafel lines gives the corrosion potential and corrosion current density.

Potentiodynamic polarization method involves changing the potential of the working electrode at a fixed rate, and monitoring the current density which is produced as a function of potential [93]. The instrumentation for carrying out the polarization study consist of a potentiostat which maintains the potential of the working electrode according to the preset value. A current measuring device (electrometer) for measuring the current produced by the applied potential. Polarization cells for carrying out polarization study consists of, (a) working electrode i.e. specimen to be tested, (b) a non-polarizable counter electrode for completing the circuit, and (c) reference electrode with respect to which potential has to be applied. The schematic of an electrochemical cell for carrying out polarization study is as shown in Fig. 3.8. Reference electrode often separated from the solution by luggin probe, and is placed close to the working electrode to eliminate the effect of solution resistance.

In the present investigation potentiodynamic polarization studies were carried out for unimplanted, nitrogen ion implanted 304L SS, uncoated, titanium (Ti), titanium dioxide (TiO_2) and duplex Ti-TiO_2 coated 304L SS using Solartron 1287 electrochemical interface associated with standard electrochemical cell consisting of platinum as counter electrode, Ag/AgCl as reference electrode and specimen as working electrode, respectively (Fig. 3.8). The working electrode was prepared by connecting the specimens to the back side of a brass holder covered with nail polish with silver paste and the whole arrangement was wrapped with Teflon tape exposing the top surface. In all the experiments the solution was not de-aerated. At least three sets of experiment were carried out to check the reproducibility. The polarization plots obtained were analyzed by CORR WARE software, and the quantitative values of corrosion related parameters such as corrosion potential (E_{corr}), corrosion current density (I_{corr}), passive current density (I_{pass}) and transpassive potential ($E_{transpass}$) were obtained to understand the corrosion behaviour of 304L SS as well as the effect of surface modification by nitrogen ion implantation (*sub-surface modification*), and by Ti, TiO_2 and duplex Ti-TiO_2 coating (*top-surface coating*) at different concentration of nitric acid. In the present investigation, corrosion potential (E_{corr}) and corrosion current density (I_{corr}) was calculated by Tafel extrapolation method of certain linear segments of measured potential-current density curves [105,106]. In the present studies, data were fitted 100 mV above and below the E_{corr} using non-linear least square algorithm based on the Levenberg-Marqurdt (LEV) method used along with CorrView 2 software (Scribner Associates, Inc) to simulate and obtain the measured data (Eq. 12) [105,106].

$$I = I_{Corr}\left(10^{\frac{E-E_{Corr}}{B_a}} + 10^{-\frac{E-E_{Corr}}{B_c}}\right) \qquad (12)$$

Protection efficiency of Ti, TiO_2 and duplex Ti-TiO_2 coating in nitric acid medium was evaluated using Eq. 13 to understand their performance in nitric acid medium [107].

$$\text{Protection efficiency (\%)} = \frac{I_{corr} - I_{corr(c)}}{I_{corr}} \times 100 \qquad (13)$$

Where, Icorr and Icorr(c), are the corrosion current density of uncoated and coated 304L SS in different concentration of nitric acid.

3.1.5.4 Electrochemical atomic force microscopy

Electrochemical atomic force microscope (EC-AFM) is one of the potential surface investigation techniques to study the in-situ electrode-electrolyte interface, and in recent years it has significantly contributed in understanding physico-chemical phenomenon of electrochemical process in different electrochemical environments. The main advantage of EC-AFM is that, the working electrode can be conductor or insulator. The ability to probe the local character at sub-microscopic level of the electrode-electrolyte interface with potentiostatic control has advanced its applications in various fields of fundamental and applied research in material science, biological science, physical and chemical science. Included in such type of studies are structure-reactivity of electrode surface, electro-deposition, surface reconstructions, adsorption on surfaces, corrosion and study of biological specimens in near physiological conditions [108-111]. Out of several interesting applications of EC-AFM, one of the important fields of study is the process of corrosion of different materials in simulated environments. To date its application is wide spread for understanding the passive film property, surface dissolution, surface morphological changes prior to corrosion initiation, efficiency of inhibitors, and many other branches of corrosion science.

The basic working principle for EC-AFM is similar to that of AFM as discussed in section 2.3.2, however it is designed to operate under electrochemical condition [112]. The topographical measurements in electrochemical environment are carried out by measuring the force of interaction between tip and sample in a three electrode electrochemical cell comprising of specimen as working electrode, counter electrode, and reference electrode. The schematic of an electrochemical AFM showing electrochemical cell, working electrode, counter electrode, reference electrode, potentiostat and signal detection system such as laser diode, probe and photodetector are shown in Fig. 3.11 [113].

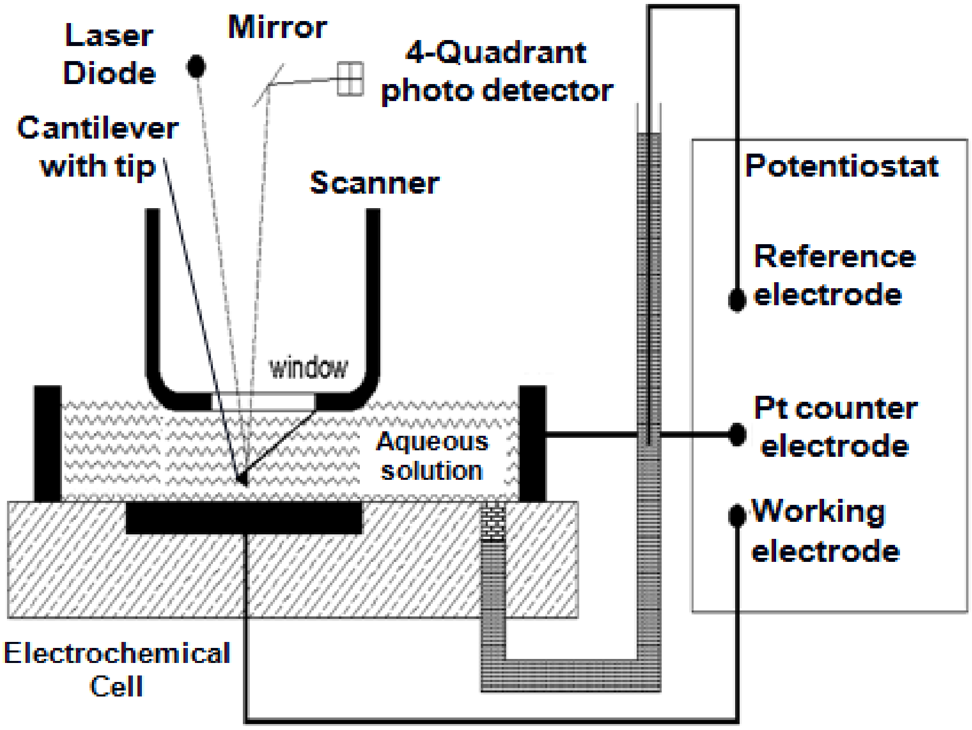

Fig. 3.11: Schematic of electrochemical atomic force microscope [113].

The mode of operation is similar to that of any standard AFM measurement such as contact or semi-contact mode. As the electrochemical cell is a three electrode cell, normal potentiostat can be used to control the working electrode potential with respect to reference electrode.

In the present investigation for studying the in-situ passive film morphology of 304L SS in nitric acid medium, surface morphological investigations were carried out using a NT-MDT make electrochemical atomic force microscope (Solver ProEC). The electrochemical cell was having volume capacity of 5 ml, and electrodes used were specimen as working electrode, platinum as counter electrode, and Ag/AgCl as reference electrode. All the component of electrochemical cell such as Teflon cell, clips were cleaned in a solution of hydrogen peroxide and sulphuric acid for 12 h in order to avoid the contamination due to impurity. The morphological investigations were carried out at fixed location of the specimen i.e. without changing specimen position in 0.1 M, 0.5 M, 0.6 M and 1 M nitric acid, respectively. The potential sweep during the scanning was varied as revealed by potentiodynamic polarization study in the aforementioned nitric acid solutions.

CHAPTER 4

Morphological and Compositional Analysis of Passive Film on AISI 304L Stainless Steel in Nitric Acid Medium

CHAPTER 4

Morphological and Compositional Analysis of Passive Film on AISI 304L Stainless Steel in Nitric Acid Medium

Passive film properties of 304L SS in nitric acid medium were investigated in both ex-situ and in-situ conditions using AFM and EC-AFM techniques. Ex-situ study in 1 M, 4 M, 8 M, and 11.5 M nitric acid revealed that variation in passive film morphology occurs depending upon the concentration, and time of immersion. In-situ passive film surface morphology investigation showed formation of chromium hydroxide layer in the form of platelet like structures at lower concentrations (0.1 M, 0.5 M), and towards higher concentration (0.6 M) the platelets formed homogenous oxide layer on the surface which started depleting at still higher concentration (1 M) leading to opening up of oxide boundaries. Compositional analysis of the passive film revealed duplex nature consisting of hydroxide and oxide layers at lower concentration, and with increasing concentration oxide layer predominates over the surface.

4.1 Introduction

Electrochemical corrosion initiation at sub-microscopic region involves several phenomenon starting from breakdown of passive film in stochastic and sporadic way to localized dissolution of oxide covered material, and mass transport of atoms across the surface to support the continuing dissolution process [114,115]. The crucial factor controlling all the above phenomenon is the passive film whose structure, property, and stability is of immense important in understanding the many details of electrochemical corrosion process as well as central to controlling corrosion, and use of metallic materials in many technologies. The desirable, and beneficial property of passivity is directly related with sustainability of material, since corrosion is encountered by all materials used for engineering applications. Although, many metals and alloys can naturally form air formed passive layer, it breaks down depending upon the process condition of the environment they are used. Thus, better understanding on the morphology, composition and “role of passivity” on the corrosion resistance of engineering materials is important for application in critical circumstances.

Passivity results from the formation of natural, ultra thin, tenacious, and self-healing oxide layer on the surface which acts as a barrier layer from the corrosive environment [3]. The protectiveness of the passive film is mostly due to insoluble nature of oxide layer, and is dependent on the corrosive nature of the electrochemical environment. If damaged, the passive film normally reforms rapidly. However, a change in the character of the environment may cause the passive material to revert to an active state. Subsequent damage to the pre-existing passive film can result in substantial increase in corrosion rate due to accelerated degradation of the passive film. As passive film constitutes a protective surface layer against localized corrosion, its chemical and structural properties play major role on the rate and extent of transient removal from the surface. The characterization of structure and composition of the passive film is thus vital for understanding their nature of interaction with corrosive environments. A large number of techniques are available to elucidate the properties of passive film, such as (a) polarization study to find out the potentials and current densities during passive film growth and dissolution, (b) AC impedance technique for analyzing capacitance, resistance and space charge within the passive film (c) electrochemical quartz crystal micro balance for studying the extent of oxide layer dissolution, (d) spectroscopic measurement to elucidate the structural information, (e) chemical study to locally resolve the chemical composition, and (f) topographical study to understand the morphological features etc.

Considerable progress have been made in the recent past towards understanding the nature of passivity with the development of optical, electro-optical, in-situ electrochemical, and morphological analysis equipments. Out of several important physico-chemical properties, surface morphological evidences are critical for understanding the passive film properties such as, growth of oxide film, possible pre-cursor sites for localized dissolution of passive film, physical changes occurring during the breakdown of passive film, and the transport process occurring over the surface [116]. Dynamic observations of the above surface morphological features in real condition are quite helpful in understanding the nucleation and growth of passive film at nano-scale, aging with increase in thickness, and the manner by which passive film breakdown occurs on the surface. Similarly, the propagation of corrosion is a surface phenomenon, and without substantial knowledge of surface morphological features it is difficult to fully understand the process of corrosion. Thus, the conceptual understanding on the surface morphological features is indispensable for understanding applied aspect of corrosion science.

Recent development of in-situ surface monitoring systems such as scanning probe microscope has opened up a new scope and dimension for understanding localized corrosion phenomenon, as it provides information regarding structural and electrochemical phenomenon occurring in a simulated electrochemical environment [112]. Considerable attempts have been made to comprehend the phenomenon of localized corrosion in stainless steel in various electrochemical environments using *in-situ* scanning probe microscope technique. Kamachi Mudali and Katada [11] have investigated the nano-mechanical properties of passive film of nitrogen-bearing austenitic stainless steel, and have predicted the decrease in stiffness value and increase in height of passivated surface in 0.5 M NaCl medium under different surface conditions. Williford et al [117] have demonstrated the growth of pit over time, and initiation of intergranular corrosion between grain boundaries adjacent to chromium carbide precipitate on the study of pitting, and intergranular corrosion of 304 SS in NaCl and oxalic acid medium. Zhang et al [118] have reported that the current density for pit growth is higher as compared to that of applied current on the analysis of the role of corrosion products on pitting corrosion of SUS 304 SS. Femenia et al [119] have shown that potential for the dissolution of austenite phase is higher as compared to ferrite phases on the investigation of surface dissolution process of 2205 duplex stainless steel in H_2SO_4 and HCl medium. Martin et al [120] have reported the initiation of the pits is along the ridged lines as a result of strain hardening due to mechanical polishing on the investigation of pitting corrosion of 304L SS in chloride media. However, to date no ex-situ or in-situ study has been carried out to understand the passive film properties of austenitic stainless steel in nitric acid medium which is mostly related to the corrosion resistance of stainless steel in nuclear fuel reprocessing environment.

The scope of the chapter is to understand the passive film morphology of 304L SS in nitric acid medium in both ex-situ and in-situ conditions with increase in concentration. The concentrations of nitric acid used in ex-situ, and in-situ study are different because process conditions have to be simulated, and experimental difficulties should be taken care. Thus for ex-situ study higher concentration, and for in-situ study lower concentration of nitric acid were used. Overview of the present investigation includes, (a) examining the time-dependent morphological changes of 304L SS in 1 M, 4 M, 8 M, and 11.5 M nitric acid after different hours of exposure using atomic force microscope, (b) analysis of polarization behaviour of 304L SS in 0.1 M, 0.5 M, 0.6 M, and 1 M nitric acid, (c) realizing the morphological changes according to polarization study using in-situ electrochemical atomic force microscope (EC-AFM), and (d) analyzing the chemical composition of the passive film as observed in in-situ study in 0.1 M, 0.5 M, 0.6 M, and 1 M nitric acid by using X-ray photoelectron spectroscopy.

4.2 Results and discussion

4.2.1 Ex-situ surface morphology study

The ex-situ results for the immersion study to monitor the surface morphology of passive film in 1 M, 4 M, 8 M, and 11.5 M nitric acid are presented in Fig. 4.1-4.4. Generally in corrosion study using AFM, increase in roughness value is considered as increase in corrosion process, and decrease in roughness value is taken as occurrence of passivation process [121,122]. Figure. 4.1a-d represents the surface morphology of 304L SS in 1 M nitric acid during the immersion up to 27 h.

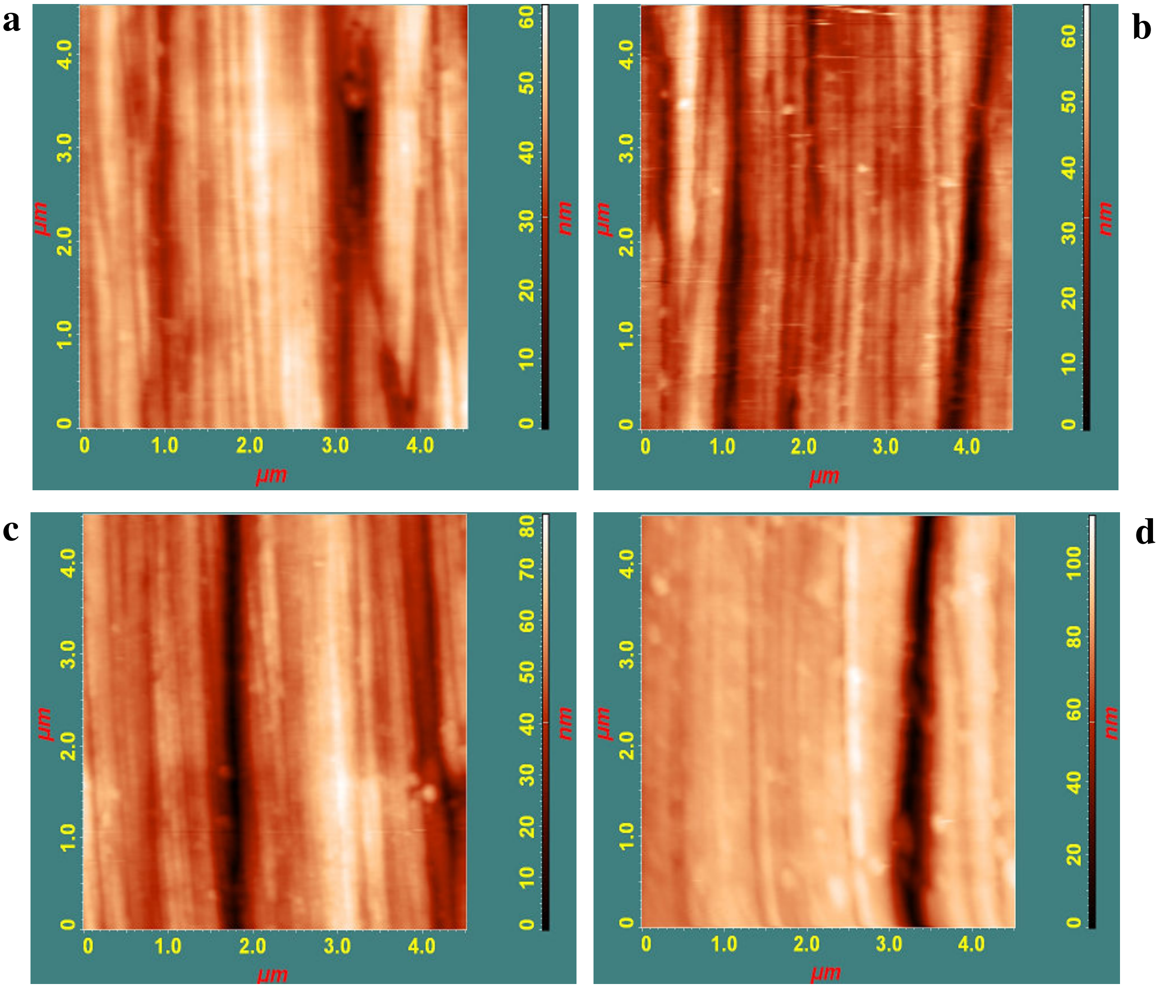

Fig. 4.1: Ex-situ surface morphology of 304L SS in 1 M HNO_3 with increase in immersion time, (a) As polished, (b) 9 h, (c) 18 h, and (d) 27 h.

The ridged structure, and lines in the same direction as observed in as polished condition (Fig. 4.1a) can also be seen after immersion up to 27 h (Fig. 4.1d) however, the ridged surface appeared smoother which is due to building up of a homogenized passive film on the surface as a result of immersion in nitric acid. Moreover, the root mean square roughness (R_q) on the surface decreased from 15 nm in as received condition to 10 nm after immersion for 27 h, which indicates the formation of uniform passive film overcoming the effect of inhomogenities, and corrugation on the surface [123]. The results for immersion study in 4 M nitric acid were by and large similar to that of in 1 M nitric acid (Fig. 4.2a-d), and with increase in immersion time the surface appeared smother with similar decrease in roughness value [123].

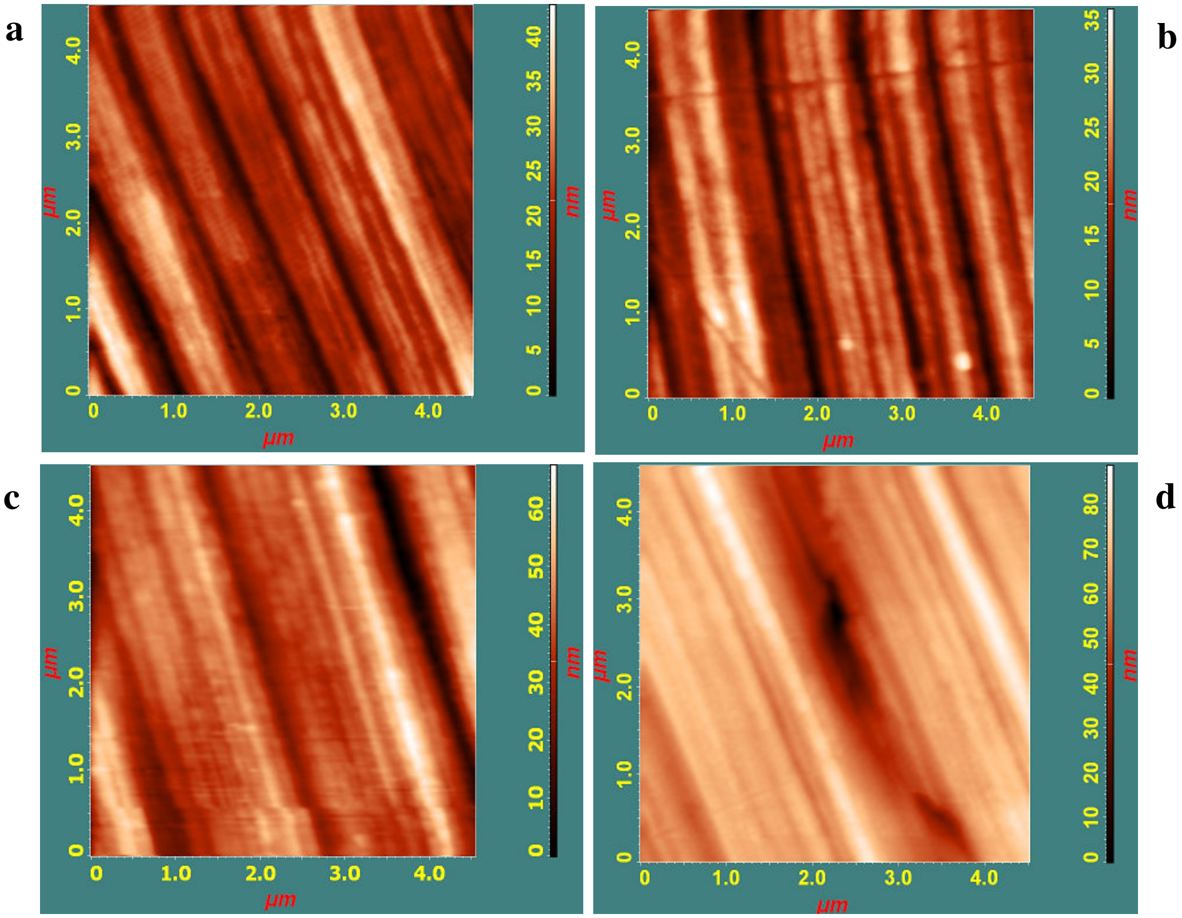

Fig. 4.2: Ex-situ surface morphology of 304L SS in 4 M HNO_3 with increase in immersion time, (a) As polished, (b) 9 h, (c) 18 h, and (d) 27 h.

However, the morphological features in 8 M nitric acid were quite different from 1 M and 4 M nitric acid, where homogenization as well as local breakdown of passive film over the ridged lines on polished surface can be observed with increase in immersion time. Figure. 4.3a-d, represents the surface morphology of 304L SS in 8 M nitric acid during the immersion up to 27 h.

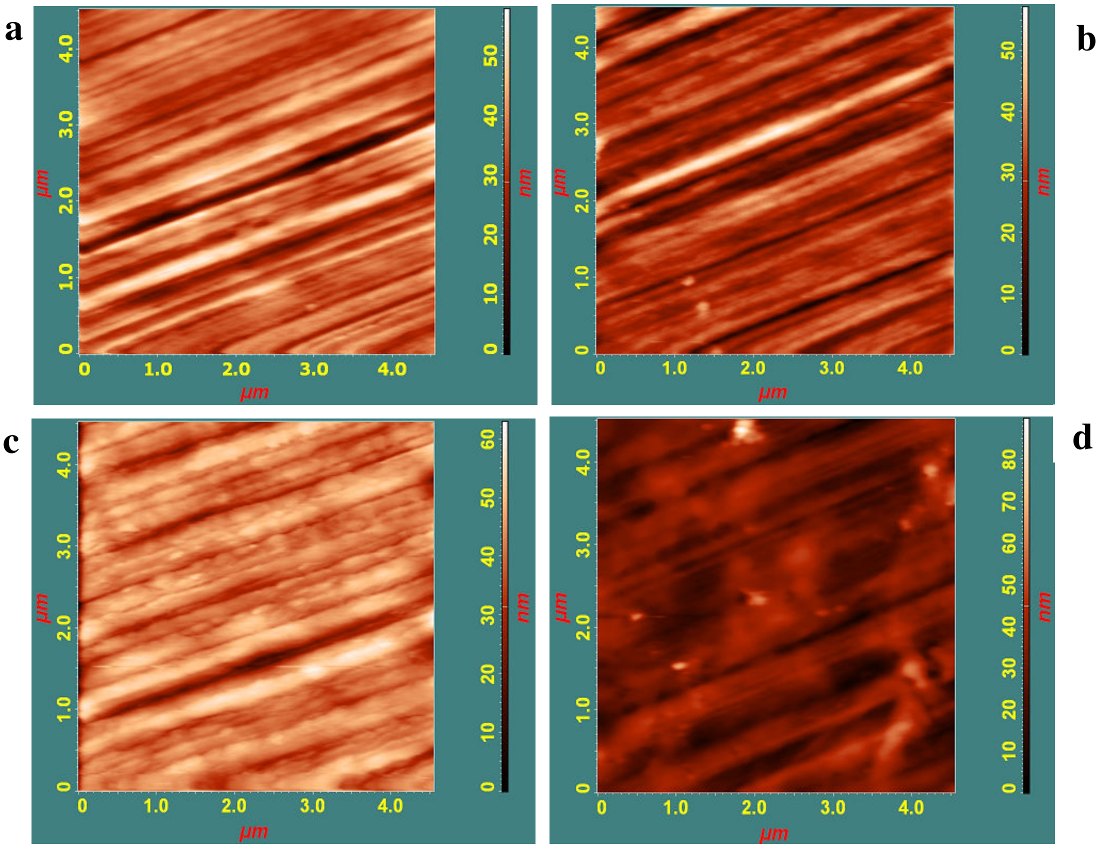

Fig. 4.3: Ex-situ surface morphology of 304L SS in 8 M nitric acid with increase in immersion time, (a) As polished, (b) 9 h, (c) 18 h, and (d) 27 h.

The morphology after 9 h of immersion (Fig. 4.3b) was mostly similar to that of as polished condition (Fig. 4.3a) showing polishing lines, and ridged structure. However, the surface appeared to be smoother by filling up of the gaps in between the ridged structures after 18 h of immersion indicating uniform passive film covering the surface. The breakdown of passive film on the surface was also observed as thin layer distorted topography over ridged structure after immersion for 27 h (Fig. 4.3d) [124]. The interesting point in 8 M nitric acid as compared to 1 M, and 4 M nitric acid is that the breakdown of passive film can be well observed due to increase in aggressivity of the medium (Fig. 4.3d). The root mean square roughness value increased from 15 nm in as polished condition to 28 nm after immersion for 27 h which indicates degradation of passive film with increase in aggressivity of the medium. The situation in 11.5 M nitric acid was totally different from 1 M, 4 M and 8 M nitric acid, where a well formed passive film was not at all observed (Fig. 4.4a-b), instead stained surface with degraded passive film and corrosion product on the polished surface was observed with increase in immersion time (Fig. 4.4c-d) [125].

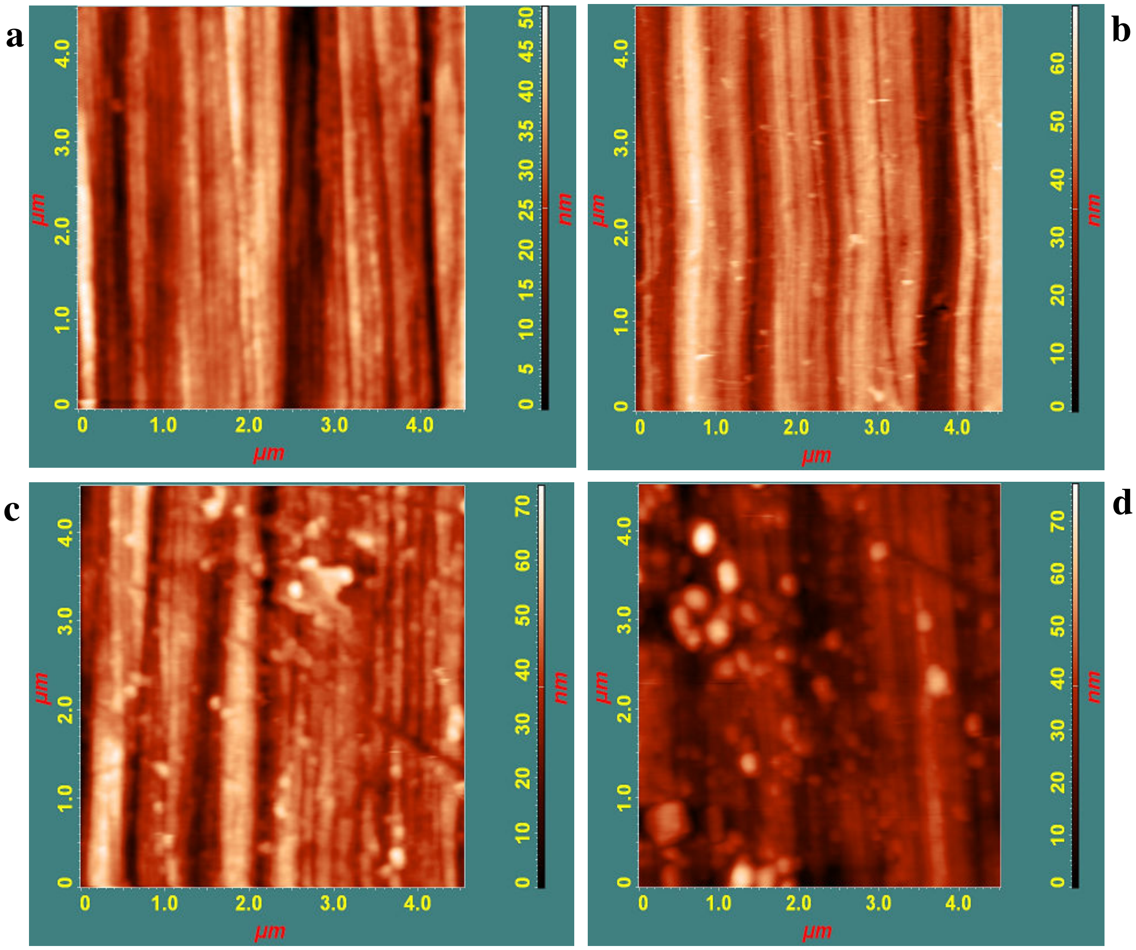

Fig. 4.4: Ex-situ surface morphology of 304L SS in 11.5 M HNO_3 with increase in immersion time, (a) As polished (b) 9 h, (c) 18 h, and (d) 27 h.

The root mean square surface roughness value increased significantly from 15 nm in as polished condition to 35 nm after 18 h of immersion to 52 nm after 27 h of immersion. The data obtained in the present study is fairly reproducible in different replicate tests, and are in accordance with data reported elsewhere [121-125].

Overall the ex-situ study demonstrates the morphological features of the developing passive film on 304L SS in nitric acid with increase in time as well as concentration of nitric acid. The observed surface morphological features in aforementioned concentrations are dependent on the passive film stability in nitric acid where aggressivity increases with rise in concentration. In 1 M and 4 M nitric acid, the surface remained in passive condition indicating high passive film stability in both the concentrations. However, in 8 M nitric acid as the aggressivity of the medium increases, the time required to attain equilibrium passive condition also increases. Moreover, the passive film formed under such condition is susceptible to rupture at structural heterogeneities. Similarly, in 11.5 M nitric acid passive film was unstable, and the surface became stained due to dissolution of passive film accumulating degraded film on the surface.

4.2.2 Potentiodynamic polarization study

The results of potentiodynamic polarization study carried out for 304L SS in 0.1 M, 0.5 M, 0.6 M, and 1 M nitric acid are as shown in Fig. 4.5, and the polarization parameters obtained from the plots are shown in Table. 4.1. The polarization plots in all the concentrations did not reveal any active-passive transition as after cathodic region entered into passive state followed by transpassive region. The results for polarization parameters showed, increase in corrosion potential (E_{corr}) by 50 mV vs. Ag/AgCl, increase in passive current density (I_{pass}) by one order of magnitude, increase in corrosion current density (I_{corr}) by two orders of magnitude, and decrease in transpassive potential ($E_{transpass}$) by 150 mV vs. Ag/AgCl, respectively from 0.1 M to 1 M nitric acid [20]. The standard deviation for E_{corr}, I_{corr}, I_{pass} and $E_{transpass}$ shown in Table. 1 are ± 6 mV vs. Ag/AgCl, $\pm 5 \times 10^{-3}$ $\mu A/cm^2$, ± 3 $\mu A/cm^2$ and ± 27 mV vs. Ag/AgCl, respectively [20].

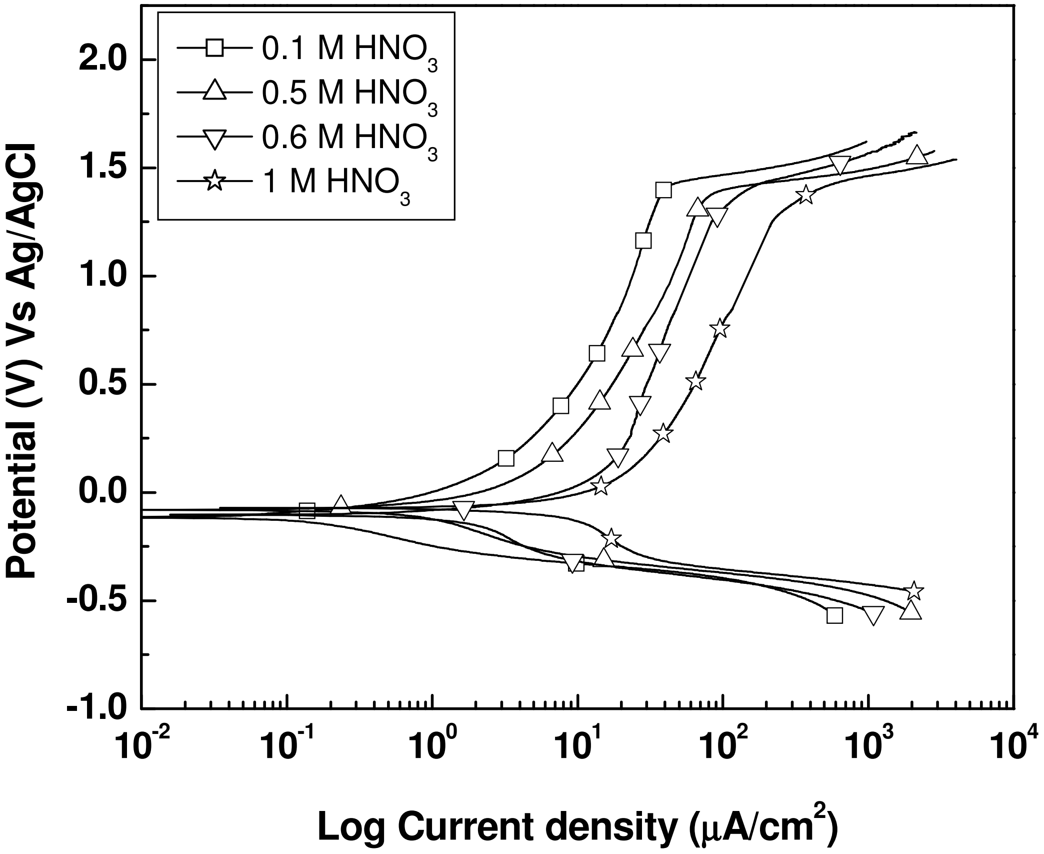

Fig.4.5: Potentiodynamic polarization study of 304L SS in 0.1 M, 0.5 M, 0.6 M and 1 M HNO$_3$ [20].

Conc of HNO$_3$	E_{corr} (mV vs Ag/AgCl)	I_{corr} (μA/cm^2)	I_{pass} (μA/cm^2)	$E_{transpass}$ (mV vs Ag/AgCl)
0.1 M HNO$_3$	-125	1.35×10^{-1}	6×10^{1}	1400
0.5 M HNO$_3$	-100	7.50×10^{-1}	9.5×10^{1}	1345
0.6 M HNO$_3$	-97	1.01×10^{1}	11×10^{1}	1330
1 M HNO$_3$	-75	1.65×10^{1}	1.45×10^{2}	1250

Table. 4.1: Average value of polarization parameters for 304L SS in 0.1 M, 0.5 M, 0.6 M and 1 M HNO$_3$ [20].

It is well known that the reduction of nitric acid is auto-catalytic in nature with the generation of aqueous HNO_2, and gaseous species such as NO and NO_2 depending up on the concentration used [3-7, 20-22, 41,42]. The sequences of reduction process of nitric acid are as given below.

$$HNO_3 \longrightarrow H^+ + NO_3^- \quad (1)$$

$$NO_3^- + 3H^+ + 2e^- \longrightarrow HNO_2 + H_2O \quad (2)$$

$$HNO_2 + H^+ + e^- \longrightarrow NO + H_2O \quad (3)$$

$$HNO_3 + NO \longrightarrow HNO_2 + NO_2 \quad (4)$$

The species which imposes redox potential to the electrochemical environment is nitrous acid (HNO_2). However, nitrous acid undergoes reduction to nitrogen monoxide (NO) by a heterogeneous charge transfer reaction (step.3) at electrode-electrolyte interface. Nitrous acid is then again regenerated along with nitrogen dioxide (NO_2) by heterogeneous chemical reaction of nitric acid and nitrogen monoxide, which is auto-catalytic in nature (step.4). Hence, with increase in nitric acid concentration the reduction rate, thus the oxidizing power also increases as the ratio of nitrous acid to nitric acid increases [20]. Consequently from kinetics point of view, the generation of nitrous acid which maintains the auto-catalytic nature, accelerates the corrosion rate due to oxidation of alloying elements such as Fe, and Cr. As a result, chromium which is key to passive film stability depletes from the surface leading to increase in passive current density, and corrosion current density. Similarly, owing to higher catalytic activity at higher concentration, the transpassive dissolution of passive film also becomes faster leading to decrease in transpassive potential [20].

4.2.3 In-situ electrochemical AFM surface morphology study

The results for in-situ passive film surface morphology study using EC-AFM of 304L SS in 0.1 M, 0.5 M, 0.6 M and 1 M HNO_3 up to 1100 mV (Ag/AgCl) at a particular location of the specimen i.e. without changing specimen position are shown in Fig. 4.6-4.9. The justification for showing morphology up to 1100 mV (Ag/AgCl) is because contrasting surface features were observed up to this potential, and especially around 1100 mV. Figure. 4.6a-d represents the surface morphology of 304L SS under immersion condition in 0.1 M nitric acid solution in as polished, 500 mV (Ag/AgCl), 900 mV (Ag/AgCl), and 1100 mV (Ag/AgCl), respectively [20].

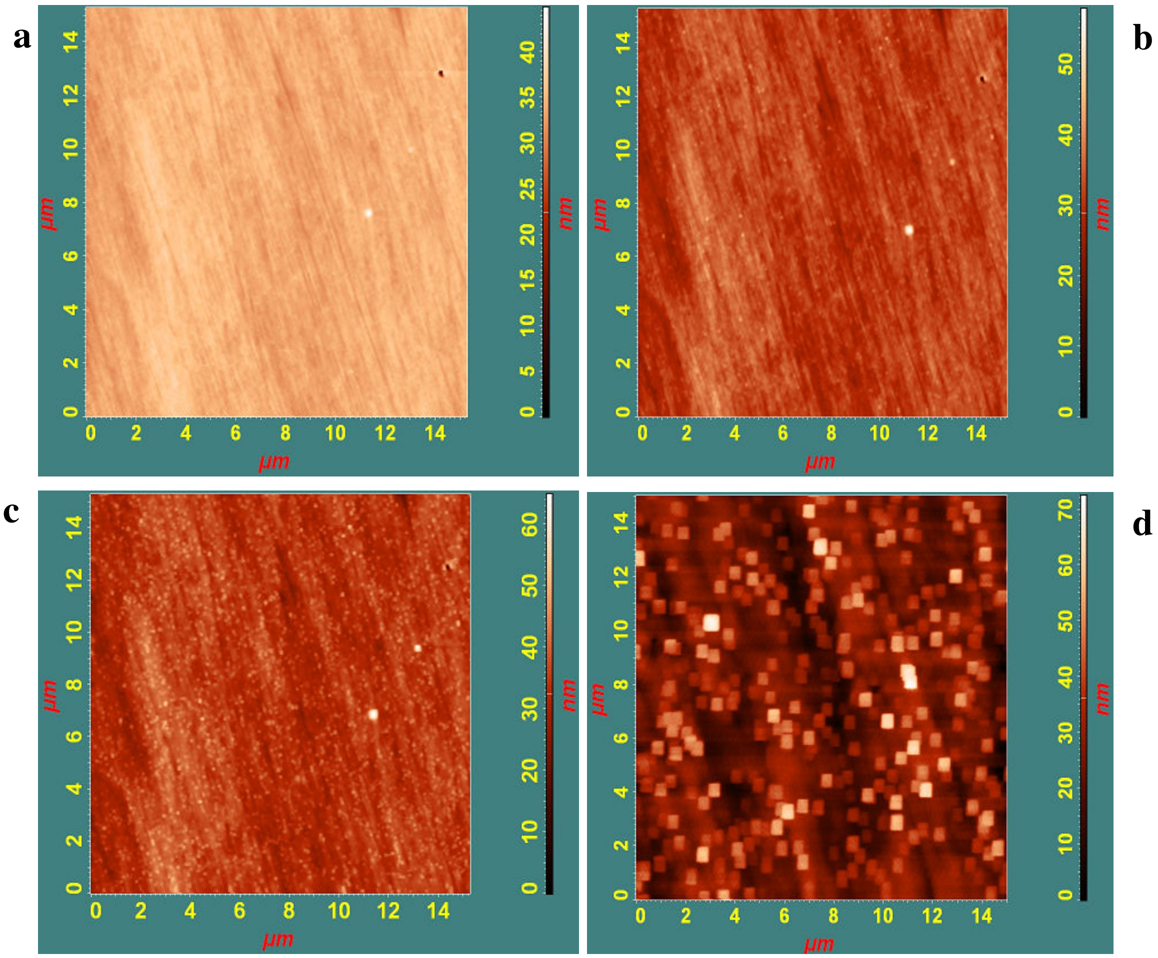

Fig. 4.6: In-situ surface morphology of 304L SS in 0.1 M HNO_3, (a) as polished, (b) 500 mV, (c) 900 mV and (d) 1100 mV vs. Ag/AgCl [20]

The results showed the growth of particles at 500 mV (Ag/AgCl), increase in size of the particle around 900 mV (Ag/AgCl), and acquired the shape of platelet [20,126] in the form of moiré-pattern around 1100 mV (Ag/AgCl). Moire-pattern is a growth process of successive layer in a stalking fashion, and arises due to small variation in the atomic scale. This type of growth mode of the platelets in aqueous solutions occurs in the nano-scopic regions of alloy-solution interface, and has been correlated with the growth of oxide layer by Viginal et al using limit height method [126]. Figure. 4.7a-d represents the surface morphology of 304L SS inside 0.5 M nitric acid solution in as polished, 500 mV (Ag/AgCl), 900 mV (Ag/AgCl), and 1100 mV (Ag/AgCl), respectively.

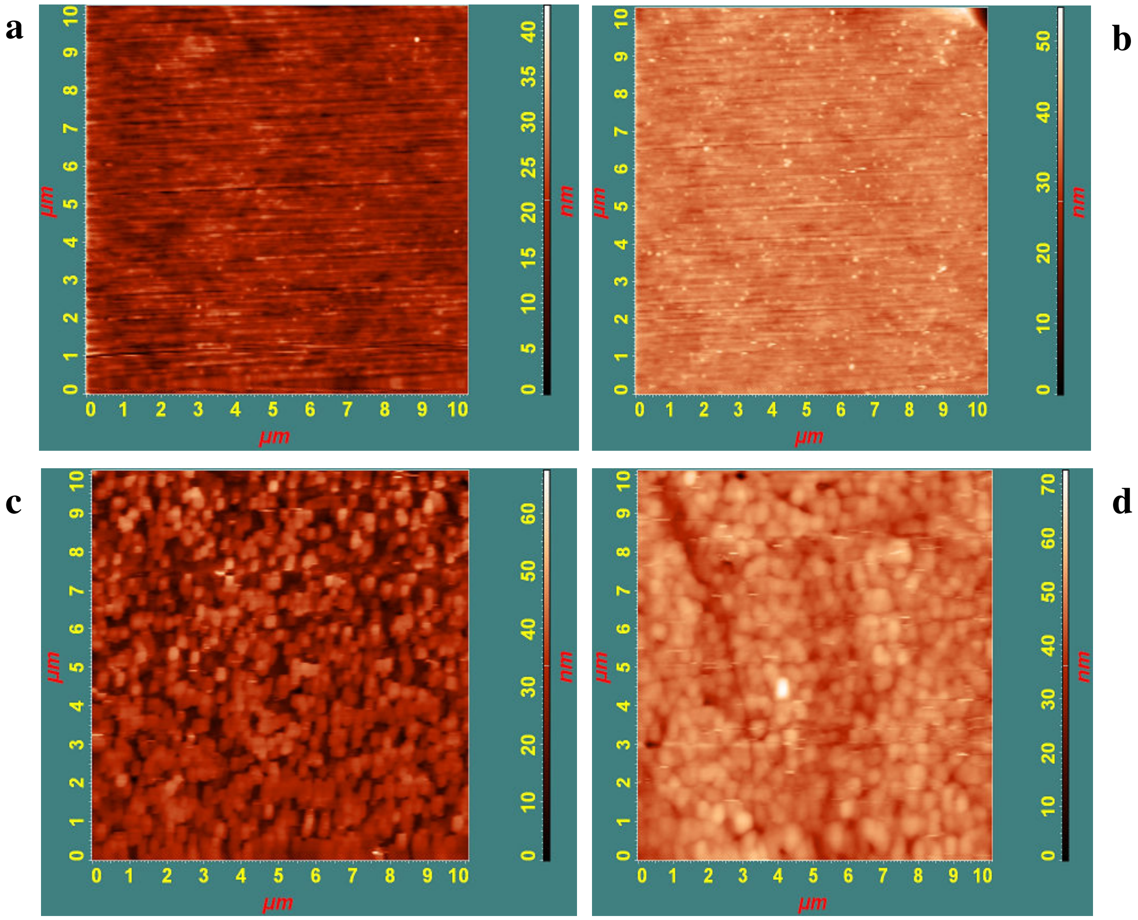

Fig. 4.7: In-situ surface morphology of 304L SS in 0.5 M HNO_3 (a) as polished, (b) 500 mV, (c) 900 mV and (d) 1100 mV vs. Ag/AgCl [20].

The surface morphologies in 0.5 M HNO_3 also shows the formation of the platelet like structures, however the platelets formed were fewer, and the size was also smaller as compared to 0.1 M HNO_3. The platelets, projected area (A_S), inclination (θ), disorientation angle (φ) between platelets for 0.1 M and 0.5 M nitric acid were calculated by using NOVA software assuming them as rectangular platelets, and the root mean square roughness on the surface are shown in Table. 4.2. Inclination (θ) was measured by taking three platelet i.e. two in the same layer and third in adjacent layer and, disorientation angle (φ) by taking three platelet in the same layer (top-bottom).

Conc of HNO_3	A_S (μm^2)	θ (Deg)	φ (Deg)	R_q (nm)
0.1 M HNO_3	0.8-1	45-65	2	9
0.5 M HNO_3	0.4-0.7	10-20	1	6
0.6 M HNO_3	-	-	-	4
1 M HNO_3	-	-	-	20

Table. 2: Statistical EC-AFM data for platelet growth in 0.1 M , 0.5 M, 0.6 M and 1 M HNO_3 [20].

It was found that, the size of the platelet decreased from 0.8 μm^2 to 0.4 μm^2, angle of inclination (θ) decreased from 45° to 10° with increase in concentration from 0.1 M to 0.5 M HNO_3. Similarly, disorientation angle decreased from 2° to 1° from 0.1 M HNO_3 to 0.5 M HNO_3. The important feature in both 0.1 M and 0.5 M HNO_3 is that, no visible corrosion process was observed on the surface and, the surface was fully covered by the platelets [20].

Figure. 4.8a-d represents the surface morphology of 304L SS under immersion condition in 0.6 M nitric acid in as polished, 500 mV (Ag/AgCl), 900 mV (Ag/AgCl), and 1100 mV (Ag/AgCl), respectively. The interesting feature observed at this concentration was the formation of platelet like structure as well as initiation of surface dissolution process around 1100 mV

(Ag/AgCl). The platelets formed were very few, and the surface dissolution occurred on brighter regions of the surface which are the topographically elevated portions on the surface (Fig. 4.8d) [20].

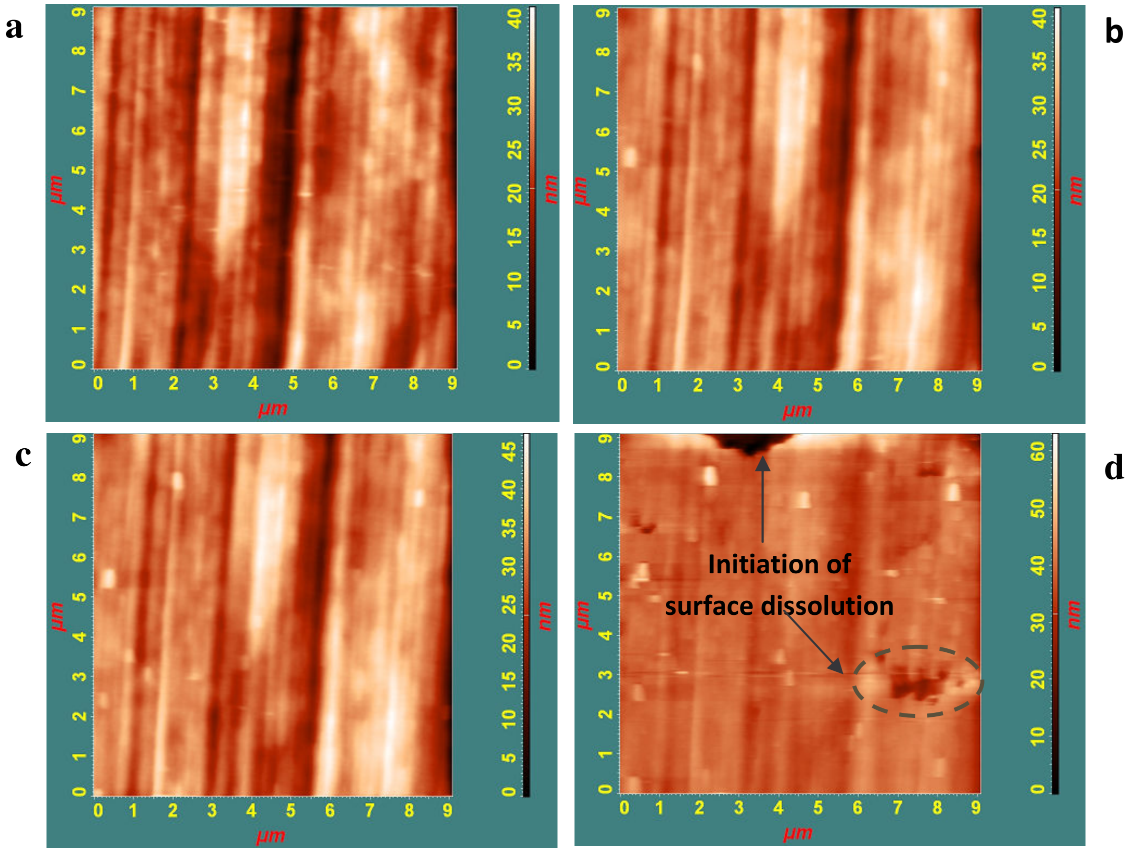

Fig. 4.8: In-situ surface morphology of 304L SS in 0.6 M nitric acid (a) as polished, (b) 500 mV, (c) 900 mV and (d) 1100 mV vs. Ag/AgCl [20].

Figure. 4.9a-d represents the surface morphology of 304L SS under immersion condition in 1 M nitric acid in as polished, 500 mV (Ag/AgCl), 900 mV (Ag/AgCl), and 1100 mV (Ag/AgCl), respectively. In 1 M HNO_3, the morphological features were different from other concentrations as formation of platelet like structure was not observed. Instead the grain boundaries opened up slowly with increase in potential showing well defined boundaries around 1100 mV (Ag/AgCl) (Fig. 4.9d). This is due to increase in oxidizing power of nitric acid owing to higher auto-catalytic activity which preferentially attacks the heterogeneous oxide boundaries [20].

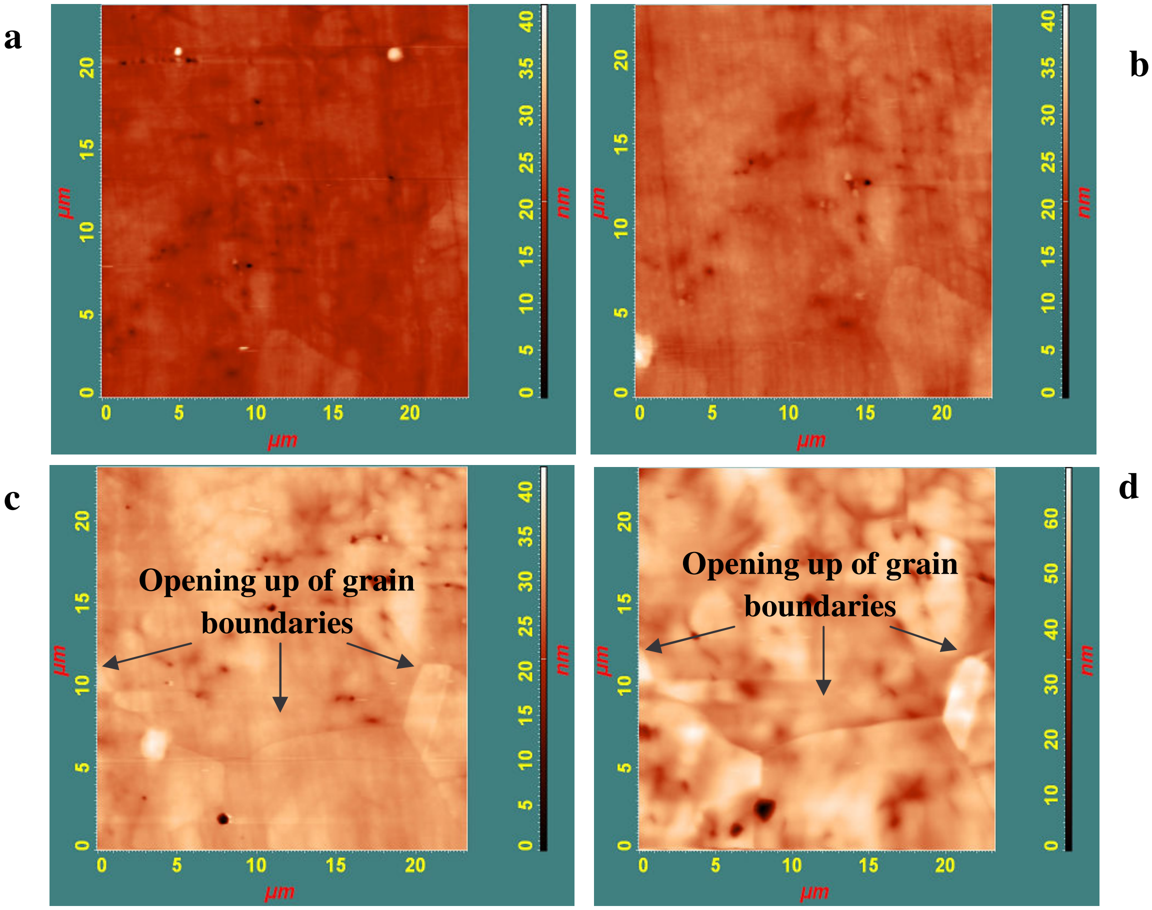

Fig. 4.9: In-situ surface morphology of 304L SS in 1 M nitric acid (a) as polished, (b) 500 mV, (c) 900 mV and (d) 1100 mV [20].

In general, the in-situ results demonstrate the formation and breakdown of passive film with increasing oxidizing power of nitric acid. According to the passivation model for austenitic stainless steel in acidic media [12, 16-19], passive film is a gel-like structure, which breaks down at local inhomogenities, thereby initiating surface dissolution. The decrease in size as well as formation of the platelets up to 0.6 M HNO_3 indicates homogenization and decay of passive film. Supportive evidence for the breakdown of passive film, and initiation of surface dissolution is apparent from morphology at 0.6 M HNO_3, where surface dissolution was observed in the presence of platelet like structures marked by arrows in Fig. 4.8d [20]. In 1 M nitric acid the platelet like structures were not observed, thus aggressive media has direct access to high energy regions on the surface such as grain boundaries. Hence, the oxide boundaries slowly opened up as potential increased showing aggressive attack around 1100 mV (Ag/AgCl) marked by arrows in Fig. 4.9c-d.

4.2.4 X-ray photoelectron spectroscopy study

X-ray photoelectron spectroscopy analysis of the passive films formed at 1100 mV (Ag/AgCl) in 0.1 M, 0.6 M, and 1 M nitric acid (Fig. 4.6d, 4.8d, 4.9d) along with specimens in as polished condition are shown in Fig. 4.10-4.13. XPS results in aforementioned concentration, and at 1100 mV are shown because characteristic change in passive film morphology was observed at these concentrations. The results presented in Fig. 4.10-4.13 represent the high resolution spectra of $Cr2p_{3/2}$ and O1s in as polished condition, and at concentrations of 0.1 M, 0.6 M, and 1 M nitric acid. Binding energy shift was observed mainly for chromium ($Cr2p_{3/2}$) and oxygen (O1s) profiles indicating changes in passive film composition. Figure. 4.10a-b represents the chromium, and oxygen profile in as polished condition.

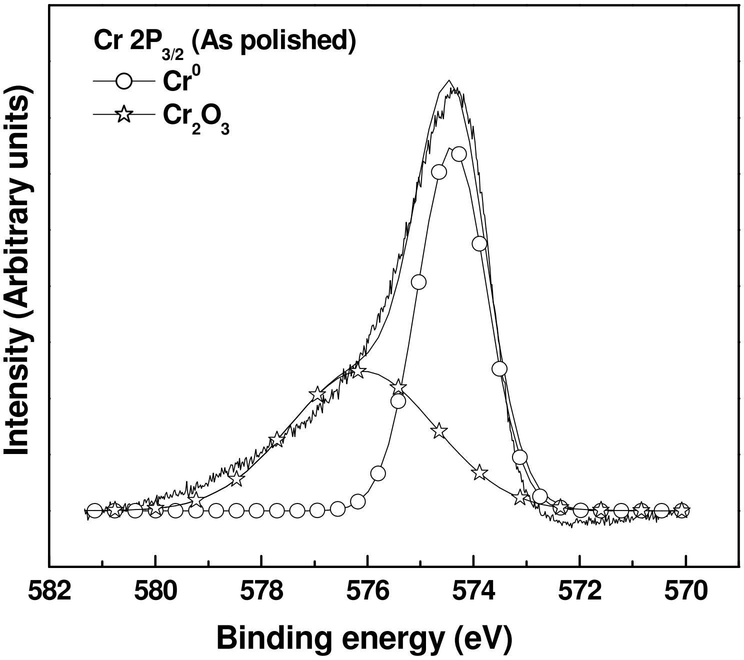

Fig. 4.10a: XPS profile of $Cr2p_{3/2}$ in as polished 304L SS.

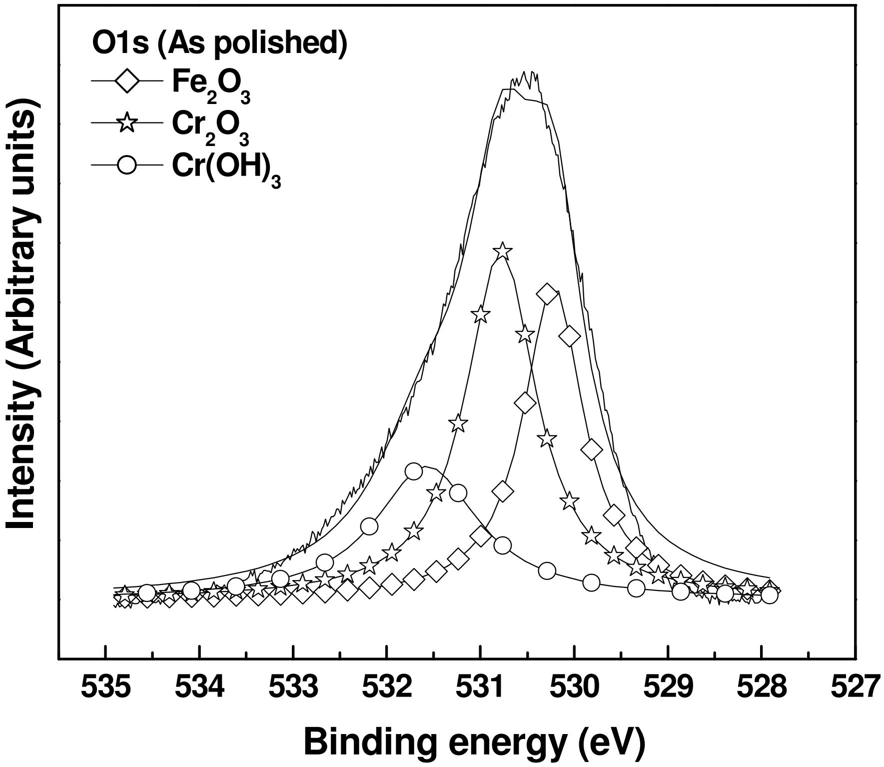

Fig. 4.10b: XPS profile of O_{1s} in as polished 304L SS.

The chromium profile showed mainly two peaks, the peak around 576.8 eV is attributed to chromium oxide (Cr_2O_3), and peak at 574.3 eV is due to elemental chromium (Cr^0) in 304L SS, respectively [127,128]. The oxygen profile in as polished condition revealed the presence of Fe_2O_3 (530.1 eV), Cr_2O_3 (530.8 eV) and $Cr(OH)_3$ (531.8 eV) respectively [127,128]. The presence of iron oxide, chromium oxide, and small amount of chromium hydroxide on the polished surface is due to naturally formed oxide, and hydroxide layer. The chromium hydroxide peak in chromium region ($Cr2p_{3/2}$) was not detected as the binding energy difference between $Cr(OH)_3$ and Cr_2O_3 is very small. At concentration of 0.1 M nitric acid, $Cr(OH)_3$ peak was observed predominantly in the chromium region around 577.7 eV, followed by chromium oxide peak at 576.8 eV, and elemental chromium at 574.3 eV, respectively (Fig. 4.11a). The shift in binding energy in chromium region was well reflected in shift in binding energy of oxygen profile also. The O1s profile at 0.1 M nitric acid showed the presence of intense $Cr(OH)_3$ peak at 531.8 eV along with normal Cr_2O_3, and Fe_2O_3 peak around 530.8 eV, and 530.1 eV, respectively (Fig. 4.11b). The chromium, and oxygen profile for 304L SS passivated in 0.5 M nitric acid were similar to that of 0. 1 M nitric acid.

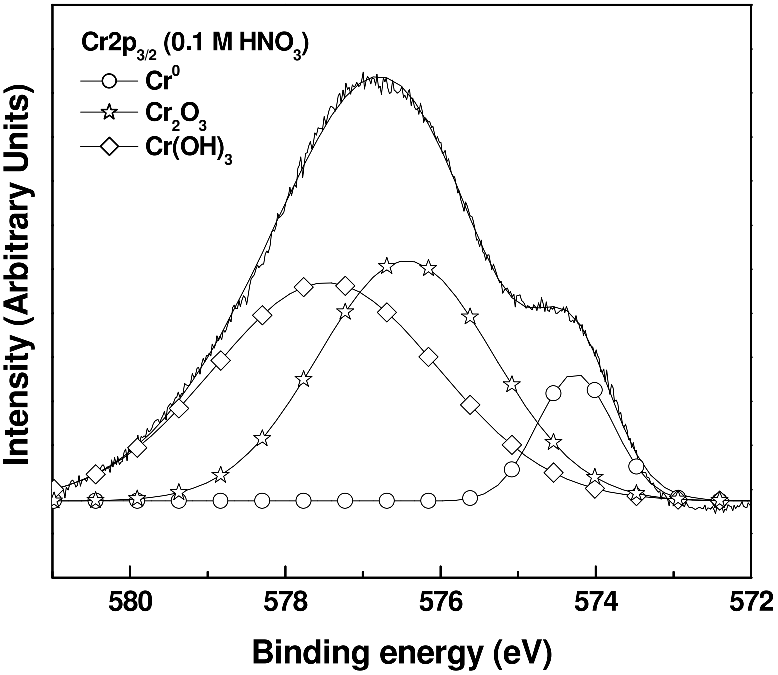

Fig. 4.11a: XPS profile of $Cr2p_{3/2}$ of 304L SS passivated in 0.1 M HNO_3.

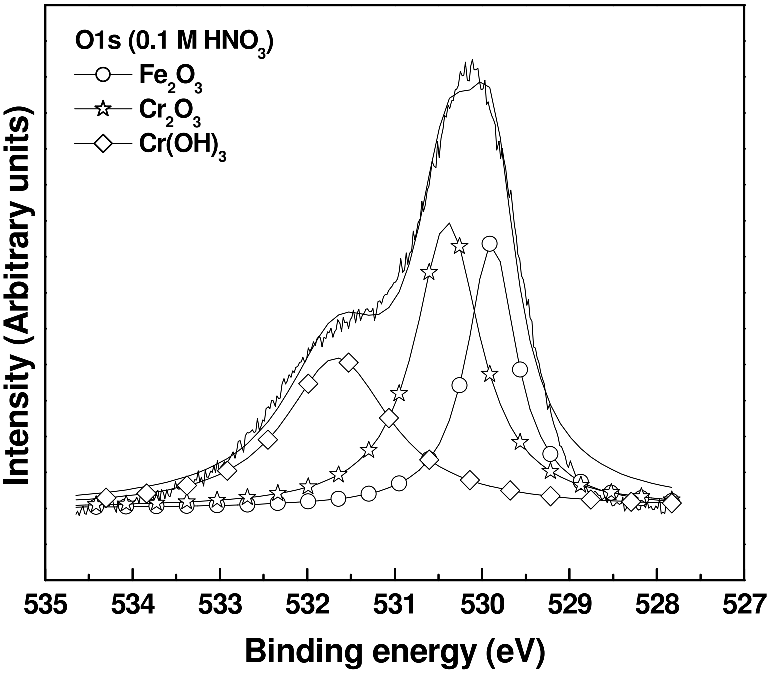

Fig.4.11b: XPS profile of O1s of 304L SS passivated in 0.1 M HNO_3.

The chromium, and oxygen profile for 304L SS passivated in 0.6 M nitric acid are shown in Fig. 4.12a-b. The chromium profile for 304L SS passivated in 0.6 M nitric acid showed the presence of $Cr(OH)_3$ peak around 577.7 eV, however the intensity was much less as compared to Cr_2O_3 around 576.8 eV (Fig. 4.12a). Similarly, the oxygen profile for 304L SS passivated in 0.6 M nitric acid also showed peak for $Cr(OH)_3$, but the intensity of Cr_2O_3 peak around 531.1 eV was much higher as compared to $Cr(OH)_3$ peak (Fig. 4.12b). The chromium, and oxygen profile for 304L SS passivated in 1 M nitric acid are shown in Fig. 4.13a-b. At 1 M nitric acid concentration the peak positions for chromium and oxygen were by and large similar to that of as polished condition. Chromium profile showed the presence of Cr_2O_3, and elemental chromium at their characteristics binding energy (Fig. 4.13a). However, no detectable peak for chromium hydroxide was observed in chromium region. The oxygen profile revealed the presence of Fe_2O_3, Cr_2O_3 and presence of $Cr(OH)_3$ (Fig. 4.13b) at their usual position as seen in case of as polished specimen.

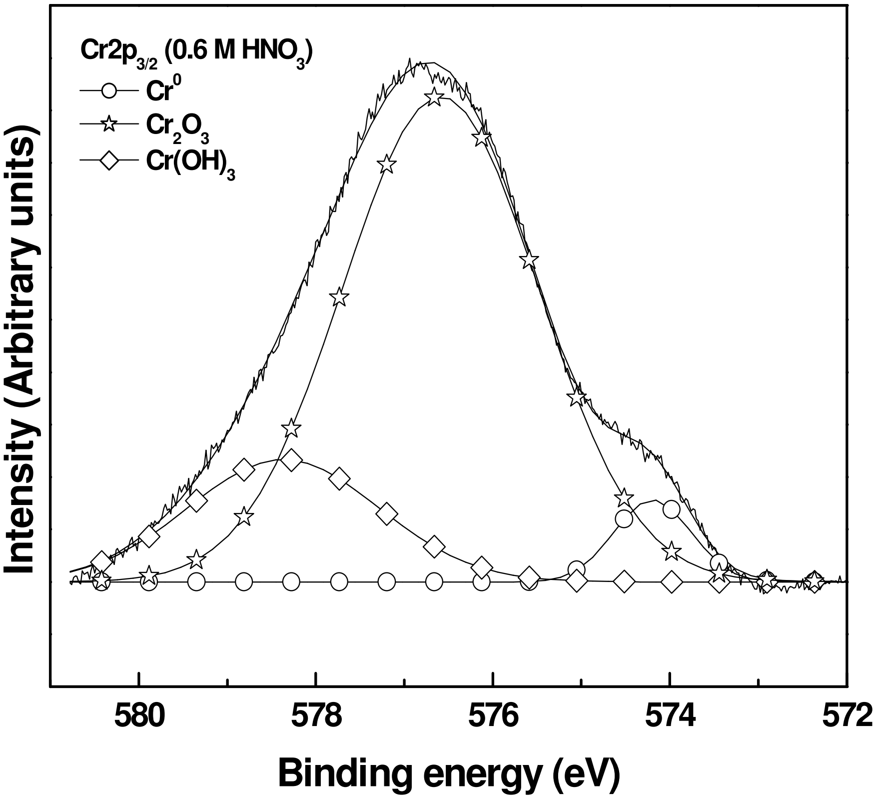

Fig. 4.12a: XPS profile of $Cr2p_{3/2}$ of 304L SS passivated in 0.6 M HNO_3.

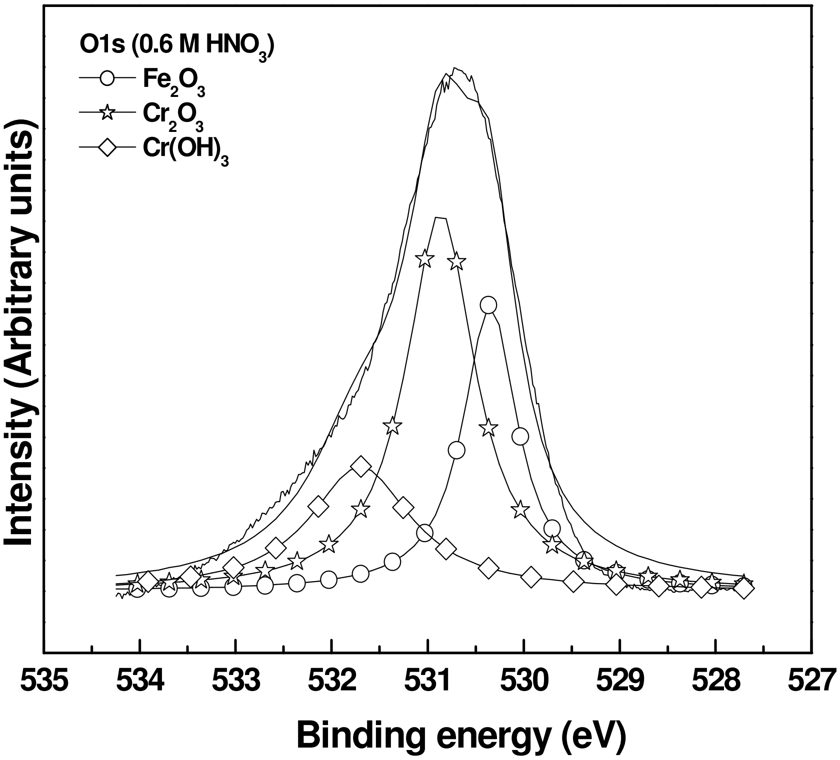

Fig. 4.12b: XPS profile of O1s of 304L SS passivated in 0.6 M HNO$_3$.

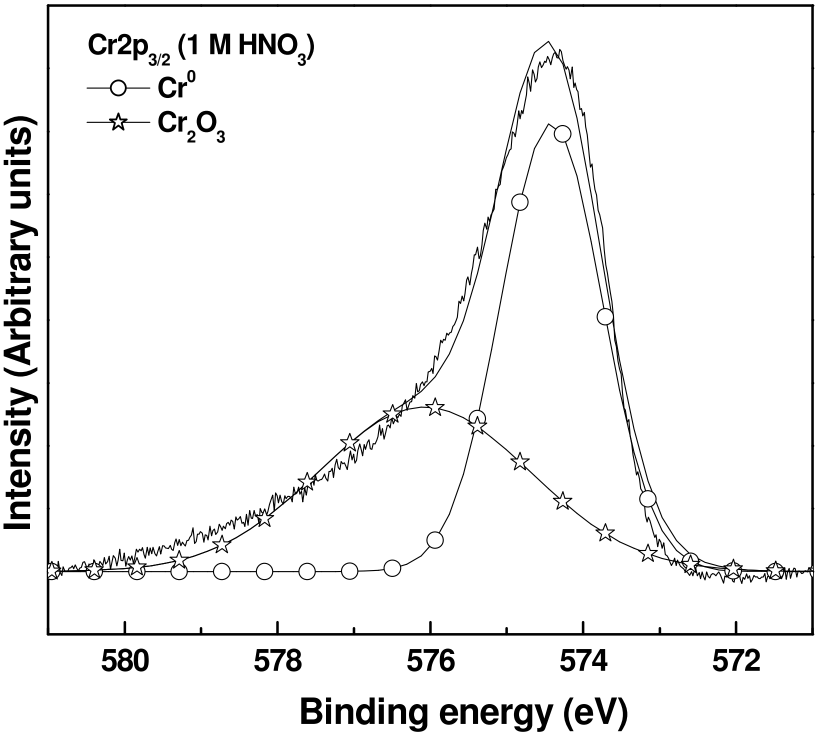

Fig. 4.13a: XPS profile of Cr2p$_{3/2}$ of 304L SS passivated in 1 M HNO$_3$.

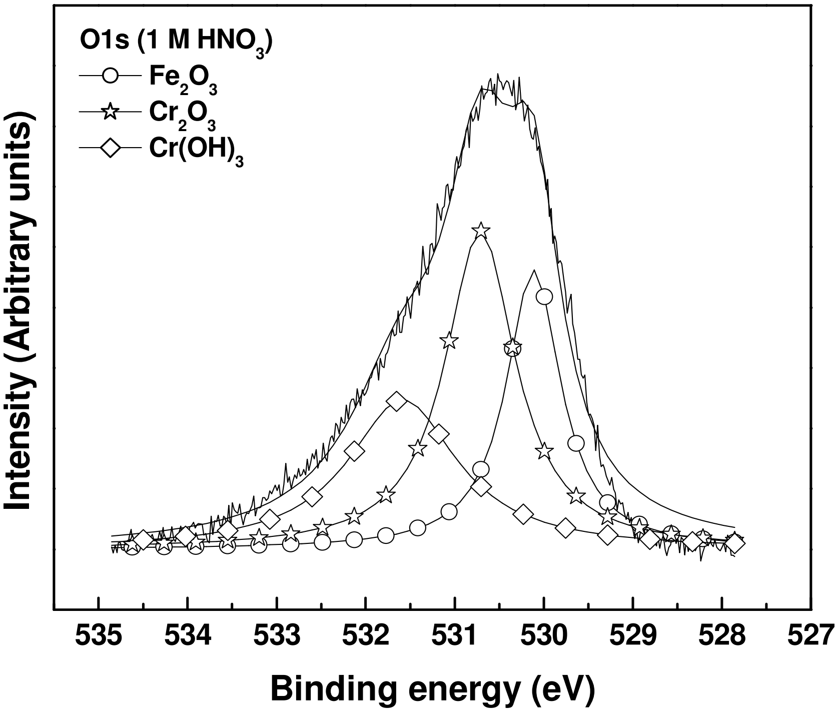

Fig. 4.13b: XPS profile of O1s region of 304L SS passivated in 1 M HNO_3.

Overall, X-ray photoelectron spectroscopy investigation in the aforementioned concentration of nitric acid revealed the generation, and decay of a duplex passive film consisting of hydroxide rich layer and oxide layer at lower concentration (0.1 M) which mostly transferred to oxide layer with increase in concentration (0.6 M, 1 M). The observed hydroxide-oxide synergism is accredited to the formation of adsorbed hydrated species of chromium, and their oxidation in the oxidizing environment of nitric acid with increase in concentration [127]. According to the passivation process of stainless steel [127-129], chromium mainly forms chromous (Cr^{2+}) species in the pre-passivation stage at lower potential, and thereby forms the hydrated species of $Cr(OH)_2$. Chromous hydroxide is electro-inactive in nature unless aggressive ions are present in electrochemical environment [130]. However, with increase in potential it transfers to chromic hydroxide [$Cr(OH)_3$], which is also a stable hydrated species of chromium. Moreover, towards higher potential, chromous ions (Cr^{2+}) also convert to chromic ions (Cr^{3+}), which subsequently forms $Cr(OH)_3$. The sequences of passivation process are as summarized below.

$$Cr \longrightarrow Cr^{2+} + 2e^- \qquad (1)$$

$$Cr^{2+} + 2H_2O \longrightarrow Cr(OH)_2 + 2H^+ \qquad (2)$$

$$Cr^{2+} \longrightarrow Cr^{3+} + e^- \qquad (3)$$

$$Cr^{3+} + 3H_2O \longrightarrow Cr(OH)_3 + 3H^+ \qquad (4)$$

Chromic hydroxide is stable in neutral and alkaline solution. However, in acidic environment with increase in oxidizing power it converts to chromium oxide by a solid state reaction as given below [128].

$$Cr(OH)_3 + Cr \longrightarrow Cr_2O_3 + 3H^+ + 3e^- \qquad (5)$$

Chromium oxide is an intermediate oxide, and has the properties between network forming (Cr-O-Cr) and modifying oxide [131]. With increasing oxidizing power of the electrochemical environment, the oxidation state of chromium increases, and the oxides formed are in general soluble in nitric acid [17-18]. Thus Cr_2O_3 which is key to passive film stability starts dissolving in acidic environment at structural heterogeneous areas and oxide layer depletes from the surface, thereby passive film disintegration initiates. The depletion of chromium oxide at weaker points such as inclusions and grain boundaries exposes the surface to aggressive medium where localized corrosion initiates. In extreme situation when potential reaches the transpassive domain most of chromium (III) is incorporated as chromium (VI) in the passive film, and these oxy-compounds dissolves faster in acidic solutions [14].

CHAPTER 5

Corrosion Behaviour of Nitrogen Ion Implanted AISI 304L Stainless Steel in Nitric Acid Medium

CHAPTER 5

Corrosion Behaviour of Nitrogen Ion Implanted AISI 304L Stainless Steel in Nitric Acid Medium

The effects sub-surface modification using nitrogen ion implantation, and its effect on the corrosion resistance of AISI 304L stainless steel in 1 M HNO_3 *medium is investigated. Nitrogen ion was implanted at 70 keV in the dose range of* 1×10^{15}, 1×10^{16}, 1×10^{17} *and* 2.5×10^{17} N^+/cm^2, *respectively. Glancing Incidence X-ray Diffraction results for unimplanted, and up to dose of* 1×10^{16} N^+/cm^2 *showed co-existence of γ-Fe & α'-Fe, and at higher doses (*1×10^{17}, 2.5×10^{17} N^+/cm^2*) preferential formation of chromium nitride was observed. X-ray photoelectron spectroscopy investigation confirmed the formation of chromium nitride at higher doses. Electrochemical corrosion investigation revealed nobler open circuit potential, decrease in passive current densities and corrosion current densities, and increase in polarization resistance with increase in dose rate. Surface morphology analysis after polarization study using atomic force microscope showed grain boundary dissolution for unimplanted specimens, and resistance to surface dissolution with increase in dose rate for implanted specimens.*

5.1 Introduction

Sub-surface modification is one of the technologically important methods to independently optimize the properties of near-surface of metallic materials, leaving underlying bulk unaffected for improved tribological properties, introduction of desired chemical properties, and to alter the metallurgical properties at nano-scale [132-136]. It is largely carried out by alloying with suitable elements, and often imparts good corrosion resistance to the base material. This approach of corrosion protection is due to the fact that alloying elements promote passivity, alter the cathodic, and anodic reaction rate to reduce the corrosion rate thereby offers greater scope for understanding the criteria of alloy design from corrosion point of view. The philosophy of selection of alloying element is based upon their ability to promote passivity by lowering the passivation potential, increasing the breakdown potential, and lowering the passive current density. Apart from this, sub-surface modification is important in locating specific species in the near-surface, and examining its usefulness as well as understanding the corrosion mechanism.

Ion implantation using accelerator is widely used as a sub-surface modification technique to modify the near-surface for improved corrosion resistance, superior mechanical, and tribological properties [49,50, 137-139]. The ability to introduce almost all elements into the surface region of material independent of thermodynamic constraints in precisely controlled way gives ion implantation advantage over other high temperature diffusion process for modifying the surface. As compared to conventional high temperature diffusion process for modifying the surface, ion implantation does not change the bulk properties of the material. Moreover, the oxide layer present on the surface also does not effect on the implantation process due to high energy of the ions. It can effectively control the structure, and composition in the near-surface region for enhancement in corrosion resistance. The improvements are attributed to amorphization of near surface layers, change in chemical composition, and formation of certain phases depending upon the chemical effects of the implanted ions, energy of the implanted ions, fluence rate, and the temperature during implantation process [140-142].

In the last decade, significant efforts have been made to study the effects of nitrogen implantation on corrosion behaviour of stainless steels due to their diversified ranges of use [21, 143-146]. Nitrogen as an alloying element in austenitic stainless steel has met with wide range of success, apart from being an austenite stabilizer, (1) it enhances passivation property in aggressive solutions, (2) provides beneficial effects from intergranular and pitting corrosion, (3) increases hardness, friction coefficient, load bearing capacity and wear behavior, and (4) improves fatigue resistance and cavitation corrosion behaviour [38, 51-54]. Song et al [147] have shown improvement in passivation property, and inhibition of anodic dissolution process of nitrogen implanted 18-8 austenitic stainless steel in acidic media. Hirvonen et al [148] have detected minor change in peak current density for nitrogen implanted AISI 420 SS in 1 N H_2SO_4 medium. Study by Kamachi Mudali et al [149] for pitting, and intergranular corrosion resistance of nitrogen implanted type 304 SS showed significant increase in pitting resistance as well as insignificant intergranular attack in acid chloride media. Picard et al [143] have indicated decrease in passive current density for nitrogen implanted AISI 304 SS as compared to untreated sample in 1 N H_2SO_4 medium, and study by Martinez et al [150] have reported improvement in corrosion property of nitrogen implanted 304L SS in chloride media. Nevertheless, nitrogen ion implantation has its own limitations, as it is not suited for very high abrasive conditions due to limited depth of implanted layer, and increase in energy of implantation to increase the depth of implanted layer deteriorates the corrosion resistance due to accumulation of surface defects owing to ballistic effect of ions [151]. Moreover, the mechanism by which nitrogen ion improves corrosion resistance is still under considerable debate.

The objective of the chapter is to evaluate the effect of sub-surface modification using nitrogen ion implantation on surface property and corrosion resistance of AISI 304L SS in nitric acid medium (1 M) using surface analytical, electrochemical, and morphological studies. The various effects of nitrogen implantation, and its correlation with passivity, and corrosion resistance are discussed and highlighted in this chapter.

5.2 Results and discussion

5.2. 1 Surface morphology study by AFM

The surface morphology of nitrogen implanted 304L SS at doses of 1×10^{15}, 1×10^{16} ,1×10^{17}, and 2.5×10^{17} N^+/cm^2 investigated using AFM are as shown in Fig. 5.1a-d [21].

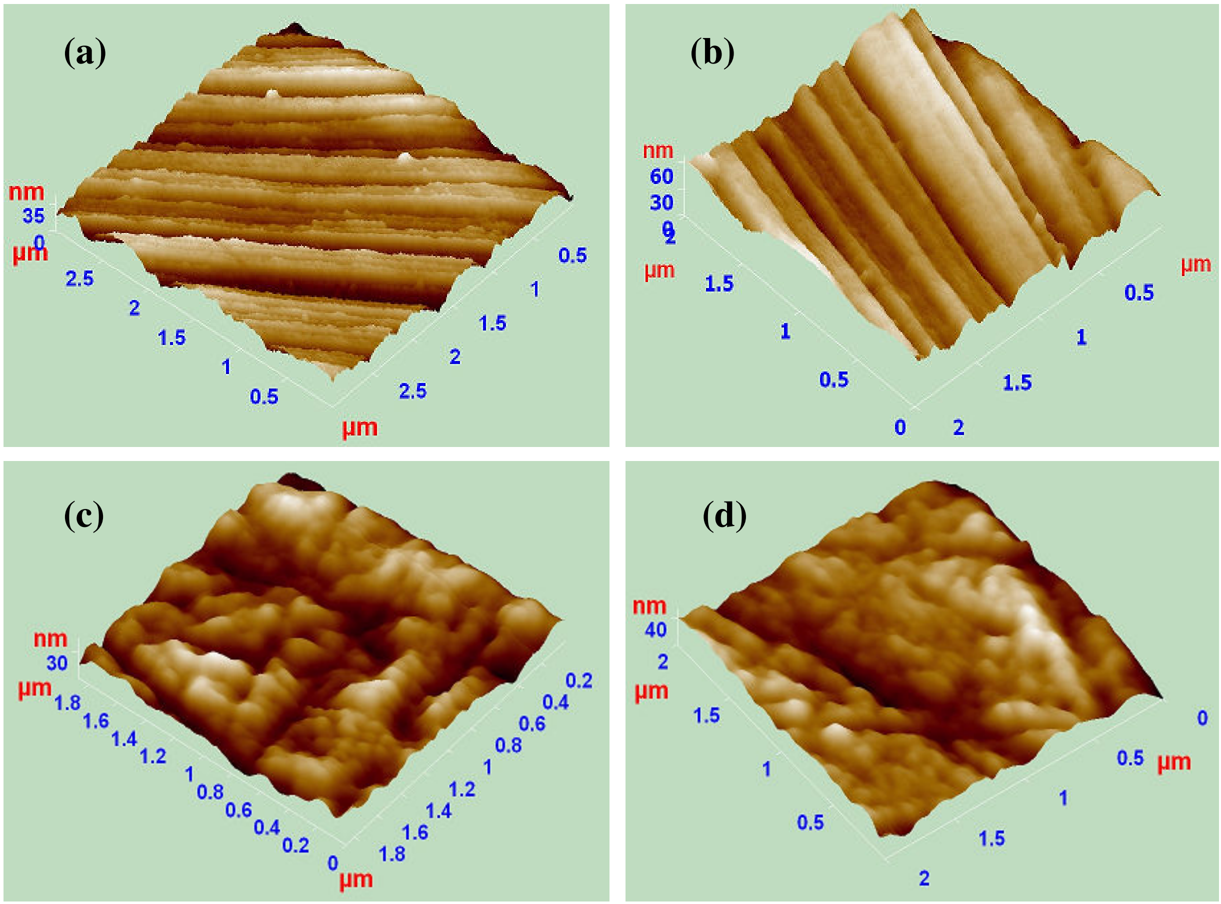

Fig.5.1: AFM surface morphology of nitrogen ion implanted 304L SS, (a) 1×10^{15} (b) 1×10^{16}, (c) 1×10^{17}, and (d) 2.5×10^{17} N^+/cm^2 [21]

Figure. 5.1a-b represents the surface morphology at dose of 1×10^{15}, 1×10^{16} N^+/cm^2. Lines in the same direction, and ridges present on the surface are due to mechanical polishing of the samples. The root mean square roughness (R_q) measured was around 12 nm. At higher dose of 1×10^{17}, 2.5×10^{17} N^+/cm^2 the surface appeared to be smooth, and the polishing lines, ridges were rarely visible with minor decrease in root mean square roughness value to 7 nm (Fig.5.1c-d). The minor decrease in root mean squre roughness value (R_q) is mainly due to homogenization of surface in the process of implantation due to preferential sputtering from the grain boundaries [143,152] overcoming the effect of surface inhomogenities. Chico et al [153] have reported the formation of pinhole like structures, and unidentified surface structures of peculiar shape at a dose of 1×10^{15} N^+/cm^2 at 80 keV energy. The occurrence of such surface features were also attributed to possible formation of interstitial nitrides of Cr and Fe. However, in the present study at a dose of 1×10^{15} N^+/cm^2 (Fig. 5.1a) such structures were not visible and the surface remained in as polished condition [21].

5.2. 2 Elemental analysis using secondary ion mass spectroscopy

The elemental depth profile analysis using SIMS of unimplanted, and nitrogen ion implanted (2.5×10^{17} N^+/cm^2) 304L SS are shown in Fig. 5.2a-b [21]. Contrast features were observed in the profiles for iron (Fe^{54}), chromium (Cr^{50}), nickel (Ni^{58}), and nitrogen (N^{14}) prior to and after nitrogen ion implantation. In case of unimplanted 304L SS specimens, iron, chromium, and nickel showed steady state with increase in depth sputtering (Fig. 5.2a).

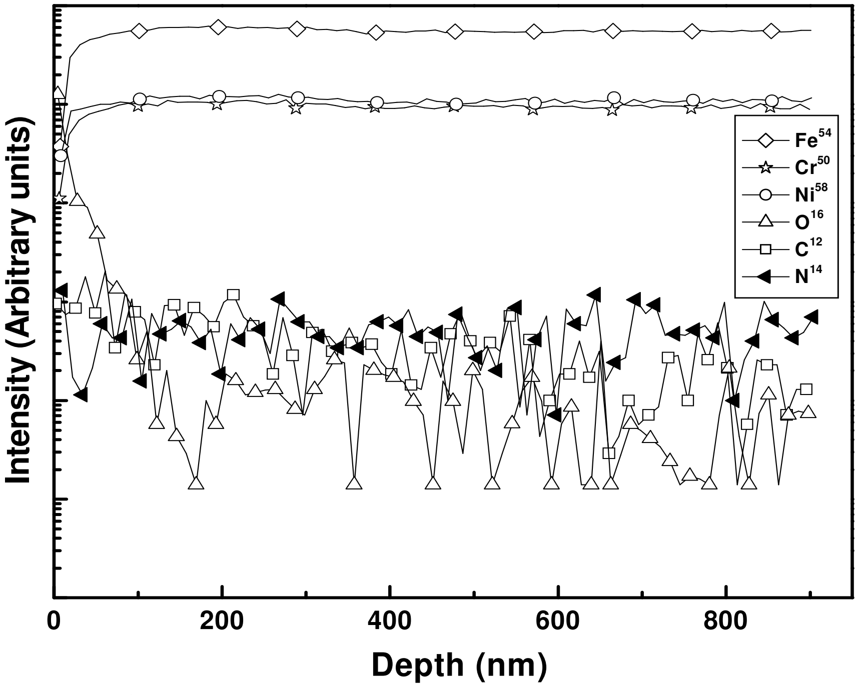

Fig. 5.2a: SIMS analysis of unimplanted 304L SS [21].

Presence of oxygen is due to the superficial oxide layers, and carbon at the surface is due to contamination during sample handling. For both the elements tailing was observed with increase in depth of sputtering, and intensity was much less as compared to major alloying elements. In case of nitrogen implanted sample (Fig. 5.2b) enrichment of nitrogen on the surface was observed in the form of two peaks. Owing to enrichment of nitrogen on the surface the corresponding profiles for Fe, Cr, and Ni showed initial decrease by passing through a shallow region, and attained steady state with increase in depth of sputtering [21].

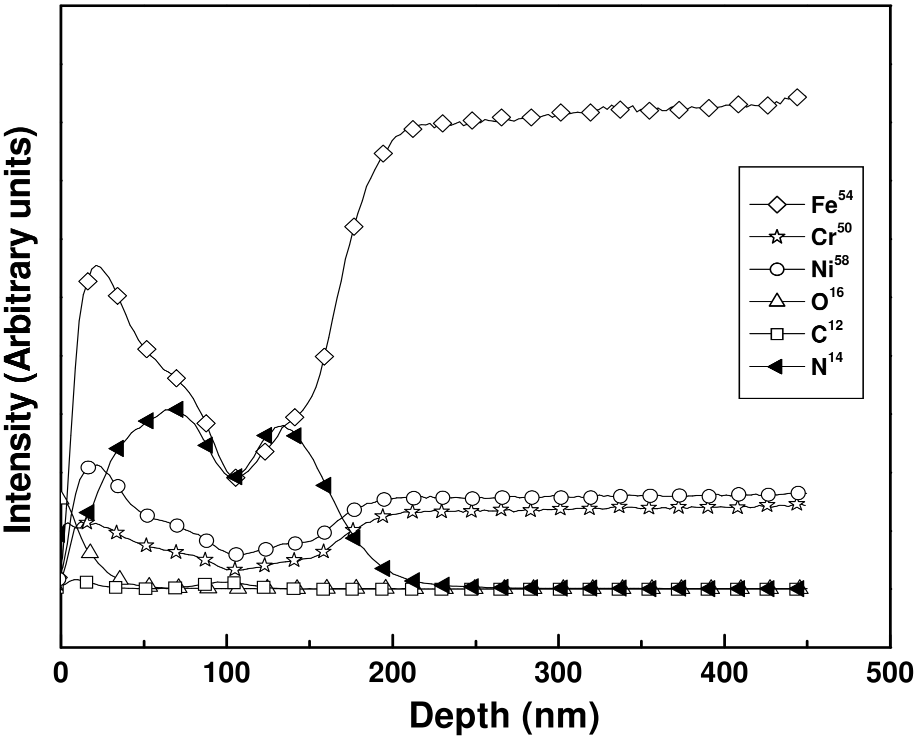

Fig. 5.2b: SIMS analysis of nitrogen implanted 304L SS (dose 2.5×10^{17} N^{+}/cm^{2}) [21].

SIMS Study by Guemmaz et al [154] for nitrogen implanted 316L SS also revealed two peaks in the nitrogen profile. The result obtained in the present study is in well agreement with study carried out by Guemmaz et al, and the possible reason for such type of peaks is attributed to different rate of sputtering of nitrogen from the surface, and from chromium nitride phase that forms at higher doses [21, 154].

5.2. 3 Study of phase formation by GIXRD

The Glancing Incidence X-Ray Diffraction patterns for unimplanted, and nitrogen implanted 304L SS at doses of 1×10^{16} N^+/cm^2 , 1×10^{17} N^+/cm^2 and 2.5×10^{17} N^+/cm^2 are depicted in Fig. 5.3 [21].

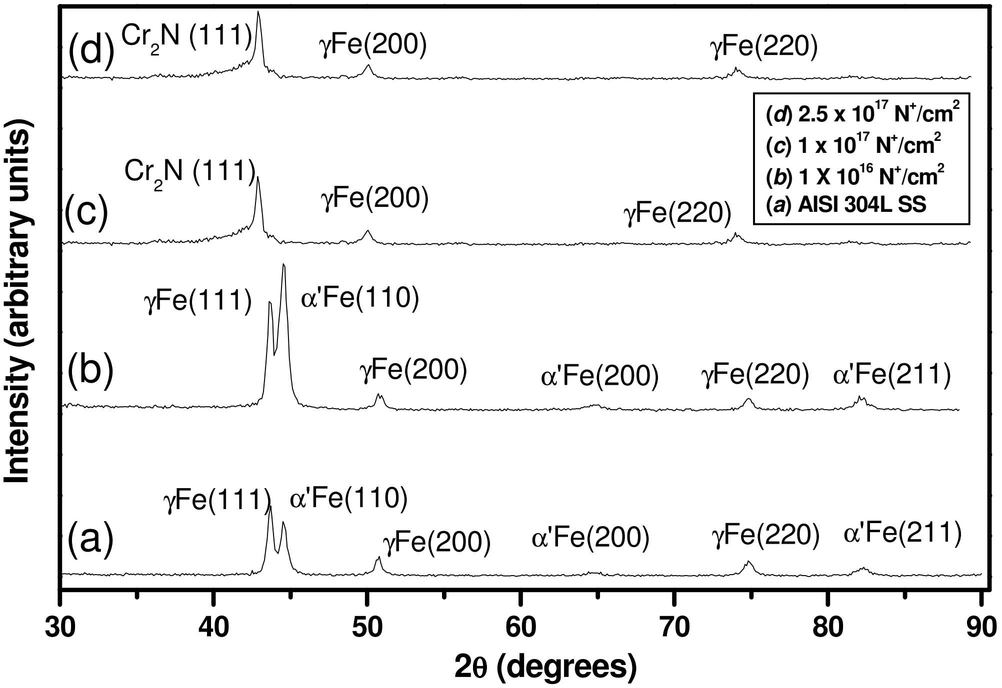

Fig. 5.3: GIXRD analysis of unimplanted, and nitrogen implanted 304L SS [21].

The profile for unimplanted specimens mostly revealed the presence of austenite peak at 43.7º [γFe(111)], and martensite peak at 44.7º [α′Fe(110)], respectively [155]. The martensite peak observed was due to work hardening of surface by mechanical grinding, and polishing during specimen preparation. Other peaks occurring at 50.7°, 65°, 74.8°, and 82.3° corresponds to γ-Fe(200), α′-Fe(200), γ-Fe(220), and α′-Fe (211) respectively [156]. The possible reason for the appearance of abnormal austenite, and martensite peaks is ascribed to existence of stacking faults on (111) plane of fcc lattice during cold rolling or most probably during mechanical preparation of specimens [157,158]. At a dose of 1×10^{16} N^+/cm^2 peaks observed were same except that, there was an increase in martensite peak intensity. The "ballistic effect" of ions implanted on the surface, can also induce shear deformation, and produce dislocations in fcc crystal structure which enhances the martensite peak character [159]. At highest dose of implantation (1×10^{17}, 2.5×10^{17} N^+/cm^2) a singlet peak was observed at 42.7° corresponding to the formation of chromium nitride [Cr_2N (111)] phase [160], and furthermore the peaks at 44.7° [α′Fe(110)], 65° [α′Fe(200)], and 82.3° [α´-Fe (211)] also disappeared [21].

5.2. 4 Metallographic characterization

The results for metallographic characterization of unimplanted, and nitrogen implanted 304L SS are shown in Fig. 5.4 [21].

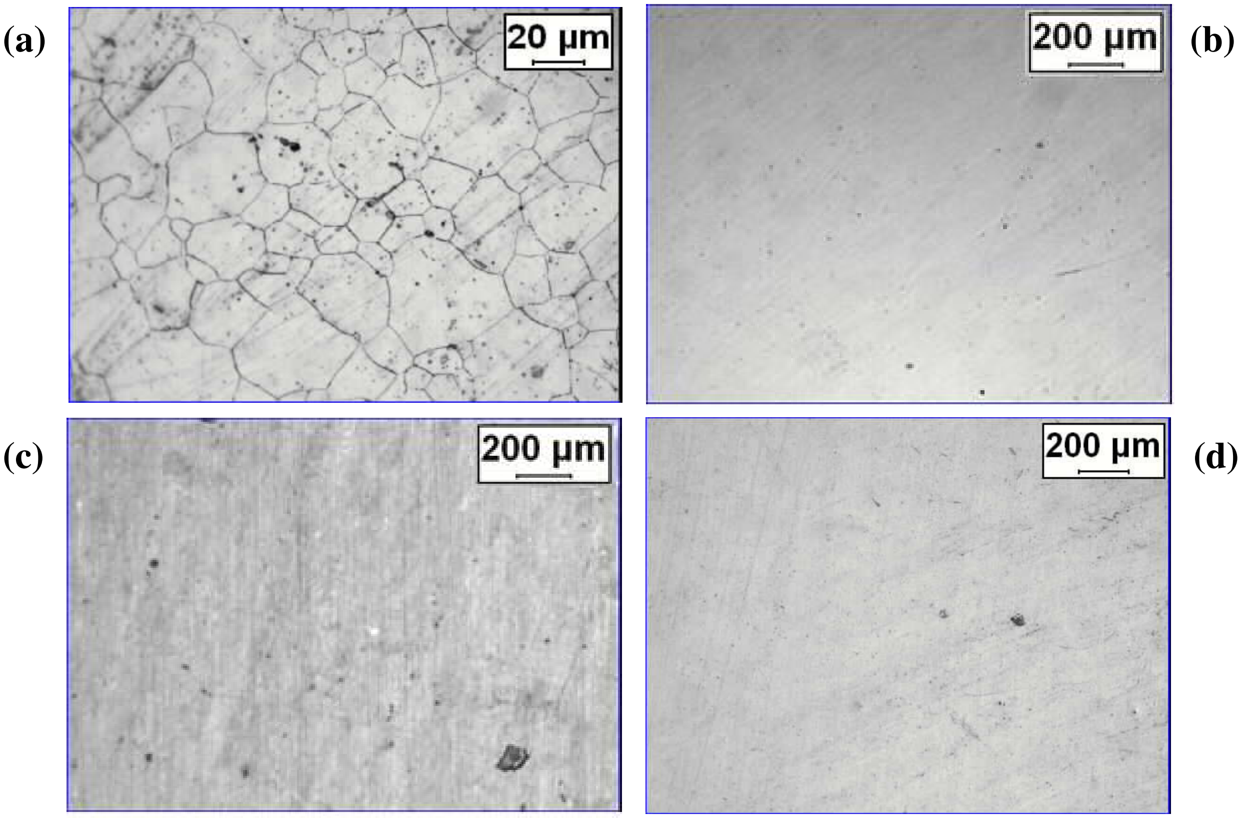

Fig. 5.4: Optical micrograph of 304L SS in (a) Oxalic acid (b) Vilella's reagent, (c) Murakami's reagent, and (d) at a dose of 1×10^{16} N^+/cm^2 in Villela's reagent [21].

The unimplanted specimen (Fig. 5.4a) revealed austenite microstructure in oxalic acid medium. However, the presence of martensite phase, and any abnormal ferrite phase present could not be confirmed by etching with Vilella's reagent, and Murakami's reagent (Fig. 5.4b-c). The reason is dissolution of superficial layer of martensite, and ferrite layer in the as polished specimens during etching. As in the case of unimplanted specimen, no ferrite microstructure was observed, for implanted specimens also it was not observed. The martensite phase at lower dose of 1×10^{16} N^+/cm^2 could not be revealed metallographically because of unknown depth, and extent of martensite formation (Fig. 5.4d). Second important factor is that the extent of martensite formation is dependent on energy of implantation, dose rate, and type of ion implanted. The degree of martensite transformation is higher for heavier ions. Study carried out by Chayahara et al [161] to investigate martensite transformation on 304 SS by high energy (1.5 MeV) implantation of heavier ions (Au^+) using TEM has revealed fewer martensite grains. However, in the present study as the energy of implantation and mass of ion implanted are small, the martensite layer formed is very thin to reveal the microstructure metallographically. As the dose rate increases the martensite layer formation is also coupled with nitride formation [162], and this has been reflected by the disappearance of main as well as additional martensite peaks at 44.7º, 65°, and 82.3° at dose of 1×10^{17} N^+/cm^2, 2.5×10^{17} N^+/cm^2, respectively. The martensite area provides defects and nitride nucleation sites, and acts as sinks for nitrogen [162]. Thus, at higher doses the martensite microstructure could not be revealed metallographically [21].

5.2. 5 X-ray photoelectron spectroscopy study

The detailed analysis of the $Cr2p_{3/2}$ and N1s energy levels has been carried out by deconvoluting the high resolution regions by asymmetric peak fitting procedure. The data presented in Fig. 5.5a-b is from the dose of 1×10^{17} N^+/cm^2 after sputtering for 3 min corresponding to erosion of 6 nm from the surface. The binding energy shift of Cr-Cr bond corresponding to the formation of Cr_2N was around 2 eV, and the shift in N1s binding energy was around 1 eV. In $Cr2p_{3/2}$ region (Fig. 5.6a) the peak around 576.7 eV corresponds to the contribution from Cr_2N, and peak around 574.6 eV corresponds to the contribution of elemental chromium from the stainless steel [163].

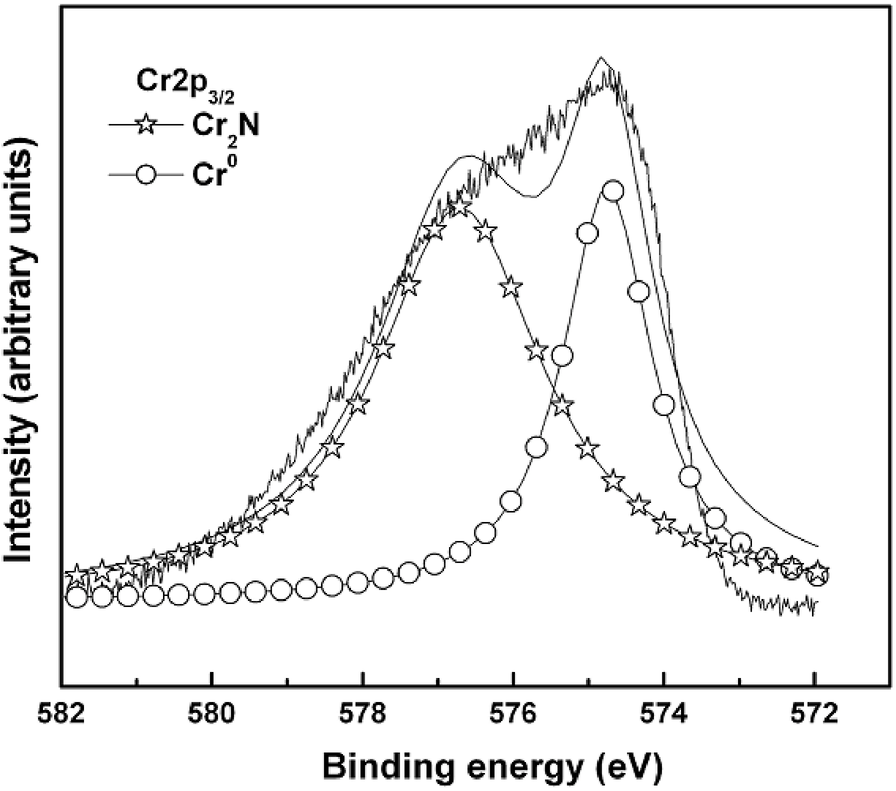

Fig. 5.5a: XPS spectra of chromium ($Cr2p_{3/2}$) region (dose 1×10^{17} N^+/cm^2)

For N1s region (Fig. 5.5b) the peak around 397.5 eV is attributed to N1s in Cr_2N compound and, the peak around 398.6 is from elemental N1s region [163]. The preferential formation of Cr_2N at this dose is attributed to the lower free energy of formation (ΔH_f = -125.4 Joule/mole) as compared to CrN (ΔH_f = -122.9 Joule/mole), and iron nitrides (ΔH_f = -10.45 Joule/mole) even though iron is the major alloying element in austenitic stainless steel [164]. At higher dose of 2.5×10^{17} N^+/cm^2, the peak position observed for $Cr2p_{3/2}$ and N1s were same. Thus, with increase in dose of nitrogen ion implantation, chromium preferentially combines with nitrogen forming Cr_2N phase in 304L SS due to limited solubility in austenitic stainless steel, as evidenced from GIXRD and XPS analysis [21].

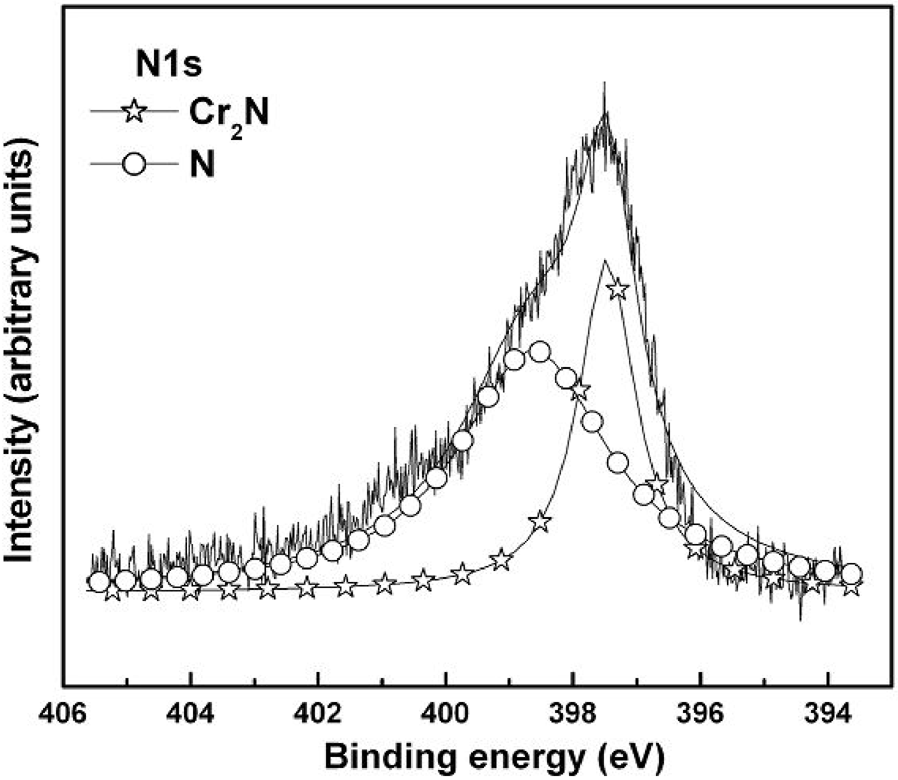

Fig. 5.5b: XPS spectra of nitrogen (N1s) region (dose 1×10^{17} N^+/cm^2) [21].

5.2. 6 Open circuit potential vs. time measurement

The OCP-time measurements for unimplanted and nitrogen implanted 304L SS during immersion for 6 h in 1 M HNO_3 are shown in Fig. 5.6 [21]. In unimplanted as well as in low dose of nitrogen implantation (1×10^{15}, 1×10^{16} N^+/cm^2), open circuit potential showed steady state indicating spontaneous, and stable passive film formation, and in case of higher dose nitrogen implanted specimens (1×10^{17} N^+/cm^2, 2.5×10^{17} N^+/cm^2), OCP shifted towards more nobler values. The OCP values improved from 100 mV vs. Ag/AgCl in unimplanted condition to 395 mV vs. Ag/AgCl with highest dose of nitrogen implantation. The improvement in open circuit potential by nitrogen implantation is an indication of stable passive film formation in nitric acid medium, and is attributed to enrichment of nitrogen at the surface of the alloy. When exposed to the electrochemical environment, nitrogen present at the surface forms ammonium ion which buffers the local *p*H, and enhance the passivation property [165]. According to study carried out by Newman et al [166], nitrogen enrichment on the surface can block the kinks and defects, making the surface homogenous, and forming uniform passive film over the surface. At higher doses the formation of chromium nitride also improves the passive film stability by forming rich oxide layer, and ammonium ions [166]. However, OCP gives only an initial indication of passive film behaviour, its actual stability in aggressive environment can be better understood from electrochemical perturbation conditions.

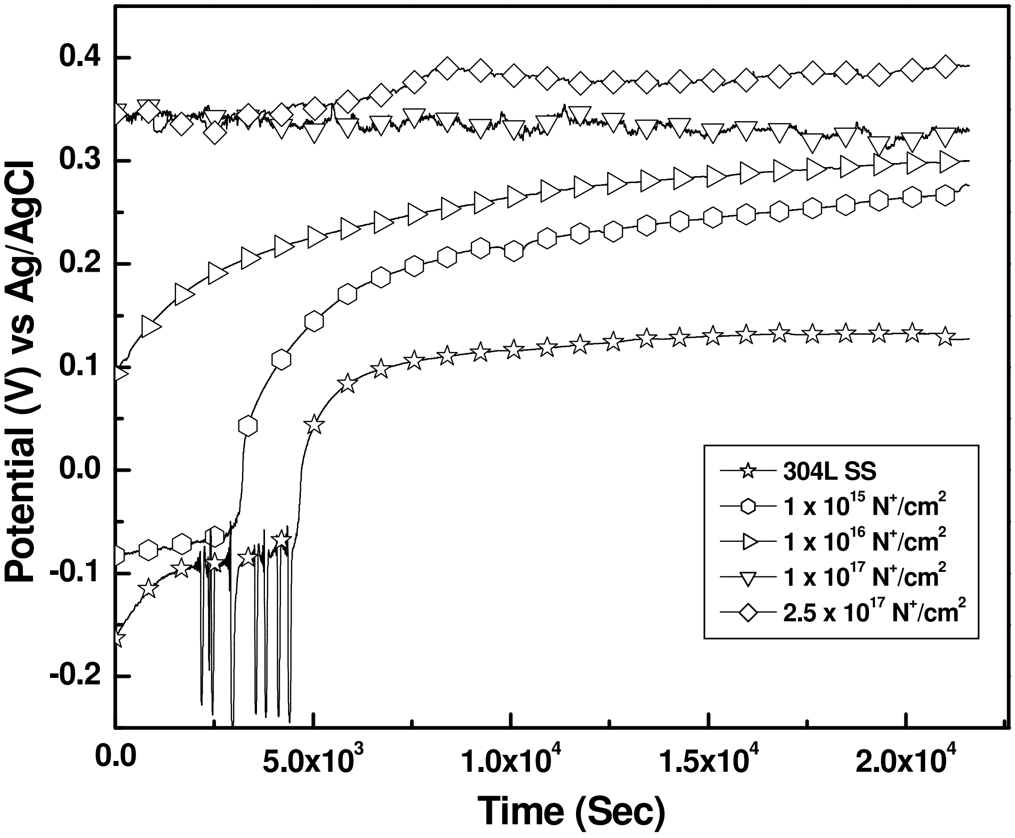

Fig. 5.6: OCP of unimplanted and nitrogen ion implanted 304L SS in 1 M HNO_3 [21]

5.2. 7 Potentiodynamic polarization study

The potentiodynamic anodic polarization results for the unimplanted, and nitrogen implanted 304L SS in 1 M HNO_3 are depicted in Fig. 5.7 [21]. The polarization plots for both unimplanted as well as nitrogen implanted specimens did not reveal any active-passive behaviour. After cathodic region it slowly translated into passive region followed by transpassive regime.

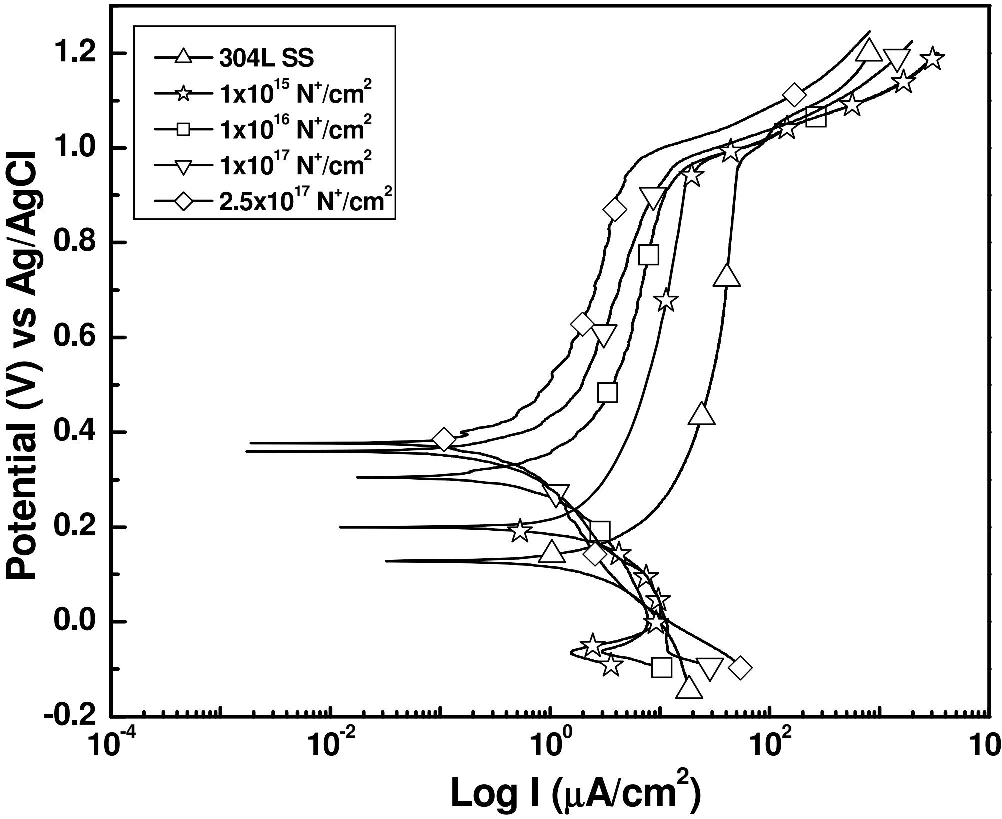

Fig. 5.7: Potentiodynamic polarization of unimplanted and nitrogen implanted 304L SS in 1 M HNO_3 [21].

The quantitative values for corrosion related parameters obtained from the polarization plots are mentioned in Table. 5.1. It is evident from Table. 5.1 that there was threefold increase in corrosion potential (E_{corr}), simultaneous decrease in corrosion current density (I_{corr}) by two order of magnitude, reduction in passivation current densities (I_{pass}) by one order, and marginal increase in transpassive potential ($E_{transapass}$) by 10 mV vs. Ag/AgCl from unimplanted to highest dose of nitrogen implantation. The maximum standard deviation for all the corrosion related parameters such as E_{corr}, I_{corr}, I_{pass} and $E_{transpass}$ mentioned in Table. 2 are within ± 15 mV vs. Ag/AgCl, ± 5×10^{-3} $\mu A/cm^2$, ± 3 $\mu A/cm^2$, and ± 7 mV vs. Ag/AgCl, respectively [21].

N^+ Dose	E_{corr} (mV vs. Ag/AgCl)	I_{corr} ($\mu A/cm^2$)	I_{pass} ($\mu A/cm^2$)	$E_{transpass}$ (mV vs. Ag/AgCl)
AISI 304L SS	120	1×10^0	6×10^1	975
1×10^{15} N^+/cm^2	195	5×10^{-1}	2×10^1	973
1×10^{16} N^+/cm^2	300	3×10^{-1}	1.6×10^1	971
1×10^{17} N^+/cm^2	354	8×10^{-2}	1.2×10^1	978
2.5×10^{17} N^+/cm^2	375	5×10^{-2}	7×10^0	985

Table. 5.1: Polarization parameters for unimplanted and nitrogen implanted 304L SS in 1 M HNO_3 [21]

Nitric acid is an oxidizing acid, and the E_{corr}, I_{corr}, I_{pass} and $E_{transpass}$ are dependent on the extent of reduction of nitric acid, which itself is concentration dependent [3-7, 20-22, 41,42]. With higher auto-catalytic activity of nitric acid, corrosion current density, passivation current density, corrosion potential increases, and transpassive potential decreases because of faster transpassive dissolution of oxide film on the surface. In the present investigation the improvement in corrosion potential, reduction in passivation current density, and corrosion current density and marginal improvement in transpassive potential reflects the beneficial effects of nitrogen on corrosion resistance of 304L SS in nitric acid medium [21, 147, 167].

The overall improvement in corrosion potential, passivation current density and corrosion current density is attributed to the combined effect of implanted nitrogen as well as formation of chromium nitride. The implanted nitrogen plays major role in modifying electrochemical properties mainly by forming ammonium ions which can further form nitrite or nitrate ions, thereby increase the local *p*H, and shift the corrosion potential in the noble direction. The formation of ammonium ion was first proposed by Osozawa et al [165] and suggested that, ammonium ions formed restricts the decrease of *p*H at active sites on the surface such as grain boundaries and kinks where passive film formation is highly unstable. However, the degree of ammonium ion formation increases with increase in amount of nitrogen, and decreases with applied potential [168]. To compensate the decreasing amount of ammonium ions at higher potential Kamachi Mudali et al proposed the subsequent formation of nitrates and nitrites ions from ammonium ion, which are well known for their strong stabilizing effect on passive film stability [169]. Similarly, it has also been observed the nitrogen implantation decreases the passive current density as well as corrosion current density owing to enrichment of nitrogen beneath the passive film, and segregation of nitrogen during polarization forming interstitial nitrides which decreases the surface dissolution process. Abundant evidence for the existence of nitrogen beneath the passive film subsist from surface analytical technique, and the decrease in passivation current is because of charge associated with passive film formation is reduced by implanted nitrogen [168]. Thus, less current is required for passive film growth with increase in nitrogen implantation dose. The decrease in corrosion current density can also be attributed to surface segregation of nitrogen to the oxide-metal interface during anodic polarization forming stable interstitial nitride phases of chromium [163, 166, 170, 171]. The formation of chromium nitride during polarization has been confirmed by several studies, and has been argued on the basis of low solubility of nitrogen in austenitic stainless steel, and thermodynamically favourable process of formation. These phases are proposed [166] to act as a kinetic barrier to the dissolution of the alloy because their dissolution reaction is slow due to multi-electron transfer process.

5.2. 8 Electrochemical impedance measurement

The electrochemical impedance measurements for both prior to, and after implantation with different doses of nitrogen in open circuit potential condition are presented in Fig. 5.8. All the Nyquist plots showed unfinished semi-circular arc and appropriate equivalent circuit is chosen as shown in Fig. 3.9 to evaluate the obtained experimental results. The fitted parameters for double layer capacitance (C_{dl}), polarization resistance (R_p), and solution resistance (R_S) are as shown in Table. 5.2 [21].

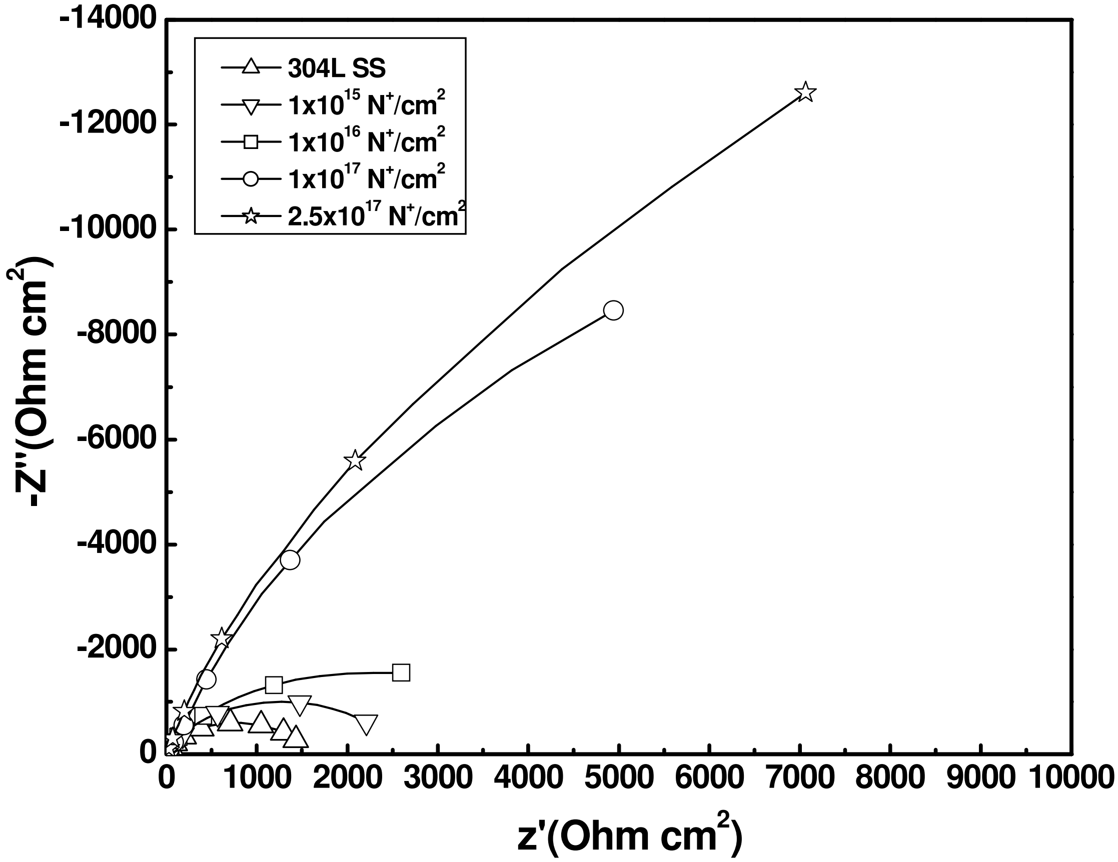

Fig. 5.8: Electrochemical impedance of unimplanted and nitrogen implanted 304L SS in 1 M HNO_3 [21].

In impedance measurement, high R_p value implies good corrosion resistance, and the low capacitance value signifies long term stability of the passive film. A comparison of Nyquist plots between unimplanted, and implanted with different doses of nitrogen revealed better passive film stability with nitrogen implantation owing to improvement in polarization resistance, and decrease in double layer capacitance. The polarization resistance increased from 1675 Ohm cm^2 in unimplanted condition to 7085 Ohm cm^2 at highest dose of nitrogen implantation. Similarly, the double layer capacitance showed a reduction in total retained charge from 1×10^{-5} F/cm^2 to 1×10^{-8}

F/cm^2 with highest dose of nitrogen indicating better passive film stability. Thus, in general with increasing dose of nitrogen ion implantation increase in the stability of the passive film was observed as compared to unimplanted condition [21].

N^+ Dose	R_S (ohm)	R_P (ohm cm^2)	C_{dl} (F/cm^2)
AISI 304L SS	5	1675	1×10^{-5}
1×10^{15} N^+/cm^2	5	2223	1×10^{-6}
1×10^{16} N^+/cm^2	5	2690	1×10^{-6}
1×10^{17} N^+/cm^2	7	4970	1×10^{-7}
2.5×10^{17} N^+/cm^2	7	7085	1×10^{-8}

Table. 5.2: EIS fitted values of unimplanted and nitrogen implanted 304L SS in 1 M HNO_3 [21].

The ennoblement observed in polarization resistance is due to stable and readily passive film formation because of presence of interfacial nitrogen at lower doses, and due to formation of chromium nitride at higher doses. At lower doses, nitrogen is present in solid solution gets enriched in passive film by bonding with chromium and thereby enhances passive film stability [168]. The implanted nitrogen can also accumulate at the surface inhomogenities such as surface defects and kinks making the passive film homogenous [166]. At higher doses presence of chromium nitride provides rich supply of chromium due to high chromium content in nitrides for oxide film formation [166].

The corrosion behaviour of stainless steels is often correlated to the protective nature of the passive oxide film, which forms on the surface. If one takes the reasonable view that corrosion initiate at flaws in the film or substrate (inclusions), then one can argue that the surface film composition will directly reflect corrosion resistance of the alloys. Based on the present results, correlation between surface analytical studies and corrosion resistance of 304L SS in 1 M nitric acid is well observed. With increase in nitrogen ion dose, decrease in passivation current density, corrosion current density and marginal increase transpassive potential revealing improvement in corrosion resistance was observed. Similarly, in both SIMS and XPS analysis increase in nitrogen intensity revealing enrichment of nitrogen as well as formation of chromium nitride was observed. Thus, the beneficial role of nitrogen from corrosion results with surface analysis using SIMS and XPS can be well correlated.

5.2. 9 Surface morphology study after potentiodynamic polarization

Surface morphology analysis of the unimplanted and nitrogen ion implanted samples with dose of 1×10^{16} and 2.5×10^{17} N^+/cm^2 after potentiodynamic polarization experiment investigated using AFM are as shown in Fig. 5.9a-c [21]. Distinctive surface morphologies were observed depending on the dose of nitrogen implantation, as clear from the topographic images indicating effect of nitrogen in slowing down the surface dissolution process leading to improvement in corrosion resistance. The unimplnated samples showed grain boundary dissolution in nitric acid medium with visibility of well demarked grain boundaries (Fig. 5.9a). The large damage, and highly corrugated surface morphology is due to intergranular corrosion of austenitic stainless steel occurring in nitric acid medium [20,21].

The extent of grain boundary dissolution lessened at a dose of 1×10^{16} N^+/cm^2 (Fig. 5.9b) as less clear grain boundaries were visible. At highest dose of implantation of 2.5×10^{17} N^+/cm^2 the grain boundary dissolution disappeared and at some places selective attack was observed (Fig. 5.10c). The selective attack is attributed to the presence of surface inhomogenities on the surface. The root mean square roughness (R_q) calculated for the aforementioned polarized test samples in 1 M nitric acid are, 238 nm for unimplanted, 110 nm for dose of 1×10^{16} N^+/cm^2 and 46 nm for dose of 2.5×10^{17} N^+/cm^2, respectively. The decrease in root mean square roughness with increase in nitrogen ion implantation dose after polarization is attributed to lesser surface dissolution [21].

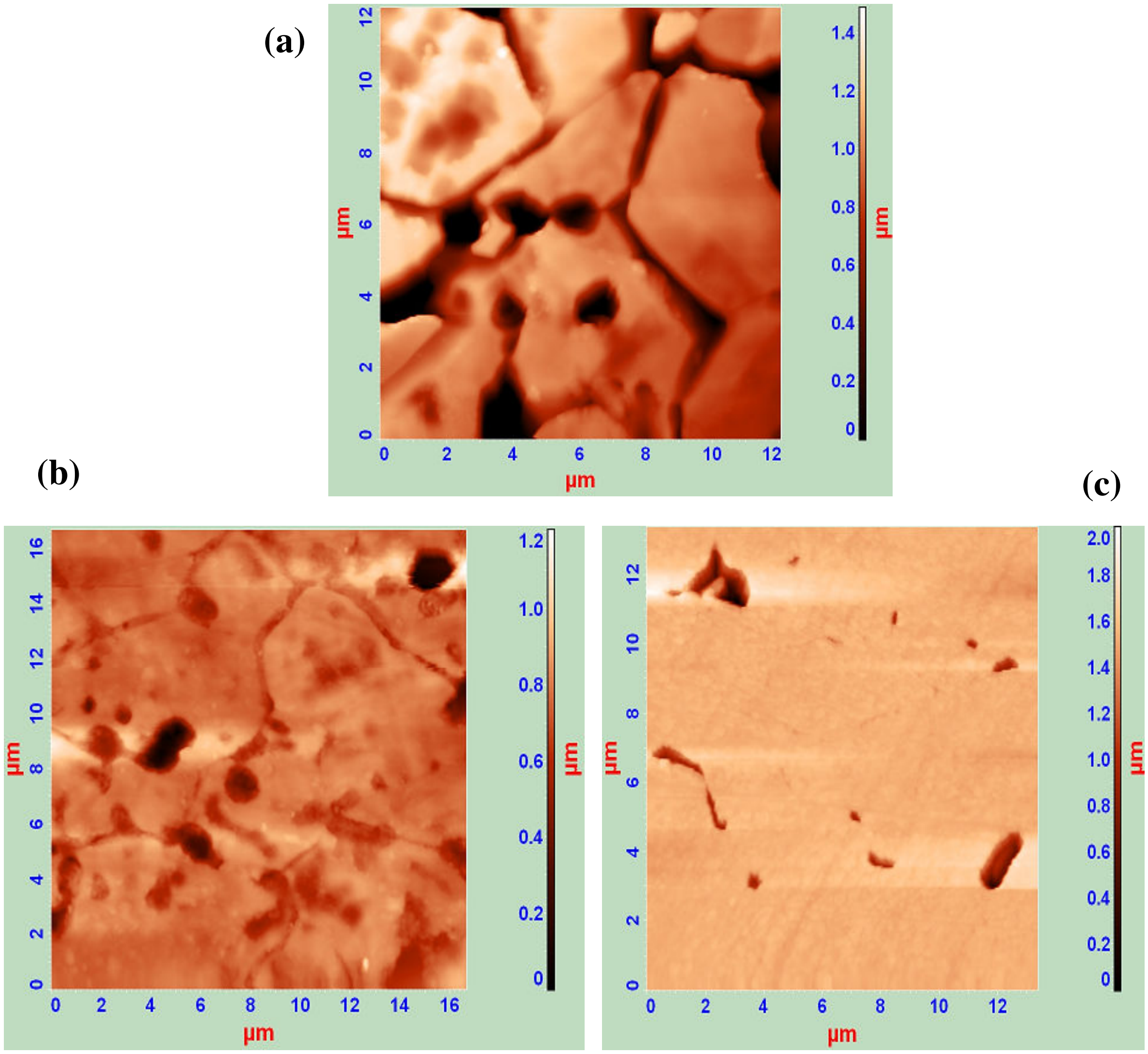

Fig.5.9: AFM surface morphology after potentiodynamic polarization study, Unimplanted (b) 1×10^{16} and (c) 2.5×10^{17} N^+/cm^2 [21]

Surface morphology investigation by Picard et al [143] on corroded samples of low energy nitrogen implanted austenitic stainless steel has revealed alternate black, and white regions in acidic media due to topographic contrasts, and preferential etching in the twinning directions. However, in the present study such topographical demarcations were not observed, and only grain boundary dissolution was observed for unimplanted and lower dose specimens, which happened due to preferential attack along the grain boundaries in nitric acid medium. The unimplanted, and implanted with highest dose of nitrogen showed completely different features. At higher doses formation of Cr_2N and segregation of nitrogen to the metal-oxide interface during polarization forming nitrides is the factor resisting surface dissolution [21].

CHAPTER 6

Corrosion Performance of Ti, TiO_2, and Duplex Ti-TiO_2 Coated AISI 304L Stainless Steel in Nitric Acid Medium

CHAPTER 6

Corrosion Performance of Ti, TiO_2 and Duplex Ti-TiO_2 Coated 304L Stainless Steel in Nitric Acid Medium

---

The chapter deals with the investigation on the corrosion performance of sputter deposited Ti, TiO_2, and duplex Ti-TiO_2 coated AISI 304L SS in nitric acid medium using electrochemical, and surface morphological studies. The results revealed that, titanium coated 304L SS showed moderate to marginal improvement in corrosion resistance in 1 M, and 8 M nitric acid, respectively. TiO_2 coated 304L SS specimens showed good corrosion resistance in both low (1 M), and high concentration (8 M), however towards higher concentration uniform dissolution of the coated surface was observed. Duplex Ti-TiO_2 coated 304L SS specimens showed improved corrosion resistance as compared to both Ti and TiO_2 coated 304L SS from dilute to concentrated medium. The percentage of protection efficiency for base material increases significantly for duplex Ti-TiO_2 coating as compared to single layer Ti and TiO_2 coatings.

6.1 Introduction

Top surface modification using protective coating is the easiest method for improving surface properties as well as corrosion resistance of the base material. The tailoring of the surface properties such as minimizing the surface irregularities and roughness on the surface, impeding the current flow between the microscopic anodic and cathodic regions on the surface, enhancing barrier layer strength thereby improving the passivation property are the essential coating properties which imparts greater resistance to the base material from corrosive environments [172-175]. Thus, protective coatings are unique, and are most widely used in varying forms in a broad range of corrosive environments to increase the performance of engineering materials. Moreover, the basis for wide spread use of coatings as well as development and advancement in coating technology is because of increasing corrosion problems, tighter economic situations, and optimal performance of technologically important materials in various industries.

The expanding use of coatings has generated the need to understand the coating-solution interaction in order to access their performance in corrosive environments. The basic approach of corrosion protection using protective coating is to cut-off the interaction between substrate and electrochemical environment by forming barrier over the surface [176-178]. The coating-solution interaction is a complex phenomenon, and involves various factors such as barrier property, topographical features, surface chemistry, and solution chemistry etc. The primary factor responsible for corrosion resistance is the barrier property of the coating which is determined by the lattice energy, bond energy, heat of formation, and band gap etc of the coated material [176,179]. Topographical features have greater influence on the corrosion resistance. The coating topography is largely anisotropic, and the presences of pores, pinholes, flaws on the coated surface are detrimental from corrosion point of view [180,181]. The surface chemistry of coating such as chemical composition of coating has its effect on the electrochemical properties at the coating-solution interface as well as coating-substrate interface [182,183]. Similarly, the solution composition also has effect on electrochemical corrosion properties such as corrosion potential, passivation tendency and corrosion current from the coated surface etc [184,185]. All the above properties decide the life time of the coating in corrosive medium.

Metallic and ceramic coatings with good passivity, low electronic conductance or insulating properties, and good tribological properties are known to protect the metals, and alloys from corrosive environments [186-189]. Titanium (Ti), and titanium dioxide (TiO_2) are widely used as coating materials for corrosion protection in a wide range of corrosive environments [190-

193]. As a single phase coating, titanium promotes passivity by spontaneous reaction in electrochemical environment owing to its reactive nature, reduces the anodic activity, and thus often used in severe conditions. Ceramic coatings such as TiO_2 is more resistant to corrosion than their metallic counterpart due to high level of chemical inertness, easily tailorable electronic properties, and good passivation ability in corrosive solutions. However, both metallic and ceramic coatings contain large number of surface defects such as flaws, pores, pinholes, and inter-columnar boundaries which have deleterious effect on the corrosion properties. Thus, in order to reduce these surface defects and improve the corrosion performance, it is quite essential to control the microstructure of the coated surface [194]. Duplex interlayer coatings are extremely effective in protecting the materials by modifying the microstructure, morphology, and passivation tendency of the base material in electrochemical solutions [195]. The interlayer reduces the number of pinholes, and restricts the capillary action of the electrolyte at coating-electrolyte interface thereby decreases the extent of sub-coating corrosion. Moreover, the interlayer can increase the passivation property in the eventuality of passive film breakdown thereby galvanic effect can be minimized which in general accelerates the corrosion rate.

In this chapter the passivation properties, and corrosion resistance of uncoated and sputter deposited Ti, TiO_2 and duplex Ti-TiO_2 coated 304L SS have been investigated by means of electrochemical studies in 1 M and 8 M nitric acid medium, and surface morphological investigations. Surface morphology analysis was carried out by atomic force microscope. Passivation property, corrosion resistance were determined by electrochemical impedance spectroscopy, and polarization study. To evaluate the performance of each coating, protection efficiency was evaluated from the polarization study. The results of the investigation are highlighted in this chapter.

6.2 Results and discussion

6.2.1 Corrosion behaviour of Ti coated 304L SS in nitric acid medium

6.2.1.1 Phase and morphology characterization

The GIXRD analysis of the sputter deposited Ti coated 304L SS specimens showed the presence of α-Ti phase, and according to PCPDF data base (65-6231), the peak position assigned were α-Ti(1 0 0) (35.10°), α-Ti(0 0 2) (38.35°), α-Ti (1 0 1) (40.15°), α-Ti (1 0 2) (52.95°), α-Ti (1 0 3) (70.65°), α-Ti (2 0 0) (74.75°) and α-Ti (1 1 2) (76.05°), respectively (Fig. 6.1).

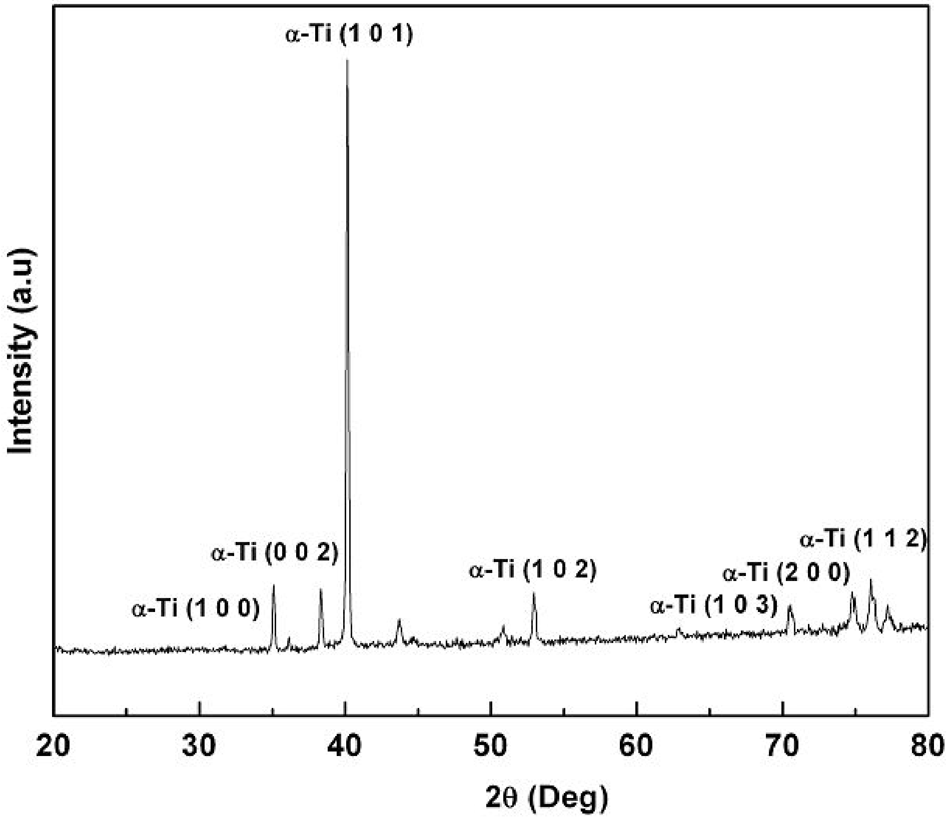

Fig. 6.1: GIXRD profile of Ti coated 304L SS.

Figure. 6.2a-d represents the morphological features of the Ti coated 304L SS. The morphology of Ti coated specimen showed the presence of globular particles with pores, and inter-columnar boundaries in the matrix (Fig. 6.2a). Figure. 6.2b shows the histogram for the distribution of the size of the particles as a function of frequency of formation. The size of the particles range from 8×10^{-3} µm^2 to 7.45×10^{-1} µm^2. However, because of agglomeration and presence of few multi-phase particles, the size increases up to 2.75 µm^2. Nevertheless, the frequency of formation of such particles is low as compared to isolated particles. The exact location of the pores, and inter-columnar boundaries present on the coated surface is shown in Fig. 6.2c. The size distribution of the pores as a function of frequency of formation is shown in Fig. 6.2d. The pore sizes range from 5×10^{-3} µm^2 to 200×10^{-3} µm^2. The root mean square roughness (R_q) on the surface was 7 nm.

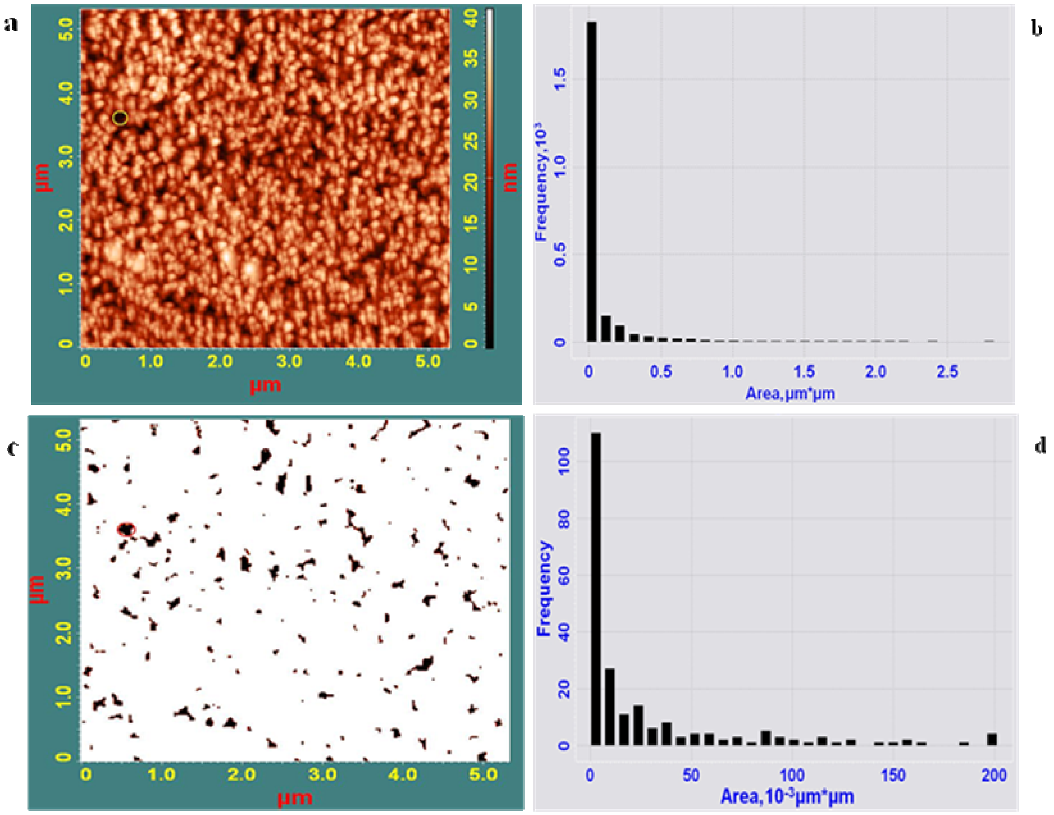

Fig. 6.2a-d: (a) Morphology of Ti coated 304L SS, (b) histogram for the particle size distribution, (c) morphology of the pores, and (d) histogram for the size distribution of the pores.

6.2.1.2 Open circuit potential vs. time measurement

The results for OCP vs. time measurement for uncoated, and Ti coated 304L SS in 1 M and 8 M nitric acid are shown in Fig. 6.3a-b.

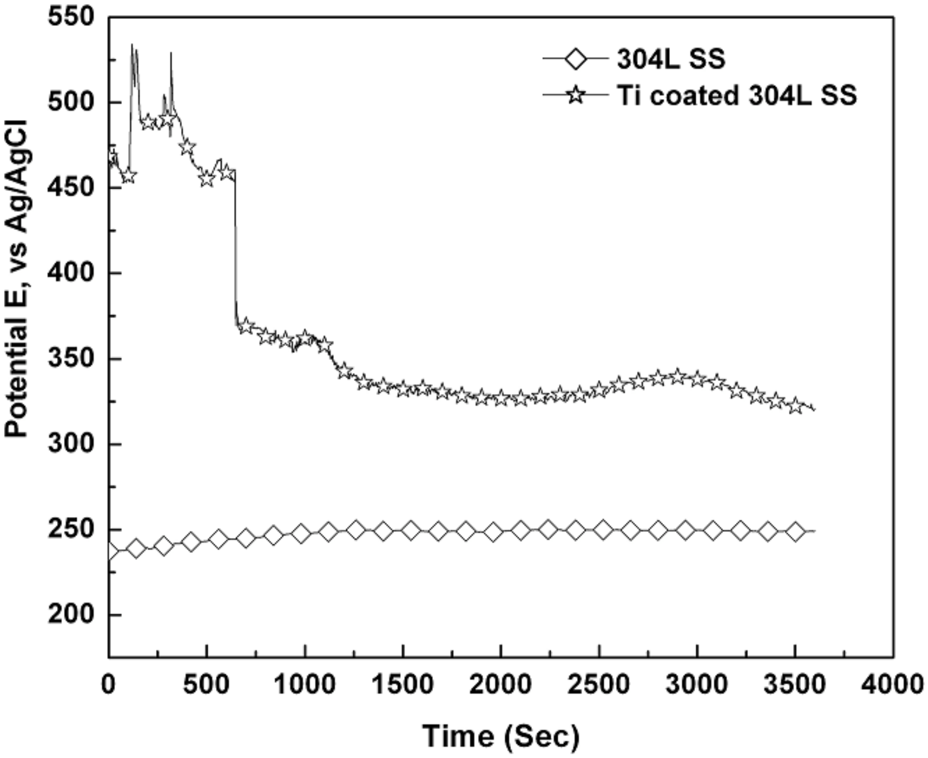

Fig. 6.3a: OCP vs. time measurement for uncoated and Ti coated 304L SS in 1 M HNO_3

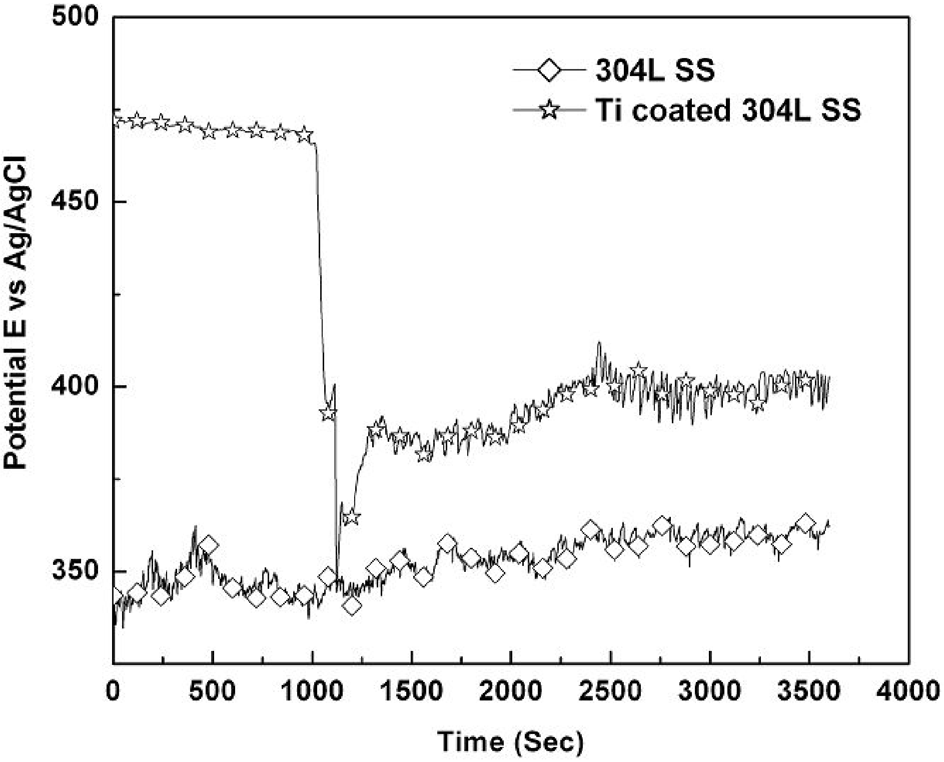

Fig. 6.3b: OCP vs. time measurement for uncoated and Ti coated 304L SS in 8 M HNO_3.

Results revealed that in both the test solutions, OCP shifted towards more noble potential for Ti coated specimens as compared to uncoated condition. For uncoated specimens OCP in 8 M nitric acid was higher as compared to that of 1 M nitric acid because of large concentration of nitrous acid (HNO_2) produced at higher concentration due to auto-catalytic reduction which imposes higher redox potential [3-7, 20-22, 41,42]. In 1 M nitric acid the uncoated 304L SS specimens attained passive state quickly, and showed steady passivation behaviour with increase in immersion time, however the OCP of titanium coated specimen started with noble potential decreased to lower value before attaining steady state (Fig. 6.3a). In 8 M nitric acid the uncoated specimens also showed steady OCP behavior. Similar to 1 M nitric acid, the Ti coated specimens initially showed higher OCP in 8 M nitric acid, and decreased abruptly to lower value before attaining steady state (Fig. 6.3b). In both the test solutions, Ti coated specimens showed one transition point before attaining steady state justifying the observed OCP behaviour in electrochemical solution [196].

The OCP of the Ti coated 304L SS specimens shows the stability of the developing oxide film in both the concentration of test solution with increase in oxidizing nature. Titanium is known to form thick oxide layer by oxidation of metallic Ti, but the composition and thickness of the oxide layer largely depends upon the nature of the electrochemical environment. In acidic solutions, the oxidation state changes from lower to higher value such as Ti_2O_3, Ti_3O_5 and TiO_2, respectively [197]. The non-stoichiometric oxides are insoluble at lower concentration of oxidizing solution, but rapidly dissolve in concentrated solution [198]. Moreover, the passive film does not stabilize properly, if Ti fails to oxidize perfectly to TiO_2, and OCP decreases to lower value justifying the observed OCP behavior [197]. The structural heterogeneities such as pinholes, and inter-columnar boundaries also effects the passive film stability because developing passive film is generally thin in these regions, and provides local sites for breakdown of passive film.

6.2.1.3 Electrochemical impedance analysis

The electrochemical impedance response in OCP condition for uncoated and Ti coated 304L SS analyzed by Bode plots (Log |Z| vs. Log f and θ vs. Log f) in 1 M and 8 M nitric acid are shown in Fig. 6.4a-d. The fitted plots for the obtained experimental results using electrical equivalent circuit model as shown in Fig. 3.10a-b are also shown along with experimental graphs in Fig. 6.4a-d. The capacitive and resistive properties of the coating were analyzed by means phase angle (θ) vs. frequency plots, and the stability of the coating was analyzed by plot of total impedance (|Z|) in the frequency domain of investigation.

The EIS spectra for uncoated specimen in 1 M nitric acid in low and high frequency region showed resistive property, and capacitive property in between the frequency region 10^1 to 10^3 Hz with one time constant feature (Fig. 6.4a). As compared to uncoated condition, the Ti coated 304L SS specimen in 1 M nitric acid showed near capacitive property in the low frequency region, and gradually changed to resistive property towards high frequency region.

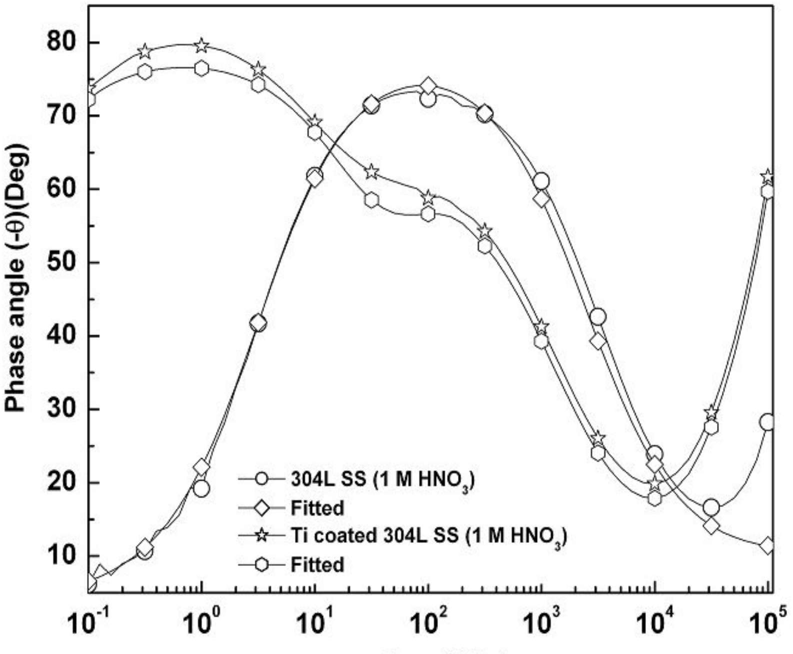

Fig. 6.4a: Log f vs. θ for uncoated and Ti coated 304L SS in 1 M HNO_3.

The change over from capacitive to resistive property has been reflected by the appearance of two time constant feature in-between 10^1 to 10^2 Hz, which indicates the alteration in passive film property as well as initiation of anodic activities. The improvement in magnitude of total impedance (|Z|) from uncoated to Ti coated condition in 1 M nitric acid was one order of magnitude (Fig. 6.4b).

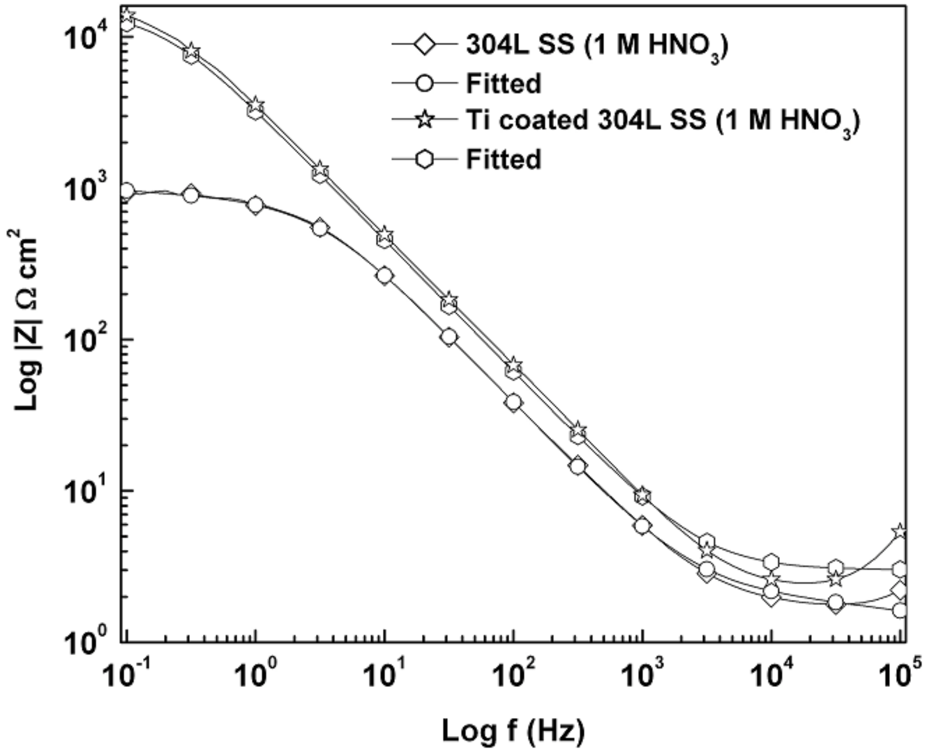

Fig. 6.4b: Log f vs. Log |Z| for uncoated and Ti coated 304L SS in 1 M HNO$_3$.

The uncoated specimens in 8 M nitric acid showed largely resistive property, and low capacitive property in the narrow region between 10^1 to 10^2 Hz (Fig. 6.4c). However, the Ti coated 304L SS specimens showed resistive property in the low frequency region, and near capacitive property in the frequency region of 10^1 to 10^3 Hz. The improvement in magnitude of total impedance (|Z|) for Ti coated specimen was five times as compared to that of uncoated condition in 8 M nitric acid (Fig. 6.4d). The low impedance value in 8 M nitric acid as compared to 1 M nitric acid, and one time constant feature in 8 M nitric acid as compared to two time constant feature in 1 M nitric acid for Ti coated specimen shows thinning down of oxide layer on the coated surface as oxidizing power of nitric acid increases.

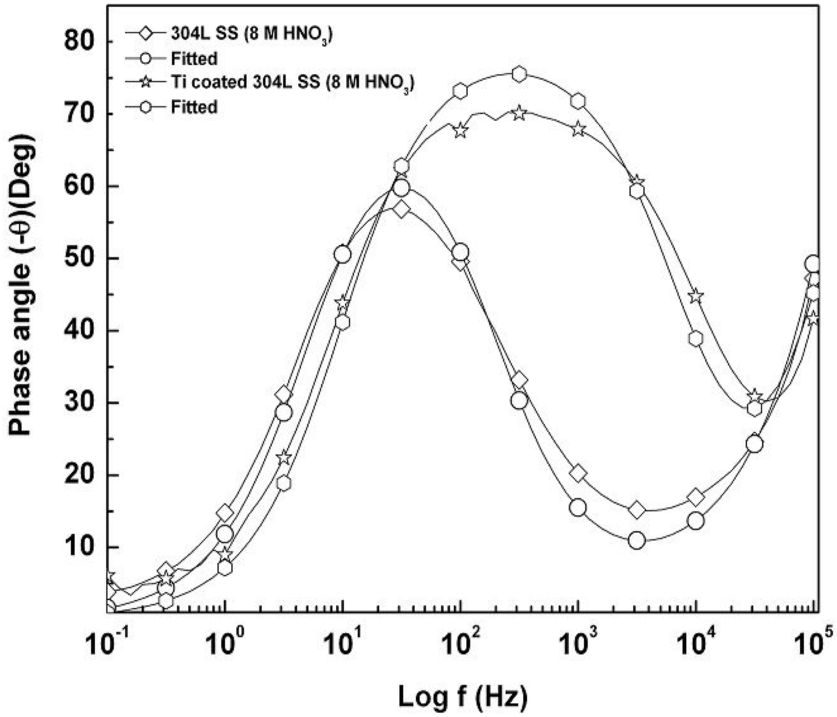

Fig. 6.4c: Log f vs. θ for uncoated and Ti coated 304L SS in 8 M HNO_3.

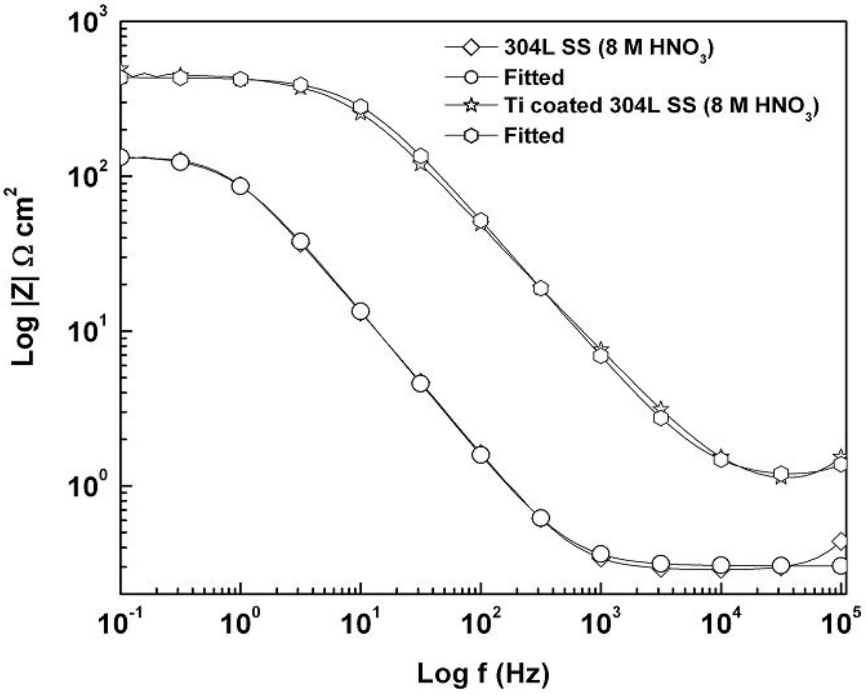

Fig. 6.4d: Log f vs. Log |Z| for uncoated and Ti coated 304L SS in 8 M HNO_3.

The impedance parameters for uncoated, and Ti coated 304L SS in 1 M and 8 M nitric acid obtained by fitting with circuit models as mentioned in Fig. 3.10a-b are shown in Table. 6.1. From Table. 6.1, it is clear that Ti coated 304L SS specimens showed improvement in polarization resistance (R_{ct2}) as compared to uncoated condition, however the polarization resistance of Ti coated specimen in 8 M nitric acid was much lower as compared to that of 1 M nitric acid. Moreover, the pore resistance (R_{ct1}) in 8 M nitric acid was also significantly lower compared to 1 M nitric acid, which shows increasing charge transfer process, and anodic activities at structural heterogeneities in the coating-substrate interface. The stability of the coating in corrosive solution is determined by the coating capacitance, and in general lower the coating capacitance value higher is the stability signifying insulating nature [199]. In 1 M nitric acid, the coating capacitance (C_{dl1}) showed lower capacitance value which indicates low amount of retained charge on the coated surface. However with increasing concentration (8 M), the retained charge capacity increased which showed higher capacitance value. The double layer capacitance (C_{dl2}) for Ti coated 304L SS specimens also showed lower capacitance value in 1 M nitric acid, which indicates good passive film stability at the coating-substrate interface. Increase in C_{dl2} value was observed at higher concentration (8 M) indicating decreasing passive film stability at the coating-substrate interface with increasing oxidizing nature.

Conc.	Substrate condition	R_s Ω cm^2	CPE$_2$		R_{ct2} Ω cm^2	CPE$_1$		R_{ct1} Ω cm^2
			C_{dl2} $\Omega^{-1}cm^{-2}S^n$	n (0-1)		C_{dl1} $\Omega^{-1}cm^{-2}S^n$	n (0-1)	
1 M	Uncoated	2	6.5×10^{-5}	0.76	9.35×10^{2}	-	-	-
1 M	Ti coated	5	4.6×10^{-5}	0.83	2.13×10^{4}	6.5×10^{-6}	0.84	4×10^{2}
8 M	Uncoated	1	5.8×10^{-4}	0.65	1.8×10^{2}	-	-	-
8 M	Ti coated	2	8.2×10^{-5}	0.71	4×10^{2}	2.7×10^{-5}	0.76	1×10^{1}

Table. 6.1: EIS fitted values for the uncoated and Ti coated 304L SS in 1 M and 8 M HNO_3.

6.2.1.4 Potentiodynamic polarization study

The results for potentiodynamic polarization study for uncoated and Ti coated 304L SS in 1 M and 8 M nitric acid are shown in Fig. 6.5a-b. The quantitative value of the polarization parameters obtained for uncoated, and Ti coated 304L SS specimens in both the test solutions are summarized in Table. 6.2.

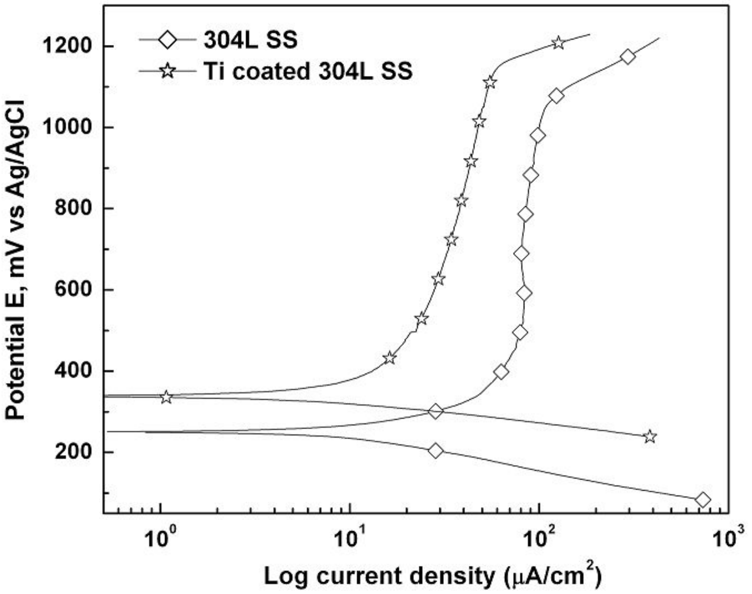

Fig. 6.5a: Polarization study for uncoated and Ti coated 304L SS in 1 HNO$_3$.

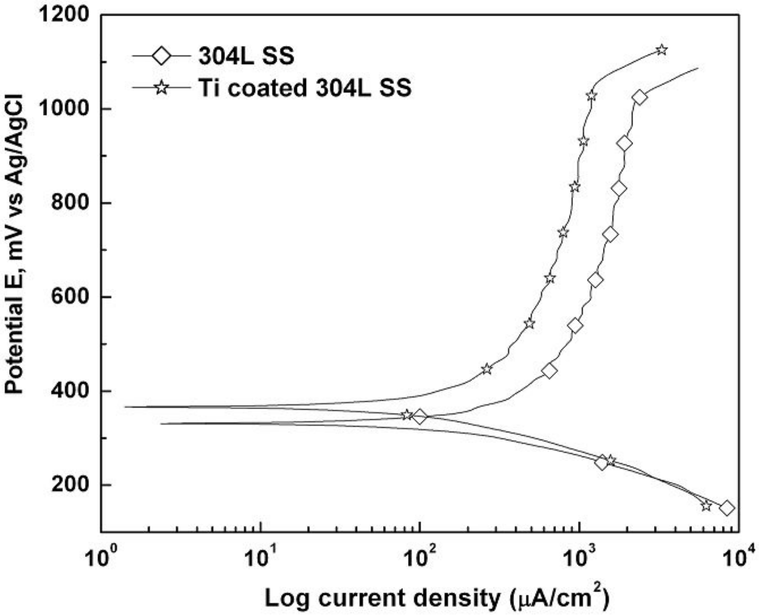

Fig. 6.5b: Polarization study for uncoated and Ti coated 304L SS in 8 M HNO$_3$.

Conc.	Substrate condition	E_{corr} mV vs Ag/AgCl	I_{pass} $\mu A/cm^2$	I_{corr} $\mu A/cm^2$	$E_{transpass}$ mV vs Ag/AgCl
1 M	Uncoated	250	1.1×10^2	10×10^0	1100
1 M	Ti coated	330	5.5×10^1	4.5×10^0	1146
8 M	Uncoated	340	1.2×10^3	7×10^1	1025
8 M	Ti coated	385	1.1×10^3	5.1×10^1	1051

Table. 6.2: Average value of polarization parameters for uncoated and Ti coated 304L SS in 1 M and 8 M HNO_3.

In both the concentrations of test solutions, Ti coated 304L SS specimens showed nobler corrosion potential (E_{corr}) as compared to uncoated condition indicating formation of protective oxide film in the oxidizing medium of nitric acid. Noticeable improvement in passive current density (I_{pass}) and corrosion current density (I_{corr}) was observed for Ti coated specimen in 1 M nitric acid, however improvement was marginal in 8 M nitric acid compared to uncoated condition (Table. 6.2). The improvement in transpassive potential for Ti coated specimens ($\Delta E_{transpassive}$ = E_{coated} - $E_{uncoated}$) in 1 M nitric acid was 46 mV (vs. Ag/AgCl), and 26 mV (vs. Ag/AgCl) in 8 M nitric acid, respectively. Overall, from Table.6.2 it is clear that at lower concentration (1 M HNO_3), lower passive current density and higher transpassive potential, and at higher concentration (8 M HNO_3) higher passive current density and lower transpassive potential was observed. Thus, the polarization parameters indicate that passive film formed on Ti coated specimens at higher concentration dissolves faster. The protection efficiency calculated using Eq. 13 was 52 % in 1 M nitric acid, and 27 % in 8 M nitric acid, respectively as compared to uncoated condition.

The protecting ability of the coated surface depends mainly on the physico-chemical properties of the developing oxide film as well as structural heterogeneities on the surface. Titanium readily forms titanium oxide in acidic solutions due to its strong affinity towards oxygen, but the kind of film formed, and its enthalpy of formation decides the stability of the oxide layer. The mechanism of passivation initiates with the formation of Ti^{3+} ions, which consequently forms certain metastable oxides which further oxidizes to TiO_2 [197]. However, the composition of oxide layer depends upon the oxidizing power of the solution, and generally consists a mixture of anatase with certain quantity of rutile phase [197]. Various oxide layers that develops in acidic solution when titanium undergoes passivation are Ti_3O_5 (ΔH_f = - 2459.15 kJ/mole), Ti_2O_3 (ΔH_f = - 1520.84 KJ/mole), TiO_2 (ΔH_f = - 944.75 KJ/mole), respectively. The non-stoichiometric oxides are having low enthalpy of formation, and are generally porous in nature [200]. The perfect stoichiometric oxides are compact and have high enthalpy of formation. The non-stoichiometric oxides are stable in low concentration, and forms good passive film but dissolve in strong acid solution due to low oxide density as well as increase in aggressivity in the exposed area of the pores [196-198]. Apart from this, the electrochemical environment at structural heterogeneities such as pinholes, flaws, and inter-columnar boundaries is more aggressive as compared to that of matrix due to accumulation of solution, and passive film formed in these regions is thinner. Thus, the protective oxide film formed electrochemically offers less resistance to corrosive medium and fails usually in the depth of the pores at higher concentration. Moreover, galvanic potentials do exist at pinholes, and inter-columnar boundaries and these regions prevent passive oxide layer formation and lead to enhanced corrosion of base material. Once initiated, corrosion proceeds at the boundaries between the coating and substrate, and the protection of base material is lost. Apart from this, accelerated corrosion reduces the coating bond strength, and uniform dissolution of the coated surface occur leading to peeling up of the coating.

6.2.1.5 Morphological investigation after potentiodynamic polarization study

The results for surface morphological study for uncoated and Ti coated 304L SS specimens after potentiodynamic polarization in both the concentration of test solution are shown in Fig.

6.6a-d. The uncoated specimens in both the concentration showed grain boundary dissolution, and the extent of dissolution was more for concentrated solution (Fig. 6.6 a and c). The large extent of dissolution at grain boundary is because, grain boundaries are structurally heterogeneous areas on the surface and are of high energy. The protective oxide film formed on these areas become susceptible to dissolution with increase in oxidizing ability of the solution leading to opening up of oxide boundaries [20-22].

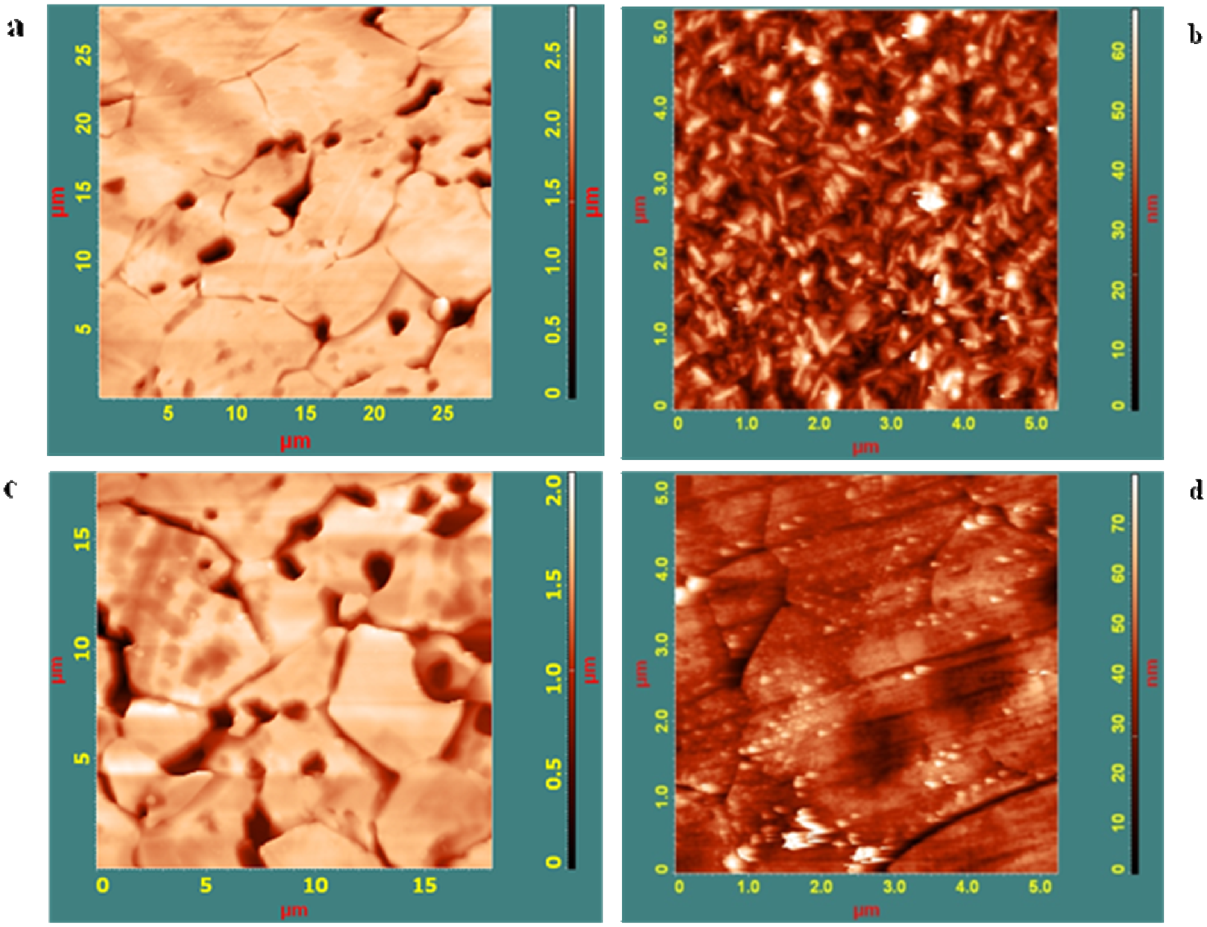

Fig. 6.6a-d: Surface morphology of uncoated and Ti coated 304L SS after polarization study in HNO_3; (a) uncoated (1 M HNO_3), (b) Ti coated 304L SS (1 M HNO_3), (c) uncoated (8 M HNO_3), (d) Ti coated 304L SS (8 M HNO_3)

As compared to uncoated specimens, the morphology of Ti coated specimens after polarization study in 1 M nitric acid (Fig. 6.6b) largely showed well separated particles, and opening up of the pores on the surface however, the particles were not detached from the surface indicating protecting ability up to certain extent. The morphology of the Ti coated specimen after polarization in 8 M nitric acid (Fig. 6.6d) showed significant depletion of the particles from the coated surface showing grain boundary regions of the base material, nevertheless very few particles sticking to the surface can also be noticed. Overall, the Ti coated 304L SS specimens in 1 M nitric acid showed resistance to surface dissolution of the base material, whereas in 8 M nitric acid depletion of the coated surface as well as attack on the base material were observed.

6.2.2 Corrosion behaviour of TiO_2 coated 304L SS in nitric acid medium

6.2.2.1 Phase and morphology characterization

The GIXRD analysis of sputter deposited f TiO_2 coated 304L SS specimens is shown in Fig. 6.7.

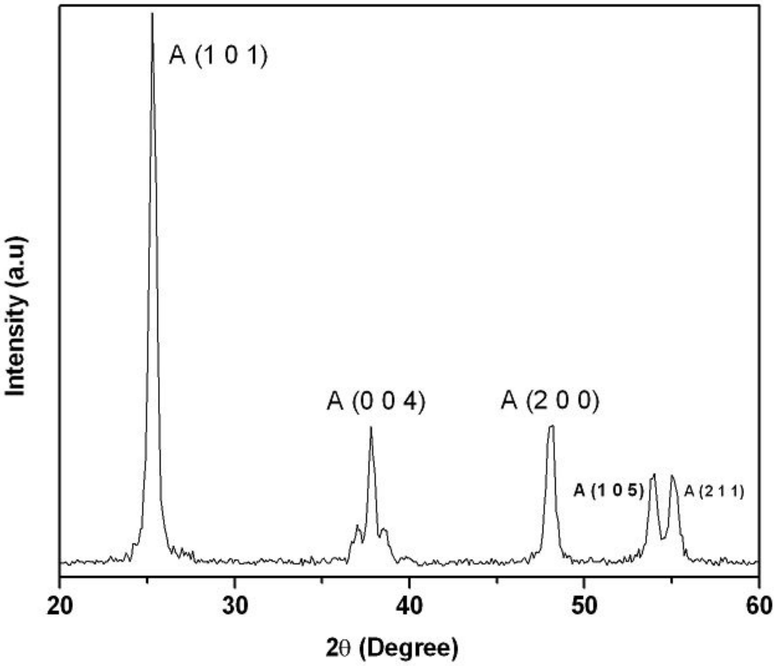

Fig. 6.7: GIXRD pattern of TiO_2 coated 304L SS [22].

The GIXRD pattern of the TiO_2 coated 304L SS surface revealed anatase phase. According to the standard PCPDF (89-4921) data base, and available literature the peak positions assigned were A (1 0 1) (25.35°), A (0 0 4) (37.84°), A (2 0 0) (48.15°), A (1 0 5) (53.97°) and A (2 1 1)

(55.18°) respectively, which are the characteristics peak of anatase phase. The surface morphological analysis of the TiO_2 coated 304L SS using AFM is shown in Fig. 6.8a-d. Figure. 6.8a represents the morphology of TiO_2 coated 304L SS. The morphology showed well organized, evenly spaced, and compact arrangement of particles covering the surface. The histogram for size distribution of the particles as a function of frequency of formation is shown in Fig. 6.8b. The particle size ranges from, $1.5\times10^{-1}\mu m^2$ to 1.12 μm^2. However, because of agglomeration the size of the particle increases up to 2.5 μm^2. The exact location, and morphology of the pores on the coated surface is shown in Fig. 6.8c. The size of the pores ranges from, 3×10^{-3} μm^2 to 450×10^{-3} μm^2 (Fig. 6.8d). The root mean square roughness (R_q) on the surface was 10 nm.

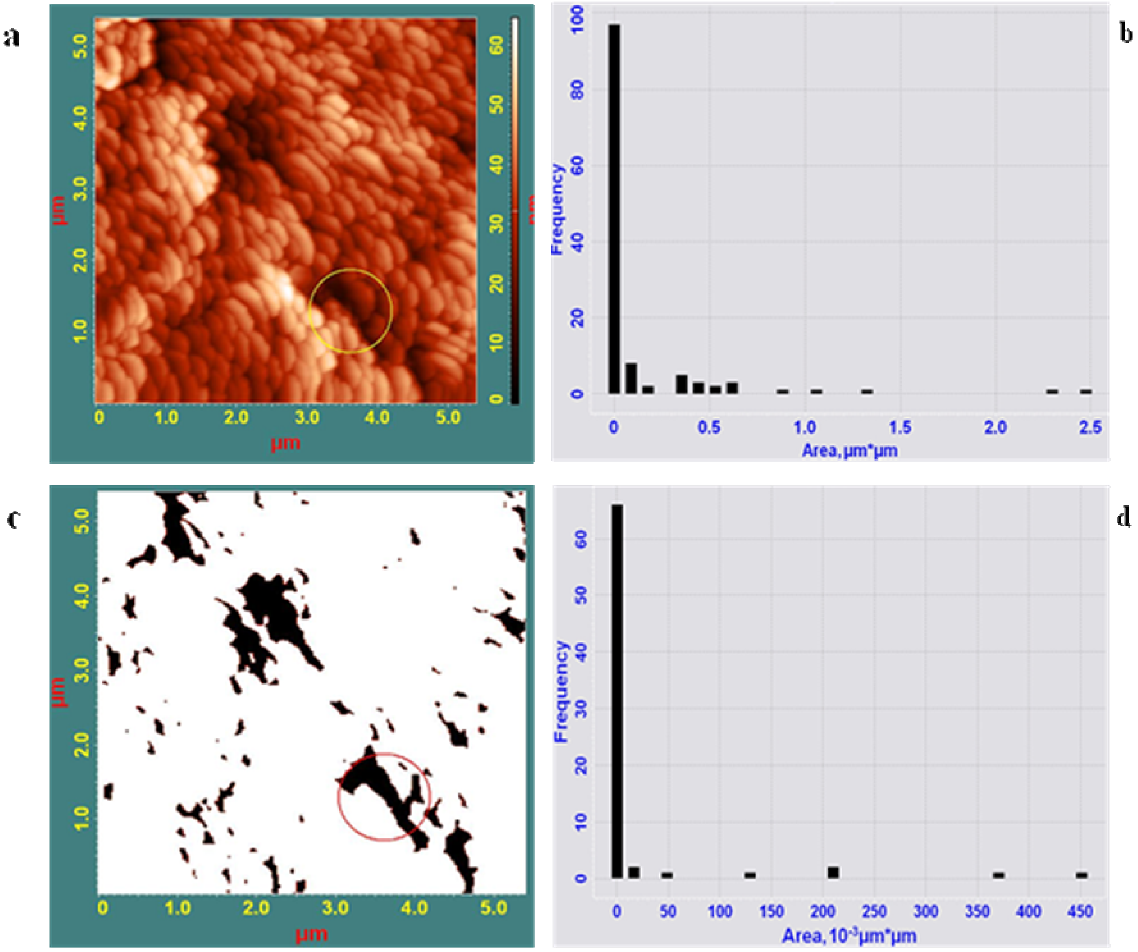

Fig. 6.8a-d: (a) Morphology of TiO_2 coated 304L SS, (b) histogram for the particle size distribution, (c) morphology of the pores and (d) histogram for the size distribution of the pores.

6.2.2.2 Open circuit potential vs. time measurement

The OCP of uncoated, and TiO_2 coated 304L SS specimens in both 1 M and 8 M nitric acid medium are shown in Fig. 6.9a-b.

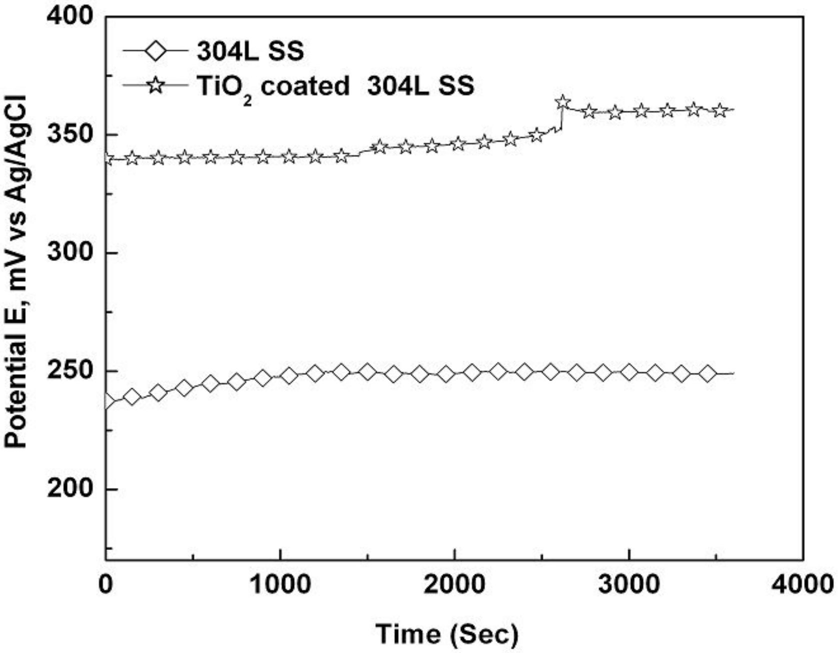

Fig. 6.9a: OCP vs. time measurement for TiO_2 coated 304L SS in 1 M HNO_3 [22].

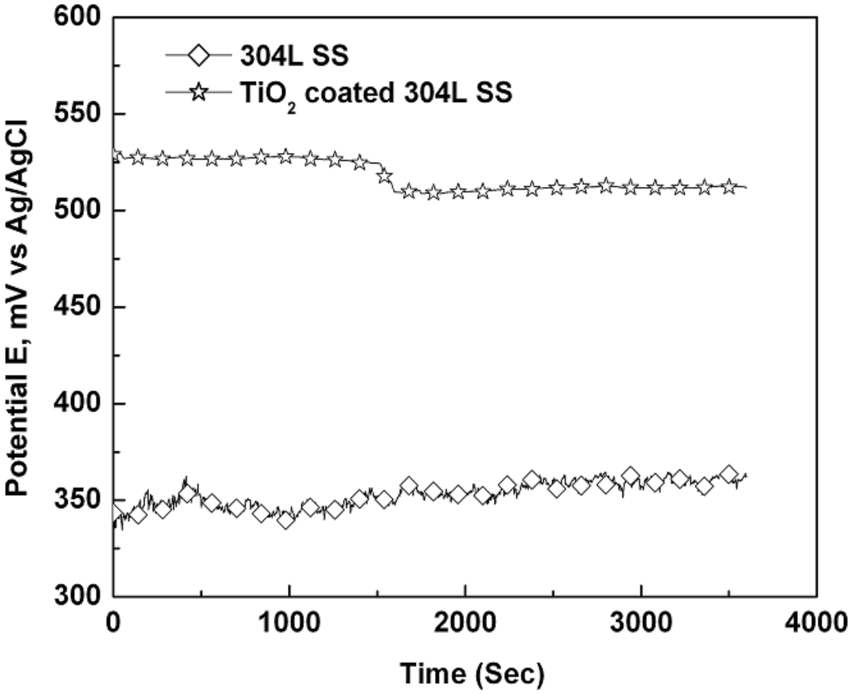

Fig. 6.9b: OCP vs. time measurement for TiO_2 coated 304L SS in 8 M HNO_3 [22].

OCP shifted in noble direction for titanium dioxide coated 304L SS specimens as compared to uncoated, and Ti coated specimen. The shift of OCP in noble direction in both the concentration of test solutions clearly indicates greater protecting power of TiO_2 coating in the oxidizing environment of nitric acid as compared to uncoated, and Ti coated specimens. As compared to Ti coated specimens, TiO_2 coated specimens showed mostly steady state with increase in immersion time. This is largely due to the presence of perfect stoichiometeric oxide layer on the surface as compared to Ti which in general forms a number of sub-stoichiometric oxides in the oxidizing environment [197]. Nevertheless, marginal increase or decrease in OCP prior to attaining of steady state in both the test solutions indicates stability of the coating-electrolyte interface by filling up of pinholes, pores, and void space at the inter-columnar boundaries [22]. The increase in OCP is attributed to the greater passivation tendency of TiO_2 in the auto-catalytic oxidizing environment of nitric acid leading to inhibition of anodic process as compared to Cr_2O_3 film which naturally occurs on stainless steel surface. In general, TiO_2 is thermodynamically more stable over a wide potential region due to high lattice energy of formation as compared to Cr_2O_3 [201]. In the eventuality of film dissolution, subsequent hydrolysis of the dissolved ions readily forms the TiO_2 film due to low free energy of formation in solution [201,202].

$$Ti^{4+} + 2\,H_2O \longrightarrow TiO_2 + 4\,H^+$$

Thus, its healing power is also quite high, unlike Cr_2O_3 [Cr(III)] where the film transfers to a soluble $Cr_2O_7^{2-}$ [Cr(VI)] form in the oxidizing environment. For uncoated specimen, OCP in 8 M HNO_3 was higher as compared to 1 M HNO_3 because of large concentration of aqueous nitrous acid (HNO_2) produced at higher concentration, which imposes higher redox potential to the electrochemical environment. Thus, the auto-catalytic reduction rate of nitric acid increases, and consequently corrosion potential rises in the noble direction. Nevertheless, the rise of OCP in the noble direction for TiO_2 coated specimens in both the test solutions is attributed to good passive film property [22].

6.2.2.3 Electrochemical impedance analysis

The electrochemical impedance analysis of the uncoated and TiO_2 coated 304L SS specimens in OCP condition are shown in Fig. 6.10a-d. The Bode plots (Log |Z| vs. Log f and θ vs. Log f) clearly showed improved protection for TiO_2 coated specimens in both the test solution compared to base material as well as Ti coated specimens. The plot of phase angle (θ), and frequency in 1 M nitric acid showed one time constant feature as compared to two time constant feature for Ti coated specimens with near capacitive property over a wide frequency indicating greater passive film stability, and resistance to anodic activity (Fig. 6.10a).

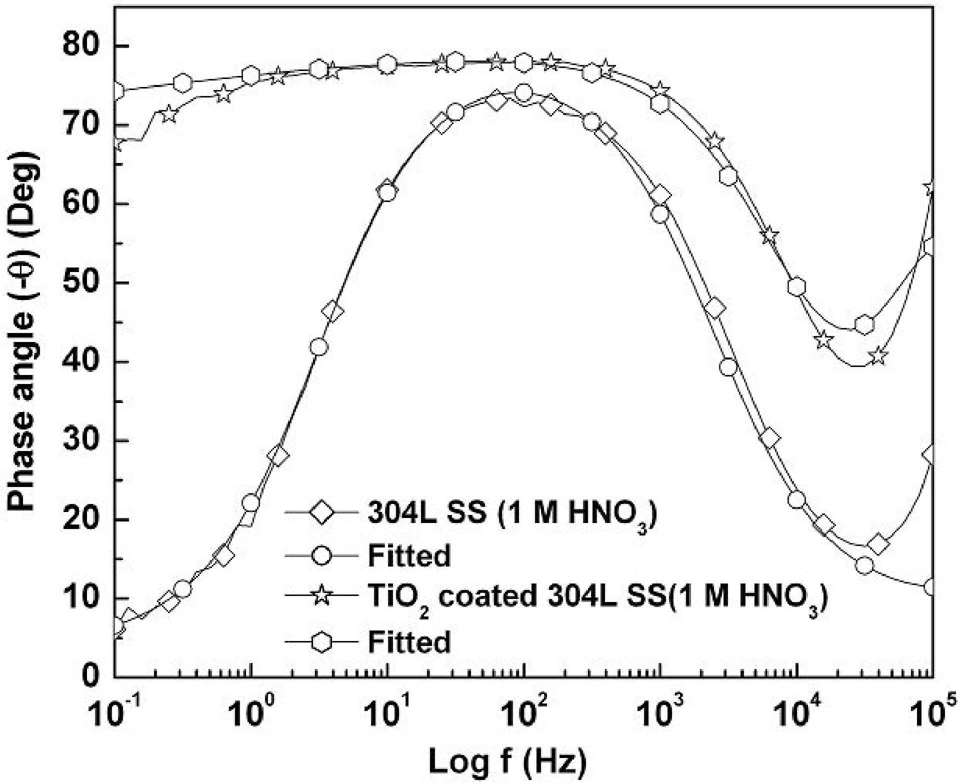

Fig. 6.10a: Log f vs. θ for uncoated and TiO_2 coated 304L SS in 1 M HNO_3 [22].

The high phase angle over wide frequency region for TiO_2 coated specimens as compared to uncoated, and Ti coated specimens is due to their capacitive property as well as high resistance to current flow in coated surface owing to insulating nature [22]. Similarly, the plot of Log f vs. Log |Z| of 304L SS at lower concentration (1 M) showed two frequency independent horizontal regions in low and high frequency region, and capacitive behaviour at intermediate frequency in middle region (Fig. 6.10b). As compared to uncoated specimens, TiO_2 coated specimens showed two order increase in magnitude of total impedance (|Z|), and slope of -1 up to high frequency region showing largely capacitive property. As compared to Ti coated specimens, the improvement in magnitude of total impedance was one order of magnitude (Fig. 6.10b)

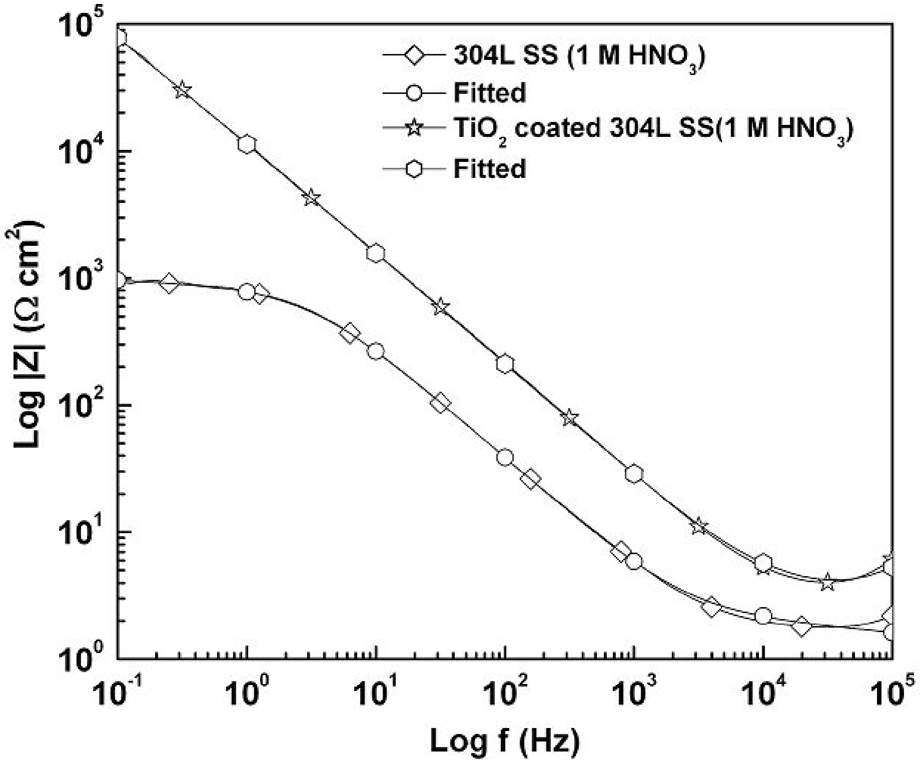

Fig. 6.10b: Log f vs. Log |Z| for uncoated and TiO_2 coated 304L SS in 1 M HNO_3 [22].

However, the TiO_2 coated specimens exhibited two time constant feature in 8 M nitric acid [203] indicating change in passive film property at higher concentration (Fig. 6.10c). The two time constant feature can be attributed to degradation of passive film at the pinholes due to permeability of the solution resulting increase in charge transfer process with increase in aggressivity of the medium [22]. Moreover, the high phase angle over wide frequency region as observed in 1 M nitric acid was not observed in 8 M nitric acid. Significant improvement in magnitude of total impedance (|Z|) was also observed in 8 M nitric acid for TiO_2 coated specimen as compared to uncoated, and Ti coated specimens. The improvement with respect to uncoated 304L SS was one order of magnitude, and two times as compared to titanium coating (Fig. 6.10d). Thus, although there is a decrease in the stability of passive film from 1 M to 8 M nitric acid for TiO_2 coated specimens, the magnitude of total impedance, and phase angle are quite superior to uncoated, and Ti coated specimen in both the solutions signifying good passive film property. The impedance parameters obtained using electrochemical circuit model as shown in Fig. 3.10a-b are presented in Table. 6.3 [22].

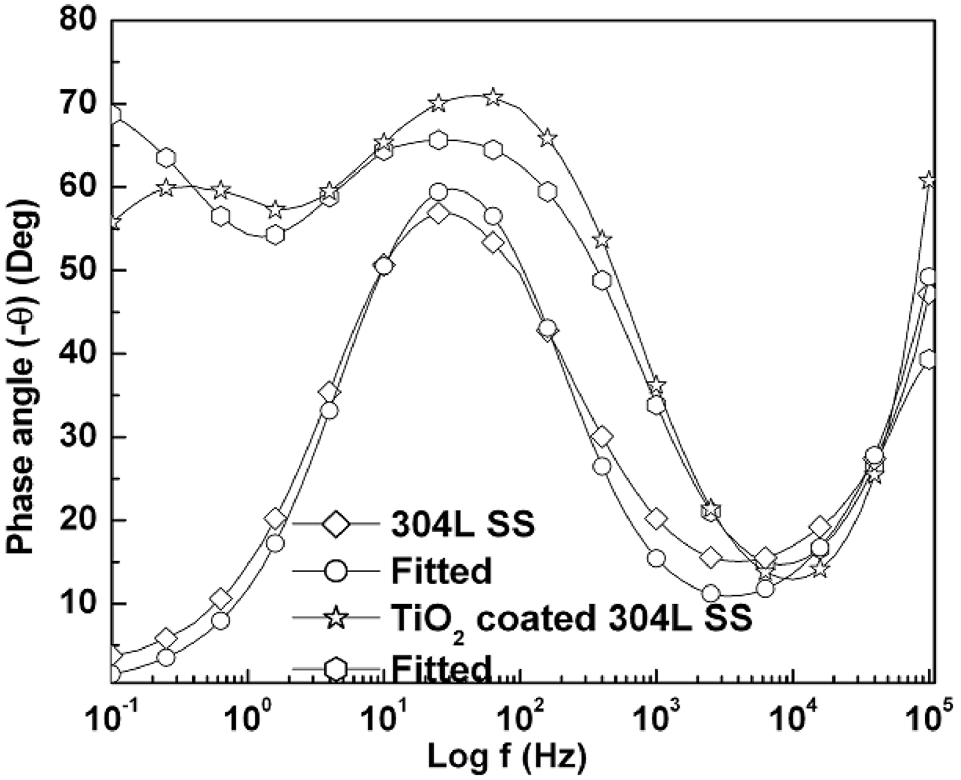

Fig. 6.10c: Log f vs. θ for uncoated and TiO_2 coated 304L SS in 8 M HNO_3 [22].

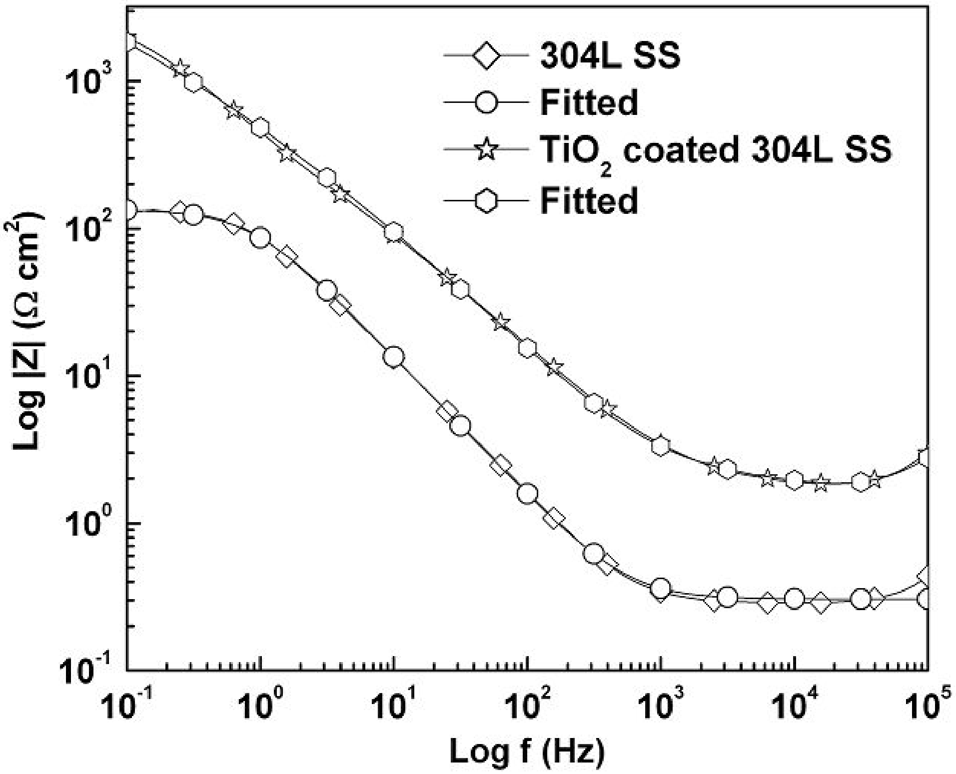

Fig. 6.10d: Log f vs. Log |Z| for uncoated and TiO_2 coated 304L SS in 8 M HNO_3 [22].

Conc.	Substrate condition	R_s Ω cm^2	CPE$_2$		R_{ct2} Ω cm^2	CPE$_1$		R_{ct1} Ω cm^2
			C_{dl2} $\Omega^{-1}cm^{-2}S^n$	n (0-1)		C_{dl1} $\Omega^{-1}cm^{-2}S^n$	n (0-1)	
1 M	Uncoated	2	6.5×10^{-5}	0.76	9.35×10^{2}	-	-	-
1 M	TiO_2coated	8	2.5×10^{-5}	0.89	3.47×10^{4}	1.3×10^{-7}	0.96	6×10^{2}
8 M	Uncoated	1	5.8×10^{-4}	0.65	1.8×10^{2}	-	-	-
8 M	TiO_2coated	10	3.6×10^{-5}	0.72	5×10^{2}	1.8×10^{-5}	0.78	3.2×10^{1}

Table. 6.3: EIS fitted values for uncoated and TiO_2 coated 304L SS in 1 M and 8 M HNO_3 [22].

From the circuit parameters in Table. 6.3, it is clear that both coating capacitance (C_{dl1}), and coating resistance (R_{ct1}) of TiO_2 coated 304L SS specimens showed good coating capacitance as well as higher pore resistance in both the test solutions compared to uncoated, and Ti coated specimens. The double layer capacitance (C_{dl2}) and polarization resistance (R_{ct2}) of TiO_2 coated 304L SS specimens also showed lower retained charge capacity, and high polarization resistance of the passive film at the coating-substrate interface as compared to uncoated condition. However, as observed in case of Ti coated specimens, the circuit parameters mentioned in Table. 6.3, such as coating capacitance, and pore resistance showed decreasing trend from 1 M to 8 M nitric acid. Similar trend was also observed for polarization resistance and double layer capacitance even though values are superior to Ti coated condition.

6.2.2.4 Potentiodynamic polarization study

The potentiodynamic polarization study carried out in 1 M and 8 M nitric acid for uncoated and TiO_2 coated 304L SS specimens are shown in Fig. 6.11a-b. The polarization parameters evaluated for the uncoated, and TiO_2 coated 304L SS specimens are shown in Table. 6.4. It is clear that, passive current density (I_{pass}) and corrosion current density (I_{corr}) decreased, and transpassive potential ($E_{transpass}$) increased for TiO_2 coated specimens compared to uncoated specimens indicating beneficial effects of titanium dioxide in nitric acid medium [22].

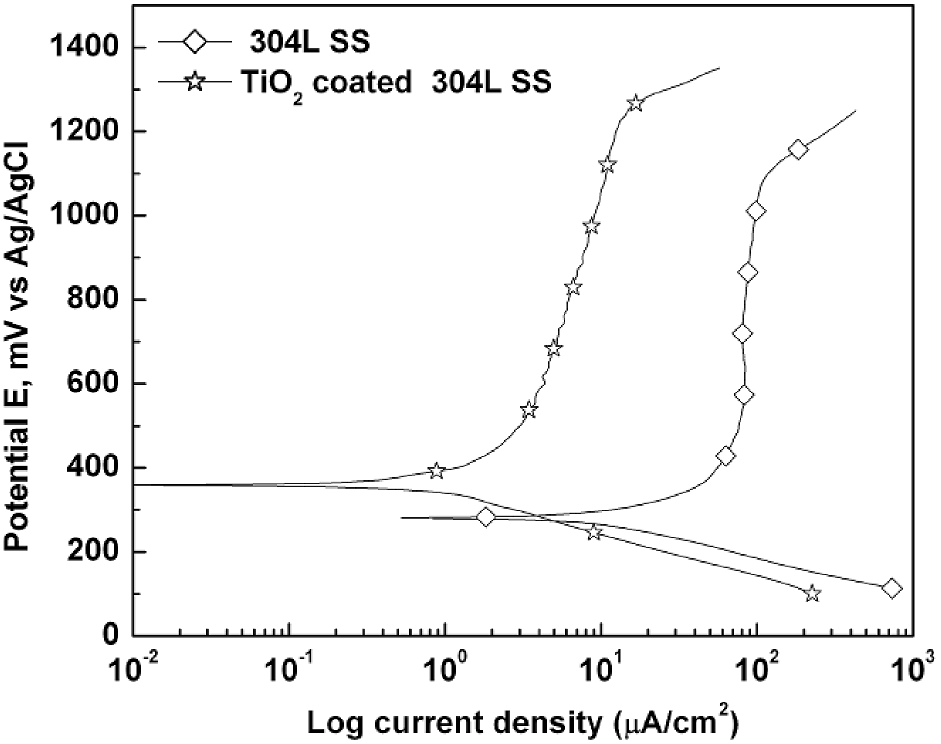

Fig. 6.11a: Polarization study of uncoated and TiO_2 coated 304L SS in 1 M HNO_3 [22].

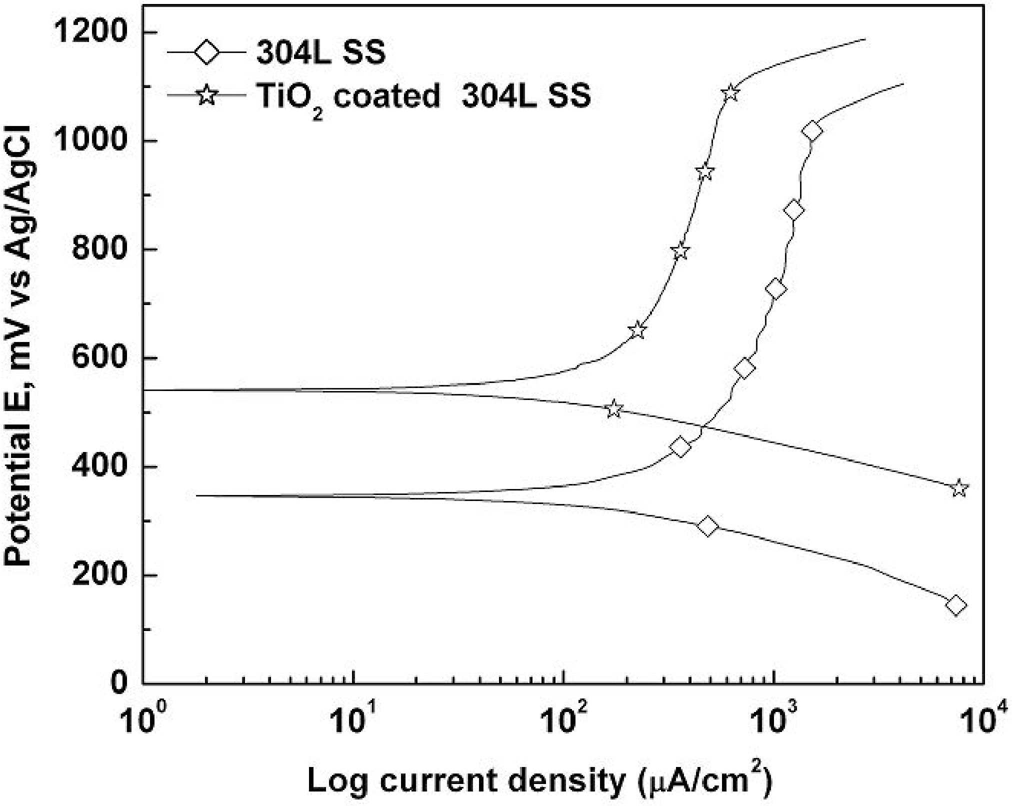

Fig. 6.11b: Polarization study of uncoated and TiO_2 coated 304L SS in 8 M HNO_3 [22].

Conc.	Substrate condition	E_{corr} mV vs Ag/AgCl	I_{pass} $\mu A/cm^2$	I_{corr} $\mu A/cm^2$	$E_{transpass}$ mV vs Ag/AgCl
1 M	Uncoated	250	1.1×10^2	10×10^0	1100
1 M	TiO_2 coated	360	10×10^0	5×10^{-1}	1250
8 M	Uncoated	340	1.2×10^3	7×10^1	1025
8 M	TiO_2 coated	550	5×10^2	4×10^1	1075

Table. 6.4: Average value of polarization parameters for uncoated and TiO_2 coated 304L SS in 1 M and 8 M HNO_3 [22].

Decrease in passive current density in 1 M nitric acid was two orders of magnitude while in 8 M nitric acid it was one order of magnitude from uncoated to TiO_2 coated specimens. As compared to Ti coated specimens, the passive current density for TiO_2 coated specimens was one-fifth in 1 M nitric acid, and half in 8 M nitric acid. The increase in transpassive potential

($\Delta E_{transpass} = E_{coated} - E_{uncoated}$) in 1 M nitric acid was 150 mV (vs Ag/AgCl), and 50 mV (vs. Ag/AgCl) in 8 M nitric acid, respectively. Similarly compared to Ti coated condition, the improvement in transpassive potential was 104 mV (vs Ag/AgCl) in 1 M nitric acid, and 24 mV (vs. Ag/AgCl) in 8 M nitric acid, respectively. Owing to decrease in passive current density and increase in transpassive potential, corresponding decrease in corrosion current density was also observed in both the test solutions. The decrease in corrosion current density for TiO_2 coated specimen compared to that of Ti coated condition was significant in 1 M nitric acid whereas in 8 M nitric acid it was marginal. This is because the transpassive dissolution of oxide layer is faster due to increase in auto-catalytic activity around 50 % concentration (8 M). Hence, breakdown of passive film i.e. transpassivity was attained quickly leading to increase in corrosion current density [22]. The protection efficiency in 1 M nitric acid was 95 % in 1 M nitric acid, and 43 % in 8 M nitric acid, respectively.

The improvement in corrosion resistance of TiO_2 coated 304L SS specimens is because of its inertness in electrochemical environment, largely due to its dielectric property, high lattice and bond energy which inhibit the anodic dissolution process and provide the alloy a stable and protective surface [179, 201]. Even though TiO_2 doesn't behave as a perfect insulator [204], the dielectric strength ensures sustain of high electric field during polarization, and thus resists field assisted collapse of the passive film at the film-solution interface, and easy dissolution of passive film. Furthermore, higher dielectric strength lowers electronic conduction through the passive film, thus charge transfer process as well as activation energy for creation of physical "faults" in passive film, which act as precursor sites for localized breakdown are also reduced. Apart from this due to high lattice energy the cohesive force in the lattice is also high. Thus, large extent of electrostatic potential barrier has to be overcome in order to polarize the surrounding environment, and consequently to pull out an ion from oxide lattice leading to initiation of surface dissolution.

Covalent aspect of lattice cohesion such as bond energy also influences the overall dissolution rate because, on dissolution bonds between constituents of a crystal have to be broken. Thus, higher energy is needed to breakdown the bond and lattice disintegration to initiate.

Although, thermodynamical and electrical properties determines the overall stability of the passive film, structural defects present on the coated surface also play a significant role in accelerating corrosion rate by increasing the accessible areas of base material to the corrosive environment. Local defects such as pinholes and continuous boundaries in between the columnar grains on the coated surface are the preferable sites for the initiation of sub-coating corrosion due to absorption of electrolyte as a result of capillary action [205]. These surface defects create solution paths, and facilitates diffusion of oxygen within the coating leading to crevice as well as galvanic corrosion between the coating and the underlying substrate. Once solution reaches the bottom of the coated surface, the exposed areas of the substrate will subject to accelerated anodic dissolution resulting increase in passive current density and corrosion current density. Moreover, unfavourable area ratio such as, large cathodic area of coating and small anodic area of the pinholes reduces the corrosion protection of the coated surface due to galvanic effect. As galvanic corrosion becomes localized, local active dissolution of the steel surface increases and consequently propagates laterally along the interface between the coating and the substrate. However, presence of porosity in the coating is inevitable, and is inversely proportional to the coating thickness. Thus by increasing the thickness and carefully selecting the deposition parameters the extent of pore formation can be reduced and consequently corrosion resistance of the coated materials can be increased. Nevertheless, by increasing thickness stresses are also generated in the coated surface leading to peeling off and flaking of the coating and thus optimum coating thickness of 1 μ is generally preferred for corrosion protection.

6.2.2.5 Morphological investigation after potentiodynamic polarization study

The surface morphology of the polarized specimens of uncoated and TiO_2 coated 304L SS specimens examined using AFM after potentiodynamic polarization in both the concentration of nitric acid are shown in Fig. 6.12a-d [22]. The morphology of uncoated 304L SS specimens revealed grain boundary structures in both the test solutions after polarization which is due to intergranular corrosion in nitric acid medium (Fig. 6.12a and c). The severity of attack was higher for higher concentration of nitric acid. At higher concentration depletion of protective Cr_2O_3 film from the surface occurs due to increase in oxidizing power of nitric acid, which exposes high energy regions such as grain boundaries to the electrochemical environment [22].

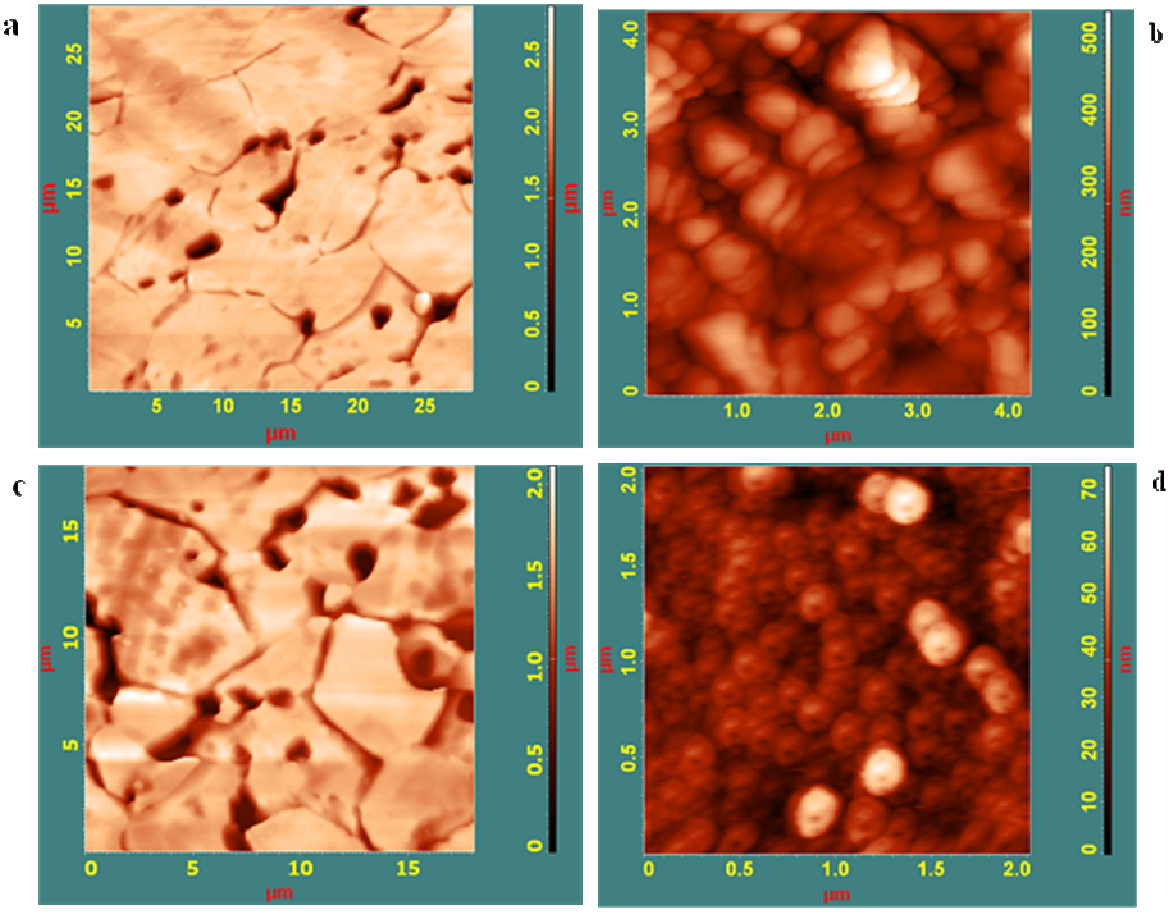

Fig. 6.12a-d: Surface morphology of uncoated and TiO_2 coated 304L SS after potentiodynamic polarization; (a) uncoated (1 M HNO_3), (b) TiO_2 coated 304L SS (1 M HNO_3), (c) uncoated (8 M HNO_3), (d) TiO_2 coated 304L SS (8 M HNO_3) [22].

As compared to uncoated specimens, morphology of TiO_2 coated specimens after polarization did not reveal any grain boundary opening up, thereby showing greater resistance to surface dissolution as well as intergranular corrosion (Fig. 6.12b and d) [22]. The improved resistance to intergranular corrosion is due to high passive film stability as well as low anodic dissolution rate of titanium dioxide in nitric acid medium. The morphology of TiO_2 coated specimens after polarization in 1 M nitric acid did not show much change in surface morphology (Fig. 6.12b). However, in 8 M nitric acid uniform dissolution of the coated surface was observed (Fig. 6.12d), leading to change in shape, and decrease in particle size of the oxide layer [22]. Moreover, the pinholes were widely open, and apparent separation between the particles were well observed. This is due to shrinkage in size of the particles as a result of dissolution along the periphery at the inter-columnar boundaries in the coated surface [22]. Nevertheless, in both concentrations, the extent of dissolution was less as compared to uncoated specimens, and no intergranular corrosion was observed [22].

6.2.3 Corrosion behaviour of duplex Ti-TiO_2 coated 304L SS in nitric acid medium

6.2.3.1 Phase and morphology characterization

The phase analysis of the duplex Ti-TiO_2 coated 304L SS revealed anatase phase as shown for TiO_2 coated 304L SS (Fig. 6.7). The morphological analysis of the duplex Ti-TiO_2 coated specimen is shown in Fig. 6.13a-d. The morphology of the coated surface showed spherical particles uniformly covering the surface (Fig. 6.13a). The histogram showing the distribution of the particles as a function of frequency of formation is shown in Fig. 6.13b. The sizes of the particles generally range from 12×10^{-3} μm^2 to 1.25 μm^2. However, certain agglomerated particles were having sizes up to 4.5 μm^2. The exact location, and morphology of the pores present on the surface is shown in Fig. 6.13c. The histogram showing the distribution of the size of the pores as a function of frequency of formation is shown in Fig. 6.13d. The size of the pores in the duplex Ti-

TiO_2 coated specimens ranges from 4×10^{-3} μm^2 to 90×10^{-3} μm^2. It is clear from Fig. 6.2d. 6.8d, and 6.13d that the size of the pores as well as the extent of formation was decreased from single layer Ti and TiO_2 coating to duplex Ti-TiO_2 coating. The prior deposition of Ti coating facilitates the nucleation and growth of TiO_2 particles at defective sites, and lead to uniform coverage of the surface which is desirable from corrosion point of view [206]. Nevertheless, pores can also be noticed in the duplex coated surface which could be due to the parallel overlap of pores in Ti, and thereafter in TiO_2 coating. The root mean square roughness (R_q) on the surface was 16 nm.

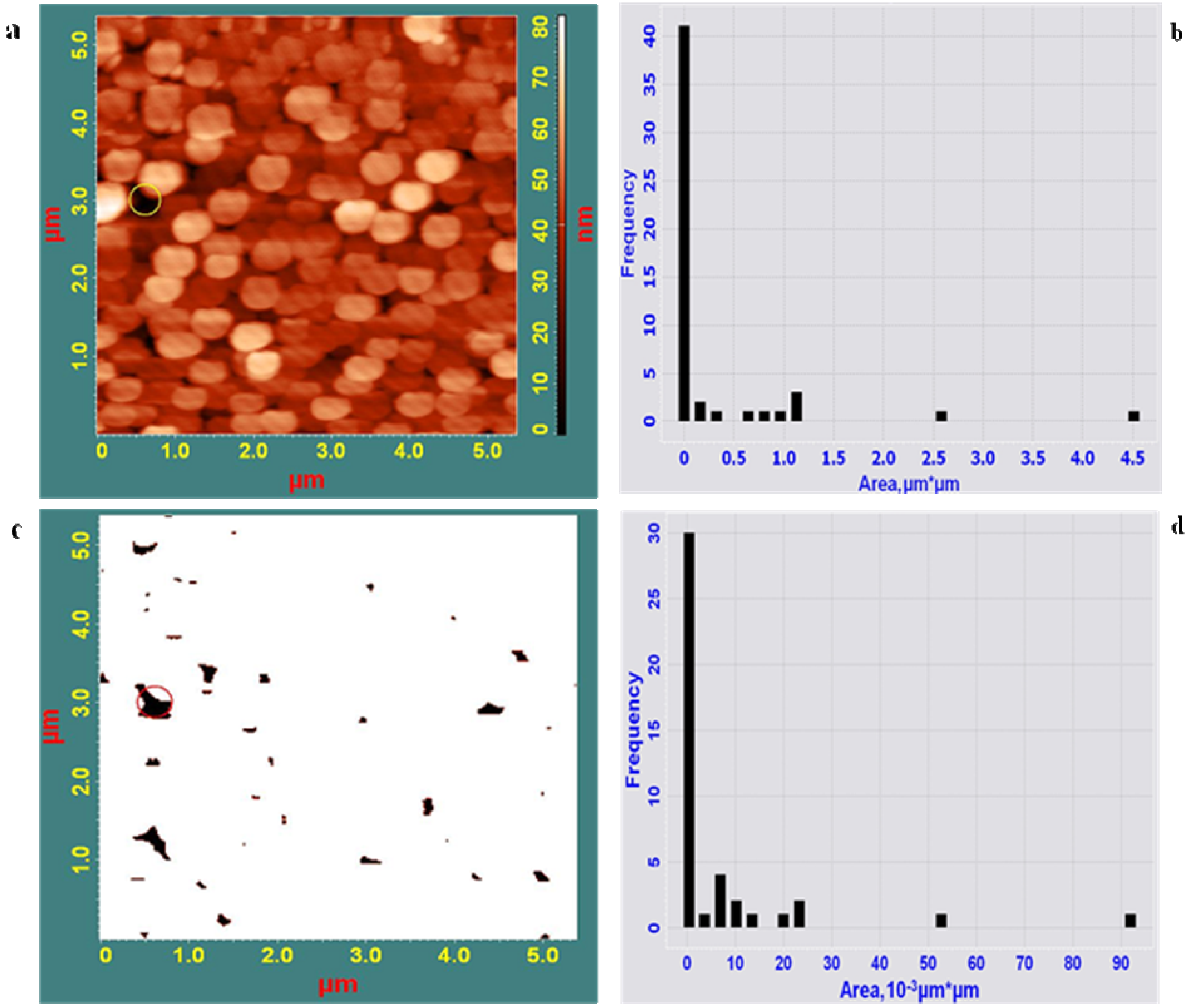

Fig. 6.13a-d: (a) Morphology of duplex Ti-TiO_2 coated 304L SS, (b) histogram for the particle size distribution, (c) morphology of the pores, and (d) histogram for the size distribution of the pores.

6.2.3.2 Open circuit potential vs. time measurement

The results of OCP vs. time measurement for uncoated, and duplex Ti-TiO_2 coated 304L SS in 1 M and 8 M nitric acid are shown in Fig. 6.14a-b. As observed earlier for the investigations with Ti and TiO_2 coated specimens, the uncoated specimens showed steady state potential with increase in immersion time, and the OCP was higher for 8 M nitric acid. The OCP for duplex Ti-TiO_2 coated specimens in 1 M nitric acid gradually increased, and attained steady state with increase in immersion time.

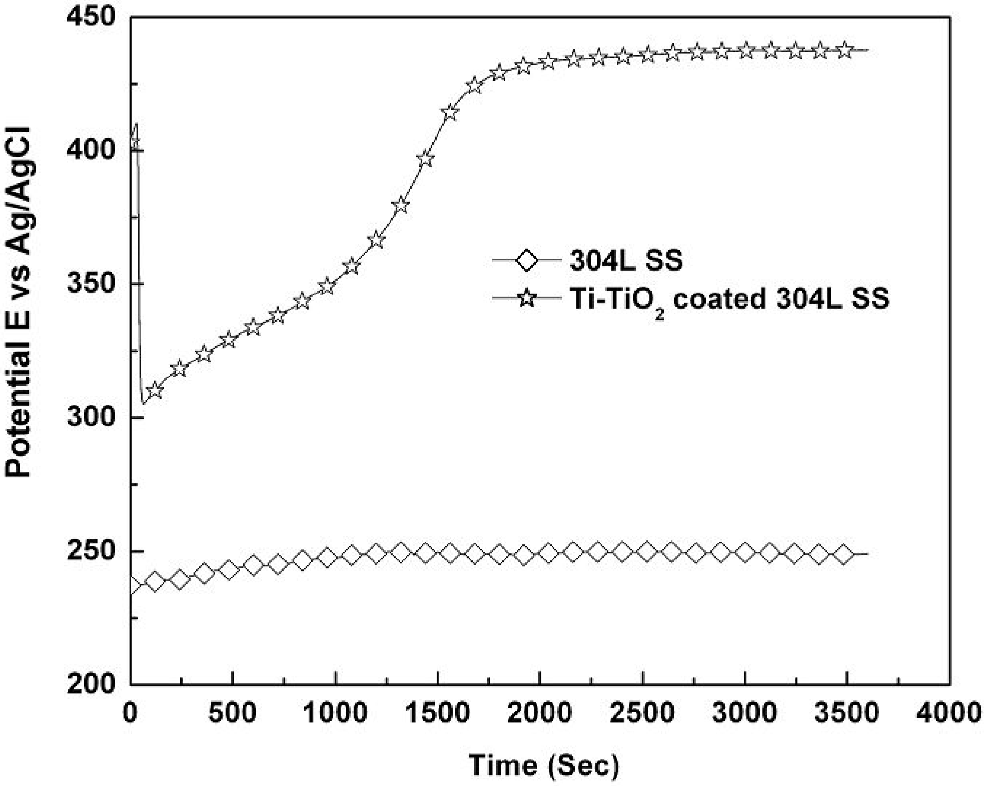

Fig. 6.14a: OCP vs. time measurement for uncoated and duplex Ti-TiO_2 coated 304L SS in 1 M HNO_3.

Steady improvement as well as attainment of stable OCP shows the effectiveness of fine grained duplex coating in minimizing the frequency of pore formation and columnar boundaries, and improving the passivation property [207]. Moreover, successive layers in duplex coating restricts the ingress of the solution, and provides stability at the coating-substrate interface giving inherent advantage over single layer coating. In 8 M nitric acid also the OCP was higher, and showed steady improvement with increase in time, however transient points were observed prior to attainment of steady state which could be due to competitive passive film formation and dissolution at the few existing structural heterogeneities such as pinholes and inter-columnar boundaries causing increase in oxidizing ability.

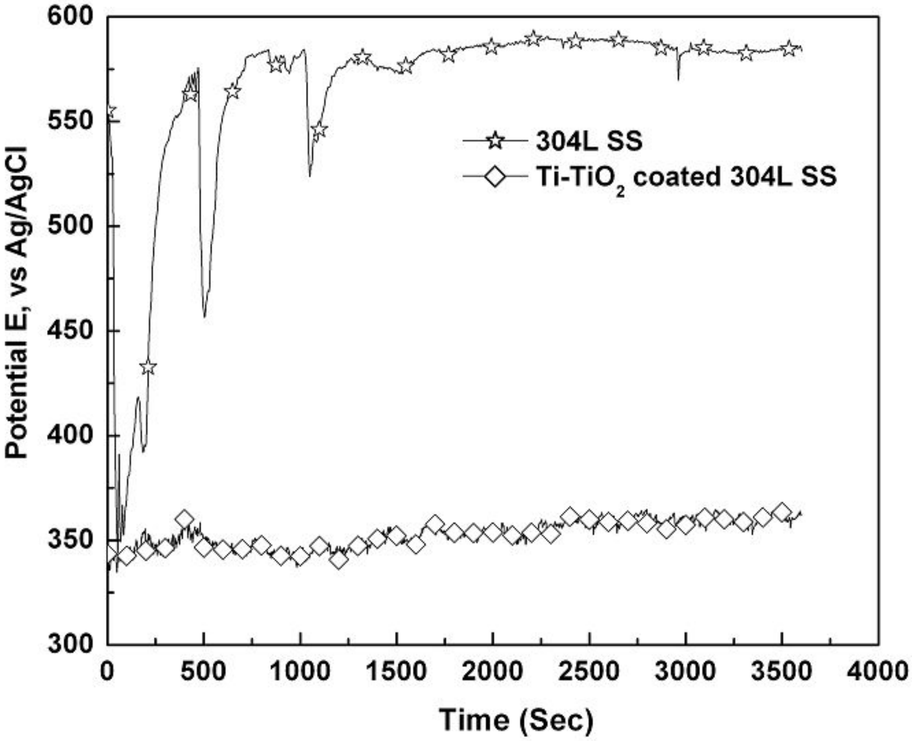

Fig. 6.14b: OCP vs. time measurement for uncoated and Ti-TiO_2 coated 304L SS in 8 M HNO_3.

6.2.3.3 Electrochemical impedance analysis

The results of electrochemical impedance analysis for uncoated, and Ti-TiO_2 coated 304L SS in 1 M and 8 M nitric acid in OCP condition are shown in Fig. 6.15a-d. As mentioned earlier, the fitted graphs obtained using electrical equivalent circuit model as shown in Fig. 3.10a-b are also shown in Fig. 6.15a-d. The plot of phase angle (θ) vs. frequency in 1 M nitric acid largely revealed near capacitive property in the entire frequency domain of investigation with one time constant feature which shows the formation of very stable passive film as well as resistance to alteration in property and initiation of anodic activities on the coated surface (Fig. 6.15a) [208].

Similarly, the plots for total impedance (|Z|) vs. frequency showed significant improvement in magnitude of total impedance as well as slope of -1 over entire frequency region for the duplex Ti-TiO_2 coating as compared to single layer Ti and TiO_2 coating indicating increase in capacitive property with duplex coating (Fig. 6.15b).

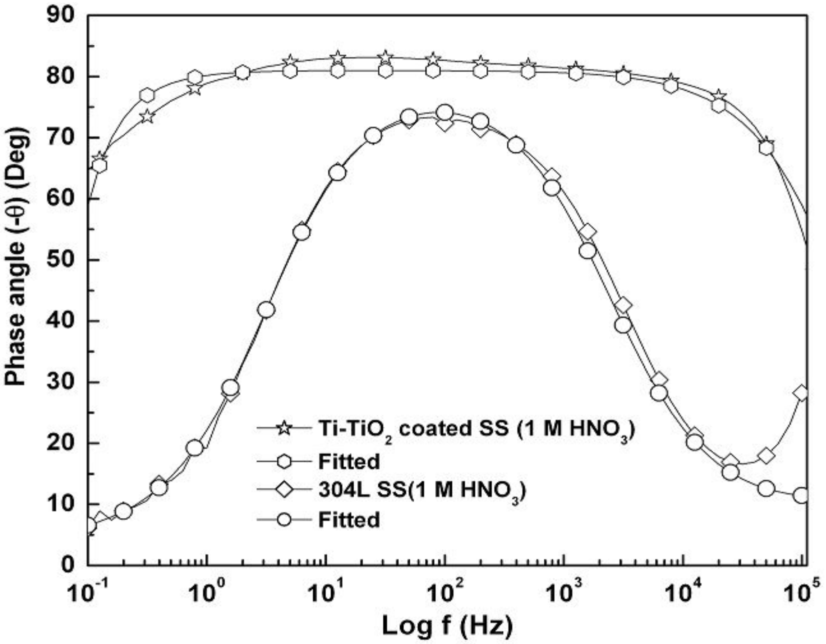

Fig. 6.15a: Log f vs. θ for uncoated and duplex Ti-TiO_2 coated 304L SS in 1 M HNO_3.

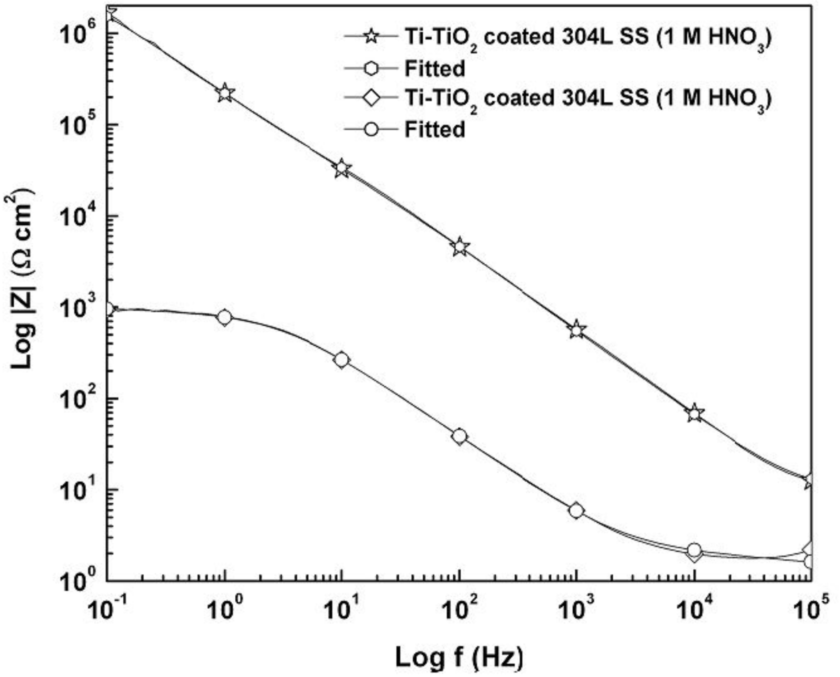

Fig. 6.15b: Log f vs. Log |Z| for uncoated and duplex Ti-TiO_2 coated 304L SS in 1 M HNO_3

The improvement in magnitude of total impedance (|Z|) for duplex Ti-TiO_2 coating in 1 M nitric acid was two orders as compared to Ti coating, and one order as compared to TiO_2 coating. The plots for phase angle (θ) vs. frequency in 8 M nitric acid revealed, near capacitive property over wide frequency region from 10^0 Hz to 10^4 Hz (Fig. 6.15c). Moreover, unique single time constant feature was observed in 8 M nitric acid what has not been observed for TiO_2 coating. It shows that presence of interlayer in duplex coating is very effective in aggressive media by containing low amount of retained charge, and hindering the charge transfer process at coating-solution as well as coating-substrate interface.

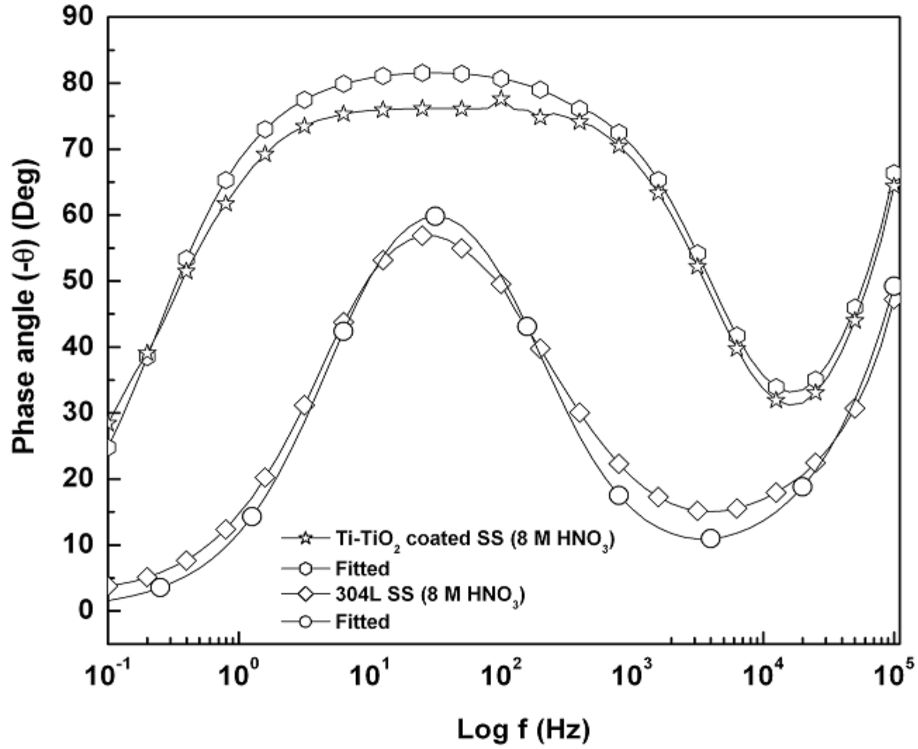

Fig. 6.15c: Log f vs. θ for uncoated and duplex Ti-TiO_2 coated 304L SS in 8 M HNO_3.

The plots of total impedance (|Z|) vs. frequency (Fig. 6.15d) predominantly showed slope of -1 up to high frequency indicating capacitive property, and is well in agreement with the plot of phase angle vs. frequency (Fig. 6.15c). The improvement in magnitude of total impedance (|Z|) for Ti-TiO_2 coated specimens in 8 M nitric acid was more than one order as compared to both Ti and TiO_2 coating. The significant improvement in total impedance shows good passivation property for the duplex coating, and greater resistance offered to the charge accumulation on the coated surface. The circuit parameters for the uncoated, and duplex Ti-TiO_2 coated specimen evaluated using circuit models as shown in Fig. 3.10a-b are given in Table. 6.5.

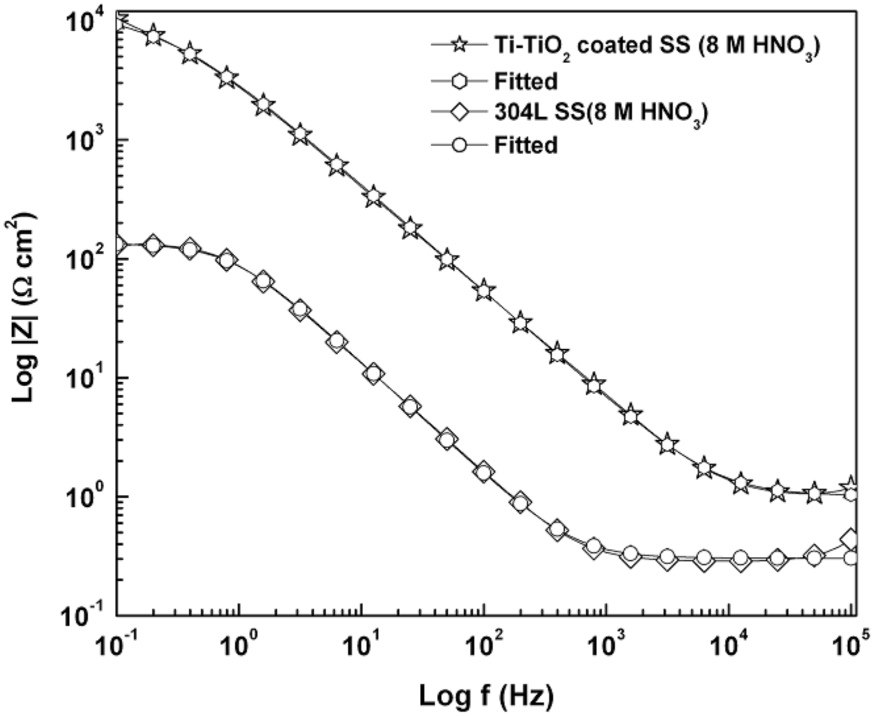

Fig. 6.15d: Log f vs. Log |Z| for uncoated and Ti-TiO_2 coated 304L SS in 8 M HNO_3.

Conc.	Substrate condition	R_s Ω cm^2	CPE$_2$		R_{ct2} Ω cm^2	CPE$_1$		R_{ct1} Ω cm^2
			C_{dl2} $\Omega^{-1}cm^{-2}S^n$	n (0-1)		C_{dl1} $\Omega^{-1}cm^{-2}S^n$	n (0-1)	
1 M	Uncoated	2	6.5×10^{-5}	0.86	9.35×10^2	-	-	-
1 M	Ti-TiO_2coated	11	1.7×10^{-7}	0.91	1.24×10^6	1.3×10^{-8}	0.98	1.1×10^3
8 M	Uncoated	1	5.8×10^{-4}	0.65	1.1×10^2	-	-	-
8 M	Ti-TiO_2coated	12	2.6×10^{-5}	0.78	1.8×10^4	1.8×10^{-6}	0.88	2.8×10^2

Table. 6.5: EIS fitted values for uncoated and duplex Ti-TiO_2 coated 304L SS in 1 M and 8 M HNO_3.

Form the circuit parameters, it is obvious that coating resistance or pore resistance (R_{ct1}) greatly improves in both the test solution with duplex coating which has not been observed either for Ti or TiO_2 single layer coating. Apart from this, the coating capacitance (C_{dl1}) also showed vary low capacitance value in both medium of investigation which indicates high insulating property of the passive film developed on the coated surface. The enhancement in pore resistance, and coating capacitance properties also has been reflected in the double layer capacitance, and polarization resistance at the coating-substrate interface. As compared to Ti and TiO_2 coating, the capacitance was low indicating presence of good protective oxide film at the interface, and the polarization resistance was also quite high showing large polarization resistance.

6.2.3.4 Potentiodynamic polarization study

The potentiodynamic polarization for the uncoated, and duplex Ti-TiO_2 coated 304L SS specimens in 1 M and 8 M nitric acid are shown in Fig. 6.16a-b. The polarization curves in both the medium of investigation showed shifting of corrosion potential in noble direction with very low passive current density, and considerable improvement in transpassive potential compared to Ti and TiO_2 single layer coating.

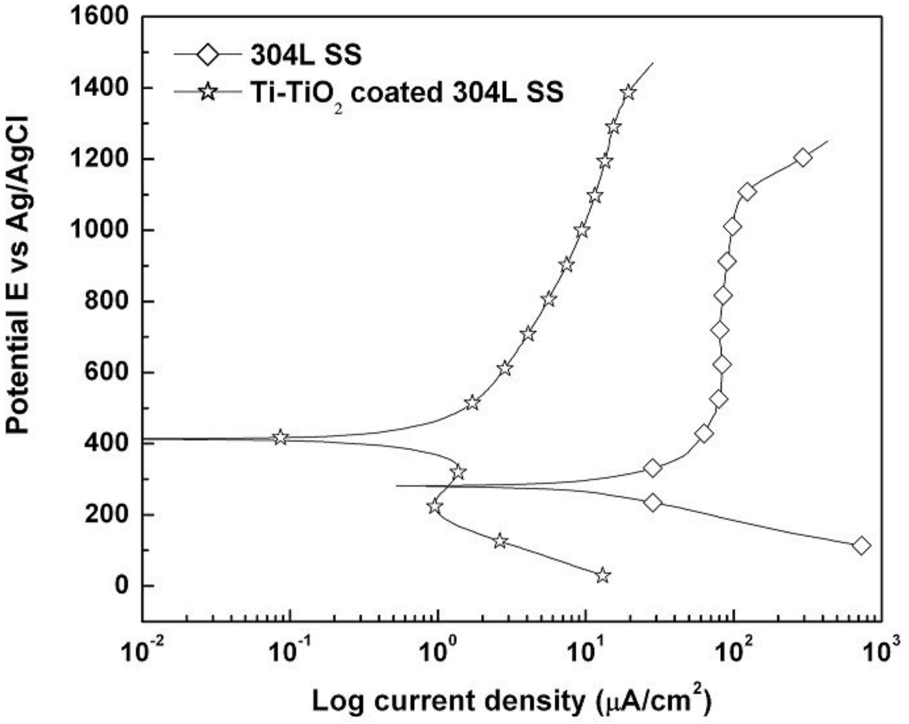

Fig. 6.16a: Polarization study of uncoated and duplex Ti-TiO_2 coated 304L SS in 1 M HNO_3.

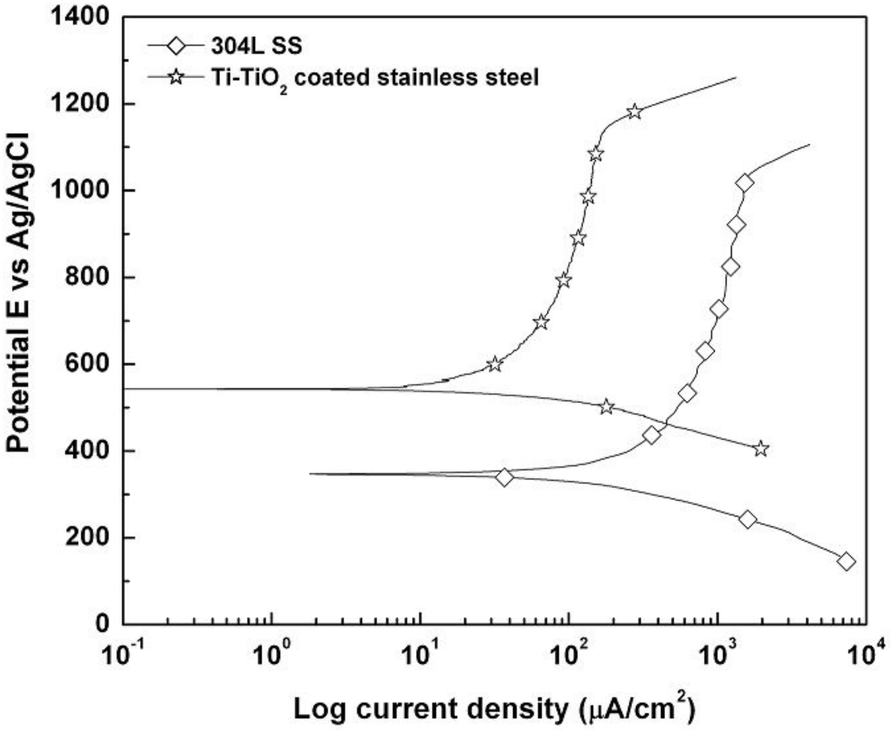

Fig.6.16b: Polarization study of uncoated and duplex Ti-TiO_2 coated 304L SS in 8 M HNO_3.

Conc.	Substrate condition	E_{corr} mV vs Ag/AgCl	I_{pass} $\mu A/cm^2$	I_{corr} $\mu A/cm^2$	$E_{transpass}$ mV vs Ag/AgCl
1 M	Uncoated	250	1.1×10^2	10×10^0	1100
1 M	Ti-TiO_2 coated	385	7×10^0	3×10^{-1}	1316
8 M	Uncoated	340	1.2×10^3	7×10^1	1025
8 M	Ti-TiO_2 coated	582	1×10^2	11×10^0	1119

Table. 6.6: Average value of polarization parameters for uncoated and duplex Ti-TiO_2 coated 304L SS in 1 M and 8 M HNO_3.

The polarization parameters evaluated for uncoated, and Ti-TiO_2 coated 304L SS are shown in Table. 6.6. The improvement in transpassive potential with respect to titanium coating is 170 mV (vs. Ag/AgCl) in 1 M nitric acid, and 68 mV (vs. Ag/AgCl), in 8 M nitric acid, respectively. Similarly as compared to TiO_2 coating, the improvement in transpassive potential was 66 mV (vs. Ag/AgCl) in 1 M nitric acid, and 44 mV (vs. Ag/AgCl) in 8 M nitric acid, respectively. From the improvement in transpassive potential it is clear that, duplex coating exhibits wide passive range as compared to both the single layer coating. It is also evident from, Table. 6.2, Table. 6.4, and Table. 6.6 that duplex Ti-TiO_2 coated specimen exhibited lowest I_{corr} value showing highest corrosion resistance out of the three different coatings investigated in the present investigation. The protection efficiency for the duplex Ti-TiO_2 coating calculated using Eq. 13 are 97 % in 1 M nitric acid, and 84 % in 8 M nitric acid, respectively.

The low passive current density as well as higher transpassive potential is due to the combination of good passivation property of outer TiO_2 layer as well as reduction in structural heterogeneity by Ti interlayer. For duplex coating the extent of structural heterogeneities has greater role in predicting the corrosion rate. If the porosity is less, the specimen behaves totally as a coating, and pores are passivated if the coating passivates showing good corrosion resistance. Similarly, if significant pores are there, the coating behaves like base material, and it fails to passivate at the pores and other structural inhomogenities regardless of how noble the coating may be. As can be observed from the Fig. 6.2d, Fig. 6.8d, and Fig. 6.13d, significant reduction of pore density in the duplex coating was observed for duplex Ti-TiO_2 coating compared to Ti and TiO_2 single layer coatings which increases the susceptibility to corrosion by increasing the dissolution rate of the base material. Moreover, from morphology and pore size analysis it is evident that the structure of duplex Ti-TiO_2 layer coating is less columnar, more compact and has fewer pinhole with small surface area as compared to Ti and TiO_2 coating which are essential to restrict the solution path to the base material. Hence, the effective isolation of the base material from oxidizing environment leads to low passive current density as well as corrosion current density. Nevertheless, pores and pinholes also can be observed from Fig. 6.13c in the duplex coating. However "repassivation" ability of the passive film in these region is higher because of small surface area and Ti intermediate layer which can oxidize itself to form protective oxide layer [195, 197, 209].

6.2.3.5 Morphological examination after potentiodynamic polarization study

The surface morphology of the polarized specimens examined using AFM after potentiodynamic polarization of uncoated and TiO_2 coated 304L SS in both the concentration of nitric acid are shown in Fig. 6.17a-d.

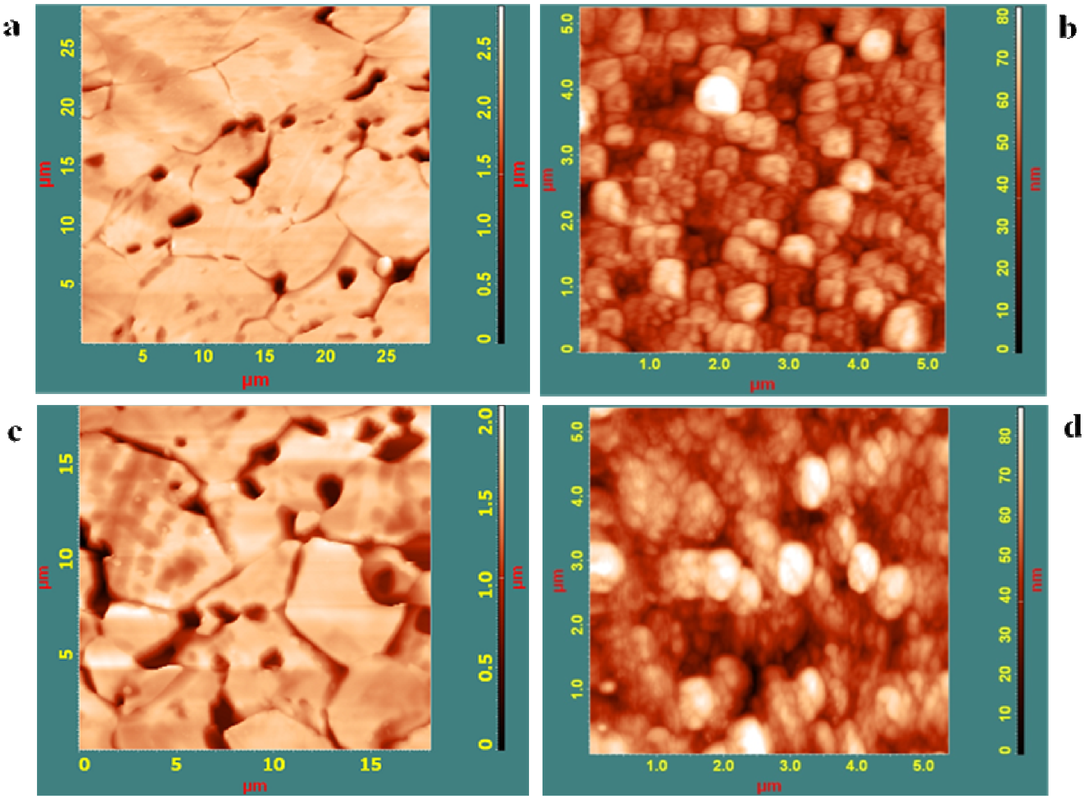

Fig. 6.17a-d: Surface morphology of uncoated and duplex Ti-TiO_2 coated 304L SS after potentiodynamic polarization; (a) uncoated (1 M HNO_3), (b) Ti-TiO_2 coated 304L SS (1 M HNO_3), (c) uncoated (8 M HNO_3), (d) Ti-TiO_2 coated 304L SS (8 M HNO_3).

As compared to Ti and TiO_2 coating, no significant dissolution of the coated surface was observed in both the medium of investigation. Moreover, no grain boundary dissolution of the base material was also observed for coated surface. The specimens before and after polarization were mostly similar, and no significant opening up of the pores as well as detaching of the particles from the base material was observed. Overall, the duplex Ti-TiO_2 coated 304L SS specimens showed greater resistance to dissolution in both the medium of investigation as compared to single layer Ti or TiO_2 coating.

CHAPTER 7

Conclusions, Summary and Scope for Future Work

CHAPTER 7

Conclusions, Summary and Scope for Future Work

The chapter provides important conclusions from the results of the investigations carried out on morphological and compositional analysis of passive film of 304L SS in nitric acid, as well as by sub-surface, and top-surface modifications on the corrosion behaviour of 304L SS in nitric acid medium. Apart from this, the chapter provides a summary and suggests additional work which may be carried out in future to further understand the corrosion behaviour 304L SS in nitric acid medium.

7.1 Conclusions from the study on morphological and compositional analysis of passive film on AISI 304L stainless steel in nitric acid medium

Following are the major conclusions from the study on “morphological and compositional analysis of passive film on AISI 304L stainless steel in nitric acid medium” to understand the passive film properties of 304L SS in nitric acid.

1. Ex-situ passive film surface morphology study after immersion in 1 M, 4 M, 8 M and 11.5 M nitric acid up to 27h showed good passive film stability in 1 M and 4 M nitric acid, respectively. In 1 M and 4 M nitric acid, homogenization of the passive film and decrease in root mean square roughness value from 15 nm to 10 nm was observed with increase in immersion time up to 27 h. In 8 M nitric acid, homogenization of the passive film as well as breakdown of passive film as distorted topography on the polished surface was observed with increase in immersion time. The root mean square roughness increased from 15 nm to 28 nm after immersion for 27 h. In 11. 5 M nitric acid formation of uniform passive film was not

observed with increase in immersion time, instead surface became stained with degraded passive film and corrosion products with increase in root mean square roughness from 15 nm in as polished condition to 52 nm after immersion for 27 h.

2. Potentiodynamic polarization study in 0.1 M, 0.5 M, 0.6 M, and 1 M nitric acid showed increase in passive current density and corrosion current density, and decrease in transpasive potential with increase in concentration of nitric acid. Passive current density increased by one order, corrosion current density increased by two order, and transpassive potential decreased by 150 mV vs. Ag/AgCl from 0.1 M to 1 M nitric acid.
3. In-situ passive film surface morphology study in 0.1 M, 0.5 M, 0.6 M, and 1 M nitric acid using EC-AFM showed the growth of passive film in the form of platelet like structure at lower concentration of 0.1 M and 0.5 M nitric acid. At concentration of 0.6 M and 1 M nitric acid the platelet like structures got agglomerated, homogenized and started depleting from the surface leading to selective dissolution and opening up of oxide boundaries.
4. X-ray photoelectron spectroscopy analysis of passive film as observed in in-situ study in 0.1 M, 0.5 M, 0.6 M, and 1 M nitric acid revealed the presence of hydroxide and oxide layer on 304L SS at lower concentration of 0.1 M and 0. 5 M nitric acid. Towards higher concentrations of 0.6 M and 1 M nitric acid, presence of oxide layer was observed. Overall, the passive film at lower concentration consists of hydroxide and oxide layer, and at higher concentration it consists of oxide layer only.

7.2 Conclusions from the study on corrosion behaviour of nitrogen ion implanted AISI 304L stainless steel in nitric acid medium

Followings are the major conclusions from the study on “corrosion behaviour of nitrogen ion implanted AISI 304L stainless steel in nitric acid medium” to understand the effect of sub-surface modification on the corrosion behaviour of 304L SS in nitric acid medium.

1. Surface morphology examination of the nitrogen ion implanted 304L SS by AFM revealed smoothening of the surface with increase in dose rate. The smoothening of the surface is due to preferential sputtering from the grain boundaries during the process of implantation.
2. SIMS analysis of the nitrogen ion implanted 304L SS specimens showed enrichment of nitrogen in the surface. With enrichment of nitrogen in the surface, the intensity profiles of the major alloying elements such as iron, chromium and nickel initially decreased, and subsequently attained steady state with increase in depth of sputtering.
3. GIXRD and XPS analysis of the nitrogen ion implanted 304L SS specimens showed preferential formation of chromium nitride at higher doses. The formation of chromium nitride (Cr_2N) at higher doses is due to their low enthalpy of formation.
4. Electrochemical corrosion investigations of unimplanted and nitrogen implanted 304L SS in 1 M nitric acid revealed decrease in passive current density and corrosion current density, and improvement in transpassive potential. The corrosion current density decreased by two order of magnitude, passive current density by one order of magnitude, and marginal improvement in transpassive potential by 10 mV vs. Ag/AgCl, respectively.
5. Surface morphology analysis of the unimplanted and nitrogen ion implanted 304L SS in 1 M nitric acid using AFM after polarization study showed aggressive grain boundary dissolution in unimplanted specimens, and resistance to grain boundary attack with increase in dose rate of nitrogen ion implantation. The results of morphological study after polarization show that nitrogen ions are effective in resisting the intergranular corrosion of 304L SS in nitric acid medium. The causative factor for the resistance to surface dissolution at higher doses is because formation of chromium nitride which increases the ability for oxide layer formation, and enrichment of nitrogen which buffers the local *p*H and decreases dissolution at grain boundaries.

7.3 Conclusions from the study on corrosion performance of Ti, TiO_2 and duplex Ti-TiO_2 coated AISI 304L stainless steel in nitric acid medium

Following are the major conclusions from the study on “corrosion performance of Ti, TiO_2, and duplex Ti-TiO_2 coated 304L stainless steel in nitric acid medium” to understand the effect of top surface modification on the corrosion behaviour of 304L SS in nitric acid medium.

1 Single Ti layer coating on 304L SS showed low capacitive and high resistive property at 1 M nitric acid showing good passive film stability. However, at 8 M nitric acid the coating capacitance increased and polarization resistance decreased indicating formation of less stable passive film. The low stability of oxide film at higher concentration is due to high dissolution rate of the oxide film developed on the surface.

2 Single Ti layer coated 304L SS specimens showed moderate to marginal improvement in corrosion resistance in 1 M and 8 M nitric acid medium, respectively. The percentage of protection efficiency was 52 % in 1 M nitric acid, and 27 % in 8 M nitric acid.

3 Titanium dioxide (TiO_2) coated 304L SS showed low capacitive and high resistive property as compared to Ti coated 304L SS in both 1 M and 8 M nitric acid.

4 The improvement in corrosion resistance of TiO_2 coated 304L SS in both 1 M and 8 M nitric acid was better than Ti coated 304L SS despite presence of pores and other structural heterogeneities. However, at 8 M nitric acid uniform dissolution of the coated surface was observed. The protection efficiency was 95 % in 1 M and 43 % in 8 M nitric acid, respectively.

5 Duplex Ti-TiO_2 coated 304L SS showed reduction in the frequency of pore formation and their size as compared to single layer Ti and TiO_2 coatings. This shows the effectiveness of interlayer coating in minimization of heterogeneities, and controlling the microstructure.

6 Duplex Ti-TiO_2 coated 304L SS showed lower capacitance and higher polarization resistance as compared to both Ti and TiO_2 coatings in both 1 M and 8 M nitric acid exhibiting excellent corrosion resistance. The protection efficiency was 97 % in 1 M nitric acid, and 84 % in 8 M nitric acid, respectively.

7 The improvement in corrosion resistance of duplex Ti-TiO_2 coating as compared to Ti and TiO_2 single layer coatings on 304L SS is attributed to the effective minimization of structural heterogeneities, and formation of uniformly distributed particles enhancing passivation property**.**

7.4 Summary

The results of the present investigation on "***Role of passivity and surface modification on the corrosion behaviour of AISI 304L stainless steel in nitric acid medium***" using surface morphological studies, analytical examinations, and electrochemical investigations is as summarized below.

Passivity of AISI 304L SS at low concentration of 0.1 M and 0.5 M nitric acid starts initially with the formation of adsorbed chromium hydroxide species which appears in the form of platelet like structures on the surface. The hydroxide layer at lower concentration is electro-inactive and provides protective film from aggressive environment of nitric acid. With increase in concentration to 0.6 M nitric acid, the hydroxide layer changes over to oxide layer, and during this platelet like structures forms homogenous oxide layer on the surface. With still rise in concentration of nitric acid to 1 M the protective oxide film depletes from structural heterogeneous areas leading to opening up of oxide boundaries. The depletion of oxide layer at structural heterogeneous areas initiate selective dissolution as well as localized corrosion in 304L SS.

Sub-surface modification using nitrogen ion implantation on 304L SS brings structural and compositional changes on the surface which significantly increases the localized corrosion resistance in the oxidizing environment of nitric acid. The factors responsible for the improvement in corrosion resistance are homogenization of the surface, enrichment of nitrogen and formation of selective chromium nitride (Cr_2N) phase. Thus the beneficial aspect nitrogen on the corrosion resistance is well reflected from the study on corrosion behaviour of nitrogen ion implanted 304L SS in nitric acid medium.

Top surface modification using Titanium (Ti) layer gives good corrosion performance in 1 M nitric acid. The oxide film developed is stable enough to resist attack at structural heterogeneous areas. At higher concentration of 8 M nitric acid, the oxidizing action in the pores and intergranular boundaries increases which decreases the protection efficiency and performance of the 304L SS. Titanium dioxide gives improved corrosion performance as compared to titanium coating in both low (1 M) and high (8 M) concentration of nitric acid despite presence of pores and other structural heterogeneities. This is mainly due to presence of perfect stoichiometric oxide with good passivation property. Even though TiO_2 shows good corrosion performance, uniform dissolution of the coating can be observed at 8 M nitric acid. Duplex Ti-TiO_2 coating is extremely effective for corrosion protection in both low (1 M) and high concentration (8 M) of nitric acid as compared to Ti and TiO_2 coatings due to combination of good passivation property of titanium dioxide and minimization of structural heterogeneities by Ti interlayer. The percentage of protection efficiency and performance is far superior to both the single layer coatings. Top surface modification is more effective than sub-surface modification for corrosion protection because of easy optimization of microstructure by tunable reduction of pores and other structural heterogeneities on the surface.

7.5 Scope for Future Work

- **EC-SPM study on effect of temperature on the passive film morphology, stability and degradation of 304L stainless steel in nitric acid medium.**

The present work, and existing literatures gives qualitative and quantitative information regarding the passive film property under in-situ condition in nitric acid medium at room temperature condition. However, variation in temperature has major role on the passive film properties such as nucleation and growth, formation and stability, change in donor-acceptor density with change in activation energy, active-passive transition behaviour etc. As nucleation and propagation of localized corrosion is related to the above mentioned properties, establishment of a correlation between protective properties of the passive film as a function temperature is vital in elucidating the many details of temperature effect on the corrosion behaviour of 304L SS in nitric acid medium. EC-SPM can play a significant role in understanding the in-situ process of nucleation and growth of passive film at different temperature condition. Morphological investigation in association with other electrochemical, and surface analytical investigation can bring out the "effect of temperature on the passive film and corrosion aspect of 304L stainless steel in nitric acid medium".

- **EC-SPM study of passive film of 304L stainless steel in mixed solution of nitric acid containing oxidizing ions.**

Oxidizing ions have greater influence on the corrosion resistance of austenitic stainless steel as they shift the corrosion potential to the transpassive domain. Since corrosion potential shifts to transpassive potential the passive film property as well as its dissolution rate also changes in the presence oxidizing ions. Oxidizing ions also change the rate of cathodic and anodic reaction rates. The rate of these reactions on the morphological consideration of the passive film has to be analyzed under in-situ condition using EC-SPM for through analysis of the "corrosion behaviour of 304L SS in nitric acid medium containing oxidizing ions". Moreover, using in-situ EC-SPM, the optimum concentration of oxidizing ions for the formation of a stable passive film can be analyzed by monitoring passive film morphology as a function of concentration of oxidizing ions.

❖ Comparison of passive film morphology of 304L stainless steel with Nitric Acid Grade (NAG) stainless steel using EC-SPM.

Nitric acid grade stainless steel possess good corrosion resistance as compared to 304L SS in nitric acid medium which is attributed to high chromium content and tighter control of impurity level. The comparison of the passive films developed in in-situ condition on both the alloys using EC-SPM will provide morphological aspect on the passive film formation and degradation in nitric acid medium.

References

V. LIST OF REFERENCES

[1] Baldev Raj, U. Kamachi Mudali, Prog Nucl Energy, 48 (2006) 283-313.

[2] U. Kamchi Mudali, R. K. Dayal, J. B. Gnanmoorthy, J. Nucl Mater, 203 (1993) 73-82.

[3] S. Ningshen, U. Kamachi Mudali, G. Amarendra, Baldev Raj, Corros Sci, 51 (2009) 322-329.

[4] S. Ningshen, U. Kamachi Mudali, S. Ramya, Baldev Raj, Corros Sci, 53 (2011) 64-70.

[5] S. Ningshen, U. Kamachi Mudali, P. Mukherjee, A. Sarkar, P. Barat, N. Padhy, Baldev Raj, Corros Sci, 50 (2008) 2124-2134.

[6] S. Girija, V. R. Raju, U. Kamachi Mudali, Baldev Raj, Corros Eng Sci Technol, 38 (2003) 309-312.

[7] S. Girija, U. Kamachi Mudali, H. S. Khatak, Baldev Raj, Corros Sci, 49 (2007) 1665-1673.

[8] L. Vehovar, M. Tendler, Nucl Eng Des, 206 (2001) 21-33.

[9] T. Yamamoto, S. Tsukui, S. Okamoto, T. Nagai, M. Takeuchi, S. Takeda, Y. Tanaka, J Nucl Mater, 228 (1996) 162-167.

[10] D. Feron, D. Crusset, J. M. Gras, J. Nucl Mater, 379 (2008)16-23.

[11] U. Kamachi Mudali, Y. Katada, Electrochim Acta, 46 (2001) 3735-3742.

[12] G. Okamoto, Corros Sci, 13 (1973) 471-489.

[13] L. Wegrelius, I. Olefjord, Mater Sci Forum, 347 (1995) 185-188.

[14] G. Song, Corros Sci, 47 (2005) 1953-1987.

[15] A. J. Sedriks, Corrosion of stainless steels, Ed: A John Sedriks, Wiley, 1979.

[16] H. Saito, T. Shibata, G. Okamoto, Corros Sci, 19 (1979) 693-708.

[17] R. P. Frankenthal, J. Kruger, Passivity of metals; Proceedings of the fourth international symposium on passivity, Ed: Robert Peter Frankenthal, Jerome Kruger, The Electrochemical society, Princeton, 1978.

[18] P. Marcus, Corrosion mechanism in theory and practice, Ed: Philippe Marcus, Marcel Dekker Inc, 2002.

[19] H. H. Uhlig, Corros Sci, 19 (1979) 777-791.

[20] N. Padhy, S. Ningshen, U. Kamachi Mudali, Baldev Raj, Scripta Mater, 62 (2010) 45-48.

[21] N. Padhy, S. Ningshen, B. K. Panigrahi, U. Kamachi Mudali, Corros Sci, 52 (2010) 104-112.

[22] N.Padhy, Subhash Kamal, Ramesh Chandra, U. Kamachi Mudali, Baldev Raj, Surf Coat Technol, 204 (2010) 2782-2788.

[23] A. Kakodkar, World Nuclear Association, Annual symposium, London, 2002.

[24] R. E. H. Sims, H-H. Rogner, K. Gregory, Energy Policy, 31 (2003) 1315-1326.

[25] Baldev Raj, H. S. Kamath, R. Natarajan, P. R. Vasudeva Rao, Prog. Nucl Energy, 47 (2005) 369-379.

[26] P. Hogselius, Energy Policy 37 (2009) 254-263.

[27] P. K. Dey, N. K. Bansal, Nucl Eng Des, 236 (2006) 723-729.

[28] C. K. Gupta, Chemical Metallurgy; principles and practices, Ed: C. K. Gupta, Wiley-VCH, 2003.

[29] H. Nagano, H. Kajimura, Corros Sci, 38 (1996) 781-791.

[30] A. Ravi Shankar, V.R. Raju, M. Narayana Rao, U. Kamachi Mudali, H.S. Khatak, Baldev Raj, Corros Sci, 49 (2007) 3527-3538.

[31] C. Bernard, J. P. Mouroux, J. Decours, R. Deamy, J. Simonnet, Proceedings of the international conference on fuel reprocessing and waste management, Sendai, Japan, RECOD 91, 2, 4-18 April (1991), 570-575.

[32] C. Kato, T. Motooka, M. Yamamoto, Stress corrosion cracking of zirconium used in the reprocessing plant, GLOBAL 2007, Boise, Idaho, September 9-13, 2007.

[33] P. Marshall, Austenitic stainless steel; microstructure and mechanical properties, Ed: P. Marshall, Elsevier Applied Science Publisher, 1984.

[34] H. S. Khatak, Baldev Raj, Corrosion of austenitic stainless steel; Mechanism, Mitigation and Monitoring, Eds: H. S. Khatak, Baldev Raj, Narosa Publishing House, 2002.

[35] G. E. Totten, Steel heat treatment hand book, Ed: G. E. Totten, Taylor and Francis, 2007.

[36] G. F. Vendor Voort, metallography and microstructure, Ed: George. F. Vendor Voort, American Society of Metals, 2004.

[37] G. Okamoto, T. Shibata, Corros Sci, 10 (1970) 371-378.

[38] U. Kamachi Mudali, Baldev Raj, high nitrogen steels and stainless steels; Manufacturing, Properties and applications, Eds: U. K. Mudali, Baldev Raj, Narosa Publishing House, 2002.

[39] K. Sugimoto, Y. Sawada, Corros Sci, 17 (1979) 425-445.

[40] K. Hasimoto, K. Asami, K. Teramoto, Corros Sci, 19 (1970) 3-14.

[41] J. A. Epstein, I. Levin, S. Raviv, Electrochim Acta, 9 (1973) 1665-1673.

[42] P. Fauvet, F. Balbaud, R. Robin, Q. T. Tran, A. Mugnier, D. Espinoux, J Nucl Mater, 375 (2008) 52-64.

[43] M. Takeuchi, G. O. H. Whillock, J Nucl Sci Tech, 41 (2004) 702-708.

[44] F. Balbaud, G. Sanchez, P. Fauvet, G. Santarini, G. Picard, Corros Sci, 42 (2000) 1685-1707.

[45] V. Bague, S. Chachoua, Q. T. Tran, P. Fauvet, J Nucl Mater, 392 (2009) 396-404.

[46] D. G. Kolman, D. K. Ford, D. P. Butt, T. O. Nelson, Corros Sci, 39 (1997) 2067-2093.

[47] J. Asher, R. F. A. Carney, T. W. Conlon, N. J. M. Wilkins, Corros Sci, 24 (1984) 411-428.

[48] M. C. Petit, D. Desjardins, M. Puiggali, A. E. Kheloui, C. Clement, Corros Sci, 32 (1991) 1315-1329.

[49] F. A. Smidt, Nucl Instrum Methods Phys Res B, 10/11 (1985) 532-538.

[50] T. D. Radjabov, Vacuum, 38 (1988) 979-985.

[51] I. Olefjord, L. Wegrelius, Corros Sci, 38 (1996) 1203-1220.

[52] A.A. Youssef, P. Budzynski, J. Filiks, A.P. Kobzev, J. Sielanko, Vacuum, 77 (2004) 37-45.

[53] L.O. Daniels, P.J. Wilbur, Nucl Instr Meth Phys Res B, 19/20 (1987) 221-226.

[54] F. M. Kustas, M. S. Misra, W. T. Tack, Mater Sci Eng, 90 (1987) 407-416.

[55] www.en.wikipedia.org.

[56] J. H. Keller, J. W. Robinson, Mater Sci Eng, 90 (1987) 423-432.

[57] J. F. Ziegler, J. P. Biersack, U. Littmark, The Stopping Range of Ions in Solids, Eds: James F. Ziegler, J. P. Biersack, U. Littmark, Pergamon, 1985.

[58] R. Constantin, B. Miremad, Surf Coat Technol, 120-121 (1999) 728-733.

[59] J. Musil, J. Vlcek, Surf Coat Technol, 112 (1999) 162-169.

[60] R.I. Bates, R.D. Arnell, Surf Coat Technol, 89 (1997) 204-212.

[61] J. Kelly, R. D. Arnel, Vacuum, 56 (2000) 159-172.

[62] S. Swann, Phys Technol, 19 (1988) 67-75.

[63] W. D. Sproul, Surf Coat Technol, 49 (1991) 284-289.

[64] www. microscopyu. com.

[65] K. C. Khulbe, T. Matsuura, Polymer, 41(2000) 1917-1935.

[66] K. L. Westra, D. J. Thomson, Thin Solid Films, 257 (1995)15-21

[67] M. R. Rodgers, M. A. Wendman, F. D. Yashar, Microelectronics Reliability, 33 (1993)1947-1956.

[68] H. J. Butt, B. Cappella, M. Kappl, Surf Sci Rep, 59(2005) 1-152.

[69] R. J. Waltman, J. Joseph, X. C. Guo, Corros Sci, 52 (2010) 1258-1262.

[70] R. J. Hamers, J. Phys. Chem, 100 (1996) 13103-13120.

[71] www.atomic force microscopy.com.

[72] J. Dudognon, M. Vayer, A. Pineau, R. Erre, Surf Coat Technol, 202 (2008) 5048-5054.

[73] H. Wulff, M. Quaas, H. Steffen, Thin Solid Films, 355-356 (1999) 395-400.

[74] J. Eymery, F. Leroy, F. Fournel, Nucl Instru Methods Phys Res B, 200 (2003) 73-78.

[75] S. Sembiring, B O.Connor, D. Li, A. V. Riessen, C Buckley, I. Low, Advances in X-Ray Analysis, 43 (2000) 319-325.

[76] B. D. Cullity, S. R. Stock, Elements of X-ray Diffraction, Eds: Bernard Dennis Cullity, Stuart R. Stock, Prentice Hall, 2001.

[77] P. Dutta, Curr Sci, 78 (2000) 1478-1483.

[78] J.M. Morabito, M.J. Rand, Thin Solid Films, 22 (1974) 293-303.

[79] M. Moens, M. Van Craen, F.C. Adams, Anal Chim Acta, 161 (1984) 53-64.

[80] E. Kossoy, Y. Khoptiar, C. Cytermann, G. Shemesh, H. Katz, H. Sheinkopf, I. Cohen, N. Eliaz, Corros Sci, 50 (2008) 1481-1491.

[81] F. M. Piras, R D Mundo, F. Fracassi, A. Magnani, Surf Coat Technol, 202 (2008)1606-1614.

[82] C. Courty, H.J. Mathieu, D. Landolt, Electrochim Acta, 36 (1991) 1623-1630.

[83] A Benninghoven, Surf Sci, 299-300 (1994) 246-260.

[84] J. C. Vickerman, A. W. Brown, N. M. Reed, Secondary ion mass spectroscopy; Principle and application, Eds: J. C. Vickerman, Alan Brown, Nicola M. Reed, Clarendon Press, 1989

[85] H. C. Swart, G. L. P. Berning, Mater Chem Phys, 41 (1995) 251-256.

[86] J. H. Liu, R. Mendonça, R.W. Bosch, M.J. Konstantinovic, J Nucl Mater, 393 (2009) 242-248.

[87] J. M. Sanz, L. Soriano, P. Prieto, G. Tyuliev, C. Morant, E. Elizalde, Thin Solid Films, 332 (1998) 209-214.

[88] B. Elsener, A. Rossi, Electrochim Acta, 37 (1992) 2269-2276.

[89] C. Donik, D. Mandrino, M. Jenko, Vacuum, 84 (2010) 1266-1269.

[90] N. Khalil, J. S. L. Leach, Electrochim Acta, 40 (1995) 1769-1772.

[91] S. J. Kerber, J. J. Bruckner, K. Wozniak, S. Seal, S. Hardcastle, T. L. Barr, J. Vac. Sci. Technol, A 14 (1996) 1314-1320.

[92] T. L. Barr, Morden ESCA, The principle and practice of photoelectron spectroscopy, Ed: Tery Lynn Barr, CRC Press, 1994.

[93] Z. Ahmad, Principle of corrosion engineering and corrosion control, Ed: Zaki Ahmad, Elsevier, 2006.

[94] S. D. Cramer, Corrosion of materials, ASM handbook; Vol: 13 (B), Ed: Stephen D. Cramer, ASM international, 2005.

[95] J. O. M. Bockris, A. K. N. Reddy, M. G. Aldeco, Modern electrochemistry, Ed: Amulya K. N. Reddy, Springer, 2006.

[96] J. R. Dygas, Solid State Ionics, 176 (2005) 2065-2078.

[97] I. Betova, M. Bojinov, V. Karastoyanov, P. Kinnunen, T. Saario, Electrochim Acta, 55 (2010) 6163-6173.

[98] R. Cabrera-Sierra, J. M .Hallen, J. Vazquez-Arenas, G. Vazquez, I. Gonzalez, J Electroanal Chem, 638 (2010) 51-58.

[99] T. Ohtsuka, T. Otsuki, Corros Sci, 40 (1998) 951-958.

[100] M. Kendig, F. Mansfeld, S. Tsai, Corros Sci, 23 (1983) 317-329.

[101] V. Freger, S. Bason, J. Membrane Sci, 302 (2007) 1-9.

[102] M. K. Orazem, B. Tribollet, Electrochemical impedance spectroscopy, Eds: Mark E. Orazem, Bernard Tribollet, Wiley Inter-Science, 2008.

[103] J. R. Macdonald, W. B. Johnson, Fundamentals of impedance spectroscopy, Eds: Evgenij Barsoukov, James Ross Macdonald, John Wiley and Sons, 2005.

[104] G.T. Burstein, Corros Sci, 47 (2005) 2858-2870.

[105] W. J. Loreenz, F. Mansfeld, Corros Sci, 21 (1981) 647-672.

[106] J. R. Galvel, Corros Sci, 47 (2005) 3053-3067.

[107] S. Sathiyanarayanan, S. Devi, G. Venkatachari, Prog Org Coat, 56 (2006) 114-119.

[108] X. M. Yang, K. Tonami, L. A. Nagahara, K. Hashimoto, Y. Wei, A. Fujishima, Surf Sci, 324 (1995) L363-L366.

[109] N. Ikemiya, S. Miyaoka, S. Hara, Surf Sci, 327 (1995) 261-273.

[110] J. R. Chen, W. T. Tsai, Electrochim Acta, doi: 10.1016/j.electacta.2010.10.024.

[111] E. P. Friis, J. E. T. Andersen, L. L. Madsen, P. Moller, J. Ulstrup, J Electroanal Chem, 431(1997) 35-38.

[112] U. Kamachi Mudali, N. Padhy, A. Ravi Shankar, Corrosion Preventation and Control, Eds: Baldev Raj, U. Kamachi Mudali, S. Rangarajan, Narosa Publication, (2009).

[113] J. Romer, M. Plaschke, G. Beuchle, J. I. Kim, J Nucl Mater, 322 (2003) 80-86.

[114] M. Hashimoto, S. Miyajima, T. Murata, Corros Sci, 33 (1992) 885-904.

[115] P. Marcus, V. Maurice, H. H. Strehblow, Corros Sci, 50 (2008) 2698-2704.

[116] T.P. Hoar, Corros Sci, 7 (1967) 341-355.

[117] R.E.Williford, C.F.Windisch Jr, R.H. Jones, Mater Sci Eng A, 288 (2000) 54-60.

[118] Q. Zhang, R. Wang, M. Kato, K. Nakasa, Scripta Mater, 52 (2005) 227-230.

[119] M. Femenia, J. Pan, C. Leygraf, P. Luukkonen, Corros Sci, 43 (2001)1939-1951.

[120] F.A. Martin, C. Bataillon, J. Cousty, Corros Sci, 50 (2008) 84-92.

[121] W. Li, D. Y. Li, Acta Mater, 54 (2006) 445-452.

[122] Ch. Kleber, M. Schreiner, Appl Surf Sci, 217 (2003) 294-301.

[123] J. SAnchez, J. Fullea, C. Andrade, J. J. Gaitero, A. Porro, Corros Sci, 50 (2008) 1820-1824.

[124] J. J. Li, D. J. Meier, J Electroanal Chem, 454 (1998) 53-58.

[125] G. Salvago, L. Magagnin, M. Bestetti, Electrochim Acta, 47 (2002) 1787-1793.

[126] V. Vignal, J. C. Roux, J. M. Olive, D.Desjardins, V.Genton, Acta Mater, 46 (1998)149-157.

[127] V. Maurice, W. P. Yang, P. Marcus, J. Electrochem. Soc, 145 (1998) 909-920.

[128] A. Machet, A. Galtayries, S. Zanna, L. Klein, V. Maurice, P. Jolivet, M. Foucault, P. Combrade, P. Scott, P. Marcus, Electochim Acta, 49 (2004) 3957-3964.

[129] J. E. Castle, C. R. Clayton, Corros Sci, 17 (1977) 7-26.

[130] T. Tsuru, Mater Sci Eng A, 146 (1991) 1-14.

[131] B. Beverskog, I. Puigdomenech, Corros Sci, 39 (1997) 43-57.

[132] G. S. Was, Prog Surf Sci. 32 (1989) 221-332.

[133] G. K. Wolf, Nucl Instru Meth Phys Res B, 46 (1990) 369-378.

[134] P. Moine, O. Popoola, J. P. Villain, N. Junqua, S. Pimbert, J. Delaford, J. Grille, Surf Coat Technol, 33 (1987) 479-486.

[135] L. Hanley, S. B. Sinnott, Surf Sci, 500 (2002) 500-522.

[136] A. M. Yacout, N. Q. Lam, J. F. Stubbins, Nucl Instru Meth Phys Res B, 42 (1989) 49-60.

[137] G. Dearnaley, Surf Coat Technol. 65(1994) l-6.

[138] C.R. Clayton, Nucl Instr Meth, 182/183 (1981) 865-873.

[139] V. Ashworth, R. P. M. Procter, W. A. Grant, Thin Solid Films, 73 (1980) 179-188.

[140] P R Gardner, Mater Des, 8 (1987) 210-219.

[141] E. Mccafferty, G. K. Hubler, P. M. Natishan, P. G. Moore, R. A. Kant, B. D. Sartwell, Mater. Sci. Eng. 86 (1987) 1-17.

[142] M. F. Stroosnijder, Surf Coat Technol, 100-l0l (1998) 196-201.

[143] S. Picard, J. B. Memet, R. Sabot, J. L. Grosseau-Poussard, J. P. Riviere, R. Meilland, Mater Sci Eng A, 303 (2001) 163-172.

[144] E. Cano, L. Martinez, J. Simancas, F. J. Perez-Trujillo, C. Gomez, J. M. Bastidas, Surf Coat Technol, 200 (2006) 5123-513.

[145] R. K. Y. Fu, D. L. Tang, G. J. Wan, P. K. Chu, Surf Coat Technol, 201 (2007) 4879-4883.

[146] C.M. Abreu, M.J. Cristobal, P. Merino, X.R. Novoa, G. Pena, M.C. Perez, Electrochim Acta, 53 (2008) 6000-6007.

[147] Sh.Song, W.Song, Zh. Fang, Corros Sci, 31 (1990) 395-400.

[148] J.P. Hirvonen, D. Ruck, S. Yan, A. Mahiout, P. Torri, J. Likonen, Surf Coat Technol 74-75 (1995) 760-764.

[149] U. Kamachi Mudali, T. Sundararajan, K.G.M. Nair, R.K.Dayal, Mater Sci Forum, 318-320 (1999) 531-538.

[150] L. Martinez Orellana, F.J. Perez, C. Gomez, Surf Coat Technol, 200 (2005) 1609-1615.

[151] G.S. Chang, J.H. Son, S.H. Kim, K.H. Chae, C.N. Whang, E. Menthe, K.T. Rie, Y.P. Lee, Surf. Coat. Technol. 112 (1999) 291-294.

[152] J.P. Riviere, P. Meheust, J.P. Villaina, C. Templiera, M. Cahoreaua, G. Abrasonis, L. Pranevicius, Surf Coat Technol, 158-159 (2002) 99-104.

[153] B. Chico, L. Martinez, F.J. Perez, Appl Surf Sci, 243 (2005) 409-414.

[154] M. Guemmaz, A. Moser, J. J. Grob, R. Stuck, Surf Coat Technol, 100-101 (1998) 353-357.

[155] Y. Arnaud, M. Brunel, A.M. De Becdelievre, M. Romand, P. Thevenard, M. Robelet, Appl Surf Sci, 26 (1986) 12-26.

[156] J. Wang, J. Xiong, Q. Peng, H. Fan, Y. Wang, G Li, B. Shen, Mater Character, 60 (2009) 197-203.

[157] N. Mottu, M. Vayer, R. Erre, Surf Coat Technol, 183 (2004) 165-173.

[158] C. Blawert, H. Kalvelage, B.L. Mordike, G.A. Collins, K.T. Short, Y. Jiraskova, O. Schneeweiss, Surf Coat Technol, 136 (2001) 181-187.

[159] H. Pelletier, P. Mille, A. Cornet, J. J Gorb, J. P. Stoquert, D. Muller, Nucl. Instr. Meth Phys Res B, 148 (1999) 824-829.

[160] S. Aggarwal, A. K. Goelt, R. K. Mohindra, P. K. Ghosh, M. C. Bhatnagar, Thin Solid Film, 237 (1994) 175-180.

[161] A. Chayahara, S. Nakashima, M. Hashimoto, T. Sasaki, M. Kurokawa, S. Kiyama, M. Satou, Nucl Inst Meth Phys Res B, 59/60 (1991) 893-896.

[162] R. Leutenecker, G. Wagner, T. Louis, U. Gonser, L. Guzman, A. Molinari, Mater Sci Eng A, ll5 (1989) 229-244.

[163] P. Marcus, M E Bussell, Appl Surf Sci, 59 (1992) 7-21.

[164] J. H. Lee, J. W. Park, J. S. Lee, C. W. Sohn, J. K. Kil, Surf Coat Technol, 196 (2005) 353-357.

[165] K. Osozawa, N. Okato, Proc: USA-Japan seminar, Passivity and its breakdown on iron and iron-based alloys, NACE (1976) 135-139.

[166] R. C. Newman, Y. C. Lu, R. Bandy, C.R. Clayton, Proc: 9th International conference on metallic corrosion, 4 (1984) 394-399.

[167] E. C. Cooney, D. I. Potter, Corros Sci, 34 (1993) 2007-2018.

[168] R.F.A Jargelius-Pettersson, Corros Sci, 41 (1999) 1639-1664.

[169] U. Kamachi Mudali, R.K.Dayal, T.P.S.Gill, J.B.Gnanmoorthy, Werkst Corros, 37 (1986) 637-643.

[170] C.O.A.Olosson, Corros Sci, 37(1995)467-479.

[171] A. Sadough Vanini, J.P. Audouard, P. Marcus, Corros Sci, 36(1994)1824-1835.

[172] U. Kamachi Mudali, N. Bhuvaneswaran, P. Shankar, Baldev Raj, Corros Sci, 46 (2004) 2867-2892.

[173] S.R. Taylor, Encyclopedia of Materials, 1259-1263, 2008

[174] H. A. Jehn, Surf Coat Technol, 125 (2000) 212-217.

[175] W. B. Nowak, Surf Coat Technol, 49 (1991) 71-77.

[176] G. Frankel, G. Grundmeier, H. McMurry, T. Shinohara, Coatings for corrosion protection, The Electrochemical Society, 2010.

[177] D.R. Gabe, G.D. Wilcox, V.E. Carter, Shreir's corrosion, 2010.

[178] H. N. McMuray, G. Willams, V. E. Carter, Shrier's corrosion, 2010.

[179] A. K. Vijh, Electrodeposition Surf Treat, 2 (1973) 461- 480.

[180] H. Park, J. A. Szpunar, Corros Sci, (1998) 525-545.

[181] M. R. Zamanzad-Gavidel, K. Raeissi, A. Saatchi, Mater Lett, 63 (2009) 1807-1809.

[182] R. Starosta, A. Zielinski, J Mater Process Technol, 157-158 (2004) 434-441.

[183] X. Z. Ding, A. L. K. Tan, X. T. Zeng, C. Wang, T. Yue, C. Q. San, Thin Solid Film, 516 (2008) 5716-5720.

[184] Y. Hamlaoui, L. Tifouti, F. Pedraza, Corros Sci, 52 (2010) 1883-1888.

[185] A. Ghasemi, V. S. Raja, C. Blawert, W. Dietzel, K. U. Kainer, Surf Coat Technol, 204 (2010) 1469-1478

[186] N. Priyantha, P. Jayaweera, A. Sanjurjo, K. Lau, F. Lu, K. Krist, Surf Coat Technol, 163-164 (2003) 31-36.

[187] F. Presuel-Moreno, M. A. Jakab, N. Tailleart, M. Goldman, J. R. Scully, Materials Today, 11 (2008) 14-23.

[188] J. T. Prater, E. L. Courtright, Surf Coat Technol, 32 (1987) 389-397.

[189] Y. Wang, Z. Jiang, Z. Yao, H. Tang, Surf Coat Technol, 204 (2010) 1685-1688.

[190] Y. Sun, Mater Lett, 58 (2004) 2635-2639.

[191] Y. Li, L. Qu, F. Wang, Corros Sci, 45 (2003) 1367-1381.

[192] C.X. Shan, X. Hou, K. L. Choy, Surf Coat Technol, 202(2008) 2399-2402.

[193] D. Siva Rama Krishna, Y. Sun, Appl Surf Sci, 252 (2005) 1107-1116.

[194] E. L. Courtright, Surf Coat Technol, 33 (1987) 327-340.

[195] H. Dong, Y. Sun, T. Bell, Surf Coat Technol, 90 (1997) 91-101.

[196] D. J. Blackwood, S. K. M. Chooi, Corros Sci, 44 (2002) 395-405.

[197] M. Metikos Hukovic, M. Ceraj Ceric, Surf Technol, 24 (1985) 273-283.

[198] D. J. Blackwood, L. M. Peter, D. E. Williams, Electrochem Acta, 33 (1988) 1143-1149.

[199] G. X. Shen, Y. C. Chen, L. Lin, C. J. Lin, D. Scantlebury, Electrochim Acta, 50 (2005) 5083-5085.

[200] N. X. Miao, D. Ling-Yan, B. Chen-Guang, C. Deng-Fu, Q. Gui-Bao. Trans Nonferrous Soc. China, 16 (2006) s723-s727.

[201] D. R. Lide, Hand book of chemistry and physics, Ed: William M Haynes, Taylor and Francis, 2010.

[202] T. Furuya, J. Kawafaku, H. Satoh, K. Shimogori, A. Aoshima, S. Tekeda, ISIJ International, 31 (1991) 189-193.

[203] M. Li, S. Luo, P. Wu, J. Shen, Electrochim Acta, 50 (2005) 3401-3406.

[204] T. Kuratomi, K. Yamaguchi, M. Yamawaki, T. Bak, J. Nowotony, M. Rekas, C. C. Sorrell, Solid State Ionics, 154-155 (2002) 223-228.

[205] F. C. Walsh, C. P. D. Leon, C. Kerr, S. Court, B. D. Barker, Surf Coat Technol, 202 (2008) 5092-5102.

[206] Y. Huang, H. Xiao, Z. Ma, J. Wang, P. Gao, Surf Coat Technol, 202 (2007) 180-184.

[207] J. H. Huang, F. Y. Quyang, G. P. Yu, Surf Coat Technol, 201 (2007) 7043-7053.

[208] S. Rudenja, C. Laygraph, J. Pan, P. Kulu, E, Telimats, V. Mikili, Surf Coat Technol, 114 (1999) 129-136.

[209] E. Soderlund, P. Ljunggern, Surf Coat Technol, 110 (1998) 94-104.

References

V. LIST OF REFERENCES

[1] Baldev Raj, U. Kamachi Mudali, Prog Nucl Energy, 48 (2006) 283-313.

[2] U. Kamchi Mudali, R. K. Dayal, J. B. Gnanmoorthy, J. Nucl Mater, 203 (1993) 73-82.

[3] S. Ningshen, U. Kamachi Mudali, G. Amarendra, Baldev Raj, Corros Sci, 51 (2009) 322-329.

[4] S. Ningshen, U. Kamachi Mudali, S. Ramya, Baldev Raj, Corros Sci, 53 (2011) 64-70.

[5] S. Ningshen, U. Kamachi Mudali, P. Mukherjee, A. Sarkar, P. Barat, N. Padhy, Baldev Raj, Corros Sci, 50 (2008) 2124-2134.

[6] S. Girija, V. R. Raju, U. Kamachi Mudali, Baldev Raj, Corros Eng Sci Technol, 38 (2003) 309-312.

[7] S. Girija, U. Kamachi Mudali, H. S. Khatak, Baldev Raj, Corros Sci, 49 (2007) 1665-1673.

[8] L. Vehovar, M. Tendler, Nucl Eng Des, 206 (2001) 21-33.

[9] T. Yamamoto, S. Tsukui, S. Okamoto, T. Nagai, M. Takeuchi, S. Takeda, Y. Tanaka, J Nucl Mater, 228 (1996) 162-167.

[10] D. Feron, D. Crusset, J. M. Gras, J. Nucl Mater, 379 (2008)16-23.

[11] U. Kamachi Mudali, Y. Katada, Electrochim Acta, 46 (2001) 3735-3742.

[12] G. Okamoto, Corros Sci, 13 (1973) 471-489.

[13] L. Wegrelius, I. Olefjord, Mater Sci Forum, 347 (1995) 185-188.

[14] G. Song, Corros Sci, 47 (2005) 1953-1987.

[15] A. J. Sedriks, Corrosion of stainless steels, Ed: A John Sedriks, Wiley, 1979.

[16] H. Saito, T. Shibata, G. Okamoto, Corros Sci, 19 (1979) 693-708.

[17] R. P. Frankenthal, J. Kruger, Passivity of metals; Proceedings of the fourth international symposium on passivity, Ed: Robert Peter Frankenthal, Jerome Kruger, The Electrochemical society, Princeton, 1978.

[18] P. Marcus, Corrosion mechanism in theory and practice, Ed: Philippe Marcus, Marcel Dekker Inc, 2002.

[19] H. H. Uhlig, Corros Sci, 19 (1979) 777-791.

[20] N. Padhy, S. Ningshen, U. Kamachi Mudali, Baldev Raj, Scripta Mater, 62 (2010) 45-48.

[21] N. Padhy, S. Ningshen, B. K. Panigrahi, U. Kamachi Mudali, Corros Sci, 52 (2010) 104-112.

[22] N.Padhy, Subhash Kamal, Ramesh Chandra, U. Kamachi Mudali, Baldev Raj, Surf Coat Technol, 204 (2010) 2782-2788.

[23] A. Kakodkar, World Nuclear Association, Annual symposium, London, 2002.

[24] R. E. H. Sims, H-H. Rogner, K. Gregory, Energy Policy, 31 (2003) 1315-1326.

[25] Baldev Raj, H. S. Kamath, R. Natarajan, P. R. Vasudeva Rao, Prog. Nucl Energy, 47 (2005) 369-379.

[26] P. Hogselius, Energy Policy 37 (2009) 254-263.

[27] P. K. Dey, N. K. Bansal, Nucl Eng Des, 236 (2006) 723-729.

[28] C. K. Gupta, Chemical Metallurgy; principles and practices, Ed: C. K. Gupta, Wiley-VCH, 2003.

[29] H. Nagano, H. Kajimura, Corros Sci, 38 (1996) 781-791.

[30] A. Ravi Shankar, V.R. Raju, M. Narayana Rao, U. Kamachi Mudali, H.S. Khatak, Baldev Raj, Corros Sci, 49 (2007) 3527-3538.

[31] C. Bernard, J. P. Mouroux, J. Decours, R. Deamy, J. Simonnet, Proceedings of the international conference on fuel reprocessing and waste management, Sendai, Japan, RECOD 91, 2, 4-18 April (1991), 570-575.

[32] C. Kato, T. Motooka, M. Yamamoto, Stress corrosion cracking of zirconium used in the reprocessing plant, GLOBAL 2007, Boise, Idaho, September 9-13, 2007.

[33] P. Marshall, Austenitic stainless steel; microstructure and mechanical properties, Ed: P. Marshall, Elsevier Applied Science Publisher, 1984.

[34] H. S. Khatak, Baldev Raj, Corrosion of austenitic stainless steel; Mechanism, Mitigation and Monitoring, Eds: H. S. Khatak, Baldev Raj, Narosa Publishing House, 2002.

[35] G. E. Totten, Steel heat treatment hand book, Ed: G. E. Totten, Taylor and Francis, 2007.

[36] G. F. Vendor Voort, metallography and microstructure, Ed: George. F. Vendor Voort, American Society of Metals, 2004.

[37] G. Okamoto, T. Shibata, Corros Sci, 10 (1970) 371-378.

[38] U. Kamachi Mudali, Baldev Raj, high nitrogen steels and stainless steels; Manufacturing, Properties and applications, Eds: U. K. Mudali, Baldev Raj, Narosa Publishing House, 2002.

[39] K. Sugimoto, Y. Sawada, Corros Sci, 17 (1979) 425-445.

[40] K. Hasimoto, K. Asami, K. Teramoto, Corros Sci, 19 (1970) 3-14.

[41] J. A. Epstein, I. Levin, S. Raviv, Electrochim Acta, 9 (1973) 1665-1673.

[42] P. Fauvet, F. Balbaud, R. Robin, Q. T. Tran, A. Mugnier, D. Espinoux, J Nucl Mater, 375 (2008) 52-64.

[43] M. Takeuchi, G. O. H. Whillock, J Nucl Sci Tech, 41 (2004) 702-708.

[44] F. Balbaud, G. Sanchez, P. Fauvet, G. Santarini, G. Picard, Corros Sci, 42 (2000) 1685-1707.

[45] V. Bague, S. Chachoua, Q. T. Tran, P. Fauvet, J Nucl Mater, 392 (2009) 396-404.

[46] D. G. Kolman, D. K. Ford, D. P. Butt, T. O. Nelson, Corros Sci, 39 (1997) 2067-2093.

[47] J. Asher, R. F. A. Carney, T. W. Conlon, N. J. M. Wilkins, Corros Sci, 24 (1984) 411-428.

[48] M. C. Petit, D. Desjardins, M. Puiggali, A. E. Kheloui, C. Clement, Corros Sci, 32 (1991) 1315-1329.

[49] F. A. Smidt, Nucl Instrum Methods Phys Res B, 10/11 (1985) 532-538.

[50] T. D. Radjabov, Vacuum, 38 (1988) 979-985.

[51] I. Olefjord, L. Wegrelius, Corros Sci, 38 (1996) 1203-1220.

[52] A.A. Youssef, P. Budzynski, J. Filiks, A.P. Kobzev, J. Sielanko, Vacuum, 77 (2004) 37-45.

[53] L.O. Daniels, P.J. Wilbur, Nucl Instr Meth Phys Res B, 19/20 (1987) 221-226.

[54] F. M. Kustas, M. S. Misra, W. T. Tack, Mater Sci Eng, 90 (1987) 407-416.

[55] www.en.wikipedia.org.

[56] J. H. Keller, J. W. Robinson, Mater Sci Eng, 90 (1987) 423-432.

[57] J. F. Ziegler, J. P. Biersack, U. Littmark, The Stopping Range of Ions in Solids, Eds: James F. Ziegler, J. P. Biersack, U. Littmark, Pergamon, 1985.

[58] R. Constantin, B. Miremad, Surf Coat Technol, 120-121 (1999) 728-733.

[59] J. Musil, J. Vlcek, Surf Coat Technol, 112 (1999) 162-169.

[60] R.I. Bates, R.D. Arnell, Surf Coat Technol, 89 (1997) 204-212.

[61] J. Kelly, R. D. Arnel, Vacuum, 56 (2000) 159-172.

[62] S. Swann, Phys Technol, 19 (1988) 67-75.

[63] W. D. Sproul, Surf Coat Technol, 49 (1991) 284-289.

[64] www. microscopyu. com.

[65] K. C. Khulbe, T. Matsuura, Polymer, 41(2000) 1917-1935.

[66] K. L. Westra, D. J. Thomson, Thin Solid Films, 257 (1995)15-21

[67] M. R. Rodgers, M. A. Wendman, F. D. Yashar, Microelectronics Reliability, 33 (1993)1947-1956.

[68] H. J. Butt, B. Cappella, M. Kappl, Surf Sci Rep, 59(2005) 1-152.

[69] R. J. Waltman, J. Joseph, X. C. Guo, Corros Sci, 52 (2010) 1258-1262.

[70] R. J. Hamers, J. Phys. Chem, 100 (1996) 13103-13120.

[71] www.atomic force microscopy.com.

[72] J. Dudognon, M. Vayer, A. Pineau, R. Erre, Surf Coat Technol, 202 (2008) 5048-5054.

[73] H. Wulff, M. Quaas, H. Steffen, Thin Solid Films, 355-356 (1999) 395-400.

[74] J. Eymery, F. Leroy, F. Fournel, Nucl Instru Methods Phys Res B, 200 (2003) 73-78.

[75] S. Sembiring, B O.Connor, D. Li, A. V. Riessen, C Buckley, I. Low, Advances in X-Ray Analysis, 43 (2000) 319-325.

[76] B. D. Cullity, S. R. Stock, Elements of X-ray Diffraction, Eds: Bernard Dennis Cullity, Stuart R. Stock, Prentice Hall, 2001.

[77] P. Dutta, Curr Sci, 78 (2000) 1478-1483.

[78] J.M. Morabito, M.J. Rand, Thin Solid Films, 22 (1974) 293-303.

[79] M. Moens, M. Van Craen, F.C. Adams, Anal Chim Acta, 161 (1984) 53-64.

[80] E. Kossoy, Y. Khoptiar, C. Cytermann, G. Shemesh, H. Katz, H. Sheinkopf, I. Cohen, N. Eliaz, Corros Sci, 50 (2008) 1481-1491.

[81] F. M. Piras, R D Mundo, F. Fracassi, A. Magnani, Surf Coat Technol, 202 (2008)1606-1614.

[82] C. Courty, H.J. Mathieu, D. Landolt, Electrochim Acta, 36 (1991) 1623-1630.

[83] A Benninghoven, Surf Sci, 299-300 (1994) 246-260.

[84] J. C. Vickerman, A. W. Brown, N. M. Reed, Secondary ion mass spectroscopy; Principle and application, Eds: J. C. Vickerman, Alan Brown, Nicola M. Reed, Clarendon Press, 1989

[85] H. C. Swart, G. L. P. Berning, Mater Chem Phys, 41 (1995) 251-256.

[86] J. H. Liu, R. Mendonça, R.W. Bosch, M.J. Konstantinovic, J Nucl Mater, 393 (2009) 242-248.

[87] J. M. Sanz, L. Soriano, P. Prieto, G. Tyuliev, C. Morant, E. Elizalde, Thin Solid Films, 332 (1998) 209-214.

[88] B. Elsener, A. Rossi, Electrochim Acta, 37 (1992) 2269-2276.

[89] C. Donik, D. Mandrino, M. Jenko, Vacuum, 84 (2010) 1266-1269.

[90] N. Khalil, J. S. L. Leach, Electrochim Acta, 40 (1995) 1769-1772.

[91] S. J. Kerber, J. J. Bruckner, K. Wozniak, S. Seal, S. Hardcastle, T. L. Barr, J. Vac. Sci. Technol, A 14 (1996) 1314-1320.

[92] T. L. Barr, Morden ESCA, The principle and practice of photoelectron spectroscopy, Ed: Tery Lynn Barr, CRC Press, 1994.

[93] Z. Ahmad, Principle of corrosion engineering and corrosion control, Ed: Zaki Ahmad, Elsevier, 2006.

[94] S. D. Cramer, Corrosion of materials, ASM handbook; Vol: 13 (B), Ed: Stephen D. Cramer, ASM international, 2005.

[95] J. O. M. Bockris, A. K. N. Reddy, M. G. Aldeco, Modern electrochemistry, Ed: Amulya K. N. Reddy, Springer, 2006.

[96] J. R. Dygas, Solid State Ionics, 176 (2005) 2065-2078.

[97] I. Betova, M. Bojinov, V. Karastoyanov, P. Kinnunen, T. Saario, Electrochim Acta, 55 (2010) 6163-6173.

[98] R. Cabrera-Sierra, J. M .Hallen, J. Vazquez-Arenas, G. Vazquez, I. Gonzalez, J Electroanal Chem, 638 (2010) 51-58.

[99] T. Ohtsuka, T. Otsuki, Corros Sci, 40 (1998) 951-958.

[100] M. Kendig, F. Mansfeld, S. Tsai, Corros Sci, 23 (1983) 317-329.

[101] V. Freger, S. Bason, J. Membrane Sci, 302 (2007) 1-9.

[102] M. K. Orazem, B. Tribollet, Electrochemical impedance spectroscopy, Eds: Mark E. Orazem, Bernard Tribollet, Wiley Inter-Science, 2008.

[103] J. R. Macdonald, W. B. Johnson, Fundamentals of impedance spectroscopy, Eds: Evgenij Barsoukov, James Ross Macdonald, John Wiley and Sons, 2005.

[104] G.T. Burstein, Corros Sci, 47 (2005) 2858-2870.

[105] W. J. Loreenz, F. Mansfeld, Corros Sci, 21 (1981) 647-672.

[106] J. R. Galvel, Corros Sci, 47 (2005) 3053-3067.

[107] S. Sathiyanarayanan, S. Devi, G. Venkatachari, Prog Org Coat, 56 (2006) 114-119.

[108] X. M. Yang, K. Tonami, L. A. Nagahara, K. Hashimoto, Y. Wei, A. Fujishima, Surf Sci, 324 (1995) L363-L366.

[109] N. Ikemiya, S. Miyaoka, S. Hara, Surf Sci, 327 (1995) 261-273.

[110] J. R. Chen, W. T. Tsai, Electrochim Acta, doi: 10.1016/j.electacta.2010.10.024.

[111] E. P. Friis, J. E. T. Andersen, L. L. Madsen, P. Moller, J. Ulstrup, J Electroanal Chem, 431(1997) 35-38.

[112] U. Kamachi Mudali, N. Padhy, A. Ravi Shankar, Corrosion Preventation and Control, Eds: Baldev Raj, U. Kamachi Mudali, S. Rangarajan, Narosa Publication, (2009).

[113] J. Romer, M. Plaschke, G. Beuchle, J. I. Kim, J Nucl Mater, 322 (2003) 80-86.

[114] M. Hashimoto, S. Miyajima, T. Murata, Corros Sci, 33 (1992) 885-904.

[115] P. Marcus, V. Maurice, H. H. Strehblow, Corros Sci, 50 (2008) 2698-2704.

[116] T.P. Hoar, Corros Sci, 7 (1967) 341-355.

[117] R.E.Williford, C.F.Windisch Jr, R.H. Jones, Mater Sci Eng A, 288 (2000) 54-60.

[118] Q. Zhang, R. Wang, M. Kato, K. Nakasa, Scripta Mater, 52 (2005) 227-230.

[119] M. Femenia, J. Pan, C. Leygraf, P. Luukkonen, Corros Sci, 43 (2001)1939-1951.

[120] F.A. Martin, C. Bataillon, J. Cousty, Corros Sci, 50 (2008) 84-92.

[121] W. Li, D. Y. Li, Acta Mater, 54 (2006) 445-452.

[122] Ch. Kleber, M. Schreiner, Appl Surf Sci, 217 (2003) 294-301.

[123] J. SAnchez, J. Fullea, C. Andrade, J. J. Gaitero, A. Porro, Corros Sci, 50 (2008) 1820-1824.

[124] J. J. Li, D. J. Meier, J Electroanal Chem, 454 (1998) 53-58.

[125] G. Salvago, L. Magagnin, M. Bestetti, Electrochim Acta, 47 (2002) 1787-1793.

[126] V. Vignal, J. C. Roux, J. M. Olive, D.Desjardins, V.Genton, Acta Mater, 46 (1998)149-157.

[127] V. Maurice, W. P. Yang, P. Marcus, J. Electrochem. Soc, 145 (1998) 909-920.

[128] A. Machet, A. Galtayries, S. Zanna, L. Klein, V. Maurice, P. Jolivet, M. Foucault, P. Combrade, P. Scott, P. Marcus, Electochim Acta, 49 (2004) 3957-3964.

[129] J. E. Castle, C. R. Clayton, Corros Sci, 17 (1977) 7-26.

[130] T. Tsuru, Mater Sci Eng A, 146 (1991) 1-14.

[131] B. Beverskog, I. Puigdomenech, Corros Sci, 39 (1997) 43-57.

[132] G. S. Was, Prog Surf Sci. 32 (1989) 221-332.

[133] G. K. Wolf, Nucl Instru Meth Phys Res B, 46 (1990) 369-378.

[134] P. Moine, O. Popoola, J. P. Villain, N. Junqua, S. Pimbert, J. Delaford, J. Grille, Surf Coat Technol, 33 (1987) 479-486.

[135] L. Hanley, S. B. Sinnott, Surf Sci, 500 (2002) 500-522.

[136] A. M. Yacout, N. Q. Lam, J. F. Stubbins, Nucl Instru Meth Phys Res B, 42 (1989) 49-60.

[137] G. Dearnaley, Surf Coat Technol. 65(1994) l-6.

[138] C.R. Clayton, Nucl Instr Meth, 182/183 (1981) 865-873.

[139] V. Ashworth, R. P. M. Procter, W. A. Grant, Thin Solid Films, 73 (1980) 179-188.

[140] P R Gardner, Mater Des, 8 (1987) 210-219.

[141] E. Mccafferty, G. K. Hubler, P. M. Natishan, P. G. Moore, R. A. Kant, B. D. Sartwell, Mater. Sci. Eng. 86 (1987) 1-17.

[142] M. F. Stroosnijder, Surf Coat Technol, 100-l0l (1998) 196-201.

[143] S. Picard, J. B. Memet, R. Sabot, J. L. Grosseau-Poussard, J. P. Riviere, R. Meilland, Mater Sci Eng A, 303 (2001) 163-172.

[144] E. Cano, L. Martinez, J. Simancas, F. J. Perez-Trujillo, C. Gomez, J. M. Bastidas, Surf Coat Technol, 200 (2006) 5123-513.

[145] R. K. Y. Fu, D. L. Tang, G. J. Wan, P. K. Chu, Surf Coat Technol, 201 (2007) 4879-4883.

[146] C.M. Abreu, M.J. Cristobal, P. Merino, X.R. Novoa, G. Pena, M.C. Perez, Electrochim Acta, 53 (2008) 6000-6007.

[147] Sh.Song, W.Song, Zh. Fang, Corros Sci, 31 (1990) 395-400.

[148] J.P. Hirvonen, D. Ruck, S. Yan, A. Mahiout, P. Torri, J. Likonen, Surf Coat Technol 74-75 (1995) 760-764.

[149] U. Kamachi Mudali, T. Sundararajan, K.G.M. Nair, R.K.Dayal, Mater Sci Forum, 318-320 (1999) 531-538.

[150] L. Martinez Orellana, F.J. Perez, C. Gomez, Surf Coat Technol, 200 (2005) 1609-1615.

[151] G.S. Chang, J.H. Son, S.H. Kim, K.H. Chae, C.N. Whang, E. Menthe, K.T. Rie, Y.P. Lee, Surf. Coat. Technol. 112 (1999) 291-294.

[152] J.P. Riviere, P. Meheust, J.P. Villaina, C. Templiera, M. Cahoreaua, G. Abrasonis, L. Pranevicius, Surf Coat Technol, 158-159 (2002) 99-104.

[153] B. Chico, L. Martinez, F.J. Perez, Appl Surf Sci, 243 (2005) 409-414.

[154] M. Guemmaz, A. Moser, J. J. Grob, R. Stuck, Surf Coat Technol, 100-101 (1998) 353-357.

[155] Y. Arnaud, M. Brunel, A.M. De Becdelievre, M. Romand, P. Thevenard, M. Robelet, Appl Surf Sci, 26 (1986) 12-26.

[156] J. Wang, J. Xiong, Q. Peng, H. Fan, Y. Wang, G Li, B. Shen, Mater Character, 60 (2009) 197-203.

[157] N. Mottu, M. Vayer, R. Erre, Surf Coat Technol, 183 (2004) 165-173.

[158] C. Blawert, H. Kalvelage, B.L. Mordike, G.A. Collins, K.T. Short, Y. Jiraskova, O. Schneeweiss, Surf Coat Technol, 136 (2001) 181-187.

[159] H. Pelletier, P. Mille, A. Cornet, J. J Gorb, J. P. Stoquert, D. Muller, Nucl. Instr. Meth Phys Res B, 148 (1999) 824-829.

[160] S. Aggarwal, A. K. Goelt, R. K. Mohindra, P. K. Ghosh, M. C. Bhatnagar, Thin Solid Film, 237 (1994) 175-180.

[161] A. Chayahara, S. Nakashima, M. Hashimoto, T. Sasaki, M. Kurokawa, S. Kiyama, M. Satou, Nucl Inst Meth Phys Res B, 59/60 (1991) 893-896.

[162] R. Leutenecker, G. Wagner, T. Louis, U. Gonser, L. Guzman, A. Molinari, Mater Sci Eng A, ll5 (1989) 229-244.

[163] P. Marcus, M E Bussell, Appl Surf Sci, 59 (1992) 7-21.

[164] J. H. Lee, J. W. Park, J. S. Lee, C. W. Sohn, J. K. Kil, Surf Coat Technol, 196 (2005) 353-357.

[165] K. Osozawa, N. Okato, Proc: USA-Japan seminar, Passivity and its breakdown on iron and iron-based alloys, NACE (1976) 135-139.

[166] R. C. Newman, Y. C. Lu, R. Bandy, C.R. Clayton, Proc: 9th International conference on metallic corrosion, 4 (1984) 394-399.

[167] E. C. Cooney, D. I. Potter, Corros Sci, 34 (1993) 2007-2018.

[168] R.F.A Jargelius-Pettersson, Corros Sci, 41 (1999) 1639-1664.

[169] U. Kamachi Mudali, R.K.Dayal, T.P.S.Gill, J.B.Gnanmoorthy, Werkst Corros, 37 (1986) 637-643.

[170] C.O.A.Olosson, Corros Sci, 37(1995)467-479.

[171] A. Sadough Vanini, J.P. Audouard, P. Marcus, Corros Sci, 36(1994)1824-1835.

[172] U. Kamachi Mudali, N. Bhuvaneswaran, P. Shankar, Baldev Raj, Corros Sci, 46 (2004) 2867-2892.

[173] S.R. Taylor, Encyclopedia of Materials, 1259-1263, 2008

[174] H. A. Jehn, Surf Coat Technol, 125 (2000) 212-217.

[175] W. B. Nowak, Surf Coat Technol, 49 (1991) 71-77.

[176] G. Frankel, G. Grundmeier, H. McMurry, T. Shinohara, Coatings for corrosion protection, The Electrochemical Society, 2010.

[177] D.R. Gabe, G.D. Wilcox, V.E. Carter, Shreir's corrosion, 2010.

[178] H. N. McMuray, G. Willams, V. E. Carter, Shrier’s corrosion, 2010.

[179] A. K. Vijh, Electrodeposition Surf Treat, 2 (1973) 461- 480.

[180] H. Park, J. A. Szpunar, Corros Sci, (1998) 525-545.

[181] M. R. Zamanzad-Gavidel, K. Raeissi, A. Saatchi, Mater Lett, 63 (2009) 1807-1809.

[182] R. Starosta, A. Zielinski, J Mater Process Technol, 157-158 (2004) 434-441.

[183] X. Z. Ding, A. L. K. Tan, X. T. Zeng, C. Wang, T. Yue, C. Q. San, Thin Solid Film, 516 (2008) 5716-5720.

[184] Y. Hamlaoui, L. Tifouti, F. Pedraza, Corros Sci, 52 (2010) 1883-1888.

[185] A. Ghasemi, V. S. Raja, C. Blawert, W. Dietzel, K. U. Kainer, Surf Coat Technol, 204 (2010) 1469-1478

[186] N. Priyantha, P. Jayaweera, A. Sanjurjo, K. Lau, F. Lu, K. Krist, Surf Coat Technol, 163-164 (2003) 31-36.

[187] F. Presuel-Moreno, M. A. Jakab, N. Tailleart, M. Goldman, J. R. Scully, Materials Today, 11 (2008) 14-23.

[188] J. T. Prater, E. L. Courtright, Surf Coat Technol, 32 (1987) 389-397.

[189] Y. Wang, Z. Jiang, Z. Yao, H. Tang, Surf Coat Technol, 204 (2010) 1685-1688.

[190] Y. Sun, Mater Lett, 58 (2004) 2635-2639.

[191] Y. Li, L. Qu, F. Wang, Corros Sci, 45 (2003) 1367-1381.

[192] C.X. Shan, X. Hou, K. L. Choy, Surf Coat Technol, 202(2008) 2399-2402.

[193] D. Siva Rama Krishna, Y. Sun, Appl Surf Sci, 252 (2005) 1107-1116.

[194] E. L. Courtright, Surf Coat Technol, 33 (1987) 327-340.

[195] H. Dong, Y. Sun, T. Bell, Surf Coat Technol, 90 (1997) 91-101.

[196] D. J. Blackwood, S. K. M. Chooi, Corros Sci, 44 (2002) 395-405.

[197] M. Metikos Hukovic, M. Ceraj Ceric, Surf Technol, 24 (1985) 273-283.

[198] D. J. Blackwood, L. M. Peter, D. E. Williams, Electrochem Acta, 33 (1988) 1143-1149.

[199] G. X. Shen, Y. C. Chen, L. Lin, C. J. Lin, D. Scantlebury, Electrochim Acta, 50 (2005) 5083-5085.

[200] N. X. Miao, D. Ling-Yan, B. Chen-Guang, C. Deng-Fu, Q. Gui-Bao. Trans Nonferrous Soc. China, 16 (2006) s723-s727.

[201] D. R. Lide, Hand book of chemistry and physics, Ed: William M Haynes, Taylor and Francis, 2010.

[202] T. Furuya, J. Kawafaku, H. Satoh, K. Shimogori, A. Aoshima, S. Tekeda, ISIJ International, 31 (1991) 189-193.

[203] M. Li, S. Luo, P. Wu, J. Shen, Electrochim Acta, 50 (2005) 3401-3406.

[204] T. Kuratomi, K. Yamaguchi, M. Yamawaki, T. Bak, J. Nowotony, M. Rekas, C. C. Sorrell, Solid State Ionics, 154-155 (2002) 223-228.

[205] F. C. Walsh, C. P. D. Leon, C. Kerr, S. Court, B. D. Barker, Surf Coat Technol, 202 (2008) 5092-5102.

[206] Y. Huang, H. Xiao, Z. Ma, J. Wang, P. Gao, Surf Coat Technol, 202 (2007) 180-184.

[207] J. H. Huang, F. Y. Quyang, G. P. Yu, Surf Coat Technol, 201 (2007) 7043-7053.

[208] S. Rudenja, C. Laygraph, J. Pan, P. Kulu, E, Telimats, V. Mikili, Surf Coat Technol, 114 (1999) 129-136.

[209] E. Soderlund, P. Ljunggern, Surf Coat Technol, 110 (1998) 94-104.

Publications

VI. LIST OF PUBLICATIONS

1. Referred international journals, conference proceedings and chapter in book

(A) International journals

1. **N. Padhy,** Ranita Paul, U. Kamachi Mudali, Baldev Raj, Morphological and compositional analysis of passive film on AISI type 304L stainless steel in nitric acid medium, Applied Surface Science, 257 (2011) 5088-5097.

2. **N. Padhy,** S. Ningshen, U. Kamachi Mudali, Baldev Raj, In situ surface investigation of austenitic stainless steel in nitric acid medium using electrochemical atomic force microscope, Scripta Materialia, 62 (2010) 45-48

3. **N. Padhy,** S. Ningshen, B. K. Panigrahi, U. Kamachi Mudali, Corrosion behaviour of nitrogen ion implanted AISI type 304L stainless steel in nitric acid medium, Corrosion Science, 52 (2010) 104-112.

4. **N. Padhy,** Subhash Kamal, Ramesh Chandra, U. Kamachi Mudali, Baldev Raj, Corrosion performance of TiO_2 coated type 304L stainless steel in nitric acid medium, Surface & Coatings Technology, 204 (2010) 2782-2788.

5. **N. Padhy,** U. Kamachi Mudali, Vipin Chawla, Ramesh Chandra, Baldev Raj, Electrochemical and surface morphological aspect of Ti and duplex Ti-TiO_2 coating on austenitic stainless steel, Materials Chemistry and Physics, Under Review.

6. U. Kamachi Mudali**, N. Padhy,** In-situ corrosion study of materials using electrochemical scanning probe microscope, Corrosion Review, Under Review.

(B) Conference Proceedings

1. **N. Padhy,** U. Kamachi Mudali, Electrochemical and surface investigation to understand the passive film formation and damage of austenitic stainless steel in nitric acid medium using AFM and XPS, 1st Indo-Italian workshop on "Frontiors of Fundamental and Industrial Electrochemistry: A Challenge of Science for Better World", Aug. 30th-31st 2010, New Delhi.

2. **N. Padhy,** S. Ningshen, R. V. Subbao Rao, U. Kamachi Mudali, Morphological and compositional analysis of passive film on AISI type 304L stainless steel in nitric acid medium, International Conference on Surface Modification Technologies (SMT-23), 2-5 November 2009, Mamalapuram, India.

3. **N. Padhy,** Subhash Kamal, Ramesh Chandra, U. Kamachi Mudali,Corrosion performance of TiO_2 coated type 304L stainless steel in nitric acid medium, International Conference on Surface Modification Technologies (SMT-23), 2-5 November 2009, Mamalapuram, India

4. **N. Padhy,** S. Ningshen, B.K. Panigrahi and U. Kamachi Mudali, Corrosion behaviour of nitrogen ion implanted AISI Type 304L stainless steel in nitric acid medium, Proceedings of International Conference on Corrosion (CORCON 2007), NACE International (India Section) 26-28th September 2007, Mumbai, India.

5. **N.Padhy,** U. Kamachi Mudali, Study of passivation and corrosion behavior of AISI 304L SS in nitric acid medium using scanning probe microscope, National Convention of Electrochemists (NCE-14), 6-7 December 2007, IGCAR, Kalpakkam, India.

(C) Chapter in Book

1. U. Kamchi Mudali**, N. Padhy,** A. Ravi shankar Application of Electrochemical STM/AFM for corrosion investigation, Corrosion Prevention and Control, Eds: Baldev Raj, U. Kamachi Mudali, S. Rangarajan, Page 179-184, Narosa Publication, New Delhi, 2009.

2. Awards and honours

1. **Best Oral Presentation**, Morphological and compositional analysis of passive film on AISI type 304L stainless steel in nitric acid medium, N. Padhy, S. Ningshen, R. V. Subbao Rao, U. Kamachi Mudali, International Conference on Surface Modification Technologies (SMT-23), 2-5 November 2009, Mamalapuram, India.

2. **Best Poster Presentation,** Corrosion behaviour of nitrogen ion implanted AISI Type 304L stainless steel in nitric acid medium, N. Padhy, S. Ningshen, B.K. Panigrahi and U. Kamachi Mudali, Proceedings of international conference on corrosion (CORCON 2007), NACE International (India Section) 26-28th September 2007, Mumbai, India**.**


Thanks